CHARACTERIZATION AND USE OF GENETICALLY ENCODED FLUORESCENT HEME SENSORS TO INTERROGATE HEME TRAFFICKING, DYNAMICS, AND SIGNALING

A Dissertation
Presented to
The Academic Faculty

by

David A. Hanna

In Partial Fulfillment
of the Requirements for the Degree
Doctor of Philosophy in the
School of Chemistry & Biochemistry at Georgia Institute of Technology

Georgia Institute of Technology
August 2019

CHARACTERIZATION AND USE OF GENETICALLY ENCODED FLUORESCENT HEME SENSORS TO INTERROGATE HEME TRAFFICKING, DYNAMICS, AND SIGNALING

Approved by:

Dr. Amit Reddi Advisor
School of Chemistry & Biochemistry
Georgia Institute of Technology

Dr. Christoph Fahrni
School of Chemistry & Biochemistry
Georgia Institute of Technology

Dr. Loren Williams
School of Chemistry & Biochemistry
Georgia Institute of Technology

Dr. Matt Torres
School of Biological Sciences
Georgia Institute of Technology

Dr. Wilbur Lam
School of Biomedical Engineering
Georgia Institute of Technology

Date Approved: May 16, 2019

ACKNOWLEDGEMENTS

I believe that direction, not intention, leads your life. Thankfully, I have had many friends and mentors who have helped me keep in the right direction. It is in large part due to their guidance and support through difficult key turning points and ordinary moments alike that I was able to complete the task of completing my dissertation, graduate school, and becoming the person I am today. I must foremost thank my parents, Marwan and Rima, my girlfriend Katherine, and my brother Michael. My ever supportive and loving parents shaped me more than anyone by instilling their values into me. Katherine always encouraged me and has given me the courage to pursue my dreams all the while being endlessly comforting and patient. Michael has always been my best friend. I am grateful for his encouragement, consistent reminders of who I am when I have felt lost, and being my extra guardian whether I wanted it or not. I thank my aunts, uncles, and cousins both far away and next door in Tennessee for their love and guidance my entire life, and my late uncle Khalil for the vision and understanding I feel he imparted onto me. I cannot thank my family enough for helping bring out the best in me and helping me see myself. Beyond my core family and Katherine, there are too many teachers, mentors, and peers to thank. They have each helped develop my curiosity, confidence, sense of purpose in my work, and my love for learning. The work here was very trying for me. I often felt separated from my natural order, yet graduate school was a great source of satisfaction and allowed me to fulfill the need I feel to learn, be inquisitive, and exercise creativity.

I would like to thank all of my teachers from Carleton College who prepared me for graduate school and mentored me. Most influential was Marion Cass. Personally, she

was always available and bolstered my confidence. Professionally, Marion always found new ways for me to take things one step further in my studies, she continually opened new avenues for me to pursue, and ultimately is why I moved to Georgia Tech to work for Amit. To my peers in the Chemistry Department, the drive that everyone had truly inspired me to engage our studies so much more intently. Continually working and interacting with people like Dan, Galen, Milan, Mia, Anna, Christian, Joe, and my entire comps group really propelled my conviction and curiosity, which were essential qualities for me to push forward in my graduate studies.

None of my work would have been possible without the training and support I got from my advisor. I cannot thank Amit enough for his continued support and giving me a direction to take in life that I could not comprehend before starting work for him as technician in an empty lab in 2013. Amit directed me in a way that gave me room to both develop as a scientist and integrate personally throughout the many changes I experienced the last several years. I want to thank Amit for teaching me how to think more critically, design experiments, have an enthusiasm for discovery, and for all of his coaching.

I would like to thank my committee members, Christoph Fahrni, Matt Torres, Loren Williams, and Wilbur Lam for their overwhelming encouragement, coaching, and academic and personal advice throughout my graduate tenure.

I would like to thank my late friend Dr. George Waring who helped me feel more at home in Atlanta and also inspired me when I was debating to apply to graduate school.

Getting to know you my first year and a half in Atlanta filled me with resolve and wild inspiration, and I still reflect on lessons George taught me.

I would like to extend my gratitude to Iqbal Hamza for inspiring me to believe in my abilities and my science. He and others I met with at the Tetrapyrroles GRCs helped renew my aspirations and my belief in myself when I was feeling low.

Thank you to Paul and Suhas who were pretty great roommates. Having them both around made everything so much easier. These guys helped lift me up, gave my life more balance, and were a consistent source for encouragement and play. I am glad for their friendships and for the help taking care of Remy.

I would like to thank Katherine again, this time for encouraging me to talk about my synesthesia with others, something I felt I should keep secret. Without my friends and therapist, Jay Dillard, who helped me make better sense of my synesthesia and how to regulate it, I would not be the man I am today.

I owe many thanks to my lab mates and all my current and old peers at Georgia Tech who I will not name for the sake of brevity. My perpetual growth was fueled by their support, encouragement, criticism, and engagement with them. I often relied on many of my peers for help learning a technique, for feedback on my data, to talk through experiments, for enhancing my presentations, or just being there when I needed a friend. Our connections made my time at Georgia Tech much more meaningful. Given all the ups and downs in graduate school, I do not believe I could have finished this work without their support. In every season, there was at least one of you who really helped drive my motivation in lab.

TABLE OF CONTENTS

LIST OF TABLES

LIST OF FIGURES

LIST OF SYMBOLS AND ABBREVIATIONS

ΔF	ΔF is the change in fluorescence due to heme binding
°C	Degrees centigrade
µL	Microliter
µM	Micromolar
µm	Micrometer
5-ALA or ALA	5-aminolevulinic acid
Ala	Alanine
ALAS	ALA synthase
atg1	Yeast gene required for vesicle formation in autophagy
BR	Bilirubin
BV	Biliverdin
BY4741	Common yeast deletion strains with selectable marker genes deletions

CG6	EGFP-Cyt b_{562} integral fusion protein
cm	Centimeter
cm^{-1}	Wavenumbers
CO	Carbon monoxide
COX4	Cytochrome c oxidase gene
ctt1	Yeast cytosolic catalase gene
CYC1	Hap1 protein target gene
Cyt b_{562}	Cytochrome b562
DAF-FM DA	Diaminofluorescein-FM diacetate
DAPI	4’,6-diamidino-2-phenylindole
DMEM	Dulbecco’s modified eagle medium
DMSO	Dimethyl sulfoxide
E coli.	*Escherichia coli*
EGFP	Enhanced green fluorescence protein

E_m(bound)	heme protein's reduction potential
E_m(free)	reduction potential of free heme
Em.	emission
EV	Empty vector plasmid
Ex.	excitation
F	Faraday's constant
F	F is the fluorescence signal at any given concentration of heme
Fe(II) or Fe^{2+}	Ferrous iron
Fe(III) or Fe^{3+}	Ferric iron
fL	Femtoliters
FL	FL is the initial fluorescence of the protein in the absence of heme
FLVCR	Feline Leukemia Virus Subgroup C Cellular Receptor 1
F_{max}^{mKATE2}	mKATE2 emission intensity when 100% of sensor is bound to heme

F_{min}^{mKATE2}	mKATE2 emission intensity when 0% of sensor is bound to heme
FPLC	Fast protein liquid chromatography
FRET	Fluorescence resonance energy transfer
G418	Geneticin; an aminoglycoside antibiotic
GAL	Galactose
GAPDH	Glyceraldehyde phosphate dehydrogenase
GlySer	Glycine-Serine
Hap1p	Heme activator protein 1
HEK293	Human Embryonic Kidney
hem1	Yeast 5-aminolevulinate synthase gene
hem15	Yeast ferrochelatase gene
HEPES	4-(2-hydroxyethyl)-1-piperazineethanesulfonic acid buffer
HG buffer	HEPES 2% Glucose buffer
His	Histidine

his3	Yeast gene, involved in histidine biosynthesis
His_6	Histidine tag comprising 6 subsequent histidine residues
Hmx1	Yeast heme oxygenase
hmx1	Yeast gene for heme oxygenase 1
HO	Heme oxygenase
HPLC	High-pressure liquid chromatography
HS1	Heme sensor 1
IAM	Iodoacetamide
iNOS	Inducible nitric oxide synthase
kanMX4	Gene that confers kanamycin resistance in yeast; selector module
KATP	ATP-sensitive Potassium Ion Channel
Katushka 2	mKATE2
K_d or K_{D1}	HS1 dissociation constant
K_{D1}	Ferric or ferrous heme dissociation constant in equation 3

kDa	Kilodalton
$K_d^{Fe(II)}$	Generic heme dissociation constant for ferrous heme
$K_d^{Fe(III)}$	Generic heme dissociation constant for ferric heme
K_d^{II}	HS1-ferrous heme dissociation constant
K_d^{III}	HS1-ferric heme dissociation constant
L	Liter
LB	Lysogeny broth
LC-MS	Liquid chromatography mass spectrophotometry
LD_{50}	Lethal dose-50
LEU	Leucine
leu2	Yeast gene, involved in leucine biosynthesis
L-NAME	N^G-nitro-l-arginine methyl ester
LT	Concentration of protein
M	Molar

MATa	Haploid a-type yeast genotype
MES	2-(N-morpholino)ethanesulfonic acid buffer
Met	Methionine
met15	Yeast gene, involved in methionine biosynthesis
Milli-Q	Millipore Corporation trademark for ultrapure Type I water
Min	Minutes
mL	Milliliter
ML	Concentration of hemoprotein complex
mM	Millimolar
MT	Concentration of heme being titrated
mV	Millivolts
n	moles
NHE	Standard hydrogen electrode

nm	nanometer
nM	nanomolar
NO	Nitric Oxide
NOS	Nitric oxide synthase
$OD_{600\ nm}$	Optical density read at 600 nm
PBS	Phosphate buffered saline
PCR	Polymerase chain reaction
pep4	Yeast gene encoding vacuolar aspartyl protease
pGAL	GAL-inducible promoter
pGAL-Cyt b_{562}	GAL-inducible Cyt b_{562}
pGAL-EV	A control EV strain expressing in the p316-GAL vector
Pi	Inorganic Phosphate
pM	Picomolar
PMSF	Phenylmethylsulfonyl fluoride
PPIX	Protoporphyrin IX

pr^{ADH1}	Truncated yeast promoter of genomic alcohol dehydrogenase
pr^{CYC1}	Truncated yeast promoter of genomic hap1p target gene CYC1
pr^{GPD}	Truncated yeast promoter of genomic GAPDH
pr^{TEF1}	Truncated yeast promoter of genomic translational elongation factor
PUG1	Protoporphyrin uptake gene; porphyrin-heme exchanger
R	Universal gas constant
RAF	Raffinose
R_{expt}	EGFP/mKATE2 fluorescence ratio under any given condition
R_{max}	EGFP/mKATE2 fluorescence ratio when 100% of sensor is bound to heme
R_{min}	EGFP/mKATE2 fluorescence ratio when 0% of sensor is bound to heme
rpn10	Yeast gene encoding 19S regulatory particle of 26S proteasome
S. cerevisiae	*Saccharomyces cerevisiae*
SA	Succinylacetone

SC	Selective complete media
SCE	SC with ergosterol and tween 80 supplements
SDS-PAGE	Sodium dodecyl sulfate polyacrylamide gel electrophoresis
SILAC	Stable isotope labeling by amino acids in cell culture
SV40	Polyomavirus simian virus 40
T	Temperature
TDH1	Isoform of yeast GAPDH
tdh1	Gene of major isoform of GAPDH
TDH2	Isoform of yeast GAPDH
tdh2	Gene of major isoform of GAPDH
TDH3	Major isoform of yeast GAPDH
tdh3	Gene of major isoform of GAPDH
TE	Tris-EDTA

TEV	Tobacco Etch Virus
TXRF	Total reflection x-ray fluorescence
ura3	Yeast gene, involved in pyrimidine biosynthesis
w/v	Weight by volume
WT	Wild type
YPD	Yeast peptone dextrose media
YPDE	YPD with ergosterol and tween 80 supplements
Δ	Deletion, referencing gene deletion strain
μg	Micrograms

SUMMARY

The current work establishes novel heme sensing technology to quantitate intracellular labile heme (LH) and provides new information concerning the amount and dynamics of LH pools. Though methods to detect both total and exchange inert intracellular heme exist, measuring exchange LH in intact cells, the pool of heme accessible for heme dependent processes and signaling, has not been possible until the development of fluorescent based genetically encoded sensors like that put forth by this work[2]. The nature of the regulatory heme pool, how it is controlled, as well as the means by which heme can be propagated to activate heme-based signals have remained mysterious phenomena. However, this body of work demonstrates the means to measure the dynamics of heme mobilization and trafficking, conditions that dynamically mobilize heme, proteins involved in buffering or controlling LH availability, and demonstrate the subsequent effects of altered LH levels on heme dependent transcription.

Before starting this thesis work, tools to monitor intracellular LH levels to investigate what controls LH availability and mobilization did not yet exist. The objective, therefore, was to develop and extensively characterize a tool to quantitate intracellular LH and apply it in multiple cell lines starting with the easily genetically tractable model eukaryote *Saccharomyces cerevisiae*. As a lab, we collectively showed that by using the heme sensors characterized in this body of work, we could measure and identify factors that induce dynamic heme mobilization and identify new heme trafficking proteins that control LH availability.

After using the heme sensor to demonstrate the first reported case that heme could be dynamically mobilized by signaling molecules like nitric oxide (NO), further stress conditions that may cause dynamic shifts in heme mobilization were investigated. Investigated stresses included heme starvation, heme chelation, and Pb^{2+} poisoning in *Saccharomyces cerevisiae*. Indeed, fluxes in LH availability under these stress conditions resulted in changes in heme dependent signaling evincing a role for this regulatory pool of heme in controlling heme signaling. Of the investigated stresses, Pb^{2+} poisoning, which was originally hypothesized to induce heme signaling in the form of a mitochondrial retrograde signal, was shown to have the most adverse effects on heme homeostasis. Our extensive characterization of our yeast model of Pb^{2+} poisoning and its effects on labile and total heme motivated the development of a heme affinity assay using hemin agarose beads to be used with quantitative mass spectrometry to identify proteins that dynamically lose or gain heme in response to Pb^{2+} poisoning. The identification of these proteins was hypothesized to shed light on new heme signaling networks activated under Pb^{2+} poisoning.

The other main goal of this thesis was to fully characterize the heme sensors in a mammalian cell line. After describing the use of our heme sensors in HEK293 cells and developing calibration protocols to quantitate LH in these cells, the sensors were used to interrogate compartment specific LH availability. Using the heme sensors, we identified how both synthesis and import of extracellular heme each impact cytosolic, nuclear, and mitochondrial heme pools. In this investigation, we discovered a preference for synthesized heme in the mitochondrial LH pool and that nuclear and cytosolic LH pools were more sensitive to exogenous heme availability than mitochondria. Next, given that

overexpressed heme oxygenase 2 (HO2) was ascribed cytoprotective roles under oxidative stress that were independent of its catalytic activity, we sought to test if HO2 overexpression had an impact on labile and total heme availability. Quite surprisingly, we found that both WT HO2 and catalytic mutants, but not heme binding mutants of HO2, sequester LH in HEK293 cells without effecting total heme availability. This unexpected result ultimately elucidated a cytoprotective role for HO2 acting as a heme sequestering or heme buffering factor. In total, the work done in HEK293 cells puts forth the means to quantify subcellular pools of LH that should be adapted to other mammalian cell lines and demonstrate the use of our heme sensors to uncover previously undescribed effectors of LH availability like HO2.

Altogether, completion of this body of work poises others to use the developed fluorescent sensor technology to shed more light on questions relevant to heme trafficking and transport, as well as LH's roles in heme related pathologies. In addition, proteins identified by the investigation in the hemin agarose mass spectrometry studies represent a new putative heme binding proteome, and the screening and characterization of these proteins may demonstrate their involvement in regulating LH availability and their potential roles in heme signaling.

CHAPTER 1. INTRODUCTION

Iron protoporphyrin IX, or heme, is an iron-containing macrocycle required for all aerobic life that functions as a protein prosthetic group to most porphyrin binding proteins[2, 3]. Heme is an extremely well characterized molecule that serves as a cofactor in numerous proteins and is involved in controlling signaling in a myriad of different ways. Even so, little is known about how heme is trafficked throughout the cell after being synthesized in the mitochondria[4]. Beyond heme being essential for life, understanding how heme is partitioned throughout the cell to be acquired by hemoproteins and control heme dependent processes is crucial to understanding the contributions of aberrant heme trafficking in several disease states[5-9]. Our understanding of heme trafficking and its involvement in pathogenesis is quite limited, largely in part by these two factors: First, there is a dearth of proper chemical and genetic tools to identify and characterize heme transporters[4]. Secondly, heme is such a promiscuous molecule that many candidate proteins could bind to it at low affinity to transport it throughout the cell, adding difficulty to designing screens for heme trafficking factors[4]. These points were large motivations to our approach to develop a ratiometric heme sensor and a more quantitative means to identify new heme trafficking factors with hemin agarose beads and mass spectrometry. This introduction will serve as a brief review of heme, its roles in cell biology as both a static cofactor and exchange labile molecule, describe the current knowledge concerning heme trafficking and transport, and provide a brief summary of heme in pathogenesis all while highlighting crucial points that motivated this body of work.

1.1 Heme in Cell Biology

Heme is an indispensable metallo-nutrient utilized in cells to facilitate a diverse set of functions that span energy production, regulating metabolism, and facilitating redox biochemistry. Heme can adapt many different conformations when bound to proteins that are often associated with the function of the associated hemoprotein[3]. The iron atom of the heme is typically in one of two oxidation states, either ferrous, Fe^{2+} or ferric, Fe^{3+}. There are 4 main types of heme; heme a, b, c, and o, which are distinguished by their side chains around the porphyrin ring[3]. Heme b is the most common form and is the cofactor of most globins like hemoglobin and myoglobin[3]. Heme a is solely known for its role as a cofactor in cytochrome c oxidase[3]. Heme o is similar to heme a but is only found in *Escherichia coli*[10]. Lastly, heme c is different from the other hemes in that it forms a covalent attachment to hemoproteins via a thioether linkage like in cytochrome c and the cytochrome bc1 complex[3]. The work in this dissertation is focused on the most abundant form, protoheme or heme b.

Most organisms including mammals, fungi, and α-proteobacteria, synthesize heme via the Shemin pathway, a highly conserved eight-step process, starting with the condensation of glycine with succinyl-coenzyme A to form δ-aminolevulinic acid (ALA)[11]. The next four steps of the Shemin pathway occur in the cytosol following mitochondrial export of ALA[3, 11]. The cytosolic steps end with the biosynthesis of coproporphyrinogen III, which is shuttled back into the mitochondria for the remaining steps of heme synthesis[12]. The final step of the pathway is the insertion of Fe^{2+} into protoporphyrin IX by ferrochelatase (FECH) to form heme b[12]. After its terminal step of

synthesis in the mitochondria, heme is shuttled by unknown mechanisms to virtually every subcellular compartment where there are heme dependent processes[13, 14].

The most commonly known roles of heme are as a static protein cofactor or prosthetic group in globins and cytochrome proteins[11]. As a cofactor in globins, heme serves multifaceted roles in gas sensing, transport, and scavenging[14, 15]. Regarding gas sensing, differential gas binding to heme regulates many metabolic switches and signaling processes[15-19]. In gas transport, hemoglobin is well known to bind and deliver diatomic oxygen and carbon dioxide via heme, but was also recently shown to control the transport of nitric oxide to regulate vasodilation[20, 21]. Finally, concerning heme's role in gas scavenging, many bacteria rely on specific globin proteins to detoxify nitric oxide imposed by environmental stresses[22, 23]. In cytochromes, heme is required as a prosthetic group to shuttle electrons in respiratory and photosynthetic pathways that require the use of an electron transport chain[11]. Additional roles for heme as an essential cofactor include in enzymatic reactions where it facilitates as part of cytochrome p450 enzymes and its involvement in scavenging hydrogen peroxide (H_2O_2) when bound to catalase or in clearing H_2O_2 in disproportionation reactions as a cofactor in peroxidases[11, 14, 24-26]. Altogether, heme is indispensable as a protein cofactor for its use in regulating signaling and metabolism, adapting to oxidative stress, and facilitating many enzymatic reactions.

Even though heme is mostly thought of as a static protein cofactor buried deep within the core of tight binding hemoproteins, more recent genetic and biochemical evidence have indicated that heme may act as a dynamic signaling molecule that regulates cell metabolism and physiology [2, 27-29]. In fact, heme dependent nuclear transcription factors, like HAP1, p53, Bach1, and Reverb, collectively serve to regulate

diverse functions from oxygen sensing, iron homeostasis, antioxidant stress response, energy metabolism, circadian rhythms, apoptosis, and cell proliferation, and are conserved from yeast to man [29-35]. Additional roles for heme in signaling extend beyond regulating metabolism and physiology via direct modulation of transcription. For instance, ferric heme has been shown to regulate the activity of the RNA-binding protein DGCR8 for primary microRNA processing[36]. Furthermore, heme transport from cytochrome c peroxidase in response to H_2O_2 produced as cells switch to respiratory metabolism is required for cells to undergo proper mitohormesis[37], and K_{ATP} channels are regulated by binding of both heme and heme degradation product, carbon monoxide (CO), to a K_{ATP} $CXXHX_{16}H$ heme-binding motif[38, 39]. Beyond direct effects of heme on signaling, variable heme transport and heme availability affect the stores of different signaling molecules. For example, heme availability to inducible nitric oxide synthase (iNOS) and cytosolic catalase, as regulated by the heme chaperone GAPDH[40], will alter intracellular levels of nitric oxide (NO) and hydrogen peroxide (H_2O_2), which are two vital signaling molecules[41-43]. These are some of many examples of heme dependent regulation that exists outside of heme directly regulating transcription.

1.2 Heme Trafficking and Transport

The roles for heme in regulating cell metabolism and signaling are exhaustive. Even so, the factors involved in mobilizing heme from its site of synthesis in the mitochondria to all these client hemoproteins that exist in virtually every subcellular compartment is poorly understood[14] (Figure 1.1). When conceptualizing the number and the diversity of heme regulated processes, it is clear that heme transport and trafficking must be tightly regulated to ensure that this metallo-nutrient is available as needed by the

cell's plethora of heme dependent functions. Even so, the dearth of knowledge regarding how heme is partitioned leaves us in the dark on whether there are distinct cellular mechanisms that actively deliver heme from where it's synthesized or from a heme store directly to different client hemoproteins or if heme is transported more passively as a passenger of heme-binding proteins that are themselves trafficked throughout the cell. The former notion points to there being a direct transfer method from synthesis or from a regulatory pool of heme that could regulate heme-dependent processes and signaling. The latter idea of heme as a passenger with heme-binding proteins describes a means to allocate heme more passively through the exchange of heme between several proteins that are themselves trafficked in a way that gets heme to equilibrate to different locales and client hemoproteins throughout the cell. Each method, active transport or passive exchange between proteins could distribute heme to meet cellular demands while buffering heme to low levels as mandated by its apparent hydrophobicity and cytoxicity. Even so, complete pathways for heme portioning throughout the cell by either means have yet to be elucidated in detail as there as the technology to monitor heme levels and heme mobilization in cells was recently developed[2, 44]. Regardless of the means for heme allocation throughout the cell, the cytotoxicity of misregulated heme dictates that the acquisition of heme by these client hemoproteins and transcription factors to regulate metabolism and signaling is ultimately reliant on the ability of cells to safely mobilize heme and use an exchange-labile source of heme, and the underlying mechanisms and proteins involved in heme trafficking and transport must be elucidated[2, 29, 45].

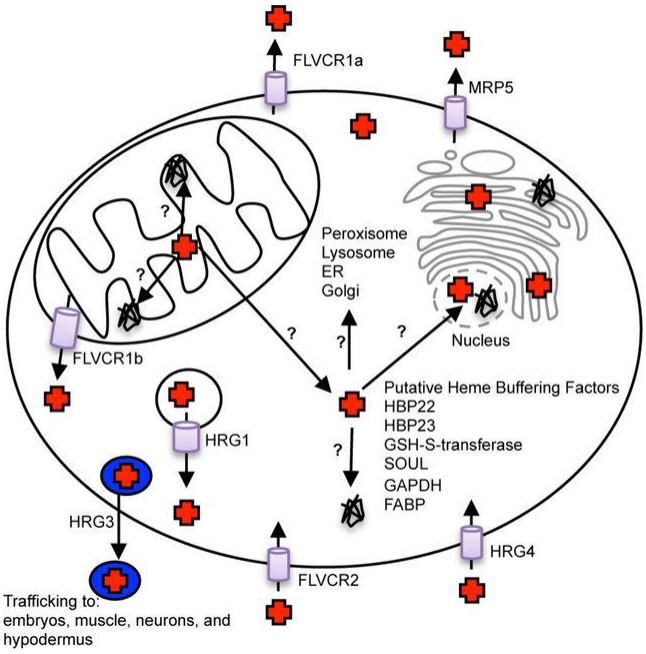

Figure 1.1 – Model of eukaryotic heme transport and trafficking. The final step of heme synthesis occurs in the mitochondrial matrix, and heme must be transported out of the mitochondria and incorporated into a multitude of hemoproteins found in different compartments. This process is likely mediated by heme chaperones and transporters. Proteins previously implicated in heme transport, trafficking, or buffering are identified, and trafficking pathways that are currently unknown are marked with question marks. Figure reproduced exactly as published by Hanna et al, Copyright © 2017 American Chemical Society[2].

Exchange labile heme (LH) is a pool of chelatable, kinetically labile heme that can readily exchange between proteins and biomolecules to be used for heme dependent processes[45]. Exchange inert heme, on the other hand, represents the fraction of heme that is too tightly bound or buried within the core of a hemoprotein, like in cytochromes or globins, so that the heme is not readily available for new heme-dependent processes[2, 29, 45]. These two pools of heme comprise the total heme within a cell, where the pool of exchangeable heme utilized for regulating heme dependent processes in non-erythroid cells has been estimated to be around 10% of a cell's total heme quota[44]. In order to elucidate how the cellular demands for heme are met, the characterization of LH,

including its concentration, speciation, oxidation state, distribution, and dynamics must be understood[29]. However, these details regarding LH, including what proteins and biomolecules affect its availability, have remained mysterious mostly due to a lack of required tools to study LH availability and trafficking[14, 28, 29].

The relevance for studying heme transport goes beyond heme being an essential protein prosthetic group and signaling molecule. Heme is also a very cytoxic molecule due to its inherent peroxidase activity and its promiscuous, nonspecific binding interactions [13, 14, 46]. Therefore, understanding the cellular mechanisms that underlie heme trafficking and transport will help elucidate mechanisms of aberrant heme trafficking apparent in different disease states like cardiovascular and neurological diseases [5, 47]. These properties that make heme cytotoxic mandate the need of dedicated pathways to facilitate the safe transfer and mobilization of heme. In much the same way that "essential toxins" like copper and iron require transporters and chaperones to bind and deliver these metals safely, I propose that heme requires this as well [2, 13, 48].

Heme is required by both membrane bound and soluble hemoproteins, requiring heme to be both soluble and able to cross membranes. However, heme is not readily soluble in aqueous media due to its hydrophobic character, and its hydrophilic propionate groups make heme unable to completely cross the lipid bilayer unassisted. Therefore, for both membrane and soluble hemoproteins to access heme, the assistance of a binding partner or heme chaperone is warranted [13, 14]. Even so, the identities of such chaperones that assist in heme transfer are mostly unknown. In fact, how heme leaves the mitochondria to be acquired by hemoproteins in virtually all subcellular compartments is a mysterious phenomenon[13, 14].

Although a complete list of required heme trafficking factors is lacking, there has been some success in identifying a number of heme transporters and chaperones within the past 10 years (Figure 1.1). Several of these heme trafficking factors were discovered using molecular genetics approaches to identify genes that were regulated differently by heme in the heme auxotroph *C. Elegans*[49, 50]. Of the identified heme responsive genes dubbed HRGs, several were characterized to have direct roles in heme trafficking and have elevated what we currently know about heme transport in cells and whole organisms (Figure 1.1)[49-56].

In addition to the identification of transporters and chaperones, small molecule oxidants like NO and H_2O_2 have proven key to facilitating heme transfer mechanisms. Recent studies have shown that H_2O_2 generated during the diauxic shift, when cells switch from fermentation to respiration, triggers a heme transfer from cytochrome c peroxidase (Ccp1) to mitochondrial catalase[37]. The peroxide labilizes heme from the otherwise exchange-inert cytochrome c peroxidase, which causes heme dissociation and heme transfer to catalase. Beyond regulating heme reallocation between these two mitochondrial hemoproteins, other instances of peroxide-dependent heme transfer have not been identified nor extensively studied[45]. Beyond peroxide based heme transfer, work by Stuehr and his colleagues has shown a more diverse set of roles for nitric oxide (NO) in regulating heme signaling and protein heme acquisition [41]. In fact, S-nitrosylation of GAPDH, a recently discovered major heme buffer and chaperone, negatively regulates inducible nitric oxide synthase (iNOS) and excess NO blocks insertion of heme to a number of hemoproteins, including iNOS, hemoglobin, catalase, and cytochrome p450s [40-43, 57, 58]. On the other hand, NO can also help facilitate heme insertion as done with the

β-subunit of soluble guanylate cyclase[59]. Beyond NO regulating protein heme acquisition, NO has been postulated to regulate heme homeostasis for years[60]. In fact, different nitrosylation mechanisms have been shown to be regulated by heme, and vice versa, various heme cleavage and heme transfer mechanisms are regulated by NO[29, 60-68]. Indeed, heme and NO signaling appear to be intimately tied, but the extent to which NO availability regulates heme trafficking and availability is undetermined[69].

1.3 Heme Related Pathology

As mentioned, heme is essential for life, serving countless roles in both facilitating and regulating biological processes. Even so, heme is also cytotoxic and causes many deleterious effects when mishandled by cells[3]. Heme is pro-oxidant that catalyzes the formation of reactive oxygen species, has the potential for non-specific binding interactions, and is known to intercalate membranes[14]. Heme is also both hydrophobic and charged, and yet, must be able to cross membranes to be incorporated into soluble hemoproteins[1]. Taken together, these characteristics enable misregulated heme to cause the peroxidation of membrane lipids, as well as damage proteins and nucleic acids [1, 14, 70]. Further, dysregulated "free heme" can act as a source of redox active iron that can facilitate the Fenton reaction to generate free hydroxyl radicals, ramping up oxidative damage and the generation of more reactive oxygen species that can negatively affect a wide-array of cellular processes (Figure 1.2)[1].

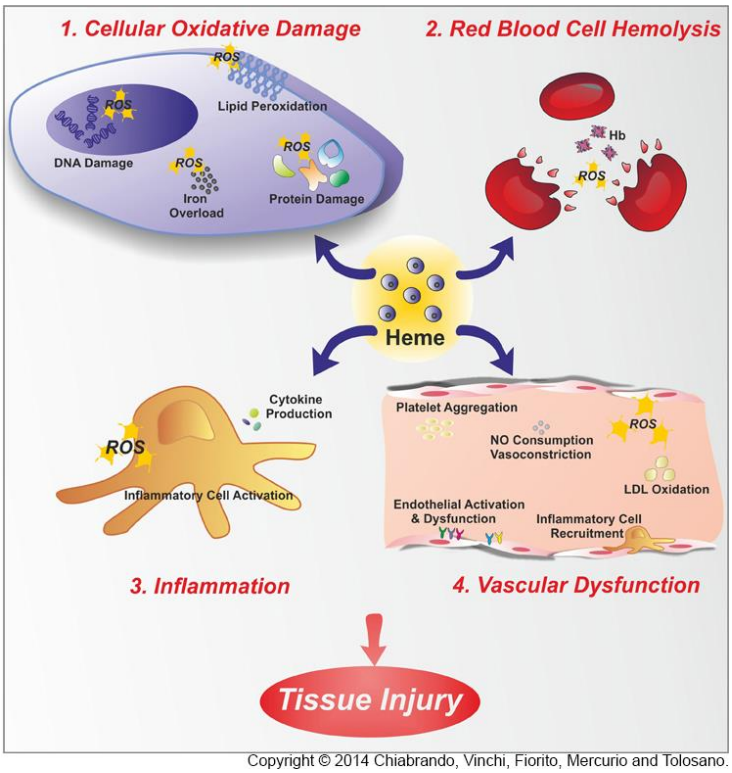

Figure 1.2 – Diagram of free heme toxicity. Heme causes tissue injury by inducing oxidative damage, hemolysis, inflammation, and vascular dysfunction. This figure was reprinted with permission from Chiabrando et al. (2014) as part of Drug Metabolism and Transport, as section of the journal Frontiers in Pharmacology[1]

Natural ways for heme to be misregulated include defects in heme synthesis and catabolism by heme oxygenase (HO) enzymes, as well as hemoprotein breakdown[1]. Heme synthesis is a very well characterized and tightly regulated process but when misregulated induces a class of metabolic disorders called porphyria, characterized by the overproduction of porphyrin intermediates, porphyrins, and heme deficiency[71-73]. The toxicity associated with heme and its biosynthetic enzymes, along with increasing amounts of biochemical evidence, support the idea that there is a heme synthesis metabolon to ensure the efficient and safe production of heme and the shuttling of its intermediates between the cytosol and mitochondria[71, 74]. This heme metabolon comprises several of the cytosolic and mitochondrial heme synthesis enzymes, several heme related

proteins, and has the potential to serve as a scaffold for interactions with other pathways, signaling molecules, and organelles[71]. Therefore, understanding defects in heme synthesis may be crucial towards understanding how heme is directed out of the mitochondria and how heme may be misregulated in porphyria, anemias, and other heme related disorders[1, 4, 70, 71, 73].

Heme catabolizing HO enzymes serve a dual protective role by regulating heme levels while also controlling cytoprotective responses to stress[1, 75]. HO's cytoprotective roles are usually attributed to its heme degradation products, biliverdin and CO, which have been shown to reduce several models of inflammation in the liver and brain[75-77]. Both free heme and the two main isoforms of HO, HMOX-1 (HO-1) and HMOX2 (HO2), are associated in a number of neurological disorders[78-81]. In Parkinson's disease, Alzheimer's disease, and multiple sclerosis, HO-1 is upregulated presumably to help manage inflammation associated with neuroinflammation and continual cell injury[82]. For undetermined reasons, however, in human immunodeficiency virus (HIV) infections of the brain, HO-1 is downregulated[82, 83]. How heme oxygenase expression and its regulation of free heme act in heme related pathology is extremely important and needs to be better understood.

Although there are dedicated heme chaperones, transporters, buffering factors, and tightly controlled mechanisms to regulate heme synthesis and induce heme degradation, heme is still inappropriately handled in cells, and there are conditions that increase free heme to pathophysiological levels[84]. Regarding high heme levels, hemolysis, hemorrhage, and myolysis all cause the release of excesses of hemoproteins and free heme into the extracellular space that is often too much for scavenging proteins

like hemopexin and haptoglobin to handle and deliver for clearing by HO[85]. Under these contexts, endothelial cells become dysfunctional leading to vascular disease (Figure 1.2)[47, 86, 87]. When heme is not in detrimental excess under hemolytic stress, heme likely acts as an alarmin to signal to TLR4 to ensure an adaptive response. However, under hemolytic conditions commonly associated with malaria, sepsis, and sickle cell disease, heme has been shown to activate innate immune receptors that contribute to lethality and the pathogenesis of these diseases (Figure 1.2)[84, 85, 87, 88]. Yet, the modes by which heme activates these extracellular signals, and specifically those contributing to lethality, are unknown and may lead to new therapeutic strategies for hemolytic diseases[84, 85].

Heme is the focus of several other diseases, including infectious diseases like tuberculosis and malaria where these pathogens rely on their host's heme as a source of iron for virulence. The mechanisms under which heme is regulated and acquired in these organisms is of high relevance in discovering new therapeutic drug targets that could selectively target the pathogen[89-91]. Therefore, in this context, understanding how heme is trafficked differently between the host and the pathogen is crucial to developing new therapeutic strategies.

Additionally, heme has been implicated in Alzheimer's disease where it can associate with the Alzheimer's disease hallmark, amyloid beta (ABeta), and intensify Abeta associated cytotoxicity with its peroxidase activity[92, 93]. Interestingly, a number of heme-associated proteins and heme degradation in Alzheimer's disease models have their expression downregulated, potentially increasing the amount of free heme that can associate with ABeta[94]. In addition, studies in primary mouse astrocytes have shown that physiological doses of heme and hemoglobin can associate with particular ABeta species

and that through their interactions with ABeta, suppress inflammatory response by preventing the induction of pro-inflammatory cytokines and prevent ABeta uptake into the astrocytes[95]. Heme has not been a central focus of Alzheimer's disease progression, but understanding the molecular mechanisms surrounding altered heme availability in the affected tissues as well as the downstream effects of heme on physiology are paramount in understanding the pathogenesis of this disease.

Before the start of this thesis, no tools existed for quantifying or monitoring dynamic changes in LH availability. Ideally, many of the questions underlying heme related pathologies relevant to mismanaged heme, disorders in heme synthesis, and perturbed regulation of HO enzymes can now be parsed out using some of the novel heme sensing technologies produced over the last several years. Now, using the heme sensors characterized as part of this dissertation, others are currently investigating heme's role in infectious diseases like tuberculosis and parsing out more details relevant to heme in Alzheimer's disease and traumatic brain injury models. Additionally, our lab is currently utilizing our heme sensors in genetic screens to identify new heme trafficking factors that will be paramount to understanding the molecular mechanisms that control heme's availability in health and disease.

1.4 Scope of Thesis

Chapter 2 describes the initial development and characterization of our genetically encoded ratiometric sensors for heme and their deployment in *Saccharomyces cerevisiae* to quantitate and reveal the nature and dynamics of LH. We found that there is cell to cell variability in cytosolic LH availability, that the subcellular distribution of LH is

heterogenous, and we revealed that the signaling molecule nitric oxide (NO) can initiate the rapid mobilization of heme in the cytosol and nucleus from certain thiol containing factors. Our heme sensing technology developed in Chapter 2 shed light on several factors regarding the nature of LH; however, the physiological importance of LH remained unclear.

Hence, in Chapter 3, we first sought to ascribe a physiological role for LH using a blend of site-specific heme chelators, molecular genetics approaches, and our fluorescent heme sensors. Using these combined approaches, we showed that LH has direct effects on physiology, and that cells rely on a LH heme pool for regulatory functions instead of solely relying on newly synthesized heme to modulate all their heme dependent processes. Additionally, in Chapter 3, we demonstrated that (1) yeast cells preferentially use LH in heme-depleted conditions; (2) sequestration of cytosolic LH suppresses heme signaling; and (3) lead (Pb^{2+}) stress contributes to a decrease in total heme, but an increase in LH, which correlates with increased heme signaling. We also observed that the proteasome is involved in the regulation of the labile heme pool and that loss of proteasomal activity sensitizes cells to Pb^{2+} effects on heme homeostasis. All these observations motivated the development of methods to probe the binding and releasing of heme in response to stress to identify new heme signaling factors that may utilize and modulate LH availability. To this end, given that Pb^{2+} had severe effects on heme homeostasis and maintained heme dependent signaling, we employed hemin agarose bead chromatography approaches coupled to SILAC labeling and LC MS-MS to identify proteins that bind and release heme in response to our model of Pb^{2+} toxicity.

Given the broader physiological relevance of heme in mammalian cells, in the following study outlined in Chapter 4, I employed our genetically encoded heme sensors in HEK293 cells and demonstrate the means to in situ calibrate the sensor for live cell quantitation of subcellular LH availability. The sensor was then used to interrogate compartment specific responses to endogenously produced or extracellularly supplied heme. Lastly, I employed our heme sensors to reveal a novel role for the constitutively expressed heme oxygenase 2 (HO2) in buffering LH, explaining previous reports of HO2 overexpression being cytoprotective independent of its catalytic activity.

CHAPTER 2. HEME DYNAMICS AND TRAFFICKING FACTORS REVEALED BY GENETICALLY ENCODED FLUORESCENT HEME SENSORS

2.1 Thesis Attribution Statement for Chapter 2.

Portions of this chapter are adapted from previously published work: "David A. Hanna; Raven M. Harvey; Osiris Martinez-Guzman; Xiaojing Yuan; Bindu Chandrasekharan; Gheevarghese Raju; F. Wayne Outten; Iqbal Hamza; and Amit R. Reddi. 'Heme Dynamics and Trafficking Factors Revealed by Genetically Encoded Fluorescent Heme Sensors. Proc Natl Acad Sci, 2016;113:7539-7544.'"

2.2 Introduction

Heme (iron protoporphyrin IX) is an essential protein cofactor and signaling molecule[1, 3, 27, 31, 34, 35, 96-100].The canonical view of heme is that it is a static cofactor buried in the active sites of hemoproteins. This view point is irreconcilable with the fact that all heme dependent processes, from heme acquisition by proteins to heme signaling, require the dynamic mobilization of heme. However, heme mobilization has never been monitored, and the mechanisms that mediate it are poorly understood. The hydrophobicity and cytotoxicity of heme necessitate that its concentration is tightly regulated and buffered to low levels, creating an apparent paradox when trying to conceptualize the movement of heme to client hemoproteins or for heme-based signal transduction[1, 44, 101]. The total heme quota is the sum of the exchange inert and labile heme (LH) pools. Inert heme, which is unavailable for new heme-dependent processes, is

more abundant and represents the large fraction of heme that is associated with high-affinity hemoproteins like cytochromes and globins. The LH pool, which is available for hemoproteins and heme signaling, is far less abundant and buffered by unknown factors[44]. The properties of LH pools, including concentration, speciation, oxidation state, distribution, and dynamics, are paramount for understanding how cells assimilate this essential nutrient, but are poorly understood. The current lack of understanding of LH is, in large part, due to the dearth of tools available to probe it. Herein, we report genetically encoded ratiometric fluorescent heme sensors and deploy them in the unicellular eukaryote *Saccharomyces cerevisiae* (Baker's yeast) to elucidate the nature and dynamics of LH. We find that LH is buffered at a concentration of 20–40 nM in the cytosol and less than 2.5 nM in the nucleus and mitochondria. Further, we find that the signaling molecule nitric oxide (NO) can initiate the rapid mobilization of heme in the cytosol and nucleus from certain thiol-containing factors. By integrating our heme sensors with genetic screens, we also find that the glycolytic enzyme glyceraldehyde phosphate dehydrogenase (GAPDH) is responsible for buffering intracellular heme and regulating the activity of the nuclear heme-dependent transcription factor heme activator protein (Hap1p). Altogether, these results reveal fundamental aspects of heme trafficking and dynamics, providing fresh insight into the cellular management of this essential nutrient.

2.3 Design and Characterization of Heme Sensors

The first-generation heme sensor, HS1, consists of a heme-binding domain, the His/Met coordinating 4-alpha-helical bundle hemoprotein cytochrome b_{562} (Cyt b_{562})[102], fused to a pair of fluorescent proteins, EGFP and Katushka 2 (mKATE2), that are expected to exhibit heme-sensitive and -insensitive fluorescence, respectively (Figure

2.1A). Holo-Cyt b_{562} is a fluorescence resonance energy transfer (FRET) acceptor for EGFP[103, 104] [excitation (ex.) = 488 nm, emission (em.) = 510 nm] but not mKATE2[105] (ex. = 588 nm, em. = 620 nm) [29]. Thus, HS1 was designed as an excitation-emission ratiometric probe [106] in which the ratio of heme-sensitive EGFP fluorescence to heme-insensitive mKATE2 fluorescence provides a readout of cellular heme independent of sensor concentration.

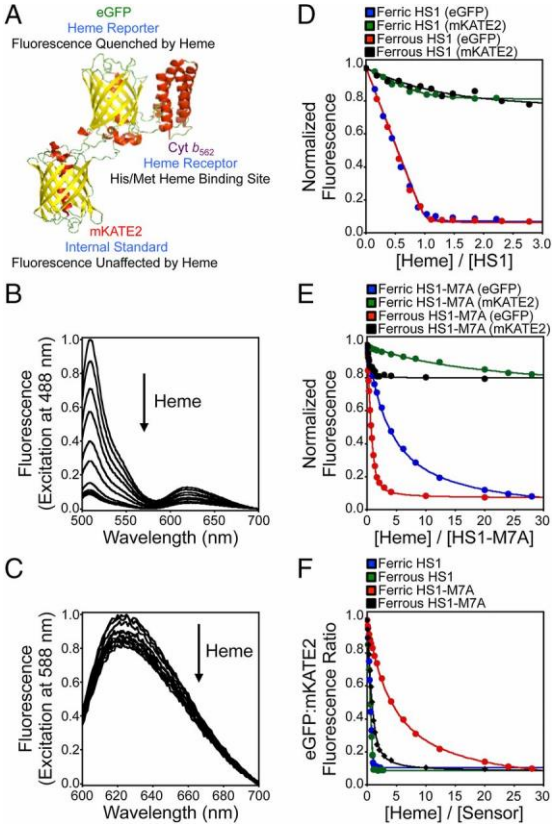

Figure 2.1 - Design and heme-dependent fluorescence properties of the heme sensors. (**A**) Molecular model and design principles of the heme sensor, HS1. The model is derived from the X-ray structures of mKATE [Protein Data Bank (PDB) ID code 3BXB] and CG6 (PDB ID code 3U8P). Ferric heme-dependent changes in the normalized fluorescence emission spectra of HS1 at pH 8.0 upon excitation of EGFP (**B**, ex.= 488 nm) and mKATE2 (**C**, ex. = 588 nm) are illustrated. Normalized changes in EGFP (ex. = 488 nm, em. = 510 nm) and mKATE2 (ex. = 588 nm, em. = 620 nm) fluorescence upon titration of heme into 0.5 μM HS1 (**D**) and HS1-M7A (**E**) at pH 8.0 are illustrated. (**F**)

Change in EGFP/mKATE2 fluorescence ratios for HS1 and HS1-M7A upon titration of heme. All titration data are fit to 1:1 heme/protein binding models.

HS1 was adapted from a previously reported EGFP-Cyt b_{562} integral fusion protein, CG6, that exhibits >99% efficient FRET between EGFP and heme [107]. mKATE2 was appended to the N terminus of CG6 with a GlySer linker. Titration of ferric and ferrous heme into an aqueous buffered solution [20 mM NaPi, 100 mM NaCl (pH 8.0)] of 0.5 μM purified HS1 resulted in visible absorbance spectra indicative of heme coordination, and quenched EGFP fluorescence (~10-fold decrease in signal), with minimal perturbation to mKATE2 fluorescence (~20% decrease in signal) (Figure 2.1B-D). Both oxidized and reduced heme quench the fluorescence of EGFP and mKATE2 to similar degrees and the change in fluorescence as a function of [heme] evinces a 1:1 heme/HS1 stoichiometry (Figure 2.1D,F).

HS1-ferric heme dissociation constants, K_d^{III}, were determined by direct titration of hemin chloride into HS1 over a broad pH range (pH 5–8) and found to be 3 nM between pH 6.0 and 7.5[29]. At pH 8.0, the 10 nM K_d^{III} value for HS1 is identical to the K_d^{III} values previously reported for Cyt b_{562} [102] and CG6 [107]. HS1-ferrous heme dissociation constants, K_d^{II} values, were too tight to measure by direct titration and are less than 1 nM. The approximate values of K_d^{II} can be estimated to be ~10 pM at pH 7.0 and by completing a thermodynamic cycle relating the reduction potential of free heme (-50 mV vs. NHE) and HS1-heme (assumed to be the reduction potential of Cyt b_{562}, 170 mV vs NHE) and by using the K_d^{III} values that were determined here by direct titration in Equation (1)[102, 108, 109]. E_m*(bound)* is the heme protein, HS1's reduction potential, and E_m*(free)* is the reduction potential of free heme[110].

$$E_m(bound) = E_m(free) + \left(\frac{RT}{nF}\right)\ln\left(\frac{K_d^{Fe(III)}}{K_d^{Fe(II)}}\right) \quad (1)$$

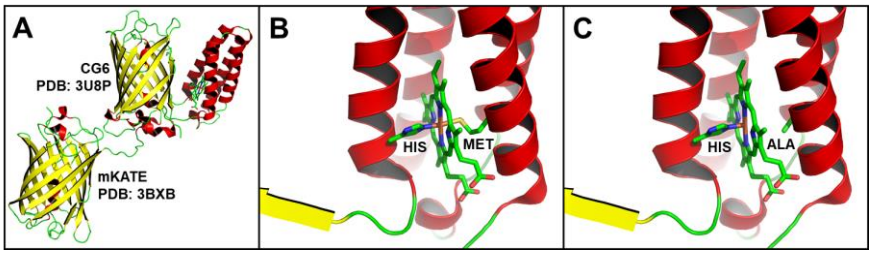

Figure 2.2 - Molecular model of the heme sensors HS1 and HS1M7A. Models are derived from the X-ray structures of mKATE (PDB: 3BXB) and CG6 (PDB: 3U8P).

Because previous estimates for the concentration of the LH pool are highly varied between nanomolar and micromolar values[44], we generated heme sensors with altered heme binding affinities. One variant, HS1-M7A, which was generated by replacing the heme axial Met7 ligand of Cyt b_{562} with Ala (Figure 2.2), exhibits fluorescence properties similar to the fluorescence properties of HS1 and binds heme in a 1:1 stoichiometry (Figure 2.1E,F). HS1-M7A binds ferrous heme with a K_d^{II} value of 25 nM between pH 6.0 and 7.5[29]. The HS1-M7A K_d^{III} values are very weak, determined to be 0.5–2.0 μM over a pH range of 5.0–8.0[29]. The K_d^{II} value of HS1-M7A is similar in magnitude to previous estimates of the "regulatory" heme pool, 10–100 nM[44, 111], as well as the affinities of proteins that may respond to this pool, including the heme-dependent transcription factor Reverbβ[112] and constitutive heme oxygenase-2 (HO-2)[113].

Both HS1 and HS1-M7A are selective for ferrous heme over other metals, protoporphyrin IX, and the heme degradation products bilirubin and biliverdin[29]. Further, apo- and ferrous heme-bound HS1 and HS1-M7A exhibit pH-independent EGFP/mKATE2 fluorescence ratios between pH 6.5 and 9.0 but are markedly pH-

dependent below pH 6.5[29].The fluorescence ratio of HS1 and HS1-M7A is independent of protein concentration between 10 nM and 1 μM, suggesting that the sensors do not aggregate over these concentrations[29]. Ferrous heme binding to HS1 and HS1-M7A is reversible because competition with excess apo-Cyt b_{562} restores the fluorescence ratio to apo-sensor[29]. Further, *in vivo*, HS1 and HS1-M7A's selectivity for heme over heme biosynthesis intermediates is shown by the EGFP:mKATE2 sensor fluorescence ratio being identical between *hem1*Δ and *hem15*Δ strains expressing HS1 (Figure 2.3). *hem1*Δ cells are heme deficient as they lack 5-aminolevulinic acid (5-ALA) synthase, the first enzyme in the heme biosynthetic pathway[114]. *hem15*Δ cells lack the ultimate enzyme in heme synthesis, which results in both heme deficiency and a build-up of heme synthesis intermediates, like protoporphyrin IX[115]. If HS1 bound heme intermediates *in vivo*, the EGFP:mKATE of *hem15*Δ cells expressing HS1 would be expected to be lower than *hem1*Δ cells expressing HS1 (Figure 2.3).

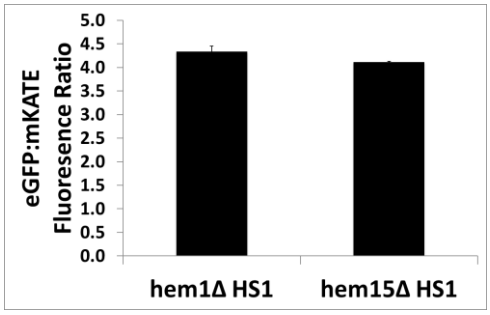

Figure 2.3 - Comparison of HS1 sensor fluorescence in *hem1*Δ vs *hem15*Δ cells. Cytosolic HS1 does not bind heme synthesis intermediates *in vivo*.

2.4 Cellular Heme Imaging: Cytosol

Using fluorimetry (Figure 2.4A), flow cytometry (Figure 2.4B), and fluorescence microscopy (Figure 2.4C), we find that HS1 and HS1-M7A can be used to sense

endogenous LH in a quantitative manner. Fluorimetry (Figure 2.4A) and fluorescence microscopy (Figure 2.4C) of WT yeast cells expressing cytosolic HS1 and HS1-M7A indicate an EGFP/mKATE2 ratio that is markedly reduced in comparison to heme-deficient *hem1Δ* cells. The difference in HS1 and HS1-M7A fluorescence ratios in WT cells reflects their differential heme binding affinities (vida infra).

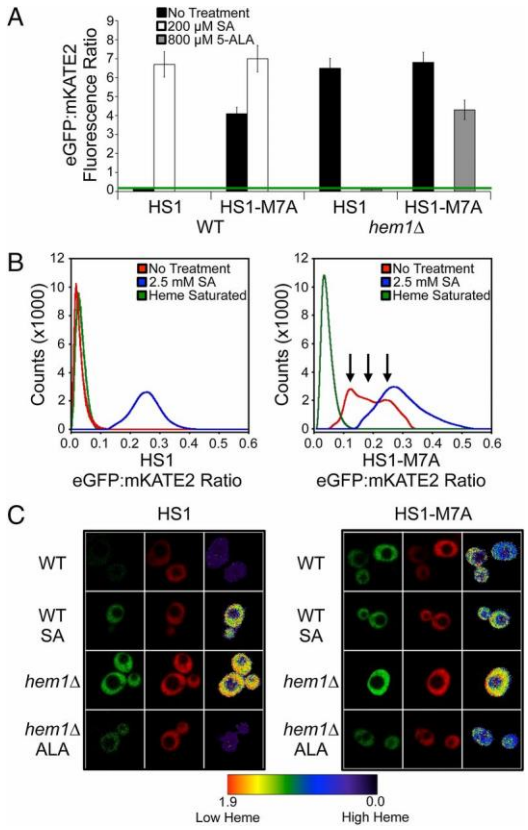

Figure 2.4 - Heme-dependent fluorescence ratios of HS1 and HS1-M7A in WT and *hem1Δ* yeast cells as measured by fluorimetry (**A**), flow cytometry (**B**), and confocal microscopy (**C**). Where indicated, cells were treated with SA or 5-ALA. Cells for microscopy experiments were treated with 0.2 mM SA or 1.5 mM 5-ALA. "Heme saturated" is the ratio recorded upon digitonin permeabilization of cells and incubation with excess heme as described in the main text for in situ calibration of the cytosolic sensors. Fluorimetry data represent the mean ± SD of triplicate cultures. The green bar indicates the eGFP/mKATE2 fluorescence ratio when the heme sensors are saturated with heme. The flow cytometry and microscopy data are representative of three independent mid-log-phase cultures grown in synthetic complete media lacking leucine and supplemented with ergosterol and tween-80 (SCE-LEU).

The HS1 and HS1-M7A EGFP/mKATE2 fluorescence ratios in *hem1Δ* cells decrease when heme synthesis is initiated due to supplementation with 5-ALA (Figure 2.4A,C) in a dose-dependent manner (Figure 2.5C,D), which is consistent with increased heme binding. Excess 5-ALA does not reduce HS1-M7A fluorescence ratios to the same extent as HS1. This effect is because excess 5-ALA (1.5 mM) results in intracellular heme levels similar to WT cells[29]; strict control of heme biosynthesis does not allow for endogenous heme levels that are sufficient to saturate the low-affinity heme sensor HS1-M7A. Conversely, the HS1 and HS1-M7A EGFP/mKATE2 fluorescence ratios in WT cells increase upon supplementation with the heme biosynthesis inhibitor succinylacetone (SA) (Figure 2.4A–C) in a dose-dependent manner (Figure 2.5A,B), which is consistent with decreased heme binding[34]. A variant of HS1 with His_{102} and Met_7 heme-coordinating ligands mutated to Ala, HS1-M7A,H102A, and an mKATE2-EGFP fusion protein lacking the Cyt b_{562} domain do not exhibit heme-dependent changes in fluorescence ratio, indicating that heme iron coordination to HS1 is required for cellular heme sensing (Figure 2.6).

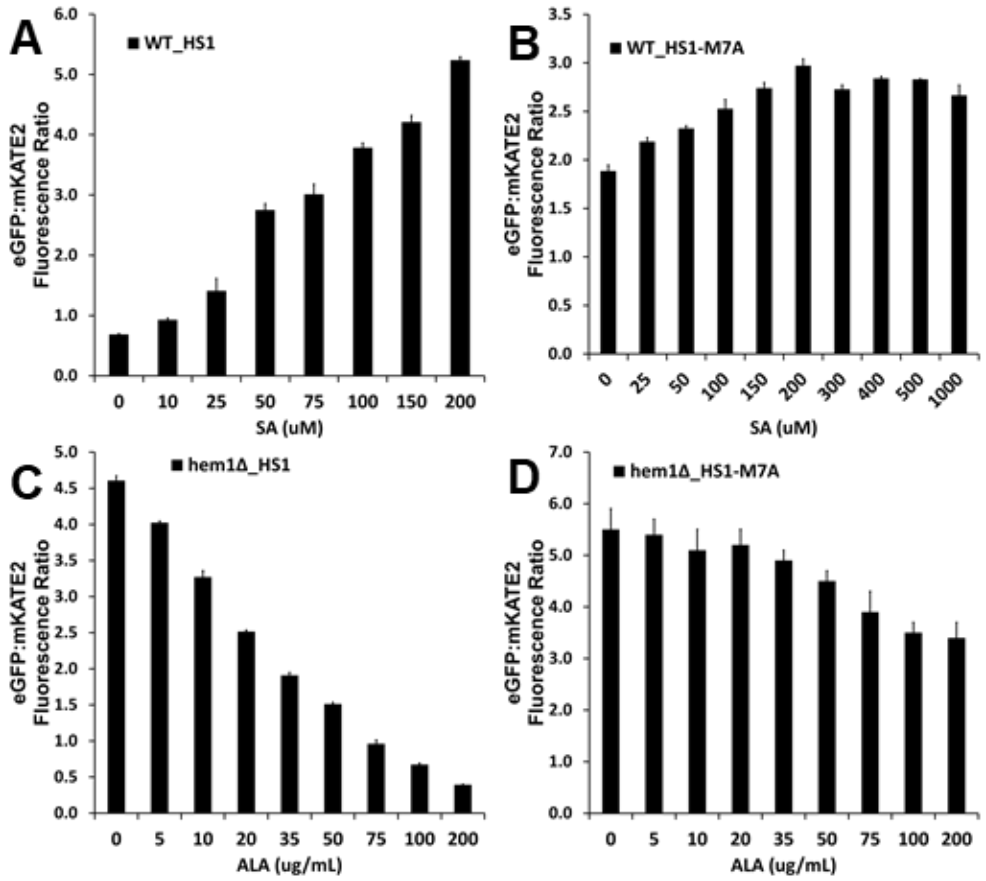

Figure 2.5 - Heme dependence of cellular EGFP:mKATE2 fluorescence ratios. (A-B) WT cells expressing (**A**) HS1 or (**B**) HS1-M7A were cultured in SCE-LEU media for 15 hours with the indicated concentrations of the heme biosynthesis inhibitor succinylacetone (SA) and EGFP:mKATE2 fluorescence ratios were recorded. (C-D) *hem1*Δ cells expressing (**C**) HS1 or (**D**) HS1-M7A were cultured in SCE-LEU media for 15 hours with the indicated concentrations of 5-aminolevulinic acid (5-ALA) and EGFP:mKATE2 fluorescence ratios were recorded. The EGFP (ex. 488, em. 510) to mKATE2 (ex. 588, em. 620 nm) fluorescence ratio was recorded by a plate reader using 100 µL of 6x107 cell/mL in PBS buffer.

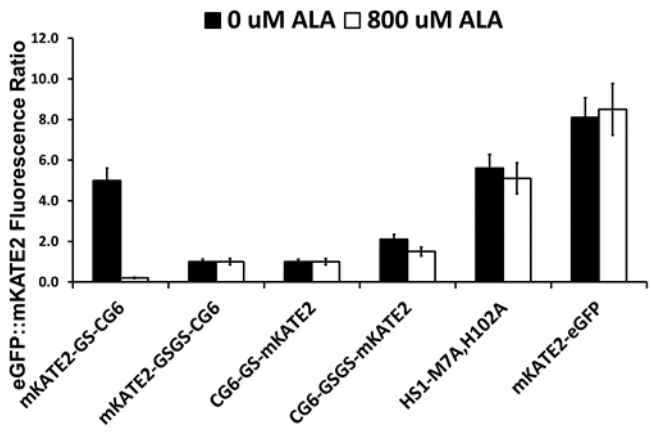

Figure 2.6 - Heme-dependence of EGFP:mKATE2 fluorescence ratios of heme binding mutants and various N- and C-terminal mKATE2-CG6 fusion proteins expressed in *hem1*Δ cells cultured with the indicated concentration of 5-aminolevulinic acid (5-ALA). Only mKATE2-(GS)1-CG6 exhibits a heme dependent EGFP to mKATE2 fluorescence ratio. The EGFP (ex. 488, em. 510) to mKATE2 (ex. 588, em. 620 nm) fluorescence ratio was recorded by a plate reader from 100 µL of 6x107 cell/mL in PBS buffer. The data represent the mean ± SD of triplicate cultures. Cells were cultured to mid-exponential phase in SCE-LEU media prior to analyses.

The heme sensor does not itself perturb heme metabolism and is a reliable reporter for endogenous LH. Titration of HS1-M7A expression using weak (pr^{ADH1}), medium (pr^{TEF1}), and strong (pr^{GPD}) promoters on centromeric plasmids do not result in a change in the observed concentration of the bioavailable heme pool, and pr^{GPD}-HS1-M7A does not affect cell growth or heme-regulated functions like total heme, catalase activity, or respiration[29].

For quantitative heme monitoring, an in situ method to calibrate the sensor was developed[111]. The concentration of [heme] accessible to the sensor is governed by the following expression[116]:

$$[heme] = K_d \times \frac{R_{expt} - R_{min}}{R_{max} - R_{expt}} \left(\frac{F_{min}^{mKATE2}}{F_{max}^{mKATE2}} \right) \quad (2)$$

where K_d is the heme-sensor dissociation constant, R_{expt} is the EGFP/mKATE2 fluorescence ratio under any given condition, R_{min} is the EGFP/mKATE2 fluorescence ratio when 0% of the sensor is bound to heme, R_{max} is the EGFP/mKATE2 fluorescence ratio when 100% of the sensor is bound to heme, F_{min}^{mKATE2} is the mKATE2 emission intensity when 0% of the sensor is bound to heme, and F_{max}^{mKATE2} is the mKATE2 emission intensity when 100% of the sensor is bound to heme. Determination of R_{max} and F_{max}^{mKATE2} involves recording EGFP and mKATE2 fluorescence after digitonin permeabilization of cells and incubation with 50 μM heme. Determination of R_{min} and F_{min}^{mKATE2} involves recording EGFP and mKATE2 fluorescence after cells are treated with SA or from *hem1Δ* cells cultured in parallel. Because the ferrous heme binding affinities are tighter than ferric affinities for both HS1 and HS1-M7A, R_{max} and F_{max}^{mKATE2} are determined in the presence of the reducing agent ascorbate (1 mM) to drive heme saturation of the sensors.

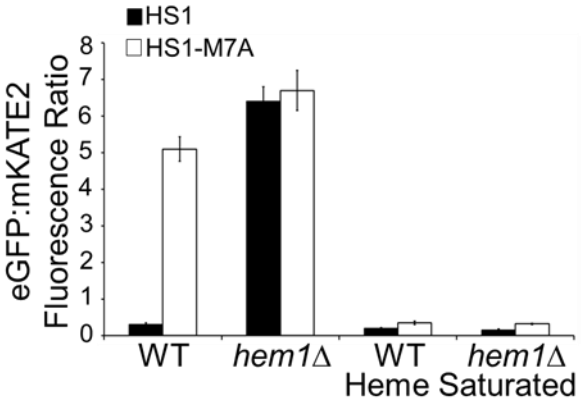

Figure 2.7 - In-situ calibration of cytosolic HS1 and HS1-M7A. 6x107 cells were harvested after 15 hours of growth and resuspended in 1 mL of PBS buffer. EGFP:mKATE2 fluorescence ratios were recorded by exciting EGFP (ex. 488) and mKATE2 (ex. 588) and collecting their emission at 510 nm and 620 nm, respectively. To calibrate the sensor and determine the ratio when they are 100% bound to heme (Heme Saturated), 6x107 cells/mL were incubated for 30 minutes at 30 °C in PBS buffer containing 1 mM ascorbate, 200 µg/mL digitonin, and 50 µM hemin chloride. After incubation, cells were washed of excess heme and fluorescence ratios were recorded as described for non-permeabilized cells. The data represent the mean ± SD of triplicate cultures. Cells were cultured to mid-exponential phase in SCE-LEU media prior to analyses.

Using fluorimetry, in situ calibration of HS1 in WT cells indicates that it is >95% saturated (Figure 2.4A, Figure 2.7), which is not ideal for imaging. On the other hand, HS1-M7A is typically 20–50% bound in exponential-phase WT cells and well poised to monitor changes in heme availability (Figure 2.4A, Figure 2.7). Estimation of the concentration of LH using equation (2) depends on assumptions made about its oxidation state. In the two limiting cases of LH being 100% reduced or oxidized, cytosolic LH can be estimated to be buffered between ~30 nM and ~1 µM, respectively, after considering the data depicted in Figure 2.4A and the K_d^{II} or K_d^{III} value of 25 nM or 1 µM at pH 7.0[29], which is the pH of the yeast cytosol[117]. Given the relatively reducing cellular environment, $E_m^{Cytosol}$ ~−320 mV vs. normal hydrogen electrode (NHE)[118], which is

governed by the ratio of oxidized-to-reduced glutathione, and the reduction potential of aqueous heme, estimated to be between −50 mV and −220 mV vs. NHE[108, 109], we propose that LH is biased toward the reduced state and assume herein that LH is 100% reduced. However, the actual fraction of LH that is reduced is dependent on its speciation and the degree to which it equilibrates with the glutathione redox buffer, both of which are unknown. However, given the weak ferric heme affinities of HS1-M7A, if [LH] is <100 nM, HS1-M7A cannot sense oxidized LH[29].

Flow cytometry of log-phase WT cells expressing HS1-M7A reveals that there are three populations of cells with distinct concentrations of cytosolic LH; 40 nM, 20 nM, and <1 nM heme (Figure 2.4B). These LH concentrations correspond to 1,200, 600, and <30 molecules of heme, respectively, assuming a cytosolic volume (V_{cyt}) of 50 fL[119]. By comparison, total cellular heme was determined to be ∼1 μM[29]. Although this trimodal distribution is highly reproducible, the relative abundance of cells with these three distinct heme levels is quite variable between experiments (Figure 2.8). This observation suggests that heme availability may be dynamically regulated. In contrast, HS1 exhibits only one population due to complete heme saturation as a result of its high heme binding affinity (Figure 2.4B, Figure 2.9). For details on how the analyzed cells were processed see the Appendix.

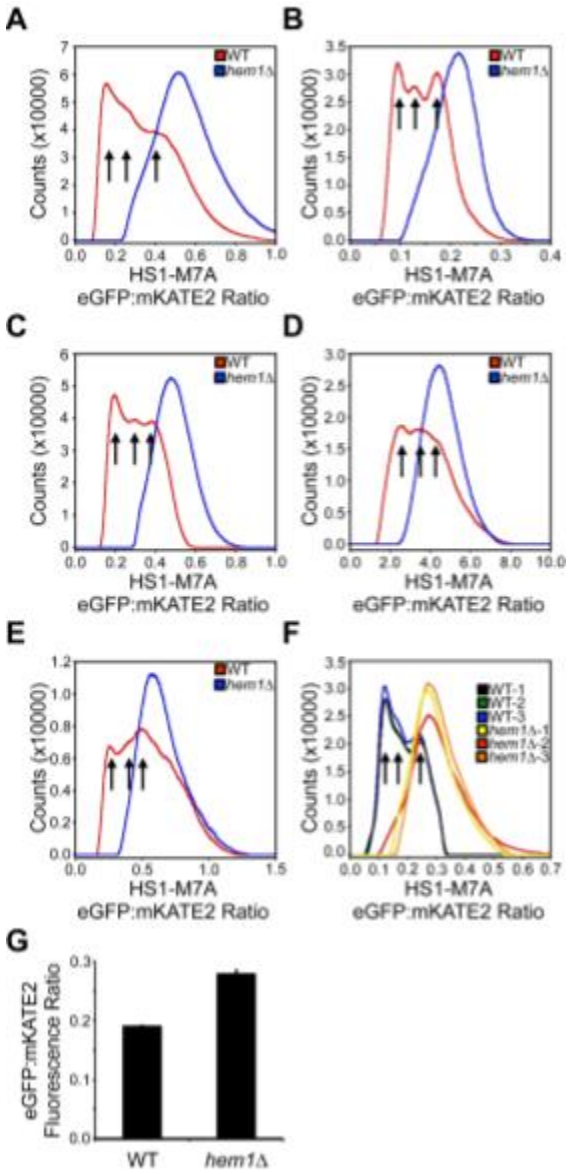

Figure 2.8 - Variation in the tri-modal distribution of labile heme as measured by HS1-M7A. (**A-F**) Flow cytometry analysis of HS1-M7A EGFP:mKATE2 ratios in WT and *hem1*Δ cells in six independent trials. In each trial, cells were cultured in SCE-LEU media to mid-exponential phase before being subject to flow cytometry. (**F** and **G**) Replicate cell cultures indicate the low amount of variation in tri-modal distribution within one experimental trial (**F**), which is also indicated by the small deviation in the cell weighted average EGFP:mKATE2 ratio between the three replicates (**G**).

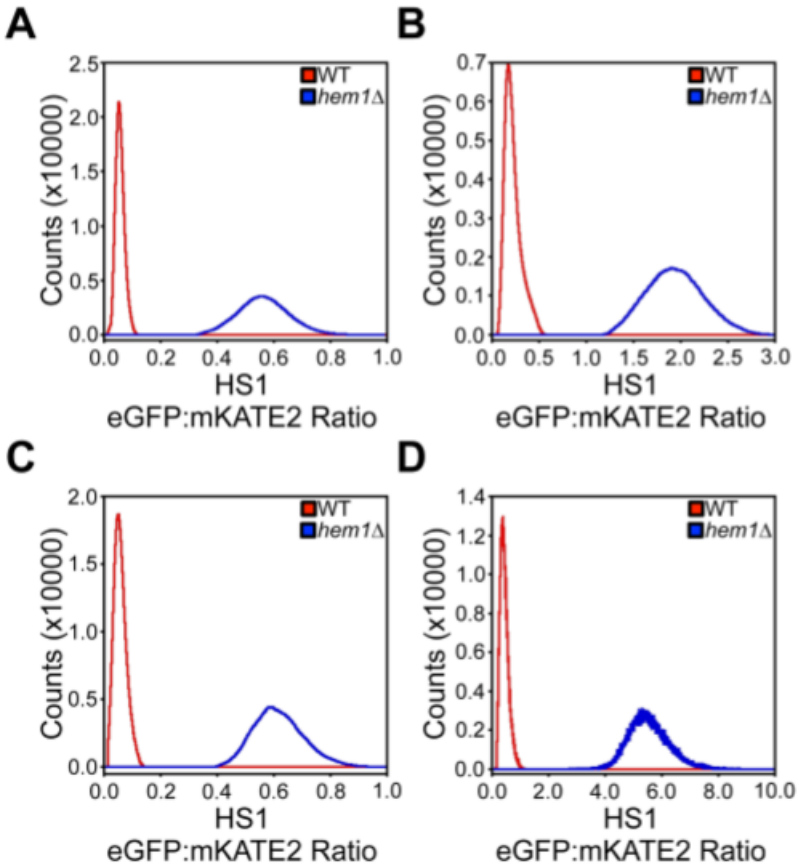

Figure 2.9 - Variation in HS1 EGFP:mKATE2 fluorescence ratios as measured by flow cytometry. (**A**-**D**) Flow cytometry analysis of HS1 EGFP:mKATE2 ratios in WT and hem1Δ cells in four independent trials. In each trial, cells were cultured in SCE-LEU media to mid-exponential phase before being subject to flow cytometry.

Given WT cells expressing HS1-M7A displayed three populations of cells with different concentrations of labile heme, we wished to ensure that each population was heme responsive. Validating this confirms that there are indeed three populations of LH in and the three populations do not arise from heme independent effects. To this end, we in situ calibrated triplicate samples of WT and *hem1Δ* cells expressing HS1-M7A, and indeed, each population in the WT cells collapsed onto the same value as in *hem1Δ* cells expressing HS1-M7A (Figure 2.10).

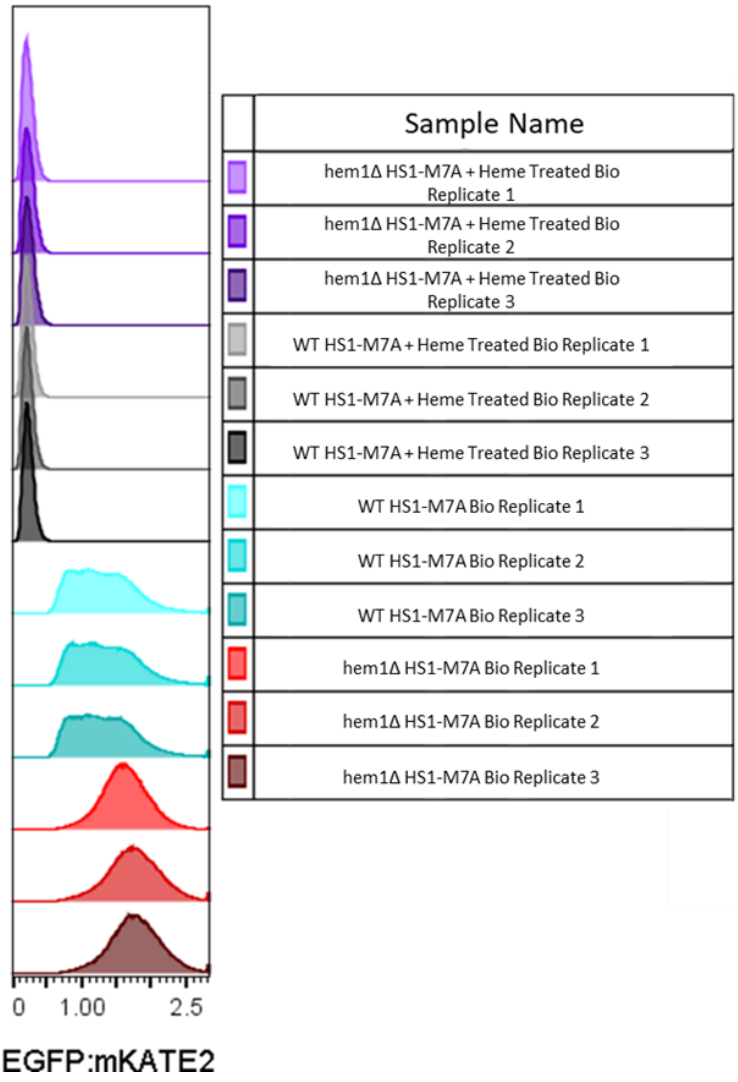

Figure 2.10 - Validation of in situ saturation protocol used in Figure 2.7 for HS1-M7A expressing cells analyzed by flow cytometry in triplicates. Like in Figure 2.7 both *hem1Δ* and WT cells expressing sensor have their EGFP levels quenched, resulting in minimized EGFP:mKATE2 ratios.

2.5 Exogenous Heme Incorporation into Labile Heme Pools in Baker's Yeast

Mechanisms underlying heme uptake in microbes is not completely understood. *Saccharomyces cerevisiae* traditionally are inefficient at importing exogenous heme, but the growth of *hem1Δ* deficient cells can be rescued be heme treatment[120]. Even so, *hem1Δ*

cells supplemented with exogenous heme are not filled with LH unlike those that are allowed to biosynthesize heme by ALA supplementation (Figure 2.11).

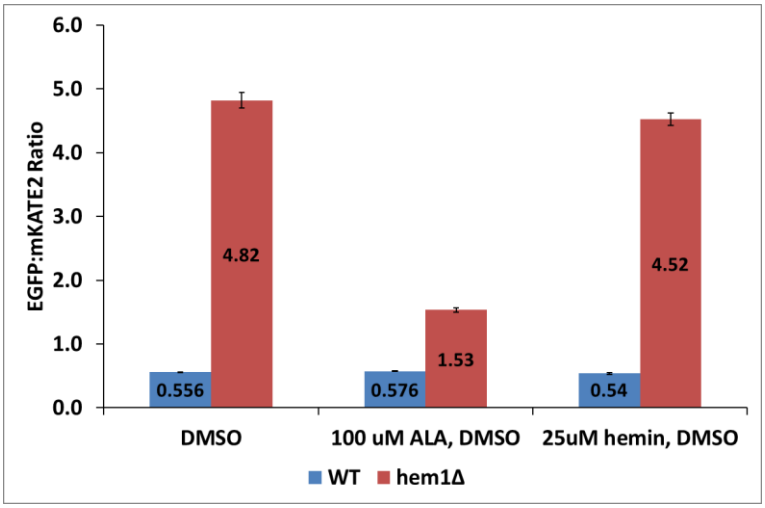

Figure 2.11 – Overnight exposure of cells to ALA but not heme decreases heme dependent EGFP:mKATE ratio of hem1Δ cells expressing HS1. WT HS1 expressing cells are unaffected by ALA or hemin chloride as HS1 is already >95% bound to heme in these cells. Heme was supplied from a 10mg/mL DMSO stock of hemin chloride.

Are *hem1Δ* cells that are rescued by extracellular heme not able to fill their LH pools with extracellular sourced heme? Is exogenous heme handled differently than biosynthesized heme? To test if heme deficient cells could incorporate exogenous heme into their labile heme pools, we tested if heme deficient *hem15Δ* cells grown in the presence of heme for prolonged periods would adapt and incorporate exogenous heme into their LH pools. Indeed, when exposed to heme plates for 9 days, then set up in liquid culture with and without hemin, *hem15Δ* cells are able to incorporate LH into their cytosol in the same fashion as *hem1Δ* cells that were fed ALA (Figure 2.12).

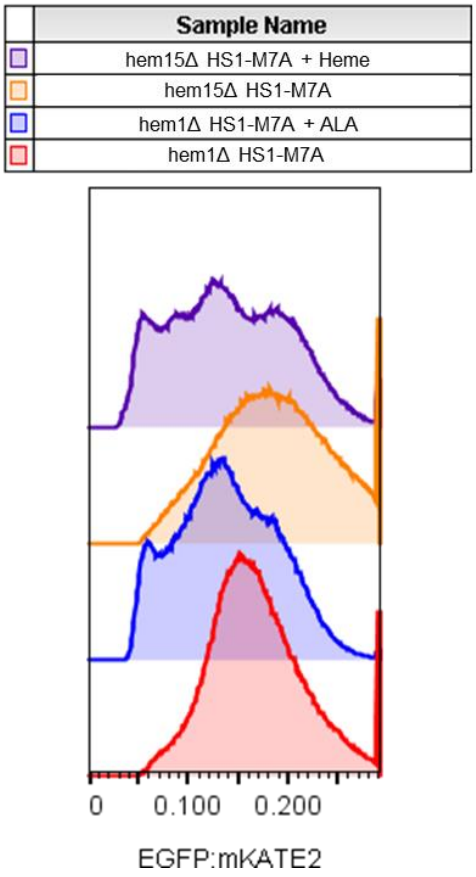

Figure 2.12 – Comparison of *hem15Δ* and *hem1Δ* LH availability in response to prolonged heme exposure with *hem15Δ* cells vs an overnight culture of *hem1Δ* with ALA HS1-M7A expressing cells. Prolonged exogenous heme exposure to *hem15Δ* cells on solid media followed by overnight culture in YPDE media supplimented with (purple) and without (orange) 25 µM heme are compared to *hem1Δ* cells treated overnight with (blue) or without (red) 800µM ALA. *hem15Δ* cells were exposed to heme for 9 days before culturing.

2.6 Hyper-expression of Cytosolic Heme Sensor Induces a Heme Sink

While the titration of HS1-M7A heme sensor does not itself perturb heme metabolism and is a reliable reporter for LH[29], we pursued if hyperexpression of the tight binding HS1 sensor could induce a heme sink inside cells. The generation of a tool that could perturb heme homeostasis by sequestering cellular LH would be instrumental in probing the roles of LH in health and disease models and could also be implemented in

high copy suppressor screens to identify new heme regulatory genes and trafficking factors. To this end, given its high promoter strength, we used a 2 micron high copy GPD promoter (p425-GPD) (Figure 2.13) to hyper-express HS1 and test its ability to sequester LH.

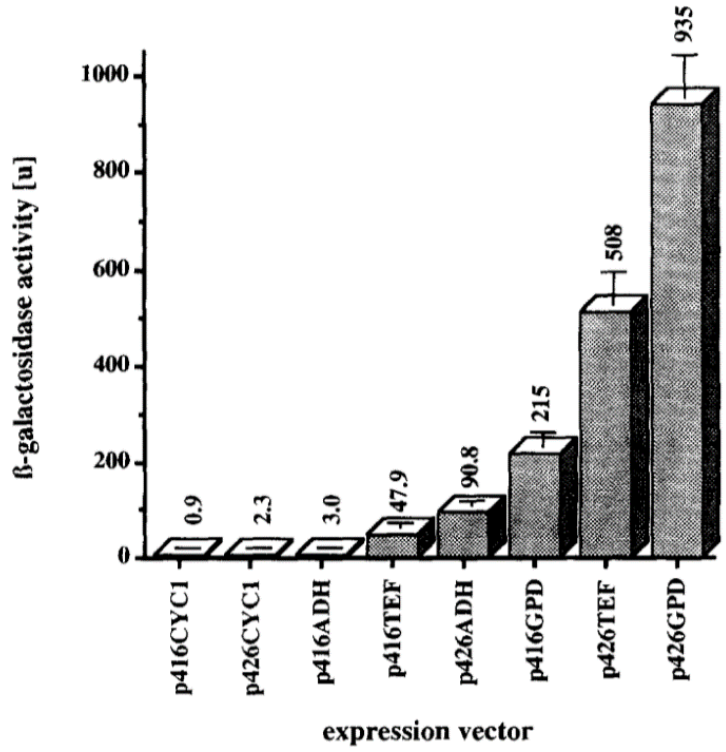

Figure 2.13 – Expression levels of different vectors. Figure was reproduced with permission from work done by Funk et al. Gene, 156 (1995) 119-122 ©1995 Elsevier Science B.V. All rights reserved.

To demonstrate that hyperexpression of HS1 induces a heme sink that perturbs cell growth, WT and *hem1Δ* cells expressing p425-GPD (EV), p425-GDP-HS1 (GPD-HS1), or a non-cytochrome containing, non-heme binding p425-GDP-mKATE-EGFP (GPD-mKATEeGFP) control, were grown in SC media with or without ALA to supply cells with heme. On SC plates, all WT strain cells grew fine regardless of expressed vector, while *hem1Δ* cells will only grow in the presence of ALA, which allows them to

synthesize heme (Figure 2.14A-D). At the low 5 µg/mL dose of ALA, *hem1Δ* cells have some rescue in their growth relative to WT cells, as seen by their highest seed density tier, 10^4 cells, having colony forming units (Figure 2.14B). In addition to this, the GPD-HS1 expressing cells, but not the EV or mKATE2-eGFP control, have their growth stunted, indicating that HS1 is sequestering enough heme to impact cell growth (Figure 2.14B). At the intermediate 10 µg/mL dose of ALA, *hem1Δ* have even more growth rescued with almost full rescue at the 10^4-cell tier for the *hem1Δ* EV and pGPD-mKATE-EGFP expressing cells (Figure 2.14C). *hem1Δ* cells hyper-expressing HS1, on the other hand, have stunted growth displaying about 10-fold less cell growth relative to the *hem1Δ* controls at the 10^3-cell tier (Figure 2.14C). Finally, at the high 50 µg/mL concentration of ALA, which typically rescues heme content in cells grown in solid media, the cell growth of the non-HS1 expressing *hem1Δ* cells has been rescued while the HS1 overexpressing cells still display impaired growth under this heme replete growth condition. The impaired growth can be seen at the 10^3- to 10^4-cell tier patches, but is most noticeable at the 10^2 cells patch, where there are only several colonies forming for HS1 expressing *hem1Δ* cells, while the *hem1Δ* controls grow like WT cells and have many colony forming units (Figure 2.14D).

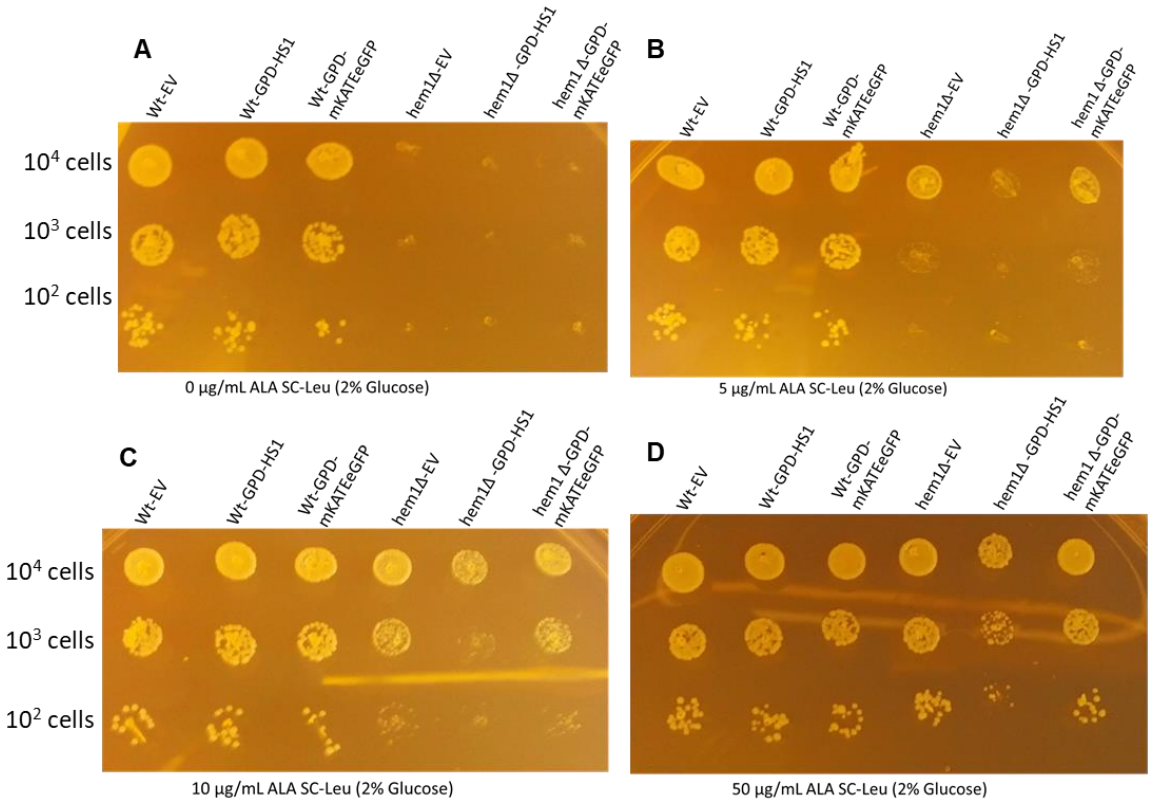

Figure 2.14 – Overexpression of HS1, but not empty vector (EV) or a non-heme binding EGFP:mKATE control, by p425-GPD expression vectors induces a heme sink in cells grown with glucose as a carbon source. WT vs *hem1Δ* cells were plated in 10^4, 10^3, and 10^2 in 4 µL patches serially diluted in Sterile MilliQ onto SC 2% glucose plates that were supplemented with either (**A**) 0, (**B**) 5, (**C**) 10, or (**D**) 50 µg/ µL ALA and grown at 30 °C for 3 days.

These results were shown both in media containing glucose, which favors fermentation, and media lacking glucose but containing glycerol, a non-fermentative carbon source, which requires cells to favor a respiratory mode of metabolism (Figure 2.15). Cells grown on glycerol containing plates for 3 vs 4 days both show that HS1 impairs growth of *hem1Δ* cells grown in the presence of 50 µg/mL ALA, while this dose nearly rescues the non-HS1 expressing *hem1Δ* cells to WT levels of growth. (Figure 2.15A-D).

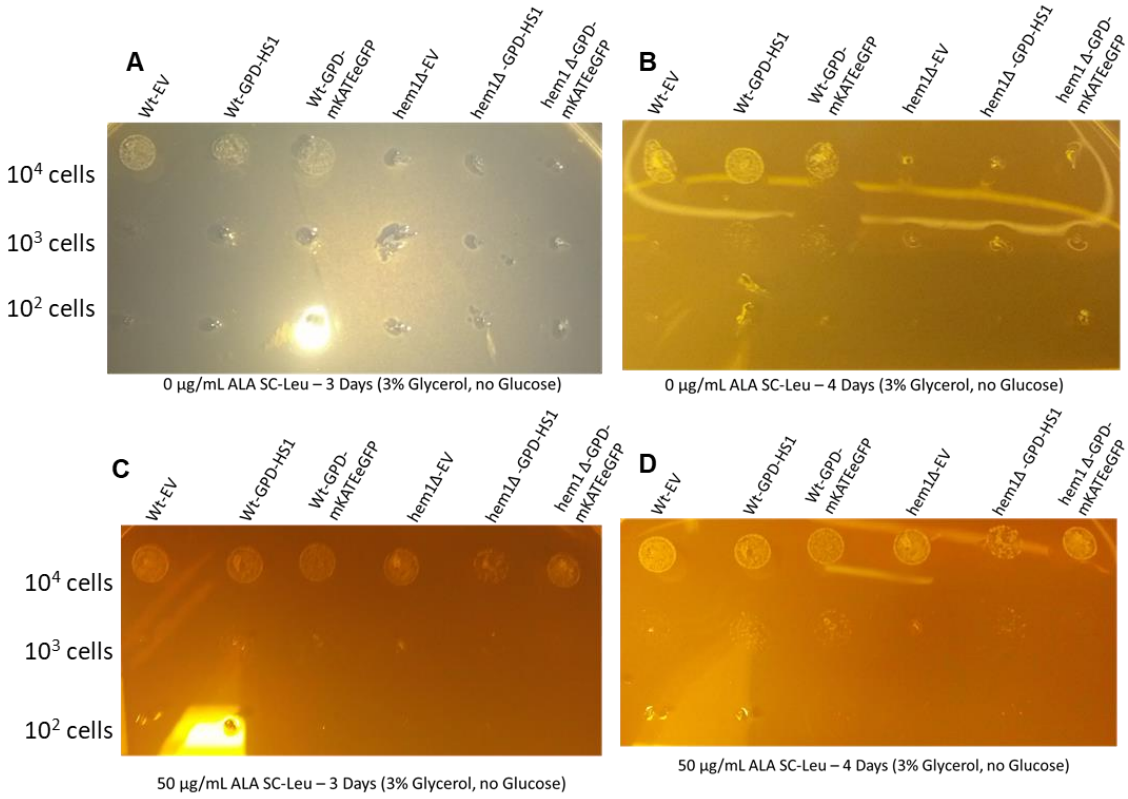

Figure 2.15 – Overexpression of HS1, but not empty vector (EV) or a non-heme binding EGFP:mKATE control, by p425-GPD expression vectors induces a heme sink in cells grown with glycerol as a carbon source. WT vs *hem1Δ* cells were plated in 10^4, 10^3, and 10^2 in 4 µL patches serially diluted in Sterile MilliQ onto SC 3% glycerol plates that were supplemented with either (**A**-**B**) 0 or (**C**-**D**) 50 µg/ µL ALA and grown at 30 °C for (**A**, **C**) 3 or (**B**, **D**) days.

To my knowledge, these are the first results showing that the overexpression of a hemoprotein in cells can induce a heme sink that impairs cell growth. The utilization of a heme sink that is targeted to different cellular locales in tandem with our heme sensors could shed light on how heme availability and heme dependent processes change when LH is sequestered. In addition, this technology could be coupled with a genetic screen to identify novel heme related proteins that could rescue the growth defect imparted by this heme sink.

2.7 Cellular Heme Imaging: Nucleus and Mitochondria

To probe the subcellular distribution of heme, we targeted HS1 and HS1-M7A to the mitochondria and nucleus by appending N-terminal COX4 mitochondrial matrix or C-terminal SV40 nuclear localization sequences, respectively[118, 121] (Figure 2.16). The localization tags do not affect heme binding to the sensors[29].

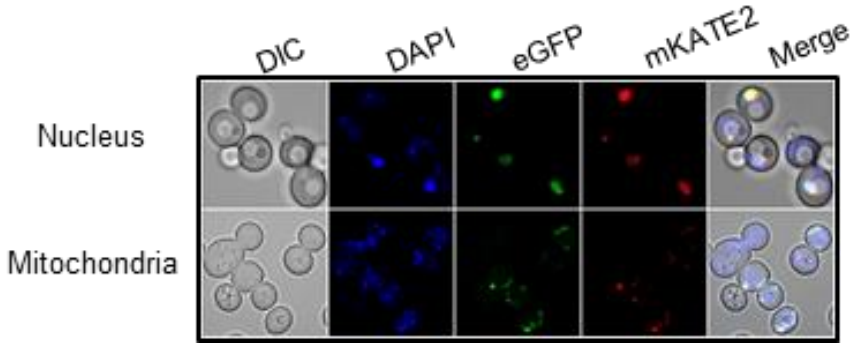

Figure 2.16 – Localization imaging of nuclear and mitochondrial heme sensors. To label DNA, hem1Δ cells expressing nuclear or mitochondrial targeted HS1-M7A were stained with DAPI. Live cells were imaged as described in Materials and Methods at a magnification of 63×. "Merge" is the merged images of DAPI, EGFP, and mKATE2.

Fluorimetry (Figure 2.17) and fluorescence microscopy (Figure 2.18) indicate that nuclear and mitochondrial HS1 exhibit EGFP/mKATE2 fluorescence ratios in WT cells that are distinctly lower than in *hem1Δ* cells, indicative of heme binding. In contrast, nuclear and mitochondrial HS1-M7A EGFP/mKATE2 fluorescence ratios are unaltered between *hem1Δ* and WT cells (Figure 2.17, Figure 2.18). To determine the fractional saturation of our sensors in these compartments, we developed an in situ sensor calibration method analogous to the one described for the cytosol. However, because digitonin cannot permeabilize nuclear or mitochondrial membranes[111], we first had to enzymatically digest the yeast cell wall with zymolyase and then incubate the resulting

spheroplasts with 0.1% Triton X-100, 50 μM heme, and 1 mM ascorbate to heme-saturate the sensors. As shown in Figure 2.7, this in situ calibration method resulted in limiting R_{max} values for HS1 and HS1-M7A that are identical within experimental error.

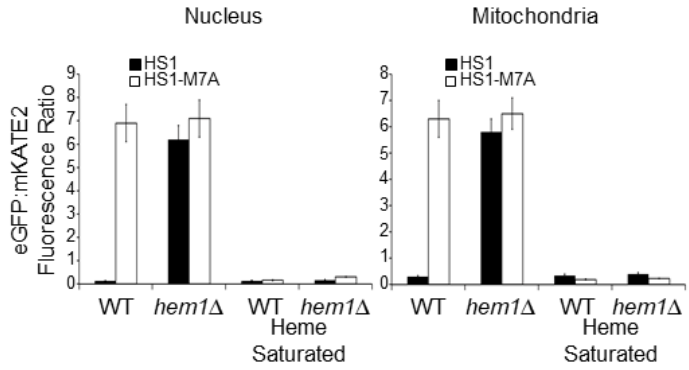

Figure 2.17 - Nuclear and mitochondrial heme monitoring with HS1 and HS1-M7A: fluorimetry. Heme-dependent EGFP/mKATE2 fluorescence ratios of nuclear and mitochondrial targeted HS1 and HS1-M7A in WT and hem1Δ yeast cells as measured by fluorimetry. "Heme-saturated" is the ratio recorded upon Triton X-100 permeabilization of yeast spheroplasts and incubation with excess heme as described in the main text for in situ calibration for the mitochondrial and nuclear sensors.

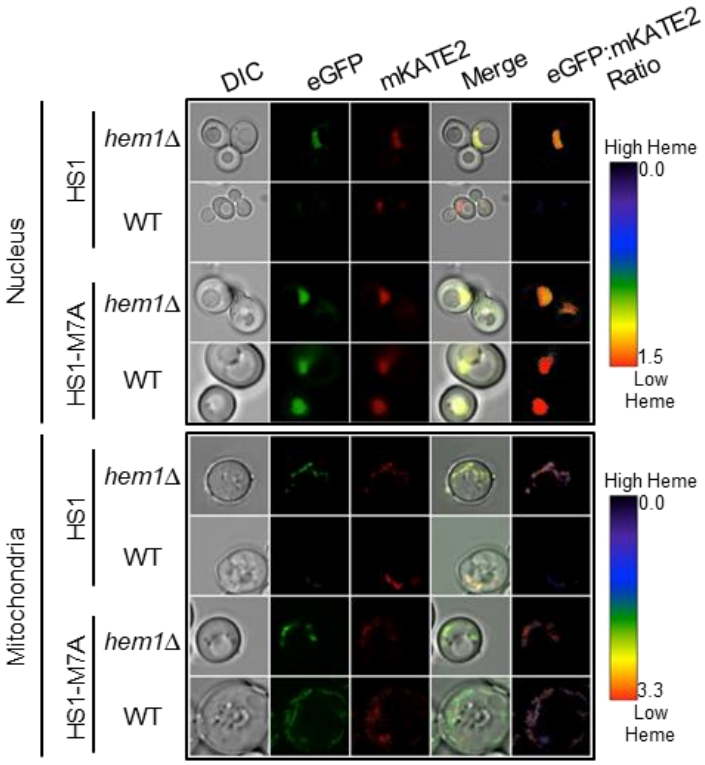

Figure 2.18 - Nuclear and mitochondrial heme monitoring with HS1 and HS1-M7A: microscopy. Confocal microscopy of WT and hem1Δ cells expressing nuclear and mitochondrial targeted HS1 and HS1-M7A. Fluorimetry data represent the mean ± SD of triplicate mid-log-phase cultures grown in SCE-LEU. Microscopy images are representative of at least two independent cultures. DIC, differential interference contrast.

In total, these data indicate that HS1 is ~100% heme-saturated in the mitochondria and nucleus, whereas HS1-M7A is ~0% heme-saturated in these organelles. Given the HS1-M7A K_d^{II} of 25 nM, we estimate that heme is buffered at an upper limit of 2.5 nM in the mitochondria and nucleus. This concentration corresponds to fewer than six molecules in the nucleus [V_{nuc} ~ 5 fL[122]] and ~0.6 molecules in the mitochondria [V_{mito} ~ 0.5 fL[119, 123]].

2.8 Nitric Oxide Mobilizes Cytosolic and Nuclear Heme

Previous work demonstrated that NO could regulate heme transfer between certain protein pairs[41]. Could NO also mobilize LH pools? Using cytosolic, nuclear, and mitochondrial targeted HS1-M7A, we found that NO derived from the small molecule NOC-7[124] rapidly increases cytosolic (Figure 2.19A) and nuclear (Figure 2.19B) LH in WT cells, but not in the mitochondria (Figure 2.19C) or in heme-deficient *hem1Δ* cells (Figure 2.20A). In the cytosol, LH increases from 17 nM to 40 nM within 20 min of adding 50 μM NOC-7 ($t_{1/2}$ = 10 min at 22 °C), which corresponds to an increase from 500 to 1,200 molecules of heme, assuming V_{cyt} ~ 50 fL[119]. This rapid increase is followed by the reestablishment of the initial steady-state heme levels over the course of ~80 min. In the nucleus, there is an even more pronounced change in the HS1-M7A EGFP/mKATE2 ratio upon NOC-7 treatment. NO results in an increase in nuclear LH from <2.5 nM to a maximum of 218 nM, corresponding to a change from fewer than six to ~650 heme molecules assuming V_{nuc} ~ 5 fL[122]. NO-mediated heme mobilization is dose-dependent (Figure 2.20B), and the observed changes in fluorescence ratios are not due to NO interactions within HS1-M7A because incubation of purified heme-bound HS1-M7A with NOC-7 does not alter sensor fluorescence[29].

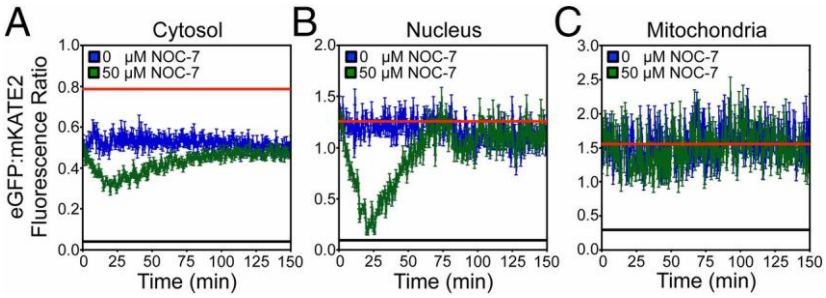

Figure 2.19 - NO-dependent mobilization of LH. WT cells expressing cytosolic (**A**), nuclear (**B**), or mitochondrial (**C**) HS1-M7A were incubated with 50μM NOC-7, and EGFP/mKATE2 fluorescence ratios were monitored by fluorimetry. The data represent

the mean ±SD of triplicate mid-log-phase cultures grown in SCE-LEU. The red and black lines indicate the fluorescence ratios of HS1-M7A when it is 0% and 100% saturated with heme as derived from hem1Δ cells expressing HS1-M7A or WT cells expressing HS1, respectively. This approach for determining R_{max} is validated by the fact that the EGFP/mKATE2 fluorescence ratio of HS1-M7A that is saturated with heme from the in situ calibration methods is identical within experimental error to HS1 (Figure 2.7, Figure 2.17).

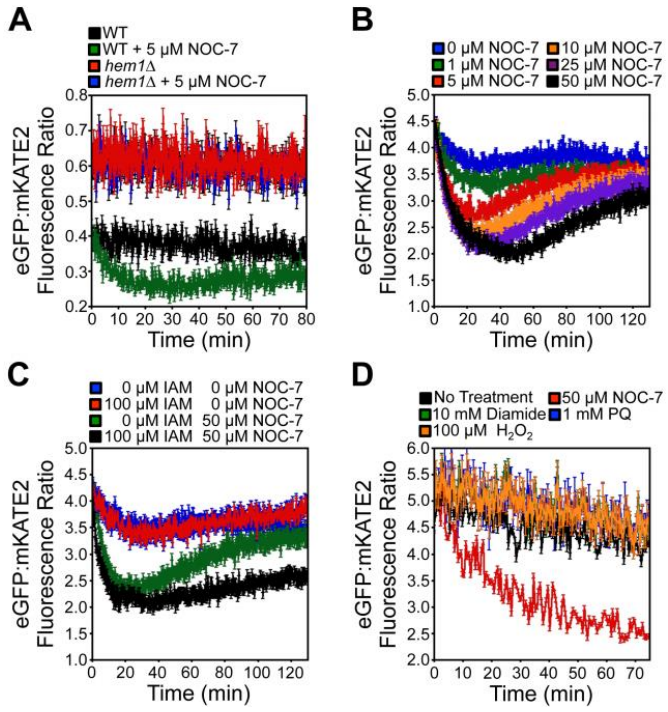

Figure 2.20 - Mobilization of cytosolic heme by NO. (**A**) WT and *hem1*Δ cells expressing HS1-M7A were incubated with 5 μM NOC-7 and EGFP:mKATE2 fluorescence ratios were monitored. (**B**) WT cells expressing HS1-M7A were incubated with the indicated concentration of NOC-7 and EGFP:mKATE2 fluorescence ratios were monitored. (**C**) WT cells expressing HS1-M7A were incubated with the indicated concentration of NOC7 and/or iodoacetamide (IAM) and EGFP:mKATE2 fluorescence ratios were monitored. (**D**) WT cells expressing HS1-M7A were incubated with the indicated concentration of NOC-7, diamide, H_2O_2 or paraquat (PQ) and EGFP:mKATE2 fluorescence ratios were monitored. Fluorimetry data represent the mean ± SD of triplicate cultures. Cells were cultured to mid-exponential phase in SCE-LEU media prior to analyses.

Given that cellular thiols are targets of NO, we sought to determine the effect of a thiol-specific alkylating agent [e.g., iodoacetamide (IAM)] on heme mobilization. Although IAM does not initiate the mobilization of heme, it does prevent the

reestablishment of the steady-state LH pool after NO treatment (Figure 2.20C). This observation suggests that IAM blocks the rebinding of heme from sites of mobilization, presumably certain thiol-containing factors.

To differentiate the effects of NO and general oxidative stress on heme mobilization, we probed the role of various oxidative insults. Diamide, a thiol-specific oxidant; paraquat, a superoxide-generating agent; and H_2O_2 had no impact on LH pools, suggesting that heme mobilization is specific to NO (Figure 2.20D).

2.9 Discussion

The mobilization of LH underlies all heme-dependent processes, including heme acquisition by client proteins and heme-based signal transduction. However, the properties of the LH pool are poorly understood. To address this fundamental gap in heme cell biology, we developed genetically encoded ratiometric heme sensors and deployed them in Baker's yeast to probe key characteristics of the LH pool, including its concentration, subcellular distribution, buffering factors, and dynamics. In addition, HS1 was tested for its ability to act as a heme sink when hyper-expressed to be used in the design of genetic screens and to probe Cyt b_{562}'s potential as a cite specific chelator of labile heme.

Using our heme sensors we see that cells do not incorporate exogenous heme into their LH pools over short exposures (Figure 2.11), even though extracellular heme rescues the growth of cells that cannot synthesize their own heme[120]. However, when cells have prolonged exposure to exogenous heme, their ability to incorporate extracellular heme into their LH pools are enhanced, where an overnight growth with

exogenous heme mirrors the effects of allowing *hem1Δ* cells to biosynthesis their own heme by ALA supplementation (Figure 2.12). What molecular changes facilitated this stark change in cells' heme management, allowing them to integrate extracellular heme into their LH pools (Figure 2.11, Figure 2.12)? Designing the proper studies to elucidate the proteins that are expressed in response to heme starvation in the presence of exogenous heme is warranted and should reveal novel heme trafficking factors that can affect cellular heme management.

Interestingly, hyper-expressed HS1 in the yeast cytosol acts as a heme sink, perturbing cell growth, mostly under heme limiting conditions. This growth phenotype could be exploited in a genetic screen to find proteins that affect heme availability. For example, looking for a high copy suppressor of the heme sink by transforming a high copy plasmid library into hyper-expressing HS1 *hem1Δ* cells grown with limited ALA could be used to detect novel heme trafficking factors that that rescue cells from the heme sink growth defect[125-127]. Conducting the screen would be done by plating enough transformed cells to get colonies under heme replete conditions that represent the entire overexpression library. Next, these colonies that represent the high copy suppressor library could be velveted to an ALA limited and an ALA replete plate[128]. Ultimately, the colonies that are able to grow well on both velveted plates represent those that are likely overexpressing a protein that rescues the heme sink phenotype seen Figure 2.14. These identified proteins would be potential heme trafficking factors and/or be involved in heme dependent signaling pathways required for cell viability.

Our heme sensors reveal that the cytosol has more LH (~20–40 nM) than the nucleus or mitochondria (<2.5 nM). Further, the cell-to-cell heterogeneity in cytosolic

heme suggests its availability may be dynamically regulated (Figure 2.4B). Given the subcellular distribution of heme, we propose that once heme is biosynthesized in the mitochondrial matrix, a fraction of heme transits to the cytosol and acts as a reservoir for signaling and/or a heme source for proteins.

The mitochondria, which have a very high demand for heme and are the site of heme biosynthesis, have exceptionally low quantities of LH, less than 2.5 nM or fewer than one molecule. By comparison, total ferrous heme in the yeast mitochondria has been estimated to be ~30 μM, or ~9,000 molecules[119]. Taken together, this low amount of mitochondrial LH suggests that mitochondrial heme is tightly regulated and trafficked in a manner that limits its availability. This observation is consistent with the identification of mitochondrial heme metabolism complexes that traffic heme via transient protein–protein interactions, thereby circumventing the LH pool[74].

The nucleus also limits LH to less than 2.5nM or fewer than six molecules. This low amount of nuclear LH is not surprising, given the cytotoxicity of heme and proximity to genetic material[1, 44]. However, this observation raises the question of how nuclear heme-regulated transcription factors acquire heme, given that the heme-regulatory motifs (HRMs) of many heme-dependent transcription factors, including Hap1p in yeast, exhibit micromolar affinities for heme[31]. Factors like Hap1p may acquire heme from transient increases in LH due to active signaling processes. Indeed, this concept is supported by our demonstration that signaling molecules like NO can result in a >10-fold increase in nuclear LH (Figure 2.19B). An alternative possibility is that the heme affinities of many HRM-containing proteins are mischaracterized. For instance, a reevaluation of the heme dissociation constants of the HRM-containing transcription factor Rev-erbβ found that

heme binds 100-fold tighter than previously estimated, with K_d^{III} and K_d^{II} of ~20 nM vs. 2–6 μM[112].

Our observation that subcellular [LH] is heterogeneous stands in striking contrast to a recent report by He and coworkers[111] that used a heme chaperone-based FRET sensor (CISDY-9) for heme in human cell lines. In that work, cytosolic, mitochondrial, and nuclear heme were all reported to be~25nM. The deviation between our two results needs to be clarified but could reflect organismal variation, difficulty in calibrating CISDY-9 in organelles, or uncertainties in LH oxidation state.

Quite surprisingly, we observed that *Saccharomyces cerevisiae*, which is not thought to import exogenous heme but solely rely on endogenously biosynthesized heme, can rely on exogenous sources of heme to fill its labile heme pools under extreme conditions such has prolonged hemin treatment of heme deficient cells (Figure 2.11, Figure 2.12). Studying the genetic differences, such as differences in mRNA transcripts, may reveal proteins that are upregulated under heme deficiency in these cells to facilitate the upregulation of heme in these cells[129-131]. And, as *Saccharomyces cerevisiae* is a model eukaryote that is genetically tractable with higher organisms, this may reveal new mechanisms by which other cell types respond to cellular stress.

We demonstrate, for the first time to our knowledge, that LH is dynamic and can be mobilized by signaling molecules like NO (Figure 2.19,Figure 2.20). Although previous studies have indicated that H_2O_2 and NO can regulate heme transfer between specific protein pairs[37, 41], our results suggest that NO can mobilize cell-wide LH pools to regulate heme-dependent processes in multiple compartments. The mechanism of NO mediated

heme mobilization is unknown, but likely involves S-nitrosation of certain hemoproteins and heme dissociation[41, 67].

NO-mediated heme mobilization provides insights into NO physiology, including NO-dependent inflammatory responses. Both heme and NO regulate inflammation, but through distinct mechanisms[99, 132, 133]. Our work indicates that NO can promote inflammation via heme mobilization. Indeed, previous observations in endothelial cells found that NO elevates cellular iron due to enhanced activity of the heme-degrading enzyme, HO[60]. This observation was proposed to occur as a result of NO-induced heme release from hemoproteins. Our current studies are the first to our knowledge, to provide direct support for this model.

Since developing and characterizing these heme sensors, they have been deployed to both mammalian cells to bacteria to study heme in neurodegeneration and infectious disease. In addition, HS1 and HS1-M7A have been used to screen for new heme homeostatic factors in genetic screens. Indeed, it was found using the sensors that GAPDH was a heme trafficking factor that regulates heme dependent transcription in Sac*charomyces cerevisiae*[29, 40]. Our findings that NO regulates heme availability and mobilization are highly reminiscent of and supported by previous studies demonstrating that GAPDH and NO cooperate to control heme insertion into nitric oxide synthase[41]. As such, it is tempting to speculate that Tdh3p is the source of NO-mobilized heme. However, NO-dependent heme mobilization is unaffected in *tdh3Δ* cells[29]. Altogether, the HS1s can be applied across prokaryotes and eukaryotes to probe heme trafficking, signaling, and dynamics in various physiological contexts.

2.10 Materials and Methods

2.10.1 Cell Lines, Culturing, and Plasmids

2.10.1.1 Yeast Strains, Media, and Growth Conditions

S. cerevisiae strains used in this study were derived from BY4741 (*MAT*a, *his3*Δ1, *leu2*Δ0, *met15*Δ0, *ura3*Δ0). *tdh1*Δ::*kan*MX4, *tdh2*Δ::*kan*MX4, and *tdh3*Δ::kanMX4 strains were obtained from the yeast gene deletion collection (Thermo Fisher Scientific). A *hem1*Δ::HIS3 strain was generated by deleting HEM1 using the hem1::HIS3 deletion plasmid, pDH001. Yeast transformations were performed by the lithium acetate procedure[134]. Strains were maintained at 30 °C on either enriched yeast extract-peptone based medium supplemented with 2% glucose (YPD), or synthetic complete medium (SC) supplemented with 2% glucose and the appropriate amino acids to maintain selection. Culturing of *hem1*Δ cells required supplementing YPD or SC media with 50 µg/mL of 5-aminolevulinic acid (5-ALA) or 15 mg/mL of ergosterol and 0.5% Tween-80 (YPDE or SCE, respectively)[114].

2.10.1.2 *E. coli*, Media, and Growth Conditions

For routine cloning, sub-cloning grade chemically competent *E. coli* cells, strain 10G E. cloni (Lucigen), were used according to the manufacturer's specifications. For recombinant protein overexpression studies, E. cloni EXPRESS BL21(DE3) chemically competent cells (Lucigen) were utilized according the manufacturer's specifications. Unless otherwise stated, all *E. coli* strains were cultured in Lysogeny broth (LB)[135] with the appropriate antibiotic selection, either 100 µg/mL ampicillin or kanamycin.

2.10.2 Experimental Methods

2.10.2.1 Instrumentation

All UV/visible absorbance spectra were recorded on a Cary 60 spectrophotometer. Fluorescence measurements were collected on a Synergy Mx multi-modal plate reader. Flow cytometry was performed on a BD FACS Aria Ill Cell Sorter or BD LSR II Flow Cytometer, with data analysis accomplished using FlowJo v9.9.3 software. Confocal laser scanning microscopy was accomplished using a Zeiss ELYRA LSM 780 Super-resolution Microscope, with all images processed in ImageJ[136]. Quantifications of metal and heme stock solutions were accomplished by total reflection x-ray fluorescence (TXRF) on a Bruker S2 Picofox TXRF. Measurement for cellular heme was accomplished by high-pressure liquid chromatography (HPLC) on an Agilent 1260 Infinity HPLC with a diode array detector.

2.10.2.2 Characterization of Heme Sensors in Yeast

For all sensor fluorescence measurements, WT and *hem1*Δ yeast cells expressing the heme sensors were cultured in SCE-LEU media for ~14-16 hours to mid-exponential phase (an optical density at 600 nm of $OD_{600\ nm}$ ~ 1-2. Unless otherwise noted, all cytosolic measurements were accomplished with the indicated sensor proteins expressed on the p415-GPD plasmid, a low copy centromeric plasmid with a GPD promoter[137]. Nuclear and mitochondrial matrix targeted sensors were expressed on p415- GPD and p415-TEF plasmids, which are low copy centromeric plasmids with GPD and TEF promoters, respectively[137]. After culturing, cells were harvested, washed in water, and resuspended in phosphate buffered saline (PBS) solution at concentrations between 3 and

5 $OD_{600\ nm}$/mL, or 6 x 10^7 to 1 x 10^8 cells/mL. For fluorimetry measurements on a population of cells, fluorescence was recorded on a Synergy Mx multi-modal plate reader using black Greiner Bio-one flat bottom fluorescence plates. EGFP and mKATE fluorescence were recorded using excitation and emission wavelength pairs of 488 nm and 510 nm and 588 nm and 620 nm, respectively. Background fluorescence of cells not expressing the heme sensors were recorded and subtracted from the EGFP and mKATE2 fluorescence values.

The impact of nitric oxide (NO), superoxide (O_2^-), hydrogen peroxide (H_2O_2), and glutathione oxidation on intracellular heme dynamics was determined by incubating 6 x 10^7 to 1 x 10^8 cells/mL of cells expressing the heme sensor in PBS with the indicated concentrations of NOC-7 (Enzo Life Sciences), paraquat, H_2O_2, and diamide, respectively. The kinetics of heme mobilization were monitored by measuring the EGFP to mKATE2 ratios as described above.

For quantitative heme monitoring, we developed an *in-situ* method to calibrate the sensor in cells similar to that previously described[111]. The concentration of [heme] accessible to the sensor is governed by the following expression[116]:

$$[heme] = K_d \times \frac{R_{expt} - R_{min}}{R_{max} - R_{expt}} \left(\frac{F_{min}^{mKATE2}}{F_{max}^{mKATE2}}\right) \quad (2)$$

K_D is the heme-heme sensor dissociation constant, R_{expt} is the EGFP:mKATE2 fluorescence ratio under any given condition, R_{min} is the EGFP:mKATE2 fluorescence

ratio when 0% of the sensor is bound to heme, R_{max} is the EGFP:mKATE2 fluorescence ratio when 100% of the sensor is bound to heme, F_{min}^{mKATE2} is the mKATE2 emission intensity when 0% of the sensor is bound to heme, and F_{max}^{mKATE2} is the mKATE2 emission intensity when 100% of the sensor is bound to heme.

Determination of R_{max} and F_{max}^{mKATE2} involves recording EGFP and mKATE2 fluorescence after digitonin permeabilization of cells and incubation with 50 μM heme. Briefly, 3 to 5 $OD_{600\ nm}$/mL of cells are resuspended in PBS with 100 μg/mL of digitonin, 1 mM ascorbate, and 50 μM hemin chloride. After a 30 minute incubation at 30 °C, cells were harvested, washed, and resuspended in PBS buffer prior to recording of fluorescence by plate reader, flow cytometry, or microscopy.

Determination of R_{min} and F_{min}^{mKATE2} involves recording EGFP and mKATE2 fluorescence after cells are treated with the heme biosynthesis inhibitor succinylacetone[138] or from *hem1*Δ cells cultured in parallel.

Since digitonin cannot permeabilize mitochondrial or nuclear membranes, we devised an alternative strategy to determine R_{max} and F_{max}^{mKATE2}. This procedure involved digesting the yeast cell wall with Zymolyase, followed by incubating yeast spheroplasts with 0.1% Triton-X100, to permeabilize all membranes, as well as 1 mM ascorbate and 50 μM hemin chloride. Briefly, cells were grown to a density of 1-2 $OD_{600\ nm}$/mL, washed in sterile Milli-Q water, and resuspended in "softening buffer" (100 mM Tris-HCl, pH = 9.4, 10 mM DTT) at a concentration of 10 $OD_{600\ nm}$/mL of cells. Cells were incubated at room temperature, with occasional swirling, for 30-60 minutes. Cells were then washed and resuspended in a sorbitol buffer containing 50 mM Tris-HCl, pH 7.4,

1.2 M Sorbitol. To this cell suspension in sorbitol buffer, 0.5 mg/mL of 100-T Zymolyase (MP Biomedicals, VWR) was added, followed by incubated for 45 minutes at 30 °C with occasional inversion. Next, cells were washed and resuspended in sorbitol buffer (50 mM Tris-HCl, pH 7.4, 1.2 M Sorbitol). 3 to 5 $OD_{600\ nm}$/mL of cells in Sorbitol buffer were resuspended in a sorbitol buffer that contained 0.1% Triton X-100, 2 mM Ascorbate, and 50 μM hemin chloride, and incubated at 30 °C for 30-45 minutes. Cells were then washed and resuspended in sorbitol buffer for fluorescence measurements.

Flow cytometric measurements were performed using a BD FACS Aria Ill Cell Sorter or BD LSR II Flow Cytometer, both equipped with an argon laser (ex 488nm) and yellow-green laser (ex 561nm). EGFP was excited using the argon laser and was measured using a 530/30nm bandpass filter. mKATE2 was excited using the yellow-green laser and was measured using a 610/20nm bandpass filter. Data evaluation was conducted using FlowJo v9.9.3 software. The number of cells measured per experiment was set to 1,000,000 unless otherwise stated. BY4741 empty vector cells were used as a negative control for fluorescence. Only mKATE2 positive cells were selected for analysis.

Confocal microscopy was done on a Zeiss ELYRA LSM 780 Super-resolution Microscope equipped with a 63x, 1.4 numerical aperture oil objective. EGFP was excited with the 488 nm line of an argon ion laser, while mKATE2 was excited using the 594 nm of a HeNe laser line. The 494-571nm and 606-686 nm band pass filters were used to filter emission for EGFP and mKATE2, respectively. Images were collected using Zeiss software and analyzed with ImageJ 1.48v (Rasband, W.S., ImageJ, U. S. National Institutes of Health, Bethesda, Maryland, USA, http://rsb.info.nih.gov/ij/, 1997-2007).

Ratio images were generated using ImageJ RatioPlus software (http://rsb.info.nih.gov/ij/plugins/ratio-plus.html) after background subtraction. To confirm mitochondrial or nuclear localization of the sensors, prior to microscopy, exponential phase cells were incubated with 2.5 μg/mL 4',6-diamidino-2-phenylindole (DAPI) (Invitrogen) in SCE-LEU media for 30 minutes to stain nuclear and mitochondrial DNA.

2.10.2.3 Immunoblotting

Yeast were cultured in 10 mL of SC media for 15 hours to a density of 1 $OD_{600\ nm}$ /mL. Cells were harvested, washed in ice-cold Milli-Q water, and lysed in two pellet volumes of phosphate buffer supplemented with protease inhibitors as described previously[139, 140]. Lysis was achieved at 4 °C using one pellet volume of zirconium oxide beads and a bead beater (Bullet Blender, Next Advance) on a setting of 8 for 3 minutes[139, 140]. Lysate protein concentrations were determined by the Bradford method (Bio-rad) and 12% tris-glycine gels (Invitrogen) were employed for SDS-PAGE[139, 141]. Anti-GFP rabbit or anti-GAPDH polyclonal antibodies (Genetex) and a goat anti-rabbit secondary antibody conjugated to a 680 nm emitting fluorophore (Biotium) were used to probe for HS1 and related variants or GAPDH, respectively. All gels were imaged on a LiCOR Odyssey Infrared imager[139, 141].

CHAPTER 3. HEME BIOAVAILABILITY AND SIGNALING IN RESPONSE TO STRESS IN YEAST CELLS

3.1 Thesis Attribution Statement for Chapter 3.

Portions of this chapter are adapted from previously published work: "David A. Hanna, Rebecca Hu, Hyojung Kim, Osiris Martinez-Guzman, Matthew P. Torres, and Amit R. Reddi. 'Heme bioavailability and signaling in response to stress in yeast cells. Journal of Biological Chemistry. 2018; DOI: 10.1074/jbc.293/32/12378.'" Regarding unpublished work investigating heme binding proteins with hemin agarose, sepharose beads, and SILAC labeling, Hyojung Kim and the Torres Lab helped set up cultures for SILAC labeling and handled these samples post bead elution up to data analysis.

3.2 Introduction

Protoheme (iron protoporphyrin IX or heme b) is an essential cofactor and signaling molecule that is also potentially cytotoxic[2, 3, 13, 49]. The molecules and mechanisms cells employ to utilize protoheme, while mitigating its inherent toxicity, are complex and poorly understood, especially during stress[2, 49]. Cells manage protoheme, which is hereafter referred to as heme, by controlling both its total concentration and bioavailability[2, 49]. Heme concentration is primarily governed by the relative rates of heme synthesis and degradation, which are well understood processes[2, 49]. Indeed, all the enzymes involved in eukaryotic heme synthesis and degradation have been structurally characterized to atomic resolution and the mechanisms of action have been largely delineated[2, 3, 13, 49]. On the other hand, the factors that control heme bioavailability are

poorly understood[2, 49]. Bioavailable heme can be operationally defined as a pool of chelatable, kinetically labile heme that can readily exchange between biomolecules and is accessible for heme-dependent processes. The identity of factors that buffer and traffic labile heme (LH) and the mechanisms employed to mobilize it for utilization are largely unknown[2, 49]. In order to mitigate heme toxicity, it is generally thought that heme is made on demand, i.e. heme synthesis and utilization are tightly coupled, and heme in excess of that required for metabolism is degraded[13, 44, 46]. As a consequence, it is unclear what role, if any, steady-state LH plays in supporting heme dependent functions. Using genetically encoded ratiometric fluorescent heme sensors to probe LH and heme homeostatic mechanisms, we have previously demonstrated the existence of a highly dynamic steady-state pool of LH in the cytosol, spanning 20-40 nM, and identified new heme trafficking factors, e.g. glyceraldehyde phosphate dehydrogenation (GAPDH), and signaling molecules that mobilize LH, e.g. nitric oxide (NO)[29]. However, the physiological importance of LH remained unclear. In the current work, using Sac*charomyces cerevisiae* as a model eukaryote and heme sensors and chelating agents, we establish the functional importance of LH in regulating heme signaling, demonstrate that LH is preferentially consumed when cells become heme depleted, and discovered that certain xenobiotics, e.g. lead ions (Pb^{2+}), can, rather paradoxically, both deplete total cellular heme, primarily through its inhibition of heme synthesis, and increase labile bioavailable heme. We further find that the proteasome is involved in the regulation of labile heme and its response to Pb^{2+} stress. In total, our results establish a functional role for LH, indicate that total and labile heme pools can be decoupled in response to certain stressors, and provide evidence for heme-based signaling in response to heavy metal stress. In light of

these discoveries under Pb^{2+} stress, in order to identify heme signaling networks activated by Pb^{2+} we designed a method to identify proteins that bind and release heme in response to stress.

3.3 Sequestering Labile Heme Impacts Heme Signaling

We first sought to determine if cytosolic LH serves a functional role in heme signaling. Towards this end, we developed an approach to sequester LH and probe its effects on the heme-regulated transcription factor Hap1[30, 142, 143]. In order to chelate cytosolic LH, we induced the expression of a high affinity hemoprotein, cytochrome b_{562} (Cyt b_{562})[102, 144-147], using a galactose (GAL)-inducible promoter (pGAL)[148]. Cyt b_{562} binds ferric heme at pH 7.0 with a dissociation constant ($K_d^{Fe(III)}$) of 10 nM[102]. Given the reduction potential (E_M) of heme-Cyt b_{562}, +200 mV vs. NHE at pH 7.0[149], and the *Em* of free heme, -38 mV vs. NHE [108, 109], one can estimate the ferrous heme dissociation constant ($K_d^{Fe(II)}$) to be ~1 pM by completing a thermodynamic cycle[109].

First, we confirmed that Cyt b_{562} overexpression could sequester heme by measuring changes in LH with the genetically encoded ratiometric fluorescent heme sensor, HS1-M7A. HS1 is a tri-domain fusion protein consisting of a heme-binding domain, the His/Met coordinating 4-alpha-helical bundle hemoprotein Cyt b_{562} fused to a pair of fluorescent proteins, EGFP and mKATE2, that exhibit heme-sensitive and –insensitive fluorescence, respectively[29] (Figure 3.1A). Heme binding to the Cyt b_{562} domain results in the quenching of EGFP fluorescence via resonance energy transfer but has little effect on mKATE2 fluorescence[29]. Thus, the ratio of EGFP fluorescence (ex: 488 nm, em: 510 nm) to mKATE2 fluorescence (ex: 588 nm, em: 620 nm) provides a

readout of cellular heme independently of sensor concentration, with the EGFP/mKATE2 ratio inversely correlating with heme binding to the sensor[29]. The high affinity of HS1 for ferric and ferrous heme, K_d^{III} = 10 nM and K_d^{II} < 1 nM at pH 7.0, renders it fully saturated with heme in WT cells[29]. On the other hand, a variant of HS1, HS1-M7A, in which the heme coordinating Met ligand is mutated to Ala, exhibits ferrous and ferric affinities of K_d^{II} = 25 nM and K_d^{III} = 2 μM at pH 7.0 and is 20-50% bound in the yeast cytosol[29]. The observed sensor EGFP/mKATE2 fluorescence ratio (R_{expt}) can be used to determine the fractional heme saturation of the sensor and the concentration of LH, assuming a 1:1 heme:sensor binding model and previously established sensor calibration protocols that involve determining the sensor ratio when the sensor is 100% (R_{max}) and 0% (R_{min}) bound to heme (see Chapters 2.10.2.2 and 3.10.5)[29]. Notably, heme binding to the sensor is reversible and expression of the heme sensor in cells does not itself perturb heme homeostasis or otherwise affect viability[29].

Wild type (WT) cells expressing heme sensor HS1-M7A and GAL-inducible Cyt b_{562} (pGAL-Cyt b_{562}) were cultured in 2% raffinose (RAF) with or without 0.1% GAL for 16 hours. As demonstrated in Figure 3.1B, induction with GAL results in an increase in the EGFP/mKATE2 fluorescence ratio, from 1.90 (.09) to 2.82 (.04), consistent with less heme binding to the sensor and diminished LH. By comparison, cells expressing an empty pGAL vector (EV) or that are heme depleted with the heme biosynthetic inhibitor, succinylacetone (SA)[29, 138, 150], are unaffected by induction of Cyt b_{562}. Using the aforementioned sensor calibration protocols the induction of Cyt b_{562} results in a decrease in the fractional saturation of the heme sensor from ~60% to ~35% heme bound, which corresponds to a change in LH from 35 to 14 nM.

Having established that LH can be sequestered by over-expression of Cyt b_{562}, we next sought to determine if this would impact the activity of the heme regulated transcription factor Hap1[30, 142, 143, 151]. Heme binding to Hap1 alters its ability to promote or repress transcription of a number of target genes, including *CYC1*, which Hap1 positively regulates[29, 30, 142, 143, 151]. In order to probe Hap1 activity, we used a transcriptional reporter that employs the promoter of a Hap1 target gene, p*CYC1*, driving the expression of enhanced green fluorescent protein (EGFP)[29]. As demonstrated in Figure 3.1, not only does heme depletion with SA decrease EGFP fluorescence, as expected, Cyt b_{562} induction with GAL also results in a decrease in EGFP fluorescence, both of which are consistent with reduced heme binding to Hap1 and diminished transcriptional activation of *CYC1*. Altogether, our results strongly suggest that over-expression of Cyt b_{562} can sequester LH and this results in diminished heme signaling and Hap1 activity.

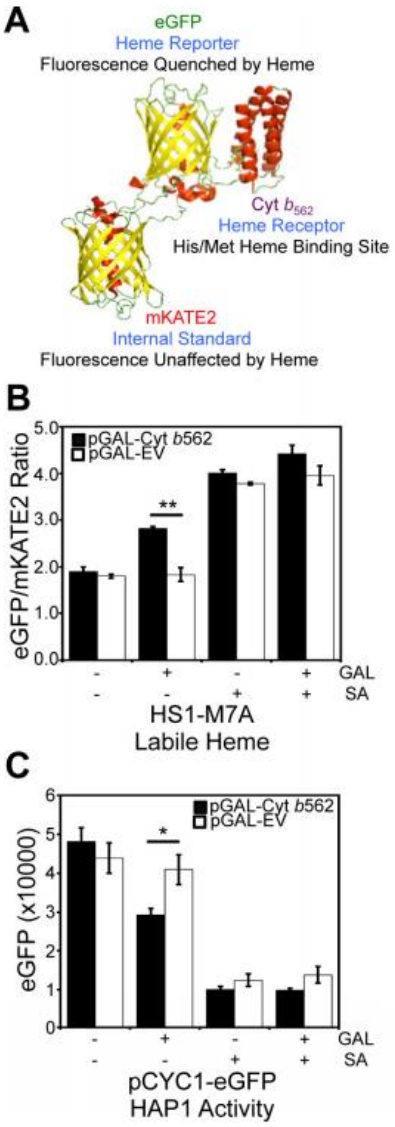

Figure 3.1 - Overexpression of a high affinity hemoprotein, Cyt b562, attenuates labile heme and the activity of heme-regulated transcription factor, Hap1. (**A**), molecular model and design principles of the heme sensor, HS1. Model derived from the X-ray structures of mKATE2 (Protein Data Bank code 3BXB) and CG6 (Protein Data Bank code 3U8P). (**B**), cells expressing the heme sensor, HS1-M7A, and an allele of Cyt b562 on a galactose (GAL)-inducible promoter (pGAL-Cyt b562) or empty vector (pGAL-EV) were cultured in 2% RAF with or without 1.0% GAL or 500 M SA for 16 h in SCE medium. After growth, HS1-M7A sensor EGFP (excitation 488 nm, emission 510 nm) and mKATE2 (excitation 588 nm, emission 620 nm) fluorescence emission ratios were recorded. (**C**), Hap1 activity was measured in cells expressing pGAL-Cyt b562 or pGAL-EV and cultured in 2% RAF with or without 1.0% GAL or 500 M SA for 16 h in SC medium using a transcriptional reporter consisting of an allele of EGFP driven by the CYC1 promoter (pCYC1-EGFP), a Hap1 target gene. All data represent the mean ± S.D.

(error bars) of triplicate cultures, and the statistical significance was assessed using a two-sample t-test. *, $p < 0.01$; **, $p < 0.001$.

3.4 Labile Heme is Preferentially Consumed Relative to Total Heme During Heme Depletion

We next sought to determine if LH is consumed preferentially relative to total heme during conditions of heme deficiency in order to ascertain if LH is mobilized for heme dependent functions when cells are confronted with defects in heme synthesis. Towards this end, we titrated the heme biosynthetic inhibitor succinylacetone (SA) in WT cells expressing the high affinity heme sensor, HS1, or the medium affinity sensor, HS1- M7A, and measured total and labile heme (Figure 3.2). Titration of SA over a broad concentration range, up to 500 μM, results in the depletion of both total (Figure 3.2C) and labile heme (Figure 3.2A,B) as expected. However, most interestingly, LH is more sensitive than total heme to SA-mediated heme depletion (Figure 3.2). When total heme is only modestly depleted by 25% using a relatively low 25 μM dose of SA (Figure 3.2), there is a much larger diminution of LH as measured by HS1- M7A and HS1 (Figure 3.2A,B); heme loading of the medium affinity sensor, HS1-M7A, shifts from ~26% bound to ~ 0% bound, and the high affinity sensor, HS1, shifts in heme loading from ~100% bound to ~60% bound. In terms of LH concentration, based on the ferrous heme dissociation constants of HS1-M7A, K_d^{II} = 25 nM[29], and HS1, assumed to be K_d^{II} ~ 1 pM based on the estimated K_d^{II} for Cyt b_{562}, we would estimate LH decreases from ~10 nM to < 1 nM (likely ~2 pM based on the predicted K_d^{II} for HS1) in response to an SA concentration that modestly depletes total heme by 25%. Taken together, these data

strongly suggest that heme deficiency mobilizes labile heme to non-exchangeable, and likely higher affinity and/or buried, heme-binding sites.

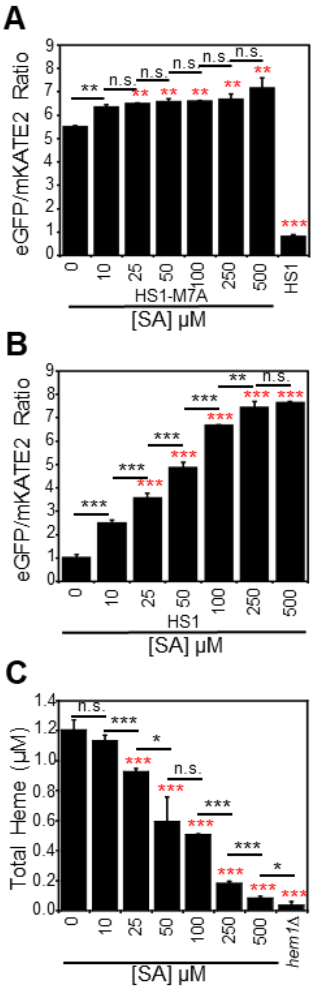

Figure 3.2 - LH is more sensitive to heme depletion using the heme biosynthetic inhibitor, SA, than total heme. Labile heme was measured in HS1- M7A– expressing (**A**) or HS1-expressing (**B**) cells cultured in SCE medium for 16 h with the indicated concentration of SA before measurement of the eGFP/ mKATE2 fluorescence ratios. (**C**) total heme was measured in the cultures depicted in A or in heme-deficient hem1Δ cells. All data represent the mean ± S.D. (error bars) of triplicate cultures, and the statistical significance was assessed using a two-sample t-test. Black asterisks, statistical significance between the indicated pairwise comparisons of conditions; red asterisks, statistical significance relative to 0M SA. *, $p < 0.05$; **, $p < 0.005$; ***, $p < 0.001$; n.s., not significant.

3.5 Pb^{2+} Depletes Total Heme but Increases Labile Heme and Heme Mediated Signaling

A number of xenobiotics and environmental toxins negatively impact heme homeostasis[152], including N-methylprotoporphyrins[153, 154], certain alkylating agents, *e.g.* 2-Allyl-2-isopropylacetamide[155], tetrachlorodibenzo-p-dioxin and various polyhalogenated biphenyls[156, 157], and heavy metals[158-163]. Pb^{2+}, in particular, is a major public health concern given the ubiquity of Pb^{2+}-based paints, piping, and munitions[163]. Among other targets, Pb^{2+} is well known to inhibit heme biosynthetic enzymes aminolevulinic acid (ALA) dehydratase (ALAD) and ferrochelatase (FECH), resulting in defects in heme synthesis, which in-turn leads to anemia, cognitive decline, and other health problems[163]. Further, Pb^{2+} and other heavy metals are known to induce HO[164, 165], which may also contribute to decreased heme levels. However, while much is known about the role of Pb^{2+} in impacting heme synthesis and degradation, virtually nothing is known about the effects of Pb^{2+} on bioavailable labile heme. Given our findings that LH is important for maintaining heme signaling to Hap1 and is preferentially consumed relative to total heme during heme deficiency, we sought to determine the effects of Pb^{2+} on LH and heme-based signaling. Towards this end, we established a yeast model of Pb^{2+} toxicity and probed the effects of Pb^{2+} on total heme, LH, and heme signaling.

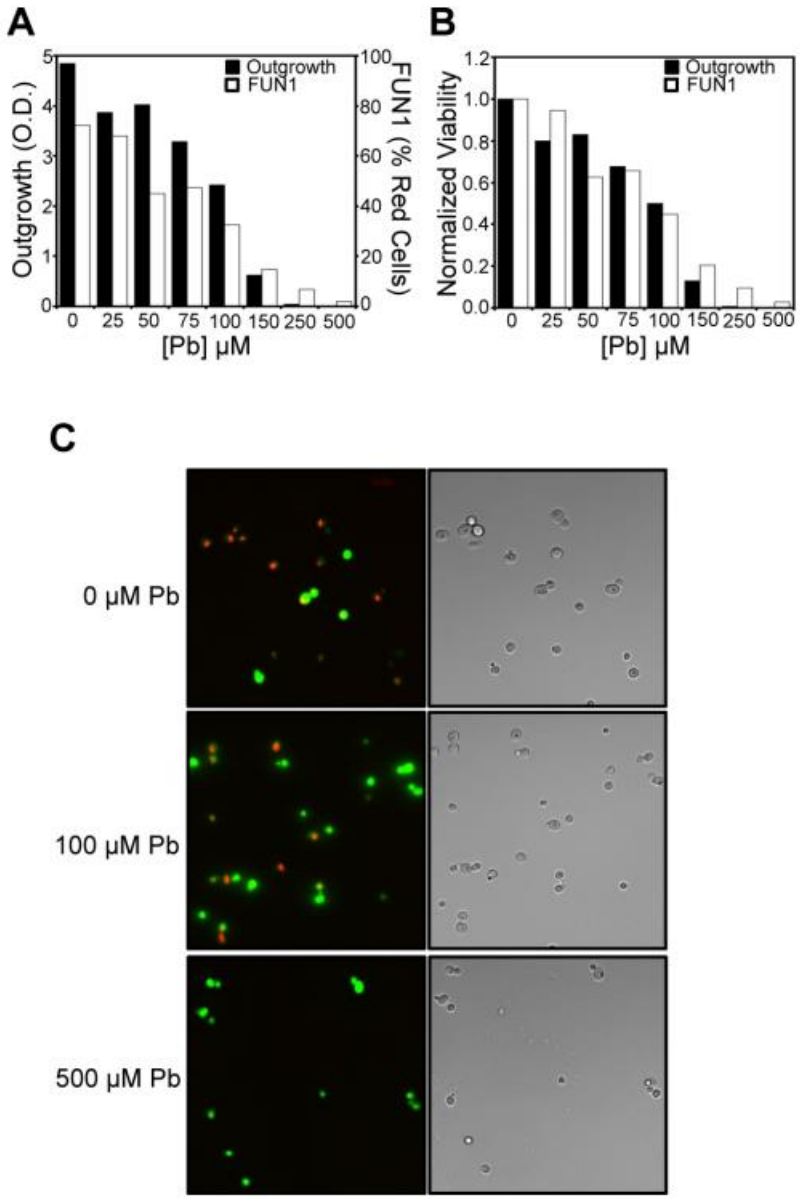

Figure 3.3 - Correlation between yeast cell viability as scored by outgrowth and a dye, FUN-1, that is sensitive to metabolic activity. (**A**) Outgrowth and FUN-1 measured viability was plotted as a function of [Pb] without normalization. Cell viability using FUN-1 was measured by taking the fraction of cells exhibiting red punctate fluorescence of the dye, which is indicative of metabolically active cells, and dividing over the total number of fluorescence positive cells that displayed either red punctate fluorescence or diffuse green fluorescence, which is indicative of metabolically inactive cells. (**B**) The data in A was normalized to the outgrowth or FUN-1 based viability at 0 µM [Pb]. These data are representative of two independent trials.

Due to the insolubility of $Pb(NO_3)_2$ in standard yeast growth medias, we employed a Pb^{2+} toxicity model similar to what was previously described in which yeast cells are subjected to an acute 3 hour exposure to varying concentrations of Pb^{2+} in 10 mM 2-(N-morpholino)ethanesulfonic acid (MES), pH = 6.0 buffer, a media in which $Pb(NO_3)_2$ is soluble and Pb^{2+} is not complexed by the buffer[166]. Following Pb^{2+} exposure, cells are washed and allowed to recover for 4 hours in an appropriate synthetic complete (SC) drop-out media prior to subsequent analyses. Cell viability is measured by diluting cells into SC media after the recovery period and monitoring growth for 20 hours. Cell viability as measured by outgrowth is virtually identical to viability measurements using FUN-1, a fluorescent dye that exhibits red punctate emission in the vacuoles of metabolically active live cells and diffuse green cytosolic emission in dead cells (Figure 3.3A-C)[166]. As shown in Figure 3.4A, yeast viability decreases with increasing $[Pb^{2+}]$. The concentration of Pb^{2+} that inhibits growth by 50%, lethal dose-50 (LD_{50}), varied between 25 and 500 μM over the course of our studies with different batches of media for reasons that are not completely understood. As a consequence, all of our analyses were done at the Pb^{2+} LD_{50} dose and not necessarily at a constant Pb^{2+} concentration.

At the Pb^{2+} LD_{50} dose, elemental analysis using total reflection X-ray fluorescence (TXRF) spectroscopy confirms a significant enrichment of Pb^{2+} in yeast cells (Figure 3.4B). In addition, a host of other bio-elements are impacted as a consequence of Pb^{2+} toxicity; P, S, K, Fe, and Zn are diminished, whereas Ca and Cu are increased[167]. These effects are consistent with prior studies in a number of organisms and cell types demonstrating the impact of Pb^{2+} on various aspects of metal[166, 168-172], phosphate[173, 174], and sulfur homeostasis[175-177].

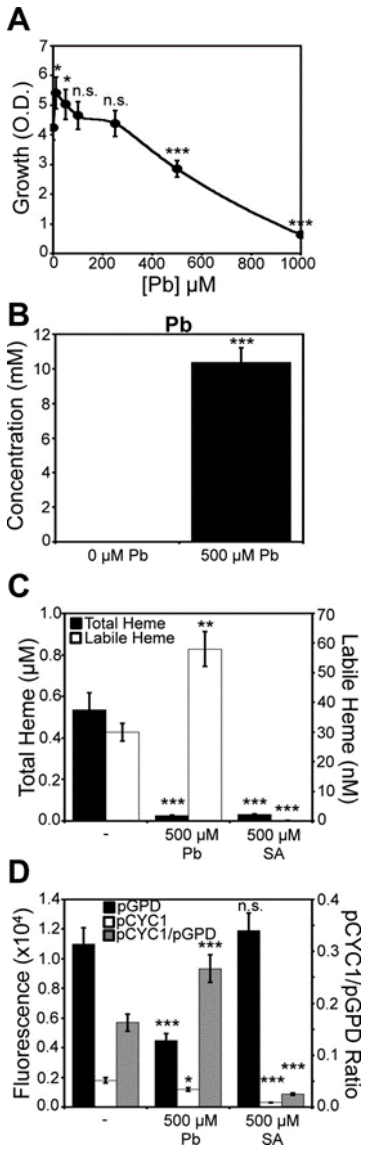

Figure 3.4 - Labile heme and heme signaling is increased, but total heme is attenuated in response to Pb^{2+} toxicity. (**A**) yeast cell viability, as measured by solution turbidity at an optical density (O.D.) of 600 nm, is diminished by exposure to Pb^{2+} in a dose-dependent manner. (**B**) at the LD50 dose of Pb^{2+} (500 µM), cells hyperaccumulate up to 10 mM Pb^{2+}, as measured by TXRF. (**C**) a dose of 500 M Pb^{2+} diminishes total heme to levels similar to 500M SA, but Pb^{2+} increases labile heme 2-fold, whereas SA does not. (**D**) Hap1p activity in response to heme depletion by SA or Pb^{2+} is measured using the pCYC1-EGFP Hap1 reporter construct (pCYC1). To control for the Hap1-independent effects of Pb^{2+} on EGFP expression, we measured EGFP fluorescence in response to Pb^{2+} or SA using an allele of EGFP driven by the heme/Hap1-independent promoter, GPD (pGPD). The ratio of pCYC1 to pGPD EGFP expression (pCYC1/pGPD) is a measure of heme/Hap1-specific activation of CYC1. All data represent the mean S.D. (error bars) of triplicate cultures, and the statistical significance relative to untreated cells was assessed using a two-sample *t-test*. *, $P < 0.05$; **, $P < 0.005$; ***, $P < 0.001$; n.s., not significant.

Interestingly, while total heme is depleted due to Pb^{2+} exposure, as expected due to its known effects on inhibiting heme synthesis[163] and up-regulating heme degradation[164, 165], LH is completely maintained, and in fact, increases by 2- fold (Figure 3.4C). In striking contrast, a dose of SA that depletes total heme to a similar degree as Pb^{2+} treatment attenuates both LH and total heme (Figure 3.4C). Titration of Pb^{2+}over a broad concentration range indicates a dose dependent increase in LH (Figure 3.5A), decrease in total heme Figure 3.5B), and decrease in cell viability (Figure 3.5C). The Pb^{2+}-dependent depletion of total heme and increase in LH primarily occurs after the recovery period in SC media; measurement of total heme and LH after the 3 hour Pb^{2+}exposure in MES buffer has minimal effects on LH (Figure 3.5D) and total heme (Figure 3.5E) relative to cells allowed to recover in SC media (Figure 3.5A,B). The changes in HS1-M7A sensor ratio are not due to artifacts associated with Pb^{2+}-dependent changes in sensor expression given that the emission of mKATE2, the heme-insensitive fluorophore, is constant over a wide-range of Pb^{2+}doses (Figure 3.6A). Furthermore, a variant of HS1 that cannot bind heme, HS1-M7A, H102A, which has the Met and His heme coordinating residues mutated to Ala, does not exhibit Pb^{2+}-dependent changes in fluorescence ratio (Figure 3.6B). Altogether, these data indicate that the total and labile heme pools can be acted upon independently of each other in response to stress and metabolically active cells are required for the observed changes in Pb^{2+}-dependent LH and total heme.

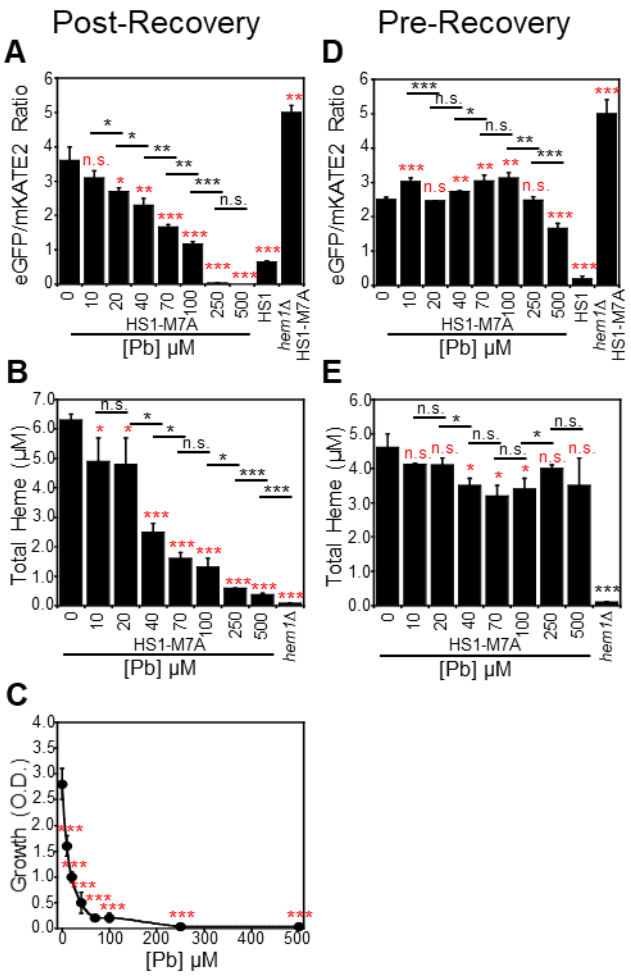

Figure 3.5 - Pb^{2+} only perturbs total and labile heme after a recovery period following exposure to Pb^{2+}. In cells expressing HS1-M7A, Pb^{2+} increases labile heme (**A**), decreases total heme (**B**), and diminishes cell viability (**C**) in a dose-dependent manner if cells are allowed to recover for 4 hr in SCE medium following Pb^{2+} exposure in MES buffer. However, labile (**D**) and total heme (**E**) in cells expressing HS1-M7A immediately after the exposure to Pb^{2+} in MES buffer are not significantly affected. All data represent the mean ± S.D. (error bars) of triplicate cultures, and statistical significance was assessed using a two-sample *t-test*. Black asterisks, statistical significance between the indicated pairwise comparisons of conditions; red asterisks, statistical significance relative to 0 M Pb. *, $P < 0.05$; **, $P < 0.005$; ***, $P < 0.001$; n.s., not significant.

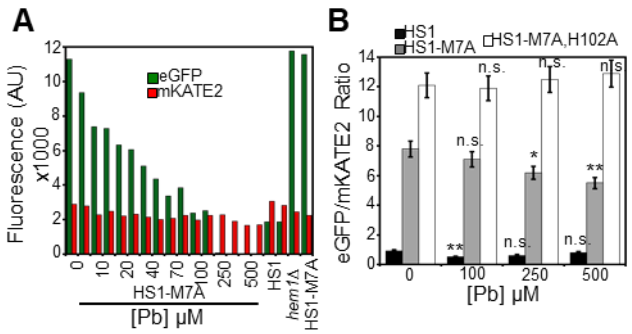

Figure 3.6 - The Pb^{2+}-dependent changes in heme sensor fluorescence ratios are not due to degradation of sensor and are heme dependent. (**A**) The EGFP (ex. 488 nm, em. 510 nm) and mKATE2 (ex. 588 nm, em. 620 nm) fluorescence channels that give rise to the HS1-M7A EGFP/mKATE2 ratios depicted in Figure 3.5A. The relatively constant mKATE2 fluorescence emission across a wide array of Pb^{2+} doses indicate that sensor expression is stable. (**B**) A sensor variant that cannot bind heme, HS1-M7A, H102A, does not exhibit Pb^{2+}-dependent changes in EGFP/mKATE2 fluorescence ratio relative to the heme sensor, HS1- M7A. This suggests that the change in sensor fluorescence emission is due to heme and not Pb^{2+}- dependent, heme-independent changes in sensor fluorescence. All data represent the mean ± SD of triplicate cultures and statistical significance was assessed using a two-sample t-test. These data support Figure 3.5. Black asterisks represent the statistical significance between the treated and untreated samples. * $P < 0.05$, ** $P < 0.01$, n.s. not significant.

Given that LH levels are changes so differently between SA and Pb^{2+} treatment, and that SA inhibits ALAD while Pb^{2+} inhibits both ALAD and FECH, we sought to analyze differences in protoporphyrin IX (PPIX) levels between these treatments. Correlating a buildup of PPIX in Pb^{2+} treated cells may indicate a preferential inhibition of FECH, and may allow us to derive insight from these results to help understand potential causes for heme mismanagement in porphyria. When comparing SA and Pb^{2+} inhibition of heme synthesis, total heme decreases to a similar degree with comparable doses of each inhibitor (Figure 3.7A,B); however, PPIX levels change differently in response to each inhibitor (Figure 3.7C,D). At low doses of Pb^{2+} PPIX levels decrease only slightly with larger absolute drops in total heme, presumably by inhibiting FECH

much more than ALAD (Figure 3.7B,D). At higher doses of Pb^{2+}, however, there appears to be more inhibition of ALAD, resulting in the tapering of PPIX levels that was not apparent at lower doses of Pb^{2+} (Figure 3.7B). SA, on the other hand, has a steady dose dependent decrease in PPIX, as reflected by its sole inhibition of ALAD (Figure 3.7C).

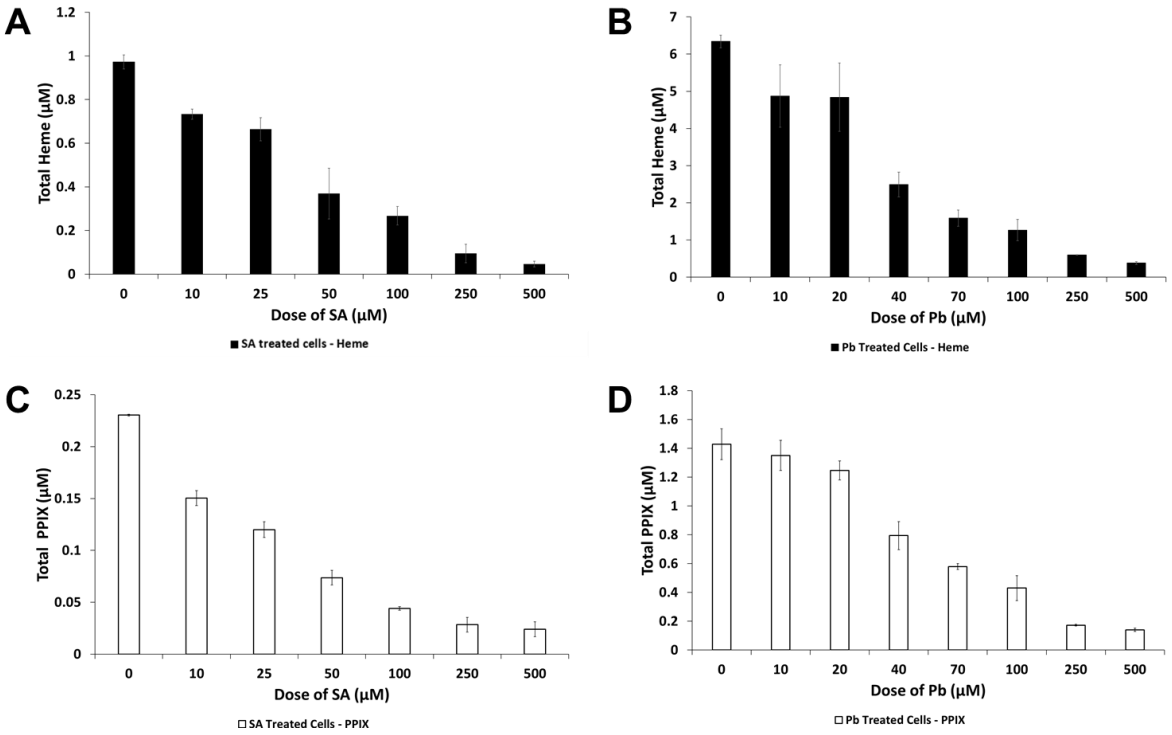

Figure 3.7 – Relative changes in total heme and total cellular PPIX levels in Pb^{2+} versus SA treated cells. (**A**) Total heme changes in response to SA. (**B**) Total heme changes in response in response to Pb^{2+} post recovery. (**C**) Total protoporphyrin IX (PPIX) changes in response to SA. (**D**) Total PPIX changes in response in response to Pb^{2+} post recovery.

We next addressed if the increase in LH in response to Pb^{2+} translates to changes in heme signaling. Towards this end, we measured Hap1 activity using the p*CYC1-EGFP* transcriptional reporter in cells conditioned with the LD_{50} dose of Pb^{2+}. In order to account for the effects of Pb^{2+} on EGFP expression independently of Hap1 activation, we also expressed EGFP under control of the *GPD* promoter (p*GPD*), which is not a transcriptional target of Hap1. As shown in Figure 3.4D, exposure to Pb^{2+} results in a

~33% decrease in the EGFP fluorescence of the Hap1 reporter while SA exposure results in a 6-fold decrease, despite a similar depletion in total heme.

Given that Pb^{2+} also affects EGFP fluorescence independently of Hap1, as evidenced by a ~60% decrease in fluorescence of parallel cultures harboring the p*GPD-EGFP* construct, we normalized the fluorescence from p*CYC1* driven expression of *EGFP* to the fluorescence from p*GPD* driven expression of E*GFP*, giving a p*CYC1*/p*GPD* ratio. Exposure to Pb^{2+} results in a nearly 2-fold increase, from .16 to .26, in the p*CYC1*/p*GPD* ratio of EGFP fluorescence, an indicator of Hap1/p*CYC1* specific activation. In striking contrast, cells conditioned with a dose of SA that results in a similar concentration of intracellular heme as the LD_{50} dose of Pb^{2+} exhibits a nearly ~10-fold decrease in the p*CYC1*/p*GPD* ratio of EGFP fluorescence, with a nearly 10-fold decrease in fluorescence of the p*CYC1-EGFP* construct and minimal perturbation to fluorescence from the p*GPD-EGFP* construct.

Taken together, at minimum, these results suggest that, in response to Pb^{2+} toxicity, Hap1 activity is largely maintained, despite a > 10-fold decrease in total heme. At maximum, these results suggest that "heme-specific" Hap1 activity, as recorded from the pCYC1/pGPD ratio, actually increases in response to Pb^{2+} stress. The maintenance of or increase in Hap1 activity, depending on the interpretation of the data, is presumably due to the Pb^{2+}-induced increase in LH.

3.6 Pb^{2+}-mediated Heme Depletion is Largely Due to a Block in Heme Synthesis

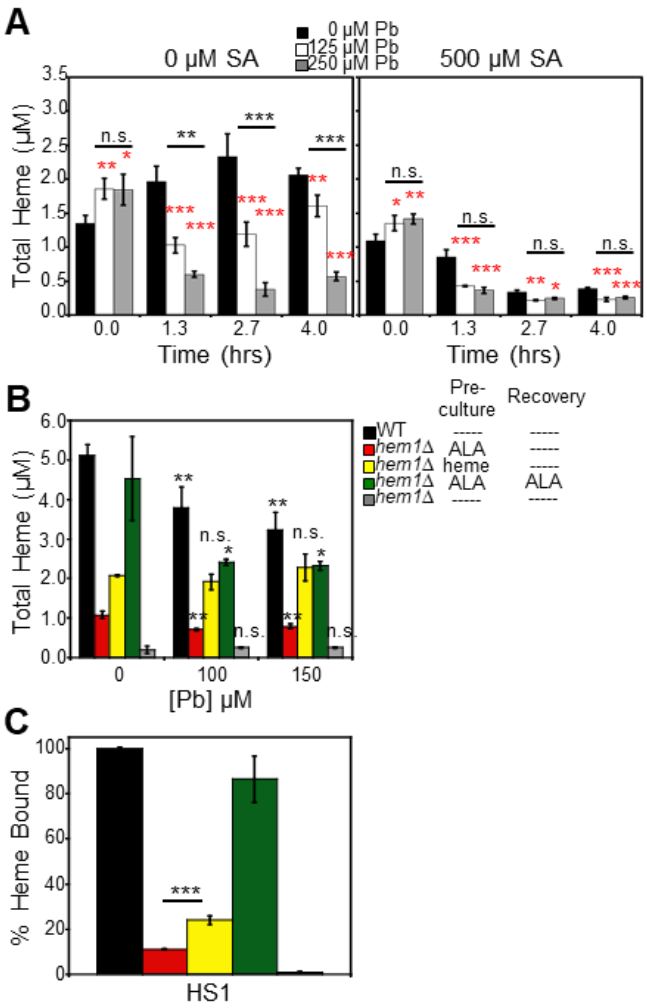

Figure 3.8 - Pb^{2+}-dependent attenuation of total heme is largely dependent on heme synthesis. (**A**) WT cells untreated (left) or treated (right) with 500 µM SA and the indicated concentrations of Pb^{2+}-demonstrate that Pb^{2+} has a larger effect on depleting total heme in cells that can properly synthesize heme. (**B**) and (**C**) endogenous heme, but not exogenous heme, is degraded in a Pb^{2+}-dependent manner. Total (**B**) and labile heme (**C**) were measured in HS1-expressing WT or hem1Δ cells conditioned with the indicated Pb^{2+} concentration and/or 200 µM ALA or 50 µM hemin chloride during the preculture and/or post- Pb^{2+} recovery period. All data represent the mean ± S.D. (error bars) of triplicate cultures, and statistical significance was assessed using a two-sample t-test. In A, black asterisks represent the statistical significance between the indicated pairwise comparisons of conditions, and red asterisks represent the statistical significance relative to 0 µM Pb for each time point. In B, black asterisks represent the statistical significance relative to 0 µM Pb foreach test condition. In C, the black asterisks represent the statistical significance between the indicated pairwise comparisons of strains. *, $P < 0.05$; **, $P < 0.01$; ***, $P < 0.001$; n.s., not significant.

We next sought to determine the mechanism by which intracellular heme is depleted in response to Pb^{2+} toxicity. The intracellular concentration of heme is governed by the relative rates of heme synthesis and degradation or export. In order to parse apart the effects of Pb^{2+} on these opposing processes, we tested the effects of Pb^{2+} on cells that had a defect in the ability to synthesize heme. First, we determined that Pb^{2+}-dependent heme depletion occurs within the first 1.5 hours of the 4-hour recovery period in SC media (Figure 3.8A, 0 μM SA). Second, we found that in cells that had a defect in heme synthesis due to conditioning with 500 μM SA, Pb^{2+} had an attenuated effect on the loss of total heme. For instance, after 2.7 hours, cells that could biosynthesize heme (Figure 3.8A, 0 μM SA) exhibited a 2-fold and 6-fold decrease in total heme when treated with 125 and 250 μM Pb^{2+}, respectively. On the other hand, in cells with ablated heme biosynthesis (Figure 3.8A, 500 μM SA), both 125 and 250 μM Pb^{2+} resulted in a relatively modest ~30% decrease in total heme. The diminished effect of Pb^{2+} on total heme in cells conditioned with the heme biosynthetic inhibitor SA suggested that Pb^{2+} depletes total heme by largely suppressing heme biosynthesis.

We next sought to further validate the observation that Pb^{2+} depletes heme by primarily affecting heme synthesis and not heme degradation or export. Towards this end, we utilized a *hem1*Δ strain, which lacks the 1st enzyme in the heme synthesis pathway, ALA synthase (ALAS), to test the effects of Pb^{2+} on the degradation of mitochondrially-derived *de novo* synthesized heme or exogenously supplied heme. *hem1*Δ cells can only acquire heme by stimulating mitochondrial heme synthesis via supplementation with ALA, the product of ALAS, or by heme uptake via hemin supplementation. We supplemented *hem1*Δ cells with ALA or heme during a 16-hour pre-culture in SCE

media, subjected them to Pb^{2+}exposure in MES buffer for 3 hours, followed by a 4-hour recovery in SCE media, and then analyzed total heme (Figure 3.8B). WT and *hem1*Δ cells supplemented with ALA in both the pre-culture and during the recovery accumulated similar amounts of intracellular heme, experienced a Pb^{2+}-dependent depletion of total heme (Figure 3.8B, black and green columns) and exhibited >80% heme-loading of the high affinity heme sensor HS1 (Figure 3.8C, black and green columns). *hem1*Δ cells treated with ALA only during the pre-culture, but not during the recovery, also exhibited a Pb^{2+}-dependent attenuation in intracellular heme (Figure 3.8B, red columns). However, the total amount of heme was ~5-fold lower (Figure 3.8B, red columns) and the heme-loading of HS1 was considerably reduced, ~10% bound, compared to *hem1*Δ cells supplemented with ALA in both the pre-culture and the recovery media (Figure 3.8C, red columns), presumably due to the fact that ALA was limiting since it is not supplied during the recovery phase. In striking contrast to ALA supplementation, *hem1*Δ cells supplemented with exogenous heme during the pre-culture, which contributed to a 2-fold increase in intracellular heme relative to ALA supplemented *hem1*Δ cells, did not exhibit the Pb^{2+}-dependent depletion of heme (Figure 3.8B, yellow columns). Exogenously supplied heme is still available to bind HS1, and in fact, its fractional saturation is similar to ALA treated cells after normalizing for the change in total intracellular heme concentration (Figure 3.8C, yellow columns). The observation that Pb^{2+} depletes endogenously synthesized heme and not exogenously supplied heme strongly suggests that Pb^{2+} primarily inhibits heme synthesis, with minor effects on heme degradation.

Given that heme synthesis is O_2-dependent and our results that Pb^{2+} largely inhibits heme synthesis, we next sought to test our prediction that Pb^{2+} should have minimal impact on total heme in the absence of O_2. To test the O_2 dependence of Pb^{2+}-induced heme depletion, we subjected aerobically grown cells to Pb^{2+} exposure in MES buffer in an anoxic or normoxic environment, followed by recovery in anoxic or normoxic culture conditions and measurement of total heme, LH, and Pb^{2+} toxicity (Figure 3.9). Quite strikingly, despite accumulating similar levels of Pb^{2+} between normoxic and anoxic Pb^{2+}-exposures (Figure 3.10), in the absence of O_2, cells do not exhibit Pb^{2+}-dependent heme depletion (Figure 3.9A). On the other hand, the increase in LH in response to Pb^{2+} is similar between both normoxic and anoxic Pb^{2+} exposures (Figure 3.9B). Notably, Pb^{2+}-mediated cell toxicity is entirely O_2-dependent given that viability is not affected in anoxic cultures (Figure 3.9C). Taken together, our data suggest that Pb^{2+}-induced depletion of total heme only occurs in cells that are synthesizing heme *de novo*, further supporting the notion that Pb^{2+} largely inhibits heme synthesis.

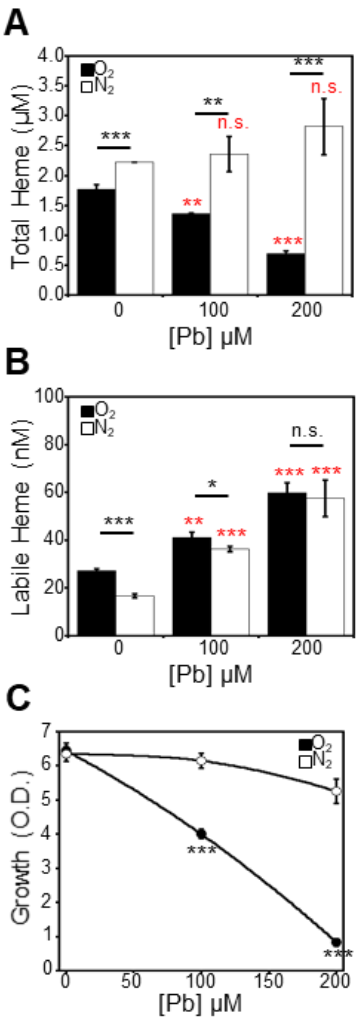

Figure 3.9 – Pb^{2+}-induced depletion of heme is O_2-dependent. Cells expressing HS1-M7A were conditioned with the indicated concentration of Pb^{2+} and allowed to recover in an anoxic, nitrogen-rich (N_2) atmosphere or in air (O_2), and total heme (**A**), labile heme (**B**), and viability (**C**) were measured. All data represent the mean ± S.D. (error bars) of triplicate cultures, and statistical significance was assessed using a two-sample *t-test*. Black asterisks, statistical significance between the indicated pairwise comparisons of conditions; red asterisks, statistical significance relative to 0 μM Pb.* *, $P < 0.05$; **, $P < 0.01$; ***, $P < 0.001$; n.s., not significant.

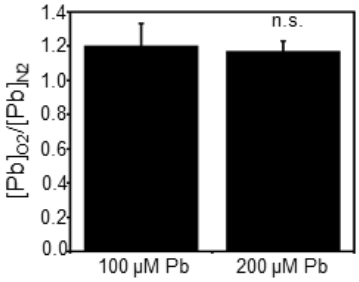

Figure 3.10 - Anaerobic and aerobic Pb^{2+} uptake are virtually identical. Intracellular Pb was measured by TXRF after treatment with a bolus of 100 µM or 200 µM $Pb(NO_3)_2$ that was administered either anaerobically (N_2) or aerobically (O_2) as described in 3.10.11. The data are presented as a ratio of aerobic (O_2) to anaerobic (N_2) cellular Pb^{2+} concentrations and represent the mean ± SD of triplicate cultures. The statistical significance was assessed using a two-sample t-test. These data support Figure 3.9. n.s. not significant.

We next sought to determine if a block in heme degradation or export could preserve total heme in the face of Pb^{2+} toxicity and affect labile heme. One established mechanism of heme degradation is via heme oxygenase (HO), an enzyme that oxidatively degrades heme into bilirubin, carbon monoxide (CO), and ferrous iron (Fe^{2+})[165]. In order to test the role of HO in Pb^{2+}-dependent heme depletion, we compared WT and *hmx1*Δ cells, which lacks heme oxygenase 1[178, 179], for Pb^{2+}-dependent heme depletion. As shown in Figure 3.11A, in the absence of Pb^{2+}, *hmx1*Δ cells exhibit a ~25% increase in total heme, consistent with prior studies in yeast and the known role of Hmx1 in heme degradation[178]. However, both WT and *hmx1*Δ cells exhibit the Pb^{2+}-induced depletion of heme to similar degrees, indicating HO does not play a role in the loss of heme during Pb^{2+} toxicity. Both WT and *hmx1*Δ cells exhibited a Pb^{2+}-dependent increase in LH (Figure 3.11B). For reasons that are not entirely clear at this time, *hmx1*Δ cells appeared to be more resistant to Pb^{2+} toxicity (Figure 3.11C). In contrast, prior work has demonstrated that Hmx1p confers resistance to various oxidative insults, including H_2O_2, diamide, and menadione[179], presumably due to released CO, bilirubin, and biliverdin.

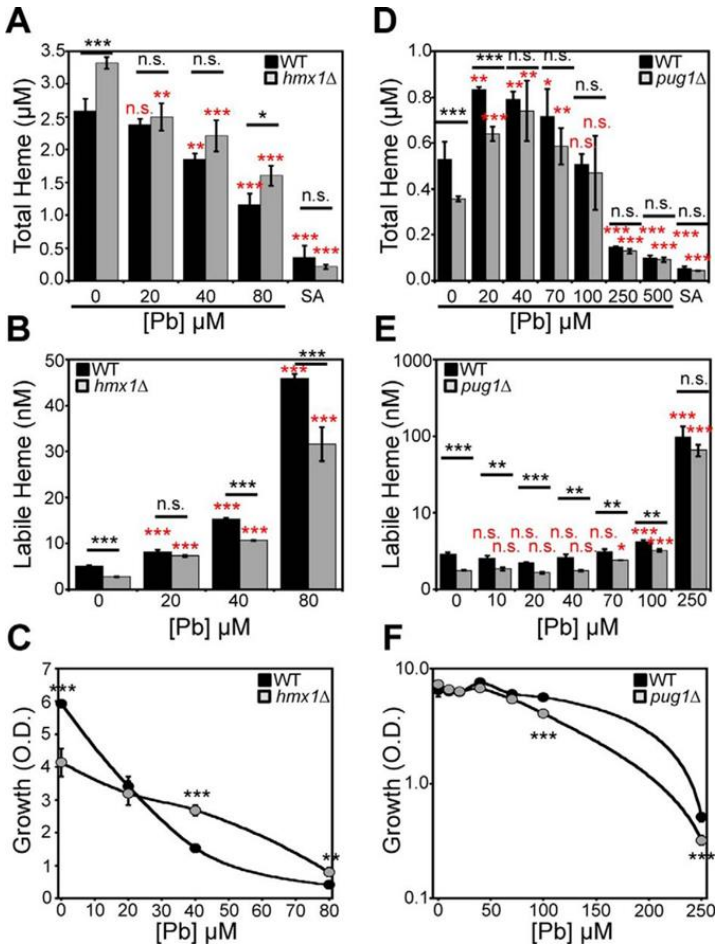

Figure 3.11 - Pb^{2+}-induced depletion of heme does not involve HMX1 or PUG1. (**A**-**C**) hmx1Δ cells exhibit a Pb^{2+}-dependent (**A**) decrease in total heme and (**B**) increase in labile heme. (**C**) hmx1Δ cells are more resistant to Pb^{2+} toxicity. (D-F) pug1Δ cells exhibit a Pb^{2+}-dependent (**D**) decrease in total heme, (**E**) increase in labile heme, and (**F**) WT-sensitivity to Pb^{2+} toxicity. All data represent the mean ± SD of triplicate cultures and statistical significance was assessed using a two-sample t-test. Black asterisks represent the statistical significance between the indicated pairwise comparisons of conditions and red asterisks represent the statistical significance relative to 0 μM [Pb]. * $P < 0.05$, ** $P < 0.01$, *** $P < 0.001$, n.s. not significant.

An alternative mechanism for cellular heme depletion is heme export. Many metazoans express heme exporters, *e.g.* FLVCR1, to aid in heme detoxification. *Saccharomyces cerevisiae* expresses a porphyrin-heme exchanger, *PUG1*, which uptakes protoporphyrin IX and expels heme[120]. In order to test the role of heme export via Pug1 during Pb^{2+} toxicity, we determined the extent to which heme is depleted in WT and

*pug1*Δ cells exposed to increasing doses of Pb^{2+}. As with *hmx1*Δ cells, *pug1*Δ cells exhibit a similar degree of Pb^{2+}-induced heme depletion as WT cells (Figure 3.11D), indicating Pug1 does not affect the loss of heme during Pb^{2+} toxicity. Both WT and *pug1*Δ cells exhibit an increase in LH in response to Pb^{2+} (Figure 3.11E) and similar sensitivities to Pb^{2+} toxicity (Figure 3.11F).

Altogether, our data indicate that: **a.** Pb^{2+} depletes total heme primarily through its ability to inhibit heme synthesis and **b.** heme degradation and export pathways do not affect Pb^{2+}-dependent changes in total and labile heme.

3.7 Pb^{2+}-dependent Increases in Labile Heme Correlate with Protein Degradation

Most heme is associated with non-exchangeable binding sites in high affinity hemoproteins. As such, we predicted that the increase in labile heme in response to Pb^{2+} may be associated with the degradation of hemoproteins and the release of heme into the labile heme pool. To test this hypothesis, we conducted 1-D PAGE analysis of cells conditioned with and without Pb^{2+} at the LD_{50} dose immediately after the 3-hour exposure to Pb^{2+} in MES buffer and after the 4-hour recovery phase (Figure 3.12A). We found that immediately following exposure to Pb^{2+}, protein expression is unaffected, whereas after the 4-hour recovery, a number of proteins are degraded (Figure 3.12A). The diminished protein expression during the recovery phase correlates with when we observe increased LH, suggesting protein turnover and an increase in LH are linked. Notably, using tandem mass spectrometry, we found that GAPDH, a component of the LH buffer[29], is retained during Pb^{2+} exposure (Figure 3.12A,B and Table 1). Another glycolytic protein, enolase, is also maintained during Pb^{2+} exposure. On the other hand,

Pb^{2+} has the capacity to degrade high affinity hemoproteins. Ctt1, which is a heme containing catalase enzyme, is degraded in a Pb^{2+}-dependent manner (Figure 3.12B). Altogether, our data is consistent with a model in which Pb^{2+} induced degradation of hemoproteins releases heme that contributes to the LH pool.

In order to test the hypothesis that Pb^{2+}-dependent protein turnover releases heme from hemoproteins and increases LH, we assayed Pb^{2+}-dependent changes in LH in yeast mutants defective in various protein degradation pathways, including vacuolar, autophagic, and proteasomal degradation. We found that a proteasome mutant, *rpn10*Δ^{180}, exhibited Pb^{2+} dependent and independent changes in LH (Figure 3.12C), whereas mutants defective in vacuolar, *pep4*Δ^{181}, (Figure 3.12D) or autophagic, *atg1*Δ^{182}, (Figure 3.12C), pathways did not have altered LH. Under non-stressed conditions, WT cells exhibited a LH concentration of ~ 5 nM, corresponding to an HS1-M7A fractional saturation of 17%. On the other hand, HS1-M7A was ~ 0% bound to heme when expressed in *rpn10*Δ cells, which corresponds to a LH concentration of < 1 nM. However, Pb^{2+} induced a greater increase in LH (Figure 3.12C) and decrease in total heme (Figure 3.12E) in *rpn10*Δ cells relative to WT. Moreover, the growth of *rpn10*Δ cells were more sensitive to Pb^{2+} toxicity that WT (Figure 3.12F). In total, these results indicate that the proteasome positively regulates LH and loss of proteasomal function sensitizes cells to Pb^{2+}-dependent effects on heme homeostasis.

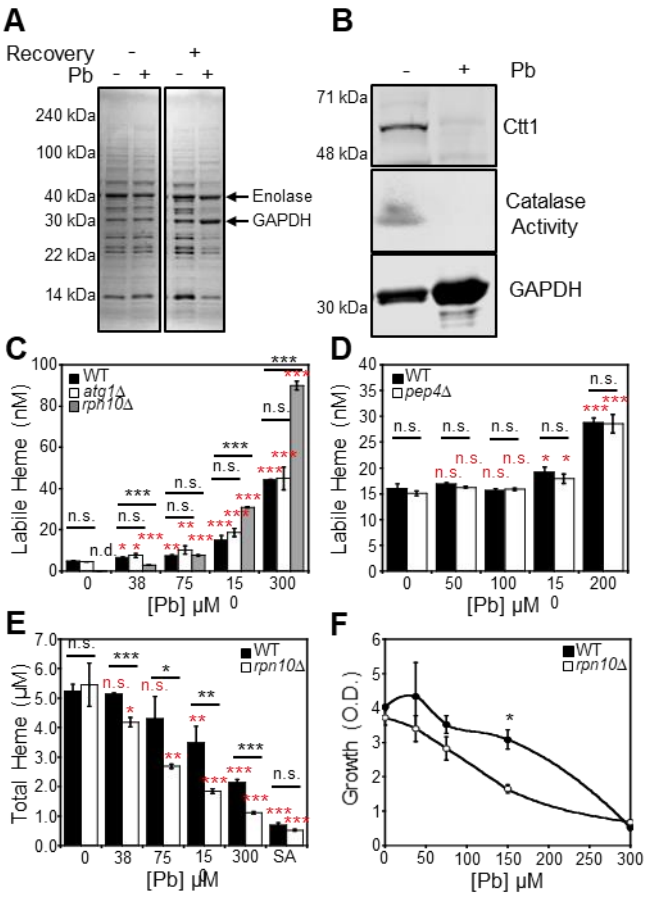

Figure 3.12 - Pb^{2+}-dependent changes in heme homeostasis correlate with the degradation of a large fraction of the proteome and are affected by the proteasome. (**A**) SDS-PAGE and Coomassie staining of lysates prepared from cells conditioned with or without an LD50 dose of Pb^{2+}, 100 μM, that did or did not undergo a post- Pb^{2+} exposure recovery period. Tandem mass spectrometry reveals that the high intensity chromatic bands that are retained under Pb^{2+}-stress, indicated by the arrows, are GAPDH and enolase (Table 1). (**B**) The expression and activity of the high affinity hemoprotein Ctt1p, a heme-catalase enzyme, is down-regulated in response to Pb^{2+} conditioning, whereas GAPDH expression, a constituent of the labile heme buffer, is maintained. All gels are representative of at least three independent cultures. (**C** and **D**) The effects of atg1Δ (**C**), rpn10Δ (**C**), and pep4Δ (**D**) deletion on Pb^{2+}-dependent changes in labile heme were assessed. (E and F) Pb^{2+}-dependent changes in total heme (**E**) and growth (**F**) were assessed in WT and rpn10Δ cells. All labile and total heme measurements represent the mean ± SD of triplicate cultures, whereas the growth data represent the mean ± SD of duplicate cultures. Statistical significance was assessed using a two-sample t-test. Black asterisks represent the statistical significance between the indicated pairwise comparisons of conditions and red asterisks represent the statistical significance relative to 0 μM [Pb]. * $P < 0.05$, ** $P < 0.01$, *** $P < 0.001$, n.s. not significant, n.d. not detectable.

Table 1 - Mass spectrometry-based protein identification of enolase and GAPDH from the SDS-PAGE gel depicted in Figure 3.12 (Hyojung Kim[167]).

Gel Band	#	Accession	Symbol	% Coverage	# Peptides	PSMs	MW [kDa]	Score Sequest HT
Upper	1	YHR174W	ENO2	65.68	19	381	46.89	1154.83
	2	YGR254W	ENO1	60.87	17	170	46.79	517.04
Lower	1	YGR192C	TDH3	43.67	9	111	35.72	357.34
	2	YJR009C	TDH2	39.76	10	106	35.82	334.19
	3	YJL052W	TDH1	46.99	12	77	35.73	254.91

3.8 Investigation of Heme Binding Proteins in Untreated vs. Pb^{2+}-shocked Cells

Up to this point, using our models of heme inhibition with SA, heme chelation by Cyt b_{562} induction, and Pb^{2+} poisoning we have divulged a great deal of details underpinning how yeast handle heme under stress. Specifically regarding Pb^{2+} poisoning, we revealed that Pb^{2+} increases cellular LH but decreases total heme, and tight binding hemoproteins like catalase among others, (data not shown), are turned over while labile heme buffering protein GAPDH is preserved. Additionally, the LH preserved under Pb^{2+} stress sustains heme signaling (Figure 3.4, Figure 3.12). Further, we have unveiled that the proteasome, which is positively regulated by Pb^{2+}, positively regulates LH availability and that the loss of proteasomal function by *RPN10* deletion sensitizes cells to Pb^{2+} dependent effects on heme homeostasis (Figure 3.12). Given all these details, and specifically that heme signaling is maintained while heme and hemoprotein availability are drastically altered between non-stressed and Pb^{2+} stressed cells, we sought to reveal what proteins are binding and releasing heme in response to stress to reveal new heme signaling networks in yeast.

To do so, we optimized the use of hemin agarose beads to affinity purify hemoproteins from cellular lysates in hopes of identifying proteins that bind or release heme in response to Pb^{2+} stress. We did this under two assumptions. 1.) These proteins that are binding and releasing heme in response to Pb^{2+} stress, by definition, are part of a heme signaling network. 2.) With this approach, proteins that change in their heme speciation or fractional saturation upon stress (Pb^{2+} poisoning) will bind differently to hemin agarose (Figure 3.13), and the abundance by which they are affinity purified with hemin agarose between two conditions reflects the relative change in fractional saturation of that protein with heme. To do this, we optimized hemin agarose chromatography methods (See Appendix) coupled to quantitative mass spectrometry (LC MS-MS) to assess the heme speciation of proteins eluted from hemin agarose beads to identify new heme binding factors involved in heme signaling.

3.8.1 Validating Approach: Hemin Agarose Binding Apo-hemoprotein

To test our approach and functional assumptions of hemin agarose illustrated in Figure 3.13, we sought to determine how well the canonical hemoprotein myoglobin would stick to hemin agarose in its unbound versus heme loaded state. 1-D PAGE analysis of elutions from hemin agarose beads treated with apo-myoglobin with and without co-treatment of hemin reveal that only apo-myoglobin sticks to the hemin agarose beads (Figure 3.14). These results served as an initial validation of our approach. See Appendix for more details regarding optimization of preparing, treating, and eluting heme-binding proteins off the beads.

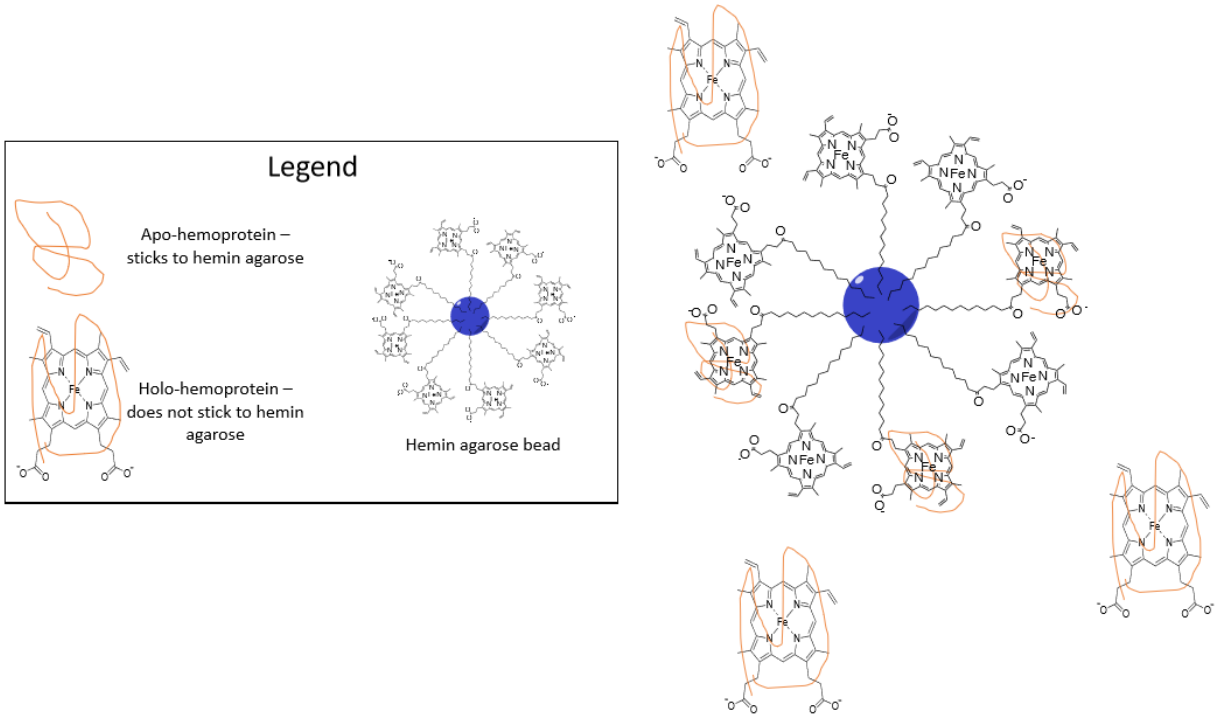

Figure 3.13 – Cartoon representation of hemin agarose beads, detailing that heme saturated, holo-hemoproteins will not stick to hemin agarose beads, while heme vacant, apo-hemoproteins will bind to hemin agarose.

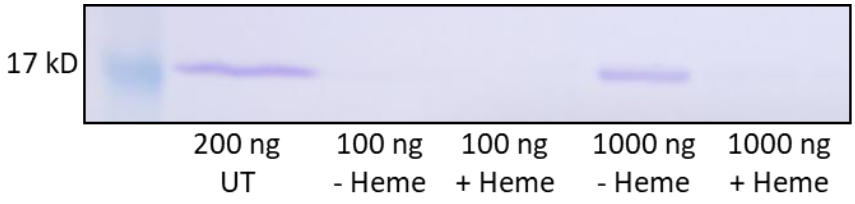

Figure 3.14 – Elution of myoglobin off of hemin agarose beads. Each heme treated sample received 30 equivalents of heme to be co-incubated with the hemin agarose beads.

From here, we further tested our original hypothesis that hemin agarose would preferentially bind with heme binding proteins based on their heme load using cellular lysates. To do this, cellular lysates from heme deficient *hem1Δ* cells and WT cells treated with and without a low or high dose of heme biosynthesis inhibitor SA to starve cells of heme were treated with hemin agarose to interrogate whether heme availability to these cells' proteins impacts their ability to bind heme (Figure 3.15). The same lysates were

treated with sepharose control beads to ensure that any eluted protein stuck to hemin agarose because of an interaction specific to the heme of the hemin agarose bead matrix (Figure 3.13, Figure 3.15). Fitting to our model, there are at least 8 noticeable protein bands visible in both contrast settings displayed in Figure 3.15 that bind hemin agarose better when extracted from heme starved cells (WT + 500 µM SA or *hem1Δ* cells) with very little abundance in the sepharose bead elutions. Interestingly, only complete depletion of heme availability by 500 µM SA, and not partial depletion by 100 µM SA treatment, has these 8 proteins bind hemin agarose more effectively (Figure 3.15).

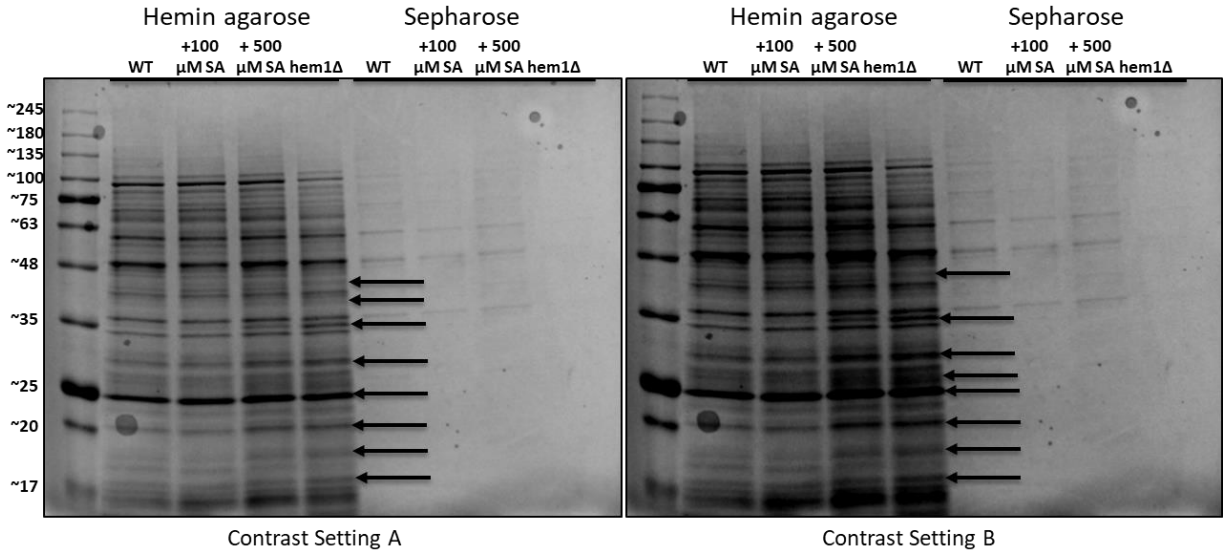

Figure 3.15 – Hemin agarose versus sepharose treated lysates from WT ± SA and *hem1Δ* cells analyzed by 1-D PAGE. Results are displayed with two different contrast settings. Bands that increased in abundance in hemin agarose elutions in heme depleted cells are pointed out with black arrows. Protein bands detected in hemin agarose treated lysates far outweigh those from sepharose treated lysates.

3.8.2 SILAC Labelling and Analysis of Heme Binding Proteins by Hemin Agarose versus Sepharose Chromatography

Given that our model and hypothesis that proteins would stick to hemin agarose preferentially based on their heme load was consistent with both analyses with myoglobin experiments and with cellular lysates (Figure 3.14, Figure 3.15), we sought to apply our hemin agarose and sepharose bead chromatography methods to study heme speciation of proteins between untreated (-Pb) vs Pb^{2+} poisoned (+Pb) cells. To comprehensively distinguish proteins that are binding or releasing heme between -Pb vs +Pb cells we devised a means to couple our hemin agarose chromatography (HAC) methods with stable isotope labeling by amino acids in cell culture (SILAC) to accurately quantify the differences in all affinity purified proteins eluted from the beads. Given the extreme differences in protein expression observed by 1-D PAGE and whole proteome (WP) analysis (Figure 3.12A, Figure 3.17A), it would be difficult to directly compare the protein abundances resulting from hemin agarose treated with -Pb or +Pb cellular lysates directly. Instead, we devised a means to use SILAC labeling to characterize the heme-binding specificity of proteins, operationally defined as the ratio of protein eluted from hemin agarose vs sepharose, measured in both -Pb lysates and +Pb lysates independently (Figure 3.16, See 3.10.3 for relevant details on our model of Pb^{2+} toxicity). Utilizing this approach, the heme binding specificity of each identified protein was plotted to compare the relative abilities of each protein to bind heme under -Pb and +Pb conditions (Figure 3.17).

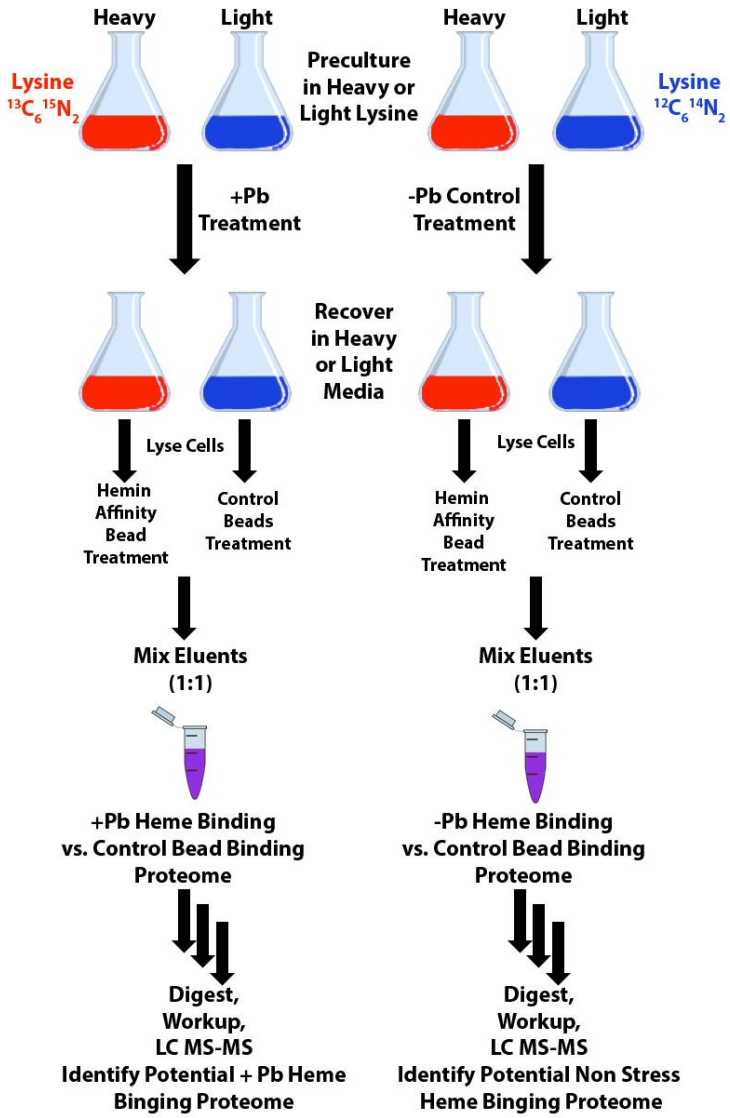

Figure 3.16 – Cartoon for SILAC growth of cells coupled to Pb^{2+} shock protocol and LC MS-MS to identify heme binding proteins in Pb^{2+} (+Pb) shocked versus non-Pb^{2+} (-Pb) treated cells. To identify specific binders of heme in Pb^{2+} treated cells, a heavy ($^{13}C_6$,$^{15}N_2$ lysine) and light ($^{12}C_6$,$^{14}N_2$) culture of cells, were grown, both subject to Pb^{2+} treatment, allowed to recover, and lysed. The lysates from the light labeled samples were treated with sepharose beads, while the heavy labeled cellular lyates were treated with hemin agarose beads. A 1:1 volume ratio of the eluents from the light labeled, sepharose treated cells was mixed with with the eluents from the heavy labeled, hemin agarose treated cells. This elution was prepped for and analyzed by LC MS-MS and the proteins that bound to hemin agarose but not sepharose beads were deemed putatitive heme binding proteins. The same procedure was conducted in tandem for the non-Pb^{2+} treated cells.

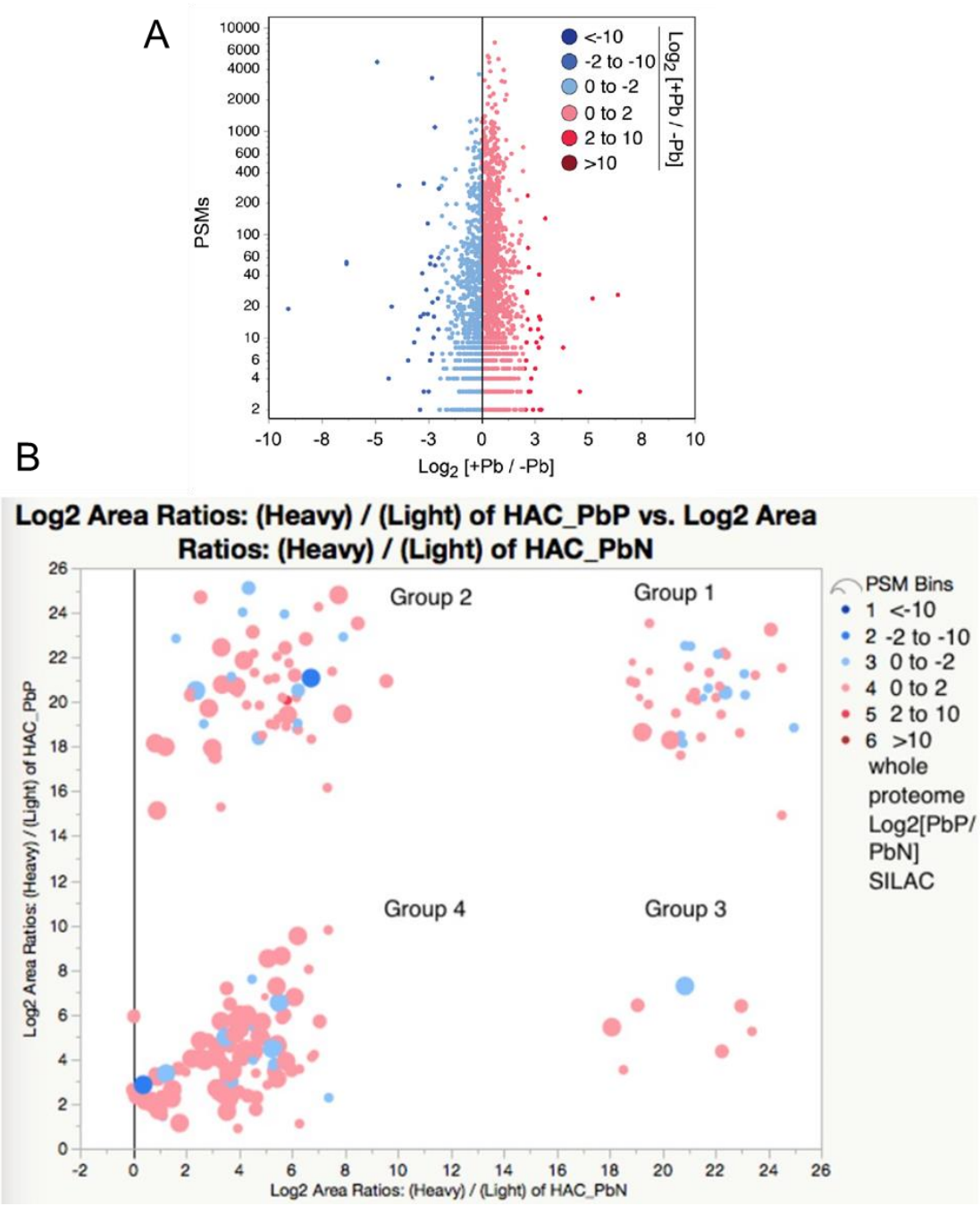

Figure 3.17 – Proteomics analysis of global protein expression and fractionally saturated heme proteins in nontreated (-Pb or PbN) versus to Pb^{2+} treated (+Pb or PbP) cells. (**A**) Whole proteome (WP) analysis of the relative abundance of proteins between -Pb and +Pb treatment conditions on a Log_2 scale. Blue circles represent proteins that decreased in abundance in response to Pb^{2+} treatment, and red circles represent proteins with increased abundance to Pb^{2+} treatment. The results indicate that protein expression changes dramatically following Pb^{2+} treatment. The WP analysis helped filter changes in protein binding to hemin agarose between -/+ Pb conditions by controlling for loss or

gain in protein abundance. (**B**) Results of SILAC labeled hemin agarose chromatography (HAC) proteomics study in both +Pb (y-axis, PbP_HAC) and -Pb (x-axis, PbN_HAC) treated cells. The hemin agarose specificity, a measure of protein abundance from hemin agarose divided by the protein abundance from sepharose elutions, from +Pb lysates was plotted against those from -Pb lysates as a Log_2 ratio. Only the proteins detected from HAC analysis in both +Pb and -Pb treatment conditions were plotted. The graphed proteins fall into 4 main groups identified in the plot. In the legend on the right, the changes in general protein abundance measured from the WP are indicated in color, and the size of the circles are direct measure of the PSM values from the WP analysis. The WP analysis metrics were essential in deciding how much a protein's change in affinity for hemin agarose was a measure of heme specificity or not, and therefore, proteins without WP detection, were excluded from analysis in panel B. This data was generated with eluents provided to Hyojung Kim and Matthew Torres, who provided this graph.

The eluted protein abundances from the heavy labeled hemin agarose were ratioed against their light labeled negative control sepharose bead abundances to give them a measure of specificity for hemin agarose, which is ideally a direct measure of their heme specificity. The resulting heme specificities, or the ratio of hemin agarose to sepharose enrichment, for the Pb^{2+} treated cells (y-axis, HAC_PbP) were plotted against those for the untreated cells (x-axis, HAC_PbN) in order to assess how the heme specificity of proteins change in response to Pb^{2+} treatment (Figure 3.17B). Only proteins that were detected by WP analysis were included in Figure 3.17B so that the changes in protein abundance in the HAC study can be assessed to be from changes in ability to be preferentially enriched by hemin agarose rather than from a change in general protein abundance between -Pb and +Pb conditions, which is quiet variable (Figure 3.17A).

Proteins that were not enriched by sepharose in either -Pb, +Pb, or both conditions represent Groups 3, 2, and 1 proteins, respectively (Figure 3.17B). When a protein was not detected in the sepharose eluents, its value for sepharose enrichment was set to a 1, yielding higher hemin agarose to sepharose enrichment ratios for many proteins in Groups 1 through 3. Group 4 proteins, on the other hand, were enriched by both hemin

agarose and sepharose with and without Pb^{2+} treatment. For these reasons, the Groups 1 to 3 protein lists were deemed more likely to contain heme binding proteins than Group 4 proteins. Even so, Group 4 proteins should not be ignored as there plenty of proteins with heme agarose to sepharose enrichment ratios that are greater than 6 on a Log_2 scale, and the heme binding chaperone protein GAPDH was identified in this group.

All in all, Group 1 proteins bind to hemin agarose specifically under both treatment conditions. Group 4 proteins may contain heme binding proteins but were enriched by both hemin agarose and negative control sepharose beads. Group 2 proteins bind to hemin agarose specifically only under Pb^{2+} treatment conditions; and therefore, Group 2 is hypothesized to contain proteins that have lost their heme in response to Pb^{2+} stress, increasing their capacity to bind to hemin agarose. Conversely, Group 3 proteins are those that only bind to hemin agarose without Pb^{2+} treatment; therefore, Group 3 proteins are hypothesized to have lost the ability to bind to hemin agarose post Pb^{2+} treatment by acquiring heme in response to Pb^{2+} stress. In total, Groups 1 to 4 represent a putative heme binding proteome in yeast, Groups 1 to 3 are easier to prioritize given their lack of enrichment with sepharose beads, and Groups 2 and 3 represent putative heme binding proteins whose fractional saturation with heme changes dramatically as a function of Pb^{2+} stress.

3.8.3 PANTHER Analysis of Group 2 and 3 Putative Heme Binding Proteomes

Given the evidence supporting Groups 2 and 3 proteins to heme binding proteins involved in heme signaling and/or trafficking in responses to stress we analyzed them by PANTER pathway analysis to investigate what types of proteins were identified by

molecular function (Figure 3.18, Figure 3.19), biological process (Figure 3.20), and protein class (Figure 3.21).

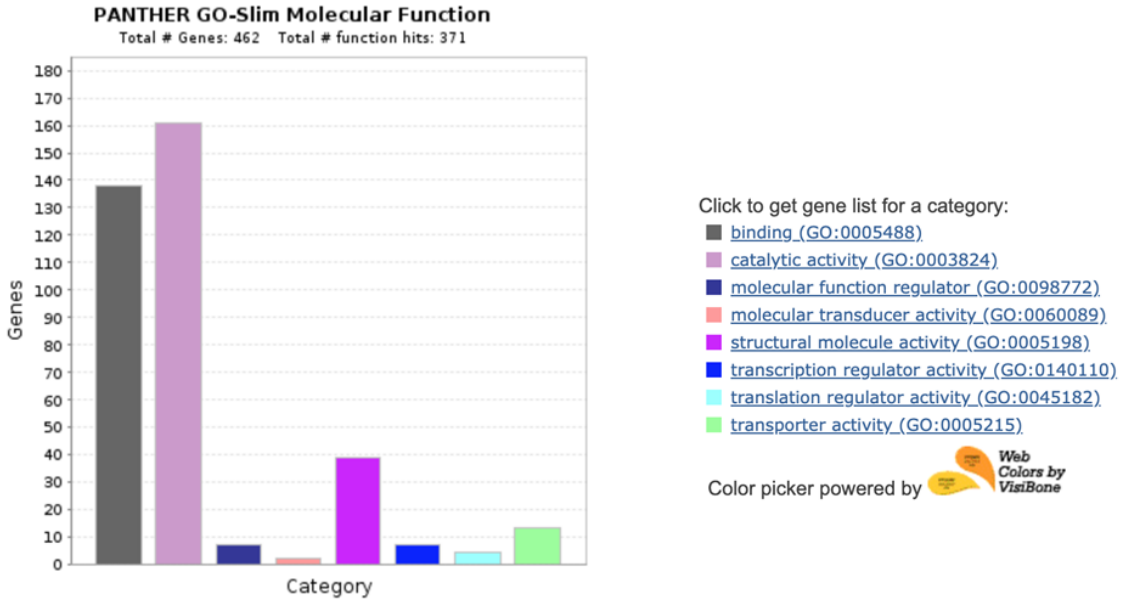

Figure 3.18 - Groups 2 and 3 catalytic proteins analyzed for their molecular function using PANTHER.

The largest subset of molecular functions ascribed to Group 2 and 3 proteins were either the class of having catalytic activity, which are further analyzed in Figure 3.19, or binding (Figure 3.18). The major class of binding proteins identified were of the class heterocyclic compound binding (77 proteins, GO:1901363), which were all nucleoside and nucleotide binding proteins. This is an overrepresented class of proteins involved in DNA and RNA binding, including many ribosomal subunits. The second major class of binding proteins identified includes proteins that are involved in protein binding (47 proteins, GO:0005515), including cytoskeleton protein binding (GO:0008092), enzyme binding (GO:0019899), unfolded protein binding (GO:0051082), heat shock protein binding (GO:0031072), and transcription factor binding (GO:0008134) among several

others. In total, the most abundant molecular functions of the identified proteins include enzymatic activity, interacting with other proteins, controlling translation and transcription, and facilitating transport within the cell (Figure 3.18).

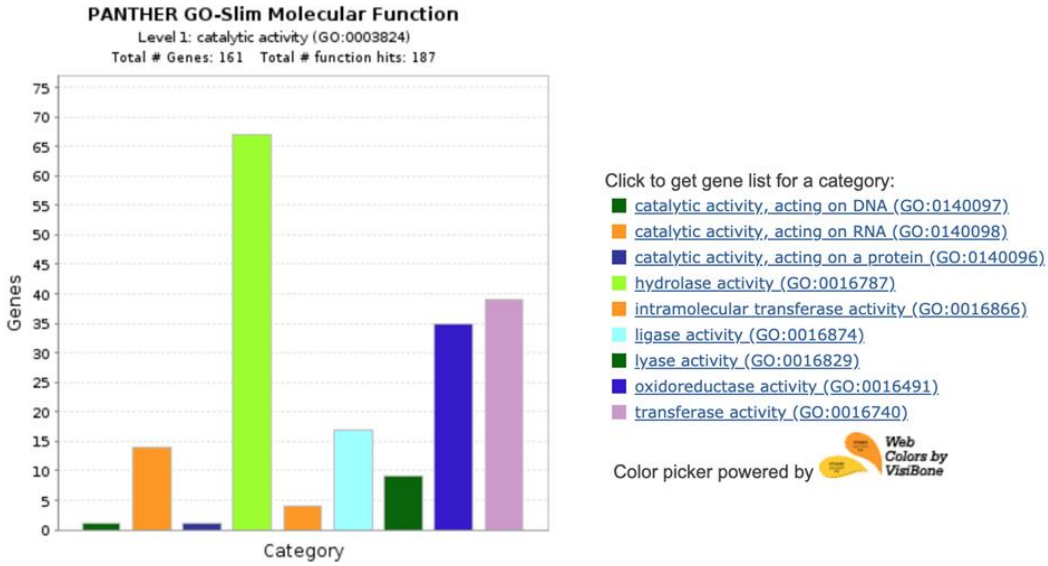

Figure 3.19 - Groups 2 and 3 catalytic proteins analyzed for their molecular function using PANTHER. The 161 catalytic proteins identified in Figure 3.18 where analyzed here for their specific catalytic function.

Of the catalytic proteins identified, the most abundant enzyme activity identified was hydrolase activity, oxidoreductase activity, and transferase activity. The proteins with transferase activity are those involved in the transfer of phosphorous containing groups, acyl groups, and several other organic functional groups (Figure 3.19).

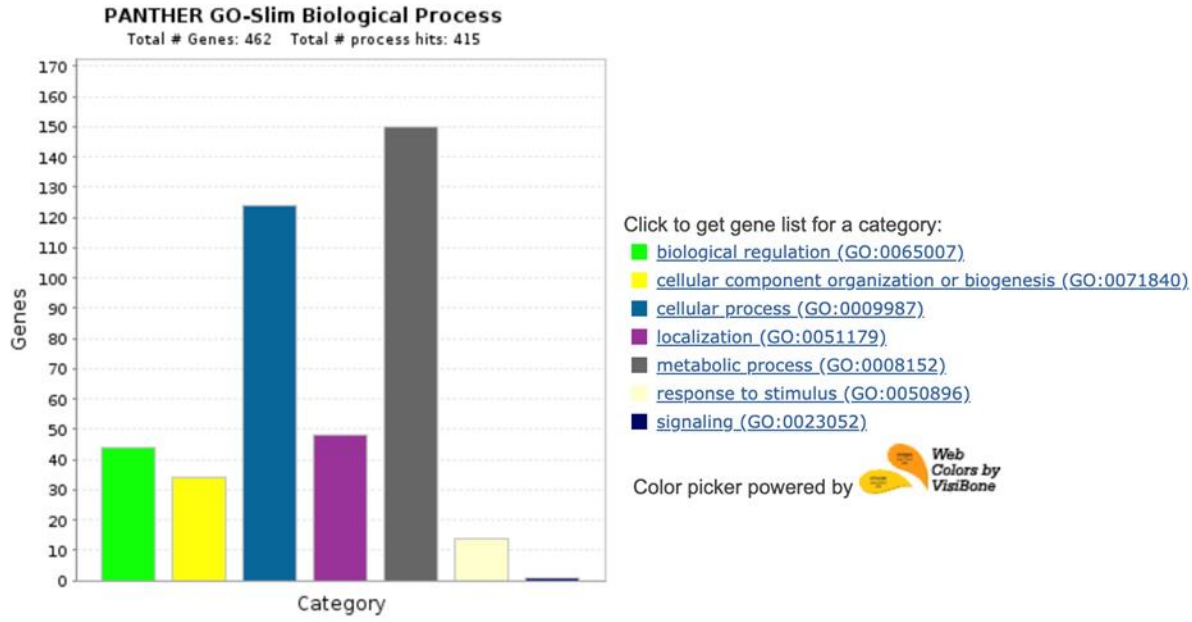

Figure 3.20 - Groups 2 and 3 proteins analyzed by biological process.

Grouping proteins by their biological process revealed that most identified proteins are involved in regulating metabolic and cellular processes (Figure 3.20). A breakdown of these processes reveal that the main biological processes regulated by these proteins include gene expression (57 proteins, GO:0010467), organelle organization (29 proteins, GO:0006996), translation (28 proteins, GO:0006412), amino acid biosynthesis (19 proteins, GO: 0008652), macromolecule catabolic processes (15 proteins, GO:0009057), and cofactor metabolic processes (14 proteins, GO:0051186).

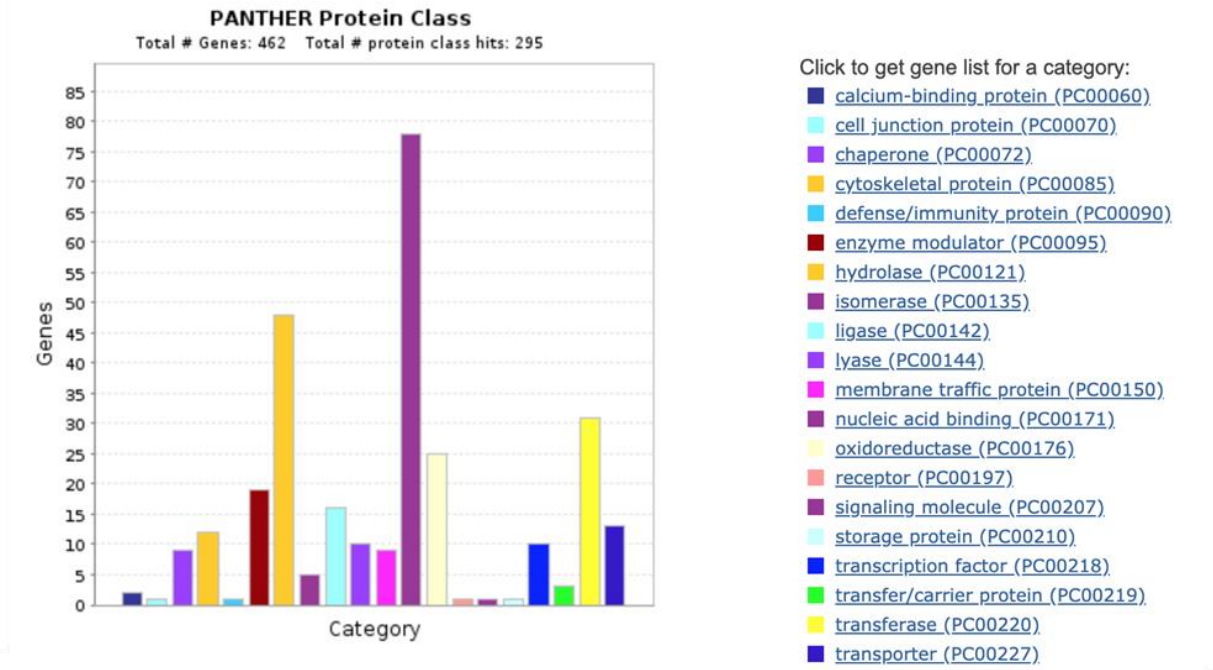

Figure 3.21 - Groups 2 and 3 proteins analyzed by Protein Class.

Additional organization by protein class further reveals the diversity of the identified proteins. Relevant to nutrient trafficking and signaling there were 13 transporters, 3 transfer/carrier proteins, 30 transferases, 9 membrane trafficking proteins, 1 storage protein, 10 transcription factors, and 7 proteins with transcription regulatory activity (Figure 3.21).

Lastly organizing proteins based on pathways using PANTHER's organization by GO:Terms reveals an exhaustive list of 149 pathways affected by these proteins. For brevity, the top 7 pathways affected were (1) ubiquitin proteasome pathway, (2) a pathway ascribed to Parkinson's disease, (3) the EGF receptor signaling pathway, (4) purine biosynthesis, (5) genes implicated in Huntington's disease (6) inflammation mediated by chemokine and cytokine signaling pathway, and the (7) integrin signaling pathway. The most represented pathway, the ubiquitin proteasome pathway included 9

subunits of the 26 S proteasome, and the Parkinson's disease pathway included several genes involved in nutrient trafficking, proteasomal proteins, stress response, and signaling proteins, including a 14-3-3 protein and a mitogen activated protein kinase.

3.9 Discussion

Heme synthesis and degradation is tightly coordinated so as to minimize the accumulation of potentially cytotoxic "free" or labile heme (LH)[13, 44, 46]. As a consequence, the concentration and physiological role of LH in biology has been controversial[2, 49]. While estimates for the concentration of LH across various cell types have spanned sub-pM to μM quantities[2, 44, 49, 183, 184], the use of genetically encoded heme sensors in yeast and various non-erythroid human cells lines have established a consensus range for cytosolic LH that spans 10-100 nM, representing up to 10% of the total heme concentration[29, 111]. However, few studies have directly probed the contribution of steady-state LH as a heme source for hemoproteins and heme signaling. Herein, we established a functional role for LH in regulating heme signaling and demonstrated that LH is preferentially consumed relative to total heme when cells become heme depleted.

We find that modestly depleting total heme by 25% with succinylacetone, an inhibitor of the second enzyme in the heme biosynthetic pathway, ALAD, results in a much larger perturbation to LH, depleting it more than 10-fold, from 10 nM to < 1 nM, possibly as low as ~ 2 pM (Figure 3.2). The sensitivity of the LH pool towards heme depletion relative to total heme is an indication that LH is mobilized to support heme-dependent processes when cells are confronted with diminished heme synthesis. In other words, LH re-equilibrates with other high-affinity and/or poorly exchangeable heme

binding sites that may become vacant when heme is depleted. These results are consistent with prior pulse-chase experiments that utilized radiolabelled ALA and/or heme sources to demonstrate that P450 enzymes equilibrate with LH[152]. Altogether, these observations may have significant implications for conceptualizing new heme-based therapies for porphyrias, a family of inherited disorders associated with defects in heme biosynthesis. For instance, treatment methods designed to increase LH via supplementation with appropriate heme complexes may form the basis for alleviating the symptoms of heme scarcity[185].

In order to address the role of LH on heme dependent functions, we induced a site-specific heme chelator in the cytosol via the overexpression of Cyt b_{562} and assessed its effect on heme signaling through the yeast heme regulated transcription factor Hap1 (Figure 3.1). We found that sequestration of LH inhibited Hap1 activity, demonstrating that LH can control heme-signaling processes. Importantly, these results indicate that increasing heme synthesis, a metabolically demanding process, is not the only means to activate heme signaling, as was previously suggested for activation of Hap1[143, 186] and metabolic cycling in yeast[187, 188], as well as heme regulation of the circadian clock through the nuclear receptors, Rev-erb-α and Rev-erb-β, in mammals[35].

In order to understand the relationship between total heme, LH, and heme signaling during adaptation to cellular stress, we subjected yeast cells to an environmentally-relevant toxicant well known to affect heme homeostasis, Pb^{2+}[163]. In yeast, Pb^{2+} toxicity suppresses metabolic activity and proliferation through a mechanism that requires new protein synthesis[166]. In addition, mitochondria are a major target of Pb^{2+} toxicity and are the source of Pb^{2+}-induced reactive oxygen species production (ROS)[189].

Heavy metal sequestration by vacuoles and binding to glutathione and metallothioneins are important detoxification pathways for Pb^{2+}[190].

A number of previously established yeast models for Pb^{2+} toxicity employ exposures spanning 0.1 – 10 mM, which is high relative to the 240 nM [Pb^{2+}] threshold in patient blood samples used to initiate public health actions[191], the 1 – 5 µM blood [Pb^{2+}] associated with inhibition of heme biosynthesis in humans[192, 193], or the 0.1 – 250 µM [Pb^{2+}] used in mammalian cell culture models of Pb^{2+} toxicity[194, 195]. However, it is important to note that the biochemical features of Pb^{2+} toxicity at these high concentrations in yeast phenocopy many of the hallmarks of Pb^{2+} toxicity in mammalian cell lines at lower concentrations[35, 166, 190, 196-198], including inhibition of heme synthesis (current work). The higher Pb^{2+} exposure concentrations required for yeast may reflect differences in Pb^{2+} uptake, efflux, or intracellular bioavailability.

While Pb^{2+} has the capacity to deplete cellular heme through its ability to inhibit two enzymes in the heme biosynthetic pathway, ALAD, also the target of SA, and FECH, and upregulate the expression of the heme-degrading enzyme HO[163-165], we found that, in yeast, Pb^{2+} significantly attenuates total heme primarily due to the inhibition of heme synthesis (Figure 3.8, Figure 3.11). However, rather surprisingly and paradoxically, we found that Pb^{2+} significantly increases LH (Figure 3.4C). When comparing heme synthesis inhibition between SA and Pb^{2+}, there is higher PPIX levels in Pb^{2+} treated cells indicating that FECH is inhibited by Pb^{2+}. If the mode of inhibition contributes to uncoupling LH from total heme, a potential explanation could be that Pb^{2+} may be affecting the proposed heme transport machinery that may associate with FECH and the heme synthesis metabolon[71]. Otherwise, given our previous findings that thiol-specific

alkylating agents impact the NO-mediated mobilization of LH[29] and the well documented interactions between Pb^{2+} and cysteine residues[199], we propose that Pb^{2+} may liberate heme in cells from certain thiol containing heme binding sites. Alternatively, since Pb^{2+}-induces the degradation of a large fraction of the proteome, the increase in LH could simply be a result of heme that is released from hemoproteins that are being turned-over. Consistent with this model, we found that a mutant that has a defect in proteasomal function, *rpn10*Δ, has less LH than WT cells (Figure 3.12C). However, it is unclear why *rpn10*Δ cells exhibit a greater magnitude increase in LH (Figure 3.12C) and decrease in total heme (Figure 3.12E) in response to Pb^{2+} stress. One explanation that could account for the former is that Pb^{2+} is directly or indirectly inducing the release of heme from a hemoprotein target that is stabilized due to the attenuation in proteasome function in *rpn10*Δ cells. Given that previous studies have demonstrated that Pb^{2+} positively regulates the proteasome[200] and heme and ALAD act as negative regulators of the proteasome[201, 202], there is a complex mosaic of competing effects that might account for the Pb^{2+}-dependent changes in heme homeostasis in WT and *rpn10*Δ cells. We are currently elucidating the molecular mechanisms underlying heme regulation of LH and the proteasome.

The Pb^{2+}-induced increase in LH seems to impact heme signaling via Hap1 (Figure 3.4D). Indeed, despite the attenuation in total heme concentration due to Pb^{2+} toxicity (Figure 3.4C), we still observe a level of Hap1 activity that is much greater relative to SA-mediated heme depletion (Figure 3.4D), which attenuates both LH and total heme (Figure 3.4C).

The observation of an increased LH pool in response to Pb^{2+} may have implications for the pathology of Pb^{2+} toxicity. For instance, the increase in LH in response to Pb^{2+} may contribute to a cytotoxic heme pool[44, 46] that leads to the oxidative stress associated with Pb^{2+} toxicity[203, 204]. Alternatively, given that there are a number of heme regulated transcription factors, kinases, and ion channels[2, 49], the increase in LH in response to Pb^{2+} may be required to activate heme-based signaling pathways important for adaptation to heavy metal stress. The specific physiological consequences of increased LH in response to Pb^{2+} stress remains to be fleshed out.

Interestingly, when optimizing and validating our methods to interrogate what proteins bind and release heme in response to stress, we found that a number of proteins preferentially stick to hemin agarose only when completely depleted of their cellular stores of heme by 500 µM SA treatment, but not with partial depletion with 100 µM SA treatment. The increased protein abundance detected between 100 and 500 µM SA treated cells may result from there still being approximately 30% total cellular heme and have LH buffered to less than 1 pM in the 100 µM SA cells, while the 500 µM SA cells are completely depleted of both total heme and LH (Figure 3.2). This suggests that the 8 protein bands that increase in affinity for hemin agarose under heme starvation, hold onto heme when cells are moderately heme starved and only release their heme when heme pools are completely depleted (Figure 3.15). Therefore, the identification of these proteins by our methods may only be possible under extreme heme depletion by SA or using *hem1Δ* cells, and their identities should be pursued as they may represent previously undisclosed, tight-binding heme trafficking factors or shed light on cellular processes for heme that are maintained even under heme limiting conditions.

To determine the specific roles and potential signaling networks employed by LH in response to Pb^{2+} stress, we sought to discover all of heme's specific heme binding partners in untreated versus LD_{50} Pb^{2+} poisoned cells by coupling SILAC with hemin agarose (heavy label) and sepharose bead (light label) chromatography (Figure 3.16). Identifying the differences in a protein's ability to stick specifically to hemin agarose between any two conditions that elicit dynamic responses in heme homeostasis, like untreated versus either NO (Ch. 2.7)[29] or Pb^{2+} poisoning, ideally represents a dynamic change in a protein's fractional saturation with heme in response to the induced signal (i.e. Pb^{2+}). Furthermore, the proteins identified to have any dynamic change in their fractional saturation with heme, by definition, are those that are involved in a heme signaling network by binding or releasing heme in response to that signal. Hence, our hemoprotein discover approach here was to identify any putative heme binding proteins that are changing in their heme fractional saturation in response to Pb^{2+} stress by identifying stark differences in protein heme binding capacity between the treated and untreated conditions. Ultimately, as identified in Figure 3.17B, when plotting the heme binding specificities of proteins in +Pb versus -Pb treated cells, we were able to identify differences in heme binding capacity of proteins. Indeed, we believe to have identified many putative hemoproteins in Group 2 that lost heme in response to Pb^{2+} stress, and therefore, stick to hemin agarose specifically only in Pb^{2+} treated cells (Figure 3.17B). And, conversely, in the smaller Group 3 list of proteins to have identified potential hemoproteins that gained heme in response to Pb^{2+} stress as indicated by their binding to hemin agarose under basal conditions but not in Pb^{2+} treated cells (Figure 3.17B). The proteins identified in Groups 1 and 4 should not be ignored, but Groups 2 and 3 proteins

were prioritized as they had the most adverse changes in their enrichment by hemin agarose relative to negative control beads in response to Pb^{2+} stress. Most prioritized proteins for screening fell into Group 2, which are hypothesized to have lost heme in response to stress. The fact that most proteins that stuck to hemin agarose seem to have lost heme in response to stress fits with our model that heme binding proteins should only be enriched by hemin agarose if their heme binding site is vacant (Figure 3.13). Additionally, this observation is consistent with the fact that most cellular heme is depleted in cells treated with this dose of Pb^{2+} and several canonical hemoproteins have their expression depleted in Pb^{2+} treated cells as indicated by our whole proteome analysis (data not shown). Pertaining to Group 3 proteins, consistent with the idea that these proteins gained heme in response to Pb^{2+}, is the fact that of 9 proteins that made our final list (Figure 3.17B), there was an isoform of the heme trafficking factor GAPDH, an iron regulated protein, and a negative regulatory of coenzyme A biosynthesis, which is required for the formation of ALA. The result regarding negative regulation of ALA synthesis is notable, because heme is known to repress ALA synthesis[205].

In support of proteins that were starkly enriched by heme agarose relative to negative control sepharose beads, within Groups 1 to 3 there were 16 heat shock proteins that stick to hemin agarose specifically in the dataset, which are of interest as there are several heat shock proteins that have implicated roles in heme trafficking[206-212]. Other promising proteins identified that may be bona fide heme binding proteins include proteins with enzymatic functions and sequence similarities to proteins identified in other species to be heme binding, including serine proteases[213-215] and alcohol dehydrogenases, which were shown to bind heme within crystal structures or at least have heme or

protoporphyrin modulated activity[216-219]. Lastly, a large subset of the proteins identified in these groups are involved in the proteasome, which heme has been shown to regulate by unknown mechanisms[201, 202]. Finally, there were a number of enzymes with reported oxidoreductase activity, which at minimum contain iron to carry out their activity and often have heme as a cofactor. Collectively, there is ample support from previous reports regarding many of our identified proteins being actual heme binding proteins. Given that the identified proteins from Groups 2 and 3 fall into classes involved in controlling gene expression, stress response, and transcription, or are transferases, transfer/carrier proteins, chaperones, and storage proteins helps solidify the notion that there may be proteins involved in direct roles in heme signaling and heme transport (Figure 3.18,Figure 3.20, Figure 3.21).

Altogether our design to interrogate the heme binding proteins that exist in untreated vs. Pb^{2+} treated cells resulted in the identification of two novel putative heme binding proteome lists. The first list, represented a list of heme specific proteins from non-stress conditions (x-axis, Figure 3.17) and the second list represented the putative heme binding proteome of cells that are recovering from an LD_{50} dose of $Pb(NO_3)_2$ (y-axis, Figure 3.17). Comparing these two heme binding proteomes resulted in the determination of Groups 2 and 3 in Figure 3.17, which represent the proteins that lost or gained heme in response to Pb^{2+}, respectively. In total, Group 2 and 3 proteins represent many candidate proteins that have the potential to be part of a heme signaling network required for cells to adapt to stress. Given the number of identified proteins and their diverse set of functions, future work entails screening prioritized proteins from each list via the development of heme binding assays and heme dependent enzymatic assays.

These screens are warranted given that some of the proteins identified having changes in heme specificity may solely be from Pb^{2+}-dependent, heme-independent reasons. One such reason would be Pb^{2+}-induced protein misfolding or protein hyper-oxidation that could allow these proteins to interact more favorably with hemin agarose independently of heme[189, 220]. Even so, confirming several promising protein hits as bona fide heme binding proteins would validate this approach to be used to identify heme signaling networks activated between any number of conditions that are known to mobilize heme, i.e. heme starvation (Figure 3.2), exogenous nitric oxide supplementation,[29] or in between two genetic backgrounds that have altered heme homeostasis, for example *tdh3Δ* vs WT cells[29].

Altogether, our studies demonstrate the functional importance of LH in heme utilization, especially during stress associated with heme depletion and Pb^{2+} toxicity. Our future work will involve probing the specific mechanisms by which LH can be coupled to heme utilization, as well as the mechanisms underlying the Pb^{2+} mediated increase in LH and the physiological consequences of this action. Furthermore, future work related to the putative heme signaling proteins identified in our screen entails using HS1 to elucidate the identified putative hemoproteins' effects on LH availability, design enzyme screens to screen many of the identified enzymatic proteins for heme dependent activity (Figure 3.19), and to canvas the role for the proteasome in regulating heme availability and signaling.

3.10 Materials and Methods

3.10.1 Yeast Strains, Transformations, and Growth Conditions

S. cerevisiae strains used in this study were derived from BY4741 (MATa, *his3*Δ1, *leu2*Δ0, *met15*Δ0, *ura3*Δ0). *pug1*::KANMX4, *hmx1*::KANMX4, *cta1*::KANMX4, and *ctt1*::KANMX4 strains were obtained from the yeast gene deletion collection (Thermo Fisher Scientific) and the *hem1*::HIS3 strain was described previously[29]. Yeast transformations were performed by the lithium acetate procedure[134]. Strains were maintained at 30 °C on either enriched yeast extract (1%)-peptone (2%) based medium supplemented with 2% glucose (YPD), or synthetic complete medium (SC) supplemented with 2% glucose and the appropriate amino acids to maintain selection[29]. Cells cultured on solid media plates were done so with YPD or SC media supplemented with 2% agar[29]. Selection for yeast strains containing the KanMX4 marker was done with YPD agar plates supplemented with G418 (200 μg/mL)[29]. WT cells treated with the heme synthesis inhibitor, succinylacetone (SA), and *hem1*Δ cells were cultured in YPD or SC media supplemented with 50 μg/mL of 5- aminolevulinic acid (ALA) or 15 mg/mL of ergosterol and 0.5% Tween-80 (YPDE or SCE, respectively)[29, 114].

For the proteomics studies, an auxotrophic yeast strain lacking lys1, lys1D::kanMX4 from the deletion library. This strain was provided by the Torres lab following verification that this was lys1D by playing on YPD vs. SD-Lys and found no growth on SD-Lys plates. See Appendix for growth conditions for SILAC labeling and the Pb^{2+} treatment using this strain.

3.10.2 Labile Heme and Total Heme Depletion

In order to sequester labile heme in the cytosol, we generated a WT yeast strain expressing an episomal plasmid (p316-GAL) containing an allele of the high affinity hemoprotein Cytochrome b_{562} (Cyt b_{562}) driven by the galactose-inducible promoter (pGAL); the plasmid is referred to as pGAL-Cyt b_{562}. A control strain expressing the empty vector (EV), (pGAL-EV), was also generated. For labile heme measurements, the strains expressing pGAL-Cyt b_{562} or pGAL-EV also co-expressed the previously described heme sensor, HS1-M7A, using an episomal plasmid (pRS415) that drives sensor expression with the GPD promoter[29]. For Hap1 activity measurements, the strains expressing pGAL-Cyt b_{562} or pGAL-EV also co-expressed the previously described pCYC1-EGFP Hap1 reporter, which is an episomal plasmid (pRS415) that drives EGFP expression using the CYC1 promoter, a transcriptional target of Hap1[29]. In order to induce Cyt b_{562} expression, cells were cultured in SC-URA-LEU media to maintain selection of both Cyt b_{562} and the heme sensor, HS1-M7A, or pCYC1-EGFP. Instead of using 2% glucose, which will repress the expression of the GAL-inducible promoter, we cultured cells in 2% raffinose and either 0.1% galactose (inducing conditions) or vehicle (sterile water, non-inducing conditions). Parallel control cultures were treated with 500 μM succinylacetone (SA) in order to deplete intracellular heme. All cultures were seeded at an initial optical density of $OD_{600\ nm}$ = 0.005 and cultured until cells reached a final density of $OD_{600\ nm}$ ~ 1.0, which typically took 14-16 hours. Following growth, cells were harvested, washed, and resuspended in phosphate-buffered saline (PBS) and sensor or EGFP fluorescence was measured as described in 3.10.5, *"Labile heme quantification"* and 3.10.7, *"Hap1 activity"*.

In order to deplete total heme, cells were cultured with the indicated concentrations of the heme biosynthetic inhibitor, succinylacetone (SA), in an appropriate SCE drop-out media. All cultures were seeded at an initial optical density of $OD_{600\ nm}$ = 0.005 and cultured until cells reached a final density of $OD_{600\ nm}$ ~ 1.0, which typically took 14- 16 hours. Following growth, cells were harvested, washed, and processed for determination of labile or total heme as described in 3.10.5, *"Labile heme quantification"* and 3.10.6, "*Total heme quantification.*"

3.10.3 Yeast Model of Pb^{2+} Toxicity

Due to the insolubility of $Pb(NO_3)_2$ in yeast media, we subjected exponential phase yeast cells to varying doses of Pb^{2+} in MES buffer for 3 hours, a media in which $Pb(NO_3)_2$ is soluble. Cells were pre-cultured in an appropriate SC drop-out media to a final density of $OD_{600\ nm}$ ~ 1.0. Following washing with sterile water, cells were resuspended in 10 mM MES buffer containing varying concentrations of $Pb(NO_3)_2$ at a density of 1 OD/mL, and mixed every 15 minutes at 25 °C for 3 hours. Following exposure to Pb^{2+} in MES buffer, cells were thoroughly washed with sterile water, resuspended in an appropriate SC drop-out mixture to a final density of $OD_{600\ nm}$ ~ 1.0 and allowed to recover for 4 hours, while shaking at 220 RPM at 30 °C. Cell viability was measured by diluting the cells to an initial density of $OD_{600\ nm}$ = 0.01 in an appropriate SC drop-out media after the recovery phase and solution turbidity was recorded by measuring $OD_{600\ nm}$ after 20 hours of growth shaking at 220 RPM and 30 °C.

In order to assess the effects of Pb^{2+} toxicity in an anaerobic environment, the Pb^{2+} toxicity model described above was modified as follows: the Pb^{2+} exposure in MES

buffer was accomplished in de-gassed MES buffer with varying concentrations of Pb^{2+} in a COY anaerobic chamber maintained with an inert atmosphere of 95% N_2 and 5% H_2. Following Pb^{2+} exposure, cells were washed with sterile de-gassed water and allowed to recover in de-gassed SC media, all anaerobically in the COY anaerobic chamber. Cell viability was measured by diluting the anaerobic cultures into in an appropriate SC drop-out media after the recovery phase and solution turbidity was recorded by measuring $OD_{600\ nm}$ after 16 hours of growth shaking at 220 RPM and 30° C in air.

All analytical analyses, including for labile or total heme, was conducted immediately after the 3 hour Pb^{2+} exposure in MES buffer (pre- recovery) or after the 4 hour recovery in SC media (post-recovery).

3.10.4 Viability Measurements Using FUN-1

Cells were grown as indicated in 3.10.3, "*Yeast model of Pb^{2+} toxicity*". After conditioning cells in MES buffer with or without Pb^{2+}, 1 OD of cells were pelleted, washed once with 1 mL sterile Milli-Q water, and once with 500 µL of 10 mM HEPES (pH 7.2) with 2% Glucose (w/v) (HG Buffer). Cells were pelleted again then resuspended in 300 µL of HG buffer, then treated with 24.5 µL of 200 µM FUN-1 (Thermo-Fisher) to a final concentration of 15 µM. The 200 µM FUN-1 working stock solution was prepared by diluting a 10 mM DMSO FUN-1 stock solution into HG buffer. Cells were allowed to incubate in the dark at 30 °C for 30 minutes and then washed three times in HG buffer. Cells were imaged on glass slides with cover slips using the Cytation 3 imaging plate reader (Biotek) with GFP and TexasRed Filter Cubes. In stained cells, the observation of red puncta was used to score viable cells and the observation of diffuse green

fluorescence was used to score dead cells. On average, ~100 cells were analyzed per sample.

3.10.5 Labile Heme Quantification

Measurements of labile heme were accomplished as previously described (Chapter 2.11.3.3)[29]. For all heme sensor fluorescence measurements, following cell growth, cells were washed in water and resuspended in phosphate-buffered saline (PBS) at a density between 3 and 5 $OD_{600\ nm}$ /mL, or 6 x 10^7 to 1 x 10^8 cells/mL. Fluorescence was recorded on a Synergy Mx multi-modal plate reader using black Greiner Bio-one flat bottom fluorescence plates. EGFP and mKATE2 fluorescence was recorded using excitation and emission wavelength pairs of 488 nm and 510 nm and 588 nm and 620 nm, respectively. Background fluorescence of cells not expressing the heme sensors were recorded and subtracted from the EGFP and mKATE2 fluorescence values. The sensor EGFP/mKATE2 fluorescence ratio (R_{expt}) is a qualitative indicator of labile or bioavailable heme, with a low ratio indicating a high concentration of labile heme and a high ratio indicating a low concentration of labile heme.

For quantitative labile heme monitoring, we can convert R_{expt} values to the fractional heme saturation of the sensor (% Heme Bound) (Equation 5) or, if the sensor heme dissociation constant is known (K_d), the concentration of labile heme (Equation 2). Both metrics require that the EGFP/mKATE2 sensor fluorescence ratio is known when the sensor is 100% bound (R_{max}) or 0% bound (R_{min})[29]. Based on a 1:1 heme-binding model, the fractional saturation, % Bound, of the sensor can be calculated according to Equation 3[29]:

$$[\%Bound] = ([R - R_{min}]/[R_{max} - R_{min}]) * 100 \quad (3)$$

$$[heme] = K_d \times \frac{R_{expt} - R_{min}}{R_{max} - R_{expt}} \left(\frac{F_{min}^{mKATE2}}{F_{max}^{mKATE2}}\right) \quad (2)$$

The labile heme concentration can be calculated according to Equation 2[29, 116]:

R_{expt} is the EGFP/mKATE2 fluorescence ratio under any given experimental condition, R_{min} is the EGFP/mKATE2 fluorescence ratio when 0% of the sensor is bound to heme, R_{max} is the EGFP/mKATE2 fluorescence ratio when 100% of the sensor is bound to heme, $F^{mKATE2}{}_{min}$ is the mKATE2 emission intensity when 0% of the sensor is bound to heme, and $F^{mKATE2}{}_{max}$ is the mKATE2 emission intensity when 100% of the sensor is bound to heme. The $F^{mKATE2}{}_{min}$ / $F^{mKATE2}{}_{max}$ ratio is typically taken to be 1 given that mKATE2 fluorescence emission is not significantly perturbed upon heme binding to the sensor[29]. Determination of R_{max} and $F^{mKATE2}{}_{max}$ involves recording EGFP and mKATE2 fluorescence after digitonin permeabilization of cells and incubation with 50 μM heme. Briefly, 3 to 5 $OD_{600\ nm}$/mL of cells are resuspended in PBS with 100 μg/mL of digitonin, 1 mM ascorbate, and 50 μM hemin chloride. After a 30 minute incubation at 30°C, cells are harvested, washed, and resuspended in PBS buffer prior to recording of fluorescence. Given that the high affinity heme sensor, HS1, is quantitatively saturated with heme and its fluorescence properties are virtually identical to HS1-M7A, we can also determine R_{max} and $F^{mKATE2}{}_{max}$ from parallel WT cultures expressing HS1[29].

Determination of R_{min} and $F^{mKATE2}{}_{min}$ involves recording EGFP and mKATE2 fluorescence after cells are treated with the heme biosynthesis inhibitor succinylacetone (SA)[138] or from *hem1*Δ cells cultured in parallel[29].

3.10.6 Total Heme Quantification

For more detailed methods with technical instructions, see Appendix.

Measurements of total heme were accomplished using a fluorometric assay designed to measure the fluorescence of protoporphyrin IX upon the release of iron from heme as described previously[221]. For all total heme measurements, following cell growth, 2 × 108 cells were harvested, washed in sterile water, and resuspended in 500 μl of 20 mM oxalic acid and stored in a closed box at 4 °C overnight (16–18 h). Next, an equal volume (500 μl) of 2 M oxalic acid was added to the cell suspensions in 20 mM oxalic acid. The samples were split, with half the cell suspension transferred to a heat block set at 95 °C and heated for 30 min and the other half of the cell suspension kept at room temperature (∼25 °C) for 30 min. All suspensions were centrifuged for 2 min on a table-top microcentrifuge at 21,000 × g, and the porphyrin fluorescence (excitation 400 nm, emission 620 nm) of 200 μl of each sample was recorded on a Synergy Mx multimodal plate reader using black Greiner Bio-one flat-bottom fluorescence plates. Heme concentrations were calculated from a standard curve prepared by diluting 500–1500 μM hemin chloride stock solutions in 0.1 M NaOH into MilliQ water, which was then added back to extra cell samples as prepared above. To calculate heme concentrations, the fluorescence of the unboiled sample (taken to be the background level of protoporphyrin IX) is subtracted from the fluorescence of the boiled sample (taken to be the free base

porphyrin generated upon the release of heme iron). The cellular concentration of heme is determined by dividing the moles of heme determined in this fluorescence assay and dividing by the number of cells analyzed, giving moles of heme per cell, and then converting to a cellular concentration by dividing by the volume of a yeast cell, taken to be 50 fL[29]. This fluorescence assay gives similar qualitative trends between samples as an HPLC assay for heme we employed previously[29], but the absolute concentrations tend to be consistently 3–5-fold higher (data not shown).

3.10.7 Hap1 Activity

After growth, cells expressing p415- *CYC1-EGFP*, or *EGFP* driven by the Hap1 regulated *CYC1* promoter, were washed in sterile water and resuspended in PBS to a concentration of 1 x 10^8 cells/mL and 100 uL was used to measure EGFP fluorescence (ex. 488 nm, em. 510 nm). Background auto-fluorescence of cells not expressing EGFP was recorded and subtracted from the p415-*CYC1-EGFP* expressing strains. In order to account for heme/Hap1 independent changes in EGFP expression/fluorescence, we also cultured cells expressing p415-*GPD-EGFP*, a plasmid expressing EGFP under control of the heme/Hap1 independent *GPD* promoter.

3.10.8 Immunoblotting

After culturing, cells were harvested, washed in ice-cold Milli-Q water, and lysed in two pellet volumes of phosphate buffer supplemented with protease inhibitors as described previously[29, 139]. Lysis was achieved at 4 °C using one pellet volume of zirconium oxide beads and a bead beater (Bullet Blender, Next Advance) on a setting of 8 for 3 minutes[29]. Lysate protein concentrations were determined by the Bradford method

(Bio-rad) and 14% tris-glycine gels (Invitrogen) were employed for SDS-PAGE[29]. α-GAPDH rabbit polyclonal antibodies (Genetex, GTX100118) and a goat α-rabbit secondary antibody conjugated to a 680 nm emitting fluorophore (Biotium) were used to probe for GAPDH. Yeast cytosolic catalase, Cttp1, was probed using a custom antibody generated by Genscript's custom antibody service (Poly Express Premium Service, SC1676). An α-Ctt1p antibody was raised in rabbit against a 1-320 amino acid fragment of Ctt1p. The α-Ctt1p antibody was validated in yeast by comparing immunoreactivity between WT, *ctt1*Δ, and *cta1*Δ cells, the latter being a deletion mutant of a peroxisomal/mitochondrial catalase, Cta1p, unrelated to Ctt1p[167]. All gels were imaged on a LiCOR Odyssey Infrared imager[29, 139].

3.10.9 Catalase Activity

After culturing, cells were harvested and lysed in phosphate buffer and 10 μg of protein lysate were subjected to native PAGE on a 10% tris-glycine gel (Invitrogen). After electrophoresis, an in-gel activity stain was utilized to measure catalase activity[26, 29]. Briefly, a catalase staining solution containing 1 part Dopamine (20mg/mL) in pH 8 0.2 M KPi buffer, 1 part para- phenylenediamine (3.5mg/mL) in pH 8 0.2M KPi, 1 part 15% H_2O_2, and 2 parts DMSO were mixed in the order listed. The staining solution was added directly to the gel and allowed to stain for 2 minutes, followed by rinsing in Milli-Q water and imaging.

3.10.10 Plasmids

All yeast expression plasmids used in this study are listed in Table 2 and were previously described, except for pDH039, the plasmid expressing Cytochrome b_{562} (Cyt

b_{562}) driven by a galactose (GAL)-inducible promoter, pGAL-Cyt b_{562}. This plasmid was constructed by amplifying the coding sequence of Cyt b_{562} from the HS1 sensor[29]. The following primers were utilized to amplify a BamHI/XbaI fragment of Cyt b_{562}:

prDH025: 5'-CCTTTGGTGGCTCTGGATCCATGGCAGATCTGGAAGACAACA TGG-3'

prDH026: 5'GGTCAGTTTGCCACCTCTAGATCATCTGTATTTCTGATGATATGC-3'

Following amplification and digestion with BamHI and XbaI, the Cyt b_{562} coding sequence was ligated into BamHI and XbaI digested p316-GAL1[148]. The amino acid sequence of Cyt b_{562} is as follows, with the heme coordinating residues highlighted in red:

ADLEDNMETLNDNLKVIEKADNAAQVKDALTKMRAAALDAQKATPPKLEDKS PDSPEMKDFRHGFDILVGQIDDALKLANEGKVKEAQAAAEQLKTTRNAYHQKY R

Table 2 – List of plasmids used in Chapter 3 studies. See Appendix for more details regarding construction of previously reported pDH plasmids, else see [29] for details regarding the construction of the pJA, pRH, and pOM plasmids.

Name	Description
p415-*GPD*	pRS415 containing the *GPD* promoter
p415-*CYC1*	pRS415 containing the *CYC1* promoter
p316-*GAL1*	pRS316 containing the *GAL1* promoter
pDH013	HS1 heme sensor subcloned into p415-*GPD*
pRH021	HS1-M7A heme sensor subcloned into p415-*GPD*
pJA010	HS1-M7A,H102A heme sensor sub-cloned into p415-*GPD*
pRH003	eGFP sub-cloned into p415-*GPD*
pOM003	eGFP sub-cloned into p415-*CYC1*
pDH039	Cytochrome b_{562} sub-cloned into p316-*GAL1*

3.10.11 Total Reflection X-ray Fluorescence (TXRF) Spectroscopy

Elemental analysis of cells, and in particular metal analysis of Pb, 1st row transition elements, P, and S, were accomplished by total reflection x-ray fluorescence (TXRF) on a Bruker S2 Picofox TXRF as described previously[29]. Briefly, following growth, cells were washed sequentially in ice-cold Tris-EDTA (TE), pH 8.0 buffer and Milli-Q water, and then finally resuspended in Milli-Q water to a density of 2 x 10^9 cells/mL. 2 µL of a cell suspension, spiked with 1 ppm of a Ga internal standard, were

spotted onto a quartz sample disc, and atomic fluorescence emission spectra were collected according to the manufacturer's recommendations[29]. The cellular metal concentrations were determined by assuming a yeast cell volume of 50 fL and that a solution turbidity of $OD_{600\ nm}$ = 1.0 is equivalent to 2 x 10^7 cells/mL[29].

CHAPTER 4. INTERROGATING COMPARTMENT SPECIFIC HEME AVAILABILITY AND TRAFFICKING DYNAMICS WITH GENETICALLY ENCODED HEME SENSORS IN MAMMALIAN CELLS

4.1 Introduction

Heme, an essential iron containing metallo-nutrient located in every subcellular compartment, has long been thought of as a static protein cofactor buried in the core of hemoproteins. However, genetic and biochemical evidence have indicated that heme may act as a dynamic signaling molecule that regulates cell metabolism and physiology[2, 27, 29]. Since heme is tightly regulated and buffered to low levels due to its toxicity, heme acquisition by client hemoproteins that regulate heme dependent functions and signaling are reliant on the ability to safely mobilize heme. This tightly buffered and controlled pool of bioavailable heme is often referred to as labile heme (LH), defined as a pool of heme chelatable, kinetically labile heme that can readily exchange between biomolecules and is accessible for heme-dependent processes[167]. The emergence and continued development of several LH sensing technologies is opening the means to characterize and understand the nature and dynamics of LH, aiding investigations for factors that control its availability, which are largely unknown[29, 111, 167, 222-224]. The use of these heme sensors has demonstrated that LH has a functional role in regulating heme signaling and can act independently of heme synthesis for regulatory purposes[167]. Truly, the development of new heme sensing technologies has aided in identifying several heme trafficking factors and insights into the importance of LH.

In this work, we find that our heme sensor associates with a pool of LH that is buffered to either low pM levels of ferrous heme or low nM levels of ferric heme in the mitochondrial, nuclear, and cytosolic fractions of HEK293 cells. These reports are in staggering contrast to the previously assessed levels demonstrated with activity based heme reporters that report ferric LH levels on the order of 100s of nM in HEK293 cells[222]. We demonstrate that cytosolic, nuclear, and mitochondrial LH availability can be replenished to varying degrees by synthesis alone, but when cells are supplied with excess heme synthesis intermediate, the heme sensor becomes saturated with heme in each compartment. Additionally, the cytosol and nucleus equilibrate with extracellularly supplied heme to a higher degree than mitochondrial LH pools. Finally, given that previous reports ascribed cytoprotective roles to heme oxygenase 2 (HO2) independent of its catalytic function, we sought to probe HO2's effects on LH availability using our sensors. Our investigation revealed novel LH heme sequestering and buffering roles for HO2 that have no effect on total heme availability and are completely independent of its catalytic function, but solely relies on HO2's ability to bind heme in its catalytic heme binding pocket. Our work demonstrates the functionality of our sensor to quantitate compartment specific LH levels and its use in characterizing new heme trafficking factors, like the unexpected role for HO2 as a heme buffering factor.

4.2 Cellular Heme Imaging: Cytosol.

To assess LH availability in HEK293 cells, we first began by testing how human codon optimized HS1 (hHS1) sensors responded to heme depletion and heme supplementation. Briefly, as mentioned in previous chapters, HS1 employs a tri-domain architecture consisting of a fusion of heme binding protein cytochrome b_{562}, plus two

proteins that exhibit fluorescence that is quenched (eGFP) or unaffected (mKATE2) by heme. Thus, heme binding to HS1 results in a decrease in the eGFP to mKATE2 fluorescence emission ratio, allowing for ratiometric [heme] measurements. In these studies, heme replete media refers to basal growth media or regular media with heme containing serum, while the heme depleted (HD) media contains heme depleted serum and a heme biosynthesis inhibitor, succinyl acetone (SA).

The high affinity hHS1 sensor, K_d^{III} = 3nM, K_d^{II} ~10 pM, is quite sensitive to heme availability in HEK293 (Figure 4.1A), while the weaker affinity variant, HS1-M7A, K_d^{III} = ~1 μM, K_d^{II} 25 nM, is much less responsive to heme in HEK293 cells[29] (Figure 4.1B). Cells expressing hHS1 have large differences in heme-dependent fluorescence in heme-depleted (HD + SA, eGFP:mKATE2 mode ~ 9) vs regular media (eGFP:mKATE2 mode ~ 4), and become saturated with heme in response to prolonged heme treatment (10, 25, or 50μM heme) or from upregulation of heme synthesis by supplementation with a bolus of heme synthesis intermediate δ-aminolevulinic acid (ALA) (modes ~ 1) (Figure 4.1A). The difference in modes between each treatment conditions exhibits the hHS1's sensitivity of heme and its ability to sense both increases and decreases of LH availability. Cells expressing hHS1-M7A, on the other hand, do not respond as well to heme depletion by HD + SA cell growth (mode ~ 6.5) compared to regular media growth (mode ~ 5). Additionally, there is no difference in the HS1-M7A ratios in regular media cell growth with and without 10 μM heme treatment or ALA supplementation, which are conditions that drastically effected hHS1 heme binding (Figure 4.1A,B). However, these cells do seem to respond to larger doses of exogenous heme treatment, indicated by the regular media mode ratio lowering from ~ 5 to a ratios

of ~2.6 with higher doses of heme (Figure 4.1B). Even though the modes do change, the overall distribution of the hHS1-M7A ratio histograms between conditions that effect its eGFP:mKATE2 mode are much broader than with hHS1 (Figure 4.1A,B). Taken together, hHS1 is very heme responsive and can sense both increases in heme availability in HEK293 cells, while hHS1-M7A is much less useful.

To further assess the heme responsiveness of the more useful sensor variant, cells expressing hHS1 were titrated with smaller doses of exogenous heme in regular versus HD + SA media. Regular media cells have a characteristically lower ratio (mode ~5.5) than HD + SA media cells (mode ~11), and the heme deficient cells have a broad range of eGFP:mKATE2 ratios, indicative of heterogeneity in the ability to heme starve cells (Figure 4.2). Both heme-starved and regular media cells have dose-dependent responses to 0.2, 0.5, and 1 μM exogenous heme treatment (Figure 4.2). HD + SA media have a mode of ~11, that decreases to 8.5 with 0.2 μM heme treatment, 4.5 with 0.5 μM heme, and sit at a mode of ~3.0 with 1 μM heme treatment. Regular media cells have a mode of ~ 5.5, and then decrease to ~4.2 with 0.2 μM, ~2.8 with 0.5 μM, and ~2.1 with 1 μM heme treatment. When comparing regular media to HD +SA grown cells at any given heme dose, the sensor fluorescence ratio is always lower in the regular media cells. However, gap between the ratios in regular vs HD + SA grown cells is much smaller at the 1 μM exogenous heme treatment dose (Figure 4.2). Based off the binding affinities of hHS1, these dose dependent responses from these low μM supplements of exogenous heme correspond to much smaller changes in intracellular labile heme (Figure 4.2).

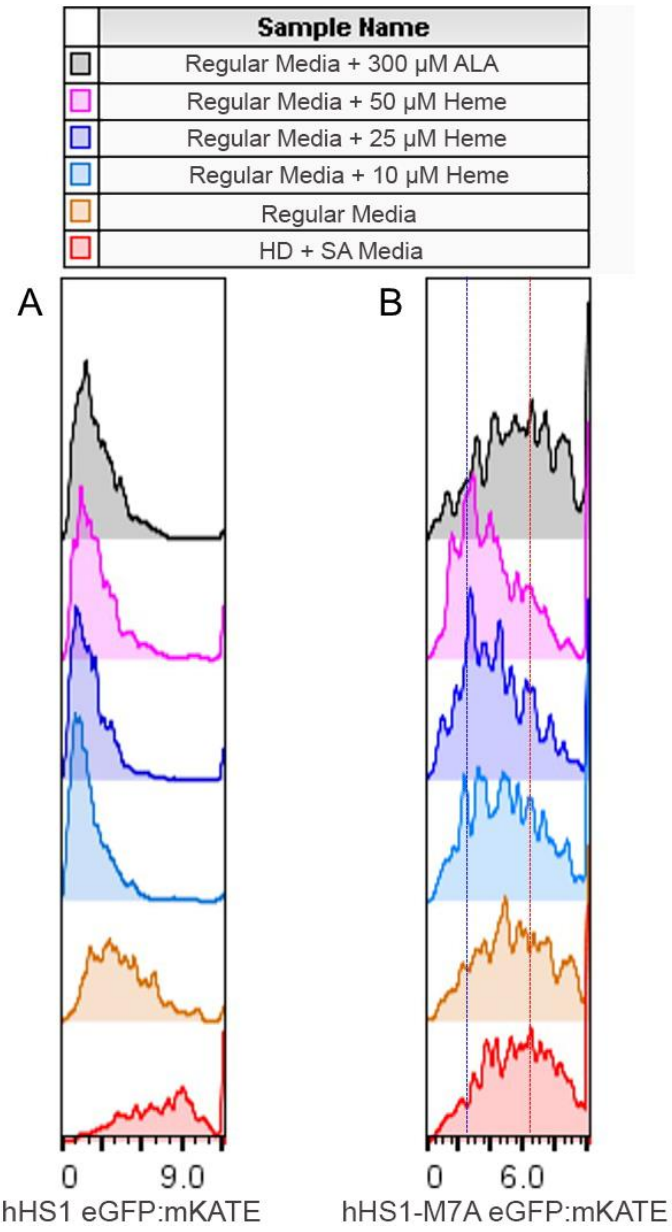

Figure 4.1 – Heme-dependent responses in heme sensor fluorescence in HEK293 cells. Flow cytometric analysis of HEK293 cells transiently transfected with (**A**) hHS1 or (**B**) hHS1-M7A sensors and cultured in heme-deficient (HD) succinylacetone (SA) treated media (HD + SA) or in regular media (heme replete) media exhibit differential responses to heme. In each panel heme replete cells were treated with 0, 10, 25, or 50 µM heme or with 350 µM δ-aminolevulinic acid (ALA), a heme synthesis intermediate, for 24 hours. In **B** dotted lines were drawn to depict a heme-dependent change in the HD + SA histogram mode (red dotted line) to the high heme treatment histogram mode (blue dotted lines).

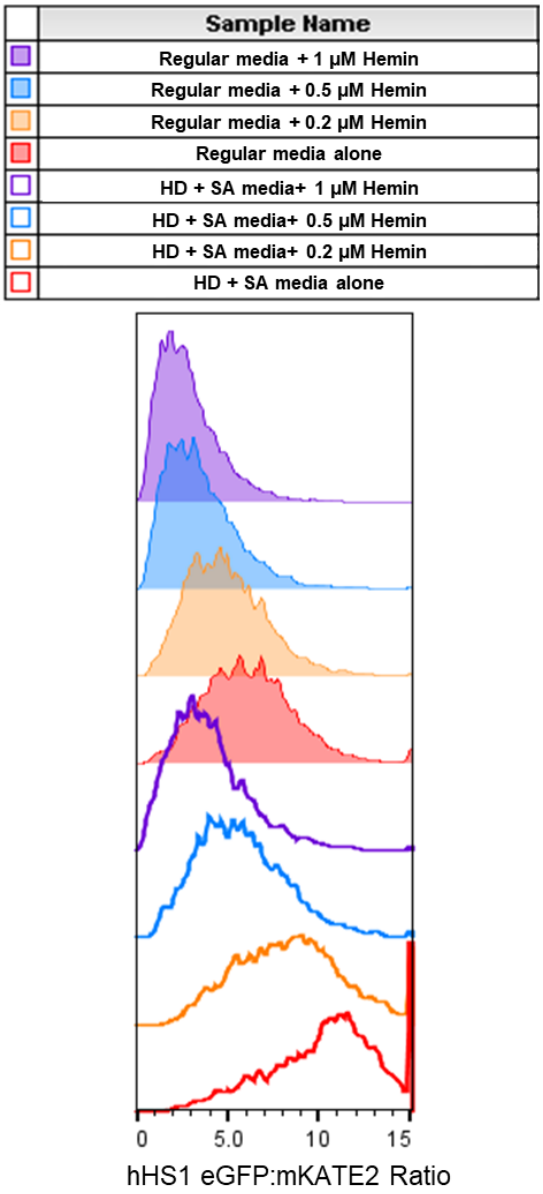

Figure 4.2 - Cytosolic expressed hHS1 heme sensor responds to low µM doses of exogenous heme. Histograms of the heme sensor of cells grown in regular media (shaded histograms) and heme depleted media HD + SA media (unshaded histograms) are plotted. Both regular and HD + SA media cells were grown in the presence of 0 (red), 0.2 (orange), 0.5 (blue), or 1 µM (purple) hemin chloride.

For quantitative measuring of labile heme availability in these cells, an in situ calibration method was developed, where the [heme] accessible to the sensor is governed by Equation 4[116]:

$$[heme] = K_d \times \frac{R_{expt} - R_{min}}{R_{max} - R_{expt}} \quad (4)$$

In Equation 4, K_d is the heme-sensor dissociation constant, R_{expt} is the eGFP/mKATE2 fluorescence ratio under any given condition, R_{min} is the eGFP/mKATE2 fluorescence ratio when 0% of the sensor is bound to heme, assumed to be the histogram eGFP:mkATE ratio mode of HD + SA media grown cells, and R_{max} is the histogram mode eGFP/mKATE2 fluorescence ratio when 100% of the sensor is bound to heme. To acquire R_{max}, digitonin permeabilized cells were treated with excess heme in the presence of ascorbate. Given the broad ratio distributions in the histograms from flow cytometric analysis, the ratio for each condition is derived from the mode of each histogram. See Appendix for more details regarding in situ calibration. Sensor fractional saturation can be calculated using Equation 5.

$$Sensor\ fraction\ bound = \frac{R_{expt} - R_{min}}{R_{max} - R_{min}} \quad (5)$$

The developed calibration method was applied to the hHS1 sensor, the weaker-affinity hHS1-M7A sensor, and a heme-insensitive mutant, hHS1-M7A, H102A (Figure 4.3). Only the hHS1 sensor has heme-dependent changes between HD + SA and regular media and is the only sensor that responds to the in situ saturation protocol (Figure 4.3). The results demonstrate the efficacy of this procedure for calibrating the hHS1 sensor, and indicate that both hHS1-M7A and hHS1-M7A, H102A are unbound to heme and do

not respond well to heme in these cells (Figure 4.3). Further, when comparing the mode of each relevant histogram to acquire R_{expt} (~2), R_{min} (~5), and R_{max} (~1) values for use in Equation 4, the mode hHS1 ratio represents 75% bound heme sensor (Figure 4.3), indicating that LH is buffered to as low as 7.5 pM ferrous heme or 2.2 nM ferric heme. Using Equation 4, and reported volumes for the HEK293 cytoplasm of 0.8 pL[225], we calculate that there are a < 4 molecules assuming all LH is reduced or a maximum of ~1350 ferric cytoplasmic LH molecules assuming all LH is oxidized[225]. Moving forward, given that the weaker affinity sensors do not respond well to heme and hHS1 is easily calibrated, all further studies focused on the use of hHS1.

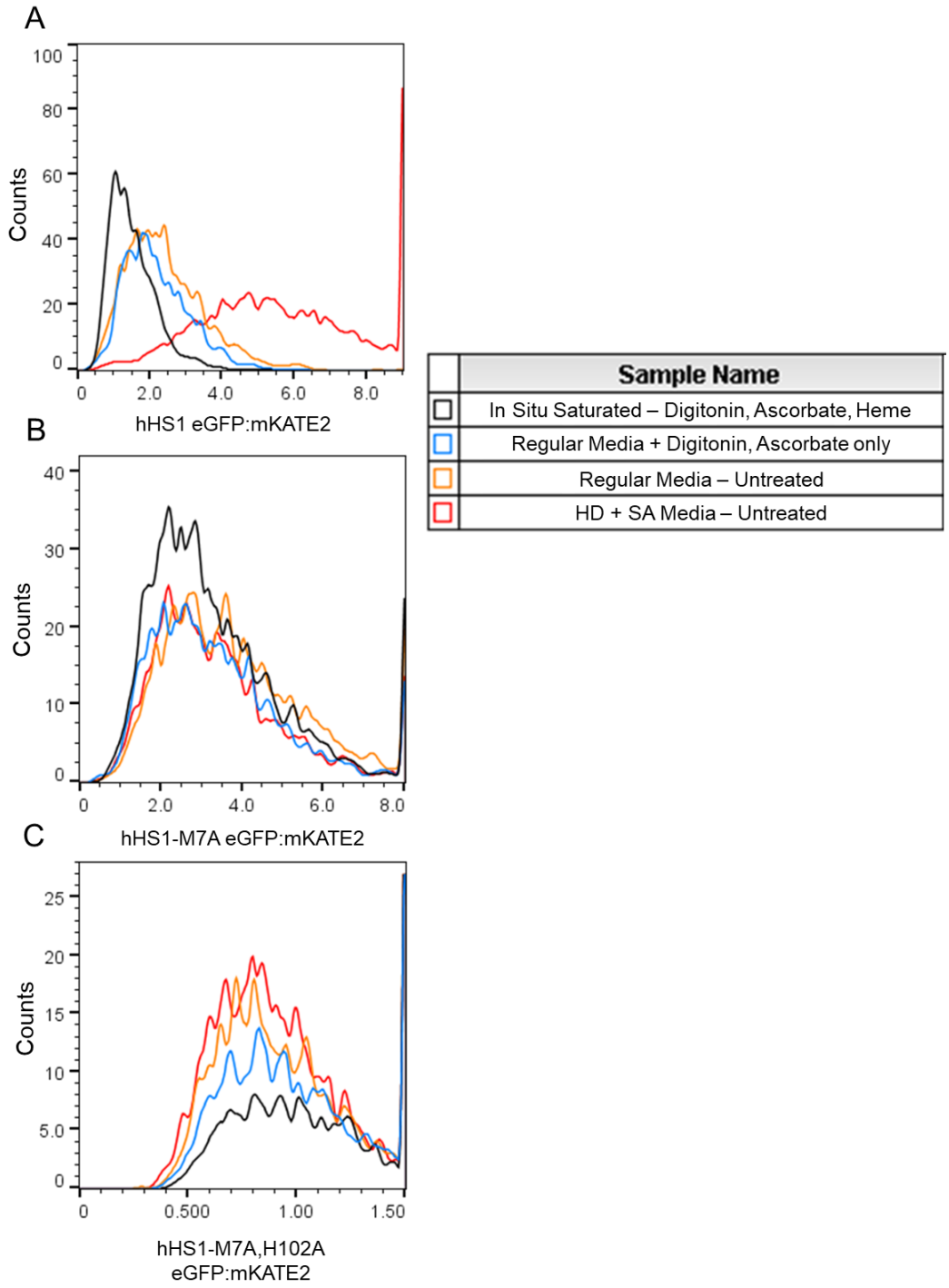

Figure 4.3 – In situ calibration of hHS1 heme sensor. (**A**) Tight binding hHS1 sensor, but not weaker affinity sensor (**B**) hHS1-M7A or heme insensitive mutant (**C**) hHS1-M7A, H102A, is heme responsive and can be saturated with heme when digitonin permeabilized and treated with excess hemin and ascorbate. Cells from 6-well plates were harvested in media by pipetting, treated with calibration reagents for 30 minutes at 30 °C, pelleted, washed in PBS, then prepped for flow cytometric analysis. Heme

depleted HD+SA represent cells that center a ratio representing 0% bound sensor (red histograms). The in situ saturation treatment, treating cells treated with digitonin, ascorbate, and 100 μM hemin (black histograms), represents 100% bound sensor in these cells.

Having determined the efficacy of using hHS1 in these cells, we sought to monitor the kinetics of LH replenishment after heme starving cells. Additionally, comparing LH versus total heme replenishment may yield information regarding how much total heme must build up before LH pools may be replenished. Understanding these factors may designate the rate at which new heme dependent processes may be activated from endogenously synthesized heme. Hence to test the dynamics of heme replenishment and cytosolic heme acquisition, total and LH heme were monitored over 24 hours in cells grown in HD or regular media after depleting their cellular heme by HD + SA growth (Figure 4.4). Surprisingly, total heme pools are replenished within the first 2 hours of recovery in each media (Figure 4.4B), but LH stores replenish much more slowly (Figure 4.4A). Additionally, there is more heme loading in cells replenished with HD media compared to regular media, but there was no difference in total heme between the media conditions (Figure 4.4A,B). Cells replenished in HD media have a mode eGFP:mKATE2 ratio of ~5.2 at time 0, ~4.7 at 2 hours, ~4.2 at 6 hours, ~4.0 at 8 hours, and ~3.2 at 24 hours. Similarly, cells replenished in regular media, have a mode eGFP:mKATE2 ratio of ~5.2 at time 0, ~5 at 2 hours, ~4.5 at 4 hours, ~4.0 at 6 hours, ~3.8 at 8 hours, and ~3.8 at 24 hours (Figure 4.4). The differences between cytosolic LH and total heme (measured by the porphyrin fluorescence assay) replenishing kinetics between HD and regular media seem to be negligible.

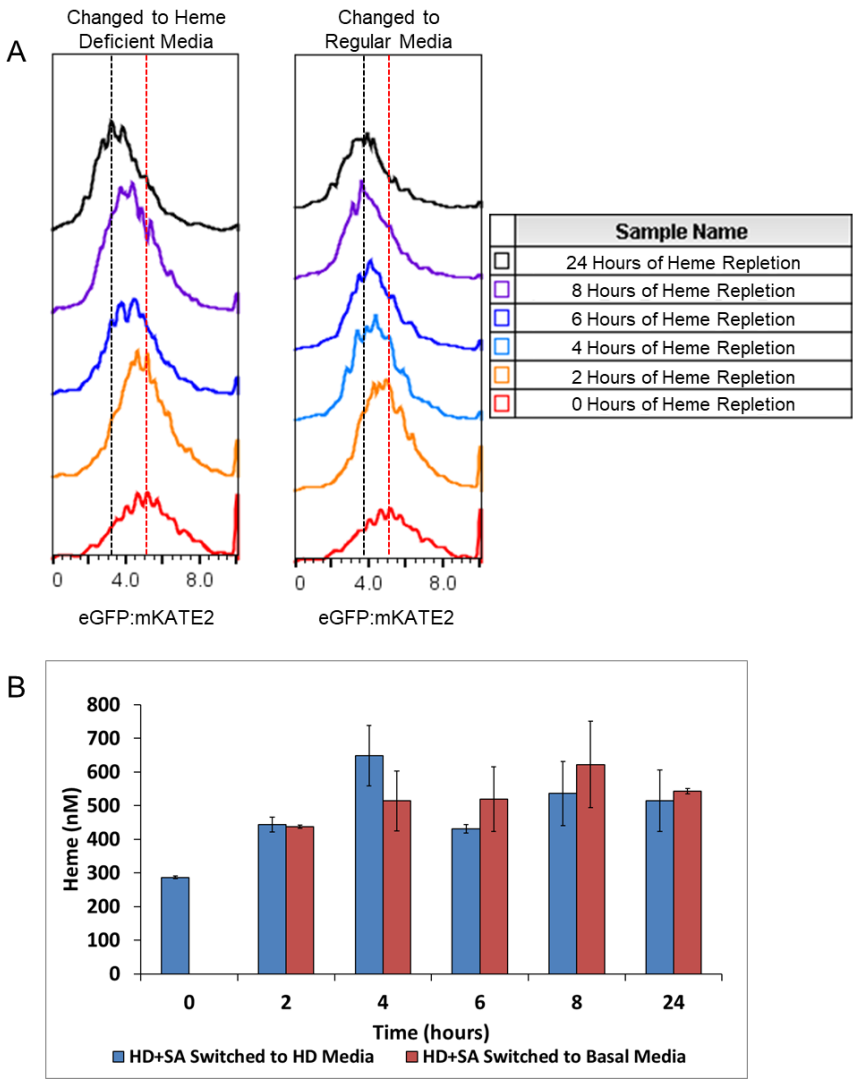

Figure 4.4 – Heme repletion kinetics of cytosolic LH and intracellular total heme. (**A**) Heme repletion kinetics of cells starved of heme for 48 hours in HD+SA media, switched to either heme deficient media (histograms on the left) to allow cells to synthesis endogenous heme, or regular media (histograms on the right) to allow cells to both synthesis and uptake any exogenous heme from the serum. The dotted red line in each histogram represents the mode of heme starved HD+SA, 0 hr replenished cells, while the dotted black line represents the mode ratio post 24 hours of heme replenishment. (**B**) Total heme repletion kinetics of biological duplicates utilized for labile heme measurements.

4.3 Cellular Heme Imaging: Cytosol, Nucleus, and Mitochondria

Heme monitoring with hHS1 and hHS1-M7A was extended to mitochondria and the nucleus, and the subcellular targeting of each sensor was validated by microscopy (Figure 4.5). To confirm heme-dependent changes in mitochondrial and nuclear localized sensors, the in situ calibration protocol developed for the cytosolically expressed sensor was applied to cells expressing cytosolic, mitochondrial, and nuclear localized hHS1 (Figure 4.6A-C). hHS1 is well poised to sense labile heme in each of these compartments as basal conditions exhibit ratios in between heme starved and the heme treated cells (Figure 4.6A-C); however, the in situ saturation protocol did not seem to saturate mitochondrially localized hHS1 (Figure 4.6A-C). Given this small decrease in the mitochondrial hHS1 eGFP:mKATE2 ratio and since digitonin treatment only permeabilizes the outer membrane of the cell, it was assumed the mitochondrial sensor was not saturated with heme.

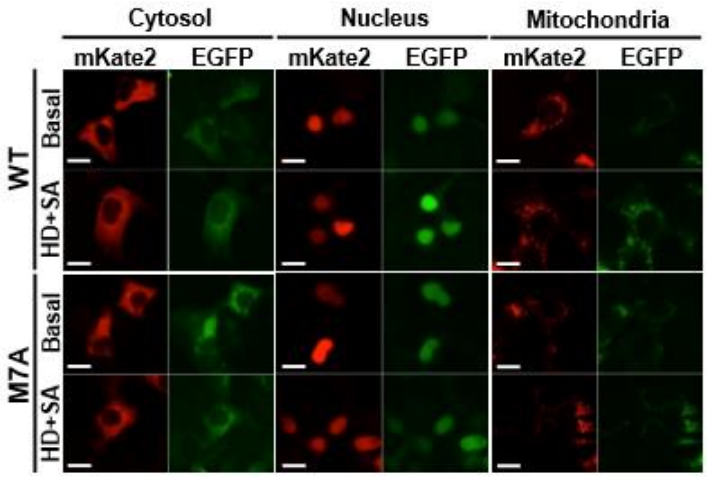

Figure 4.5 - Localization of targeted hHS1. HEK293 cells were transfected with WT and M7A sensor constructs made for targeting to the cytosol, nucleus, and mitochondria. Cells imaged 42 hours post-transfection using a Leica DM IRE2 fluorescence microscope under 63x oil immersion objective. Scale bar = 10 µm. Images were taken and provided by Xiaojing Yuan.

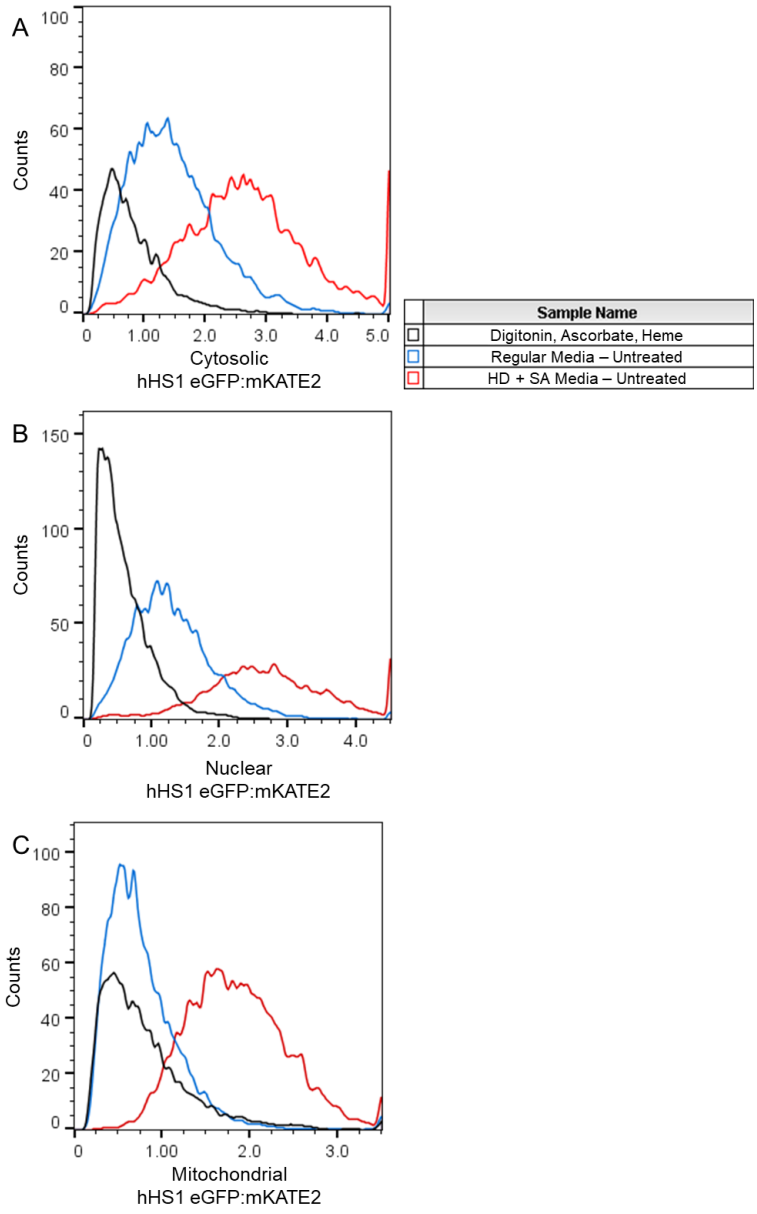

Figure 4.6 – In situ saturation protocol optimized for cytosolic hHS1 applied to cells expressing sensor in (**A**) cytosol, (**B**) nucleus, and in the (**C**) mitochrondria. Regular media cells (blue) are compared to heme starved HD + SA cells (red) and cells treated with digitonin, ascorbate, heme to saturate the sensors (black).

Since the cell permeabilizing saturation protocol does not work for mitochondrial hHS1 sensor (Figure 4.6C), a new protocol was adapted and compared to the previous method to in situ saturate hHS1. Simply, cells were treated with a large overnight dose of

heme biosynthetic intermediate ALA, which drastically increases the endogenous synthesis of heme inside HEK293 cells. This method of upregulating heme synthesis supplied each compartment with enough heme to saturate the sensor to equal degrees as the in situ saturation protocol in the cytosol and nucleus (Figure 4.7A,B), or more efficiently in the case of mitochondrial hHS1 (Figure 4.7C). The saturation of the heme sensor in each compartment reveals that regular media treated cells are ~78% bound in the cytosol (R_{expt} (~1.7), R_{min} (~2.8), and R_{max} (~0.4)), ~53% bound in the nucleus (R_{expt} (~1.4), R_{min} (~2.6), and R_{max} (~0.25)), and ~71% bound in mitochondria (R_{expt} (~0.7), R_{min} (~1.8), and R_{max} (~0.25)). Using Equation 4 and reported HEK293 cytoplasmic volume of 0.80 pL[225], nuclear volume of 1.00 pL[225], and that mitochondrial volumes are approximately 10% of the total cellular volume, 0.2 pL[226], we can calculate the concentration of LH in each compartment. If each compartment's heme is assumed to be completely reduced, cytosolic LH would be ~7.8 pM or <4 molecules of free heme, the nuclear LH would be ~5.3 pM or ~3 molecules of heme, and the mitochondrial LH would be ~7.1 pM or ~1 molecule of heme. If all LH is assumed to be completely ferric, which would only be the case if LH's redox status was determined independently of the glutathione redox system, we calculate that cytosolic LH would be ~2.3 nM or ~ 1100 molecules of heme, nuclear LH would be ~1.6 nM or < 960 molecules of heme, and the mitochondrial LH would be ~2.1 nM or ~ 250 molecules of heme. The contribution of ferrous and ferric heme in each compartment is not discernable with the hHS1 heme sensor without knowing what dictates heme's oxidation state within the cell. If heme is largely ferrous in these cells, the data suggests that LH is very tightly buffered in these cells.

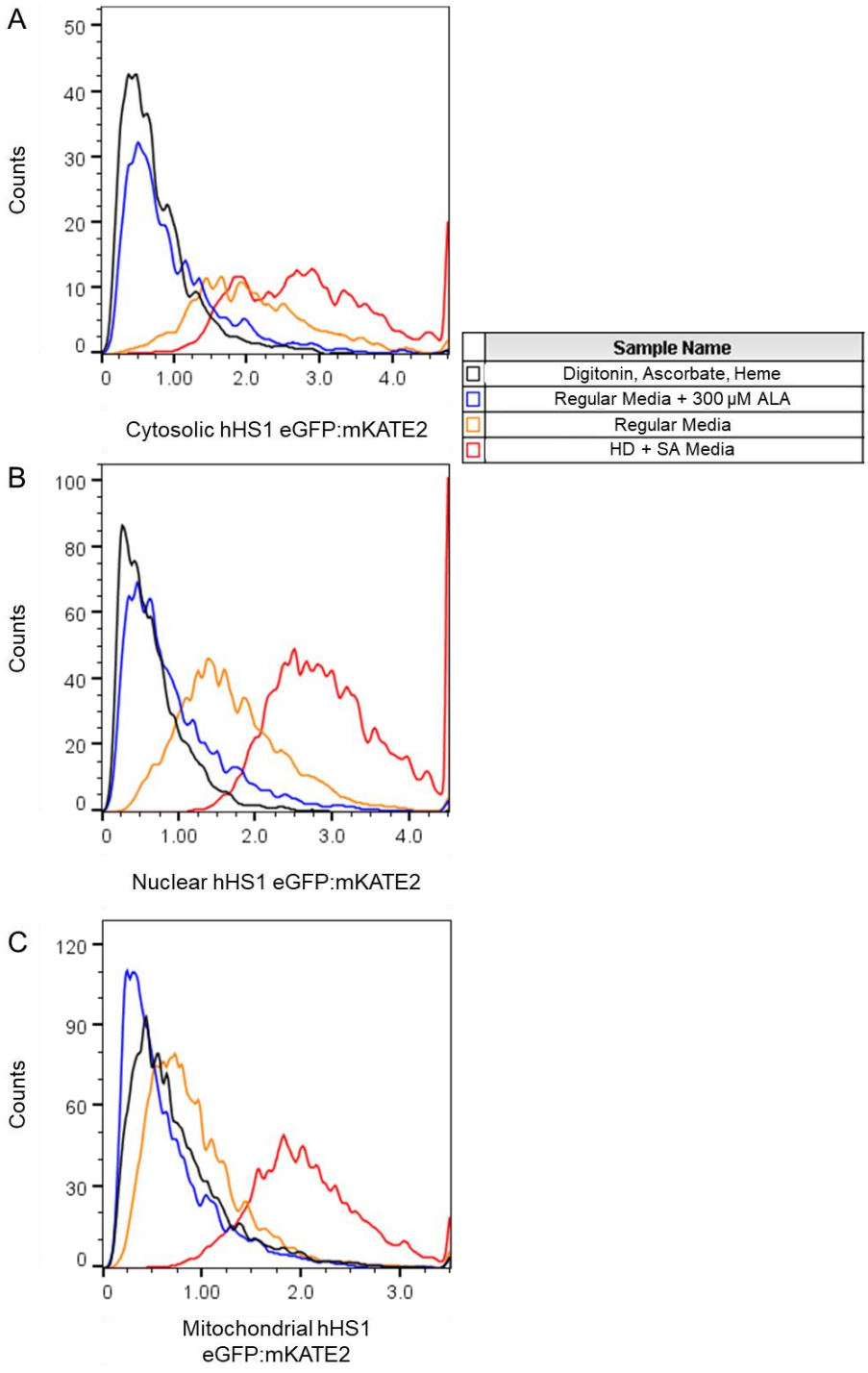

Figure 4.7 – In situ saturation of (**A**) cytosolic, (**B**) nuclear, and (**C**) mitochondrial hHS1 by prolonged exposure to δ-aminolevulinic acid (ALA). Permeabilizing cells with digitonin in the presence of heme and reducing agent ascorbate (black histograms) is

compared to a 20 hour supplementation of growth media with 300 μM (δ-aminolevulinic acid) ALA, which saturates hHS1 in each compartment (blue histograms).

Armed with the tools and methods to quantitate LH in these compartments, we sought to characterize the contributions from extracellular by derived heme vs biosynthesized heme on LH availability in each compartment. We started by investigating if endogenous heme synthesis is sufficient for cells to produce LH by interrogating the amount of LH in cells grown in HD versus regular media. The results demonstrate that heme synthesis in HD media cells is indeed sufficient to fill LH to some degree in each compartment, but there was additional LH availability in the cytosol and nucleus when grown in regular media (Figure 4.8). We next sought to address if cells that could not utilize heme synthesis to fill their LH pools, could fill their LH with extracellular heme sourced from the serum in regular media cells. To test this, we interrogated compartment specific LH availability in cells grown in regular media + SA media and compared the fraction bound of hHS1 to cells grown in other relevant growth conditions (Figure 4.8). The results show that cytosolic LH is completely depleted by inhibition of synthesis alone as the mode ratio between regular media + SA is nearly identical to that in HD + SA treated cells (Figure 4.8A). Mitochondrial and nuclear LH pools, on the other hand, are not completely depleted in regular media + SA, and contain hHS1 that is ~20% bound with heme, indicating that inhibiting synthesis does not deplete mitochondrial or nuclear labile heme stores in cells grown in media containing serum (Figure 4.8B,C).

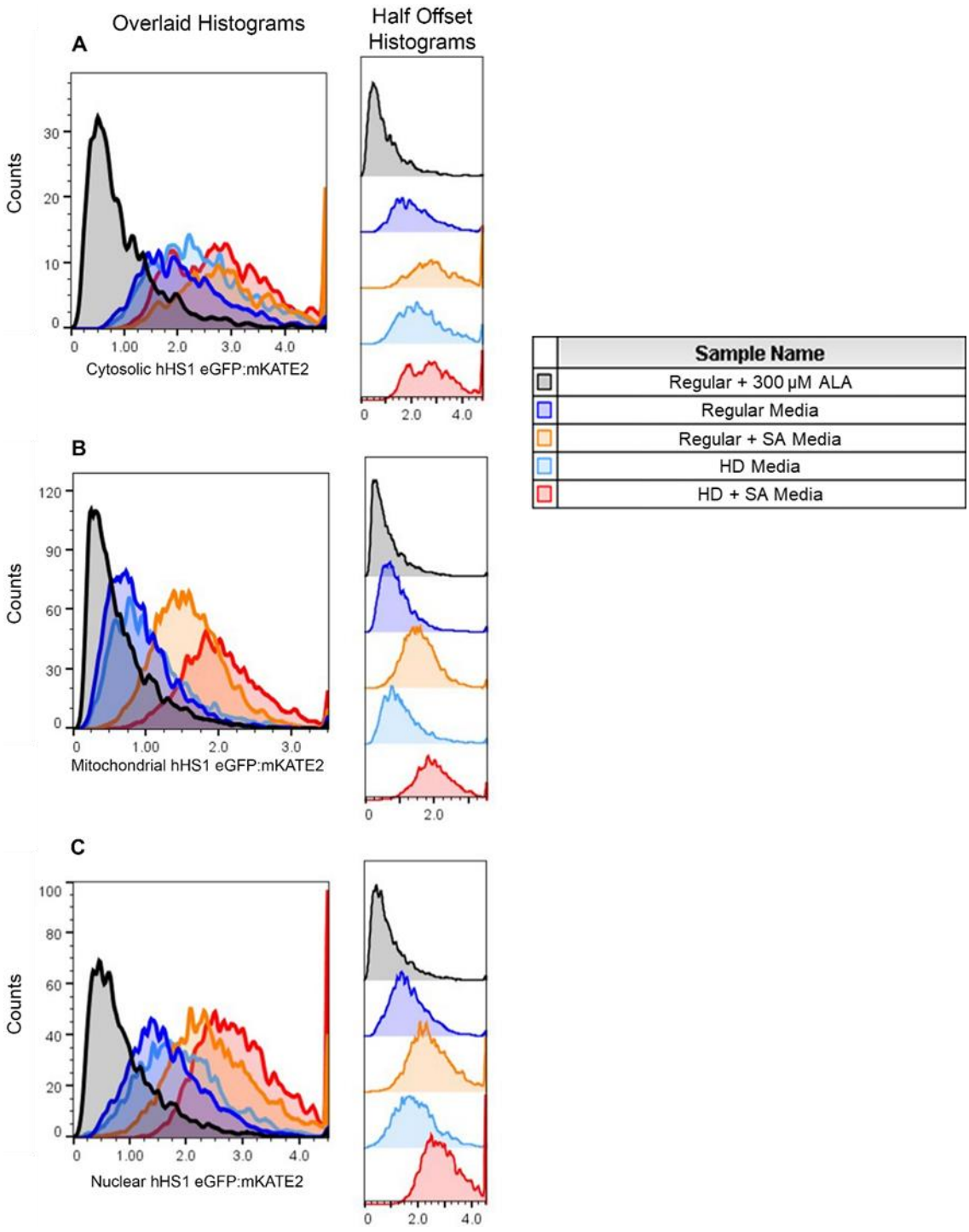

Figure 4.8 – Measuring differences in (**A**) cytosolic, (**B**) mitochondrial, and (**C**) nuclear labile heme sensed by hHS1 in response to heme starvation. Data is displayed in two different ways, with overlaid histograms in the left column, and half offset histograms in the right column.

To further parse out the details underlying compartment specific LH management from exogenous versus endogenous heme sources, changes in total and LH availabilities were analyzed for their response to treatment with different sources of exogenous and endogenous heme. Specifically, cells grown in regular or HD media treated with ALA, SA, and/or hemin were compared for their relative changes in fractional saturation of hHS1 from these treatments in each compartment (Figure 4.9B) and compared to total cellular heme (Figure 4.9A). The results reveal that total heme and the amount of LH accessible to each compartment generally correlate with one another, but there are differences in labile heme availability in each compartment that is specific to source of heme made accessible to the cells (Figure 4.9A,B). As shown previously in Figure 4.8, cytosolically expressed hHS1 in regular media + SA (~4 % bound) detects less heme than mitochondrial or nuclear hHS1 in regular media + SA treated cells (both ~20 % bound) (Figure 4.8, Figure 4.9B). Under conditions that increase heme availability via treatment with large amounts of exogenous heme or ALA, each compartment increases in LH availability, but mitochondrial hHS1 is less sensitive to exogenous heme treatment than the cytosolic and nuclear heme sensors. See Figure 4.9B; mitochondrial hHS1 is closer to 80 % bound, while nuclear and cytosolic hHS1 are closer to 90 % bound from excess exogenous heme treatment. Moreover, mitochondrial hHS1 is more saturated with heme under conditions that facilitate heme synthesis and is not impacted by heme from serum in the media. To this point: in HD media hHS1 is ~25% bound in the cytosol and ~40% bound for nucleus, while the mitochondrial hHS1 is ~65 % bound. Additionally, the cytosolic and nuclear hHS1 sensors acquire more heme when grown in regular media vs HD media than mitochondria do. When comparing the fraction bound of sensor in HD

versus regular media, there is an 11 % change in cytosolic hHS1, a 15% change in nuclear hHS1, and only a < 5% change in mitochondrial hHS1 heme loading (Figure 4.9B). In total, mitochondria are much more responsive to endogenously supplied heme while the cytosol and nucleus have the potential to acquire more extracellular heme than mitochondria while synthesis is not inhibited by SA (Figure 4.9).

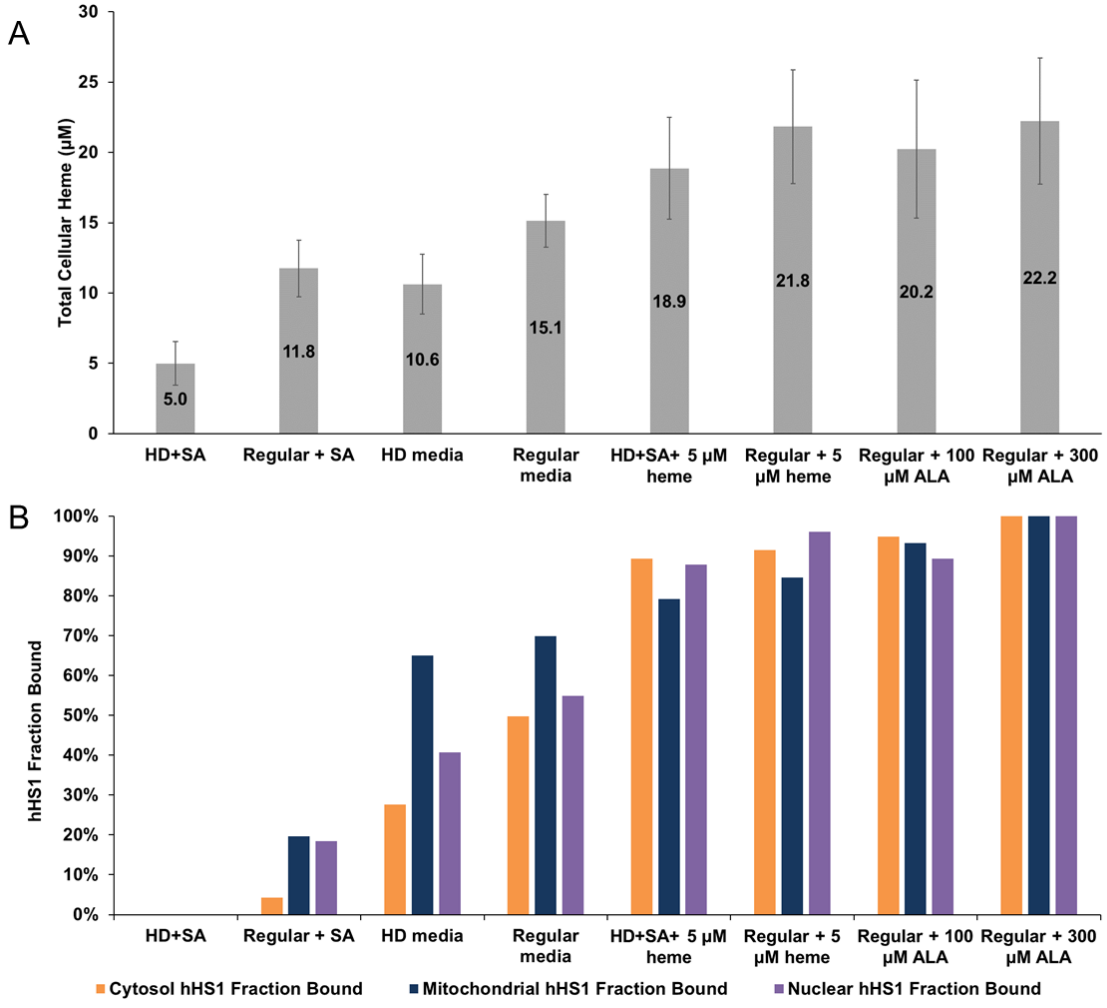

Figure 4.9 – Heme dependent changes in total cellular heme and LH sensed by cytosolic, mitochondrial, and nuclear hHS1. (**A**) Total heme values for each media condition were taken in triplicates. Regular media grown cells were supplemented with or without 500

μM SA, 5 μM hemin, 100 μM or 300 μM ALA, and HD media grown cells were grown with or without 500 μM SA ± 5 μM hemin. (**B**) The corresponding cells for the total heme measurements were used to take analyze the fraction of hHS1 bound with heme in the cytosol (orange), mitochondria (blue), and nucleus (purple), which are indicative of the LH availability sensed by hHS1 targeted to these locals. These % hHS1 fraction bound was calculated using eGFP:mKATE2 histograms generated by flow cytometric analysis of sensor expressing cells.

4.4 Heme Oxygenase 2 (HO-2) Sequesters Cellular Labile Heme Independent of Catalytic Activity and without Impacting Total Heme Availability

Previous studies found that heme oxygenase 2 (HO2) imparts cytoprotective effects to cells under oxidative stress even if catalytically inactive[227]. This suggested that part of the protection afforded by HO2 was independent of heme degradation. Given that soluble HO2 has heme binding sites with nM affinities for ferric heme, we tested if HO2 and its catalytically inactive mutants were able to perturb and/or sequester LH[113]. We first tested the effects of HO2 levels on hHS1 and its heme insensitive variants in regular versus HD + SA media (Figure 4.10). The results clearly show that WT HO2 overexpression depletes LH accessible to hHS1 (Figure 4.10A), and the effects are visibly heme-dependent as there are no HO2 dependent changes in sensor fluorescence ratio in HD + SA media or in the ratios of heme irresponsive mutants, hHS1-M7A and hHS1-M7A,H102A (Figure 4.10B,C).

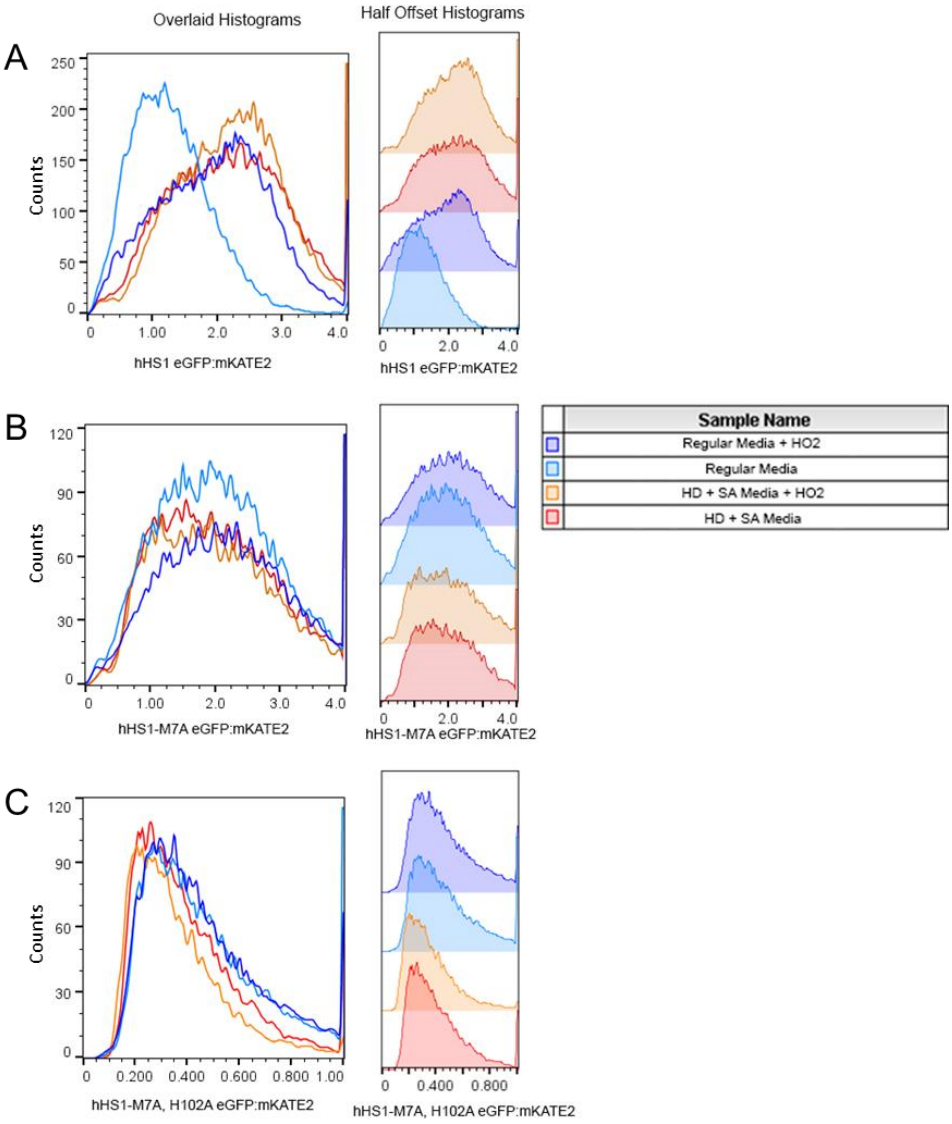

Figure 4.10 - Overexpression of HO2 lowers labile heme availability. Overlaid histograms and half offset histograms of (**A**) hHS1, (**B**) hHS1-M7A, and (**C**) hHS1-M7A, H102A sensor expressing cells with and without HO2 overexpression in regular media versus HD + SA medias. (**A**) Overexpression of HO2 in regular media lowers labile heme to the same degree as heme depleted media (HD + SA). There is no effect in seen by HO-2 in HD + SA media, indicating that the change in ratio in regular media is heme dependent. (**B**-**C**) There is no change in sensor fluorescence ratio in the heme insensitive sensors, indicating that HO-2 changes in sensor fluorescence ratio seen with hHS1 (**A**) are not heme independent changes to the sensor.

Having discovered that WT HO2 lowers LH availability, we tested the roles the catalytically inactive mutant, H45A, and HO2's heme regulatory motif (HRM) mutants,

C265A and C282A, for their role in LH depletion. None of these mutants effected the lowering of labile heme (Figure 4.11A) and there were no heme-independent perturbations in sensor fluorescence when any of these mutants were expressed in HD + SA media (Figure 4.11B). Given these results, we tested if the lowering of LH by HO2 required heme binding at the catalytical site by testing mutants that include the H45W and G159W point mutations, which completely block HO2's ability to bind heme at its catalytic core. In addition to the heme binding mutant, we examined a more expansive list of catalytic and HRM mutants to probe any potential catalytic or HRM dependence of this LH phenotype. In regular media, the heme binding mutants containing the H45W, G159W mutations do not affect labile heme at all. Additionally, every other tested mutant lowers LH to the same degree as WT HO2 in regular media (Figure 4.12B). All mutants were expressed well in regular media (Figure 4.12F), and these changes were heme dependent as there was no change in the eGFP:mKATE2 ratio of cells due to HO2 overexpression in HD+SA grown cells (Figure 4.12A). To definitely rule out the roles of the HRM and catalytic mutants in sequestering LH, we tested their effects on LH under high heme conditions with either 5 μM exogenous heme or 300 μM ALA supplementation (Figure 4.12C,D). Each mutant was able to reduce LH under these high heme conditions but not quite as much as in regular media (Figure 4.12B-D). Additionally, under excess heme availability the catalytically incompetent mutants with H45A mutations seem to have a very modest defect in its ability to lower LH relative to the other mutants, but this result was only reproducible in 2 of 4 trials (Figure 4.12C,D, additional trials not shown).

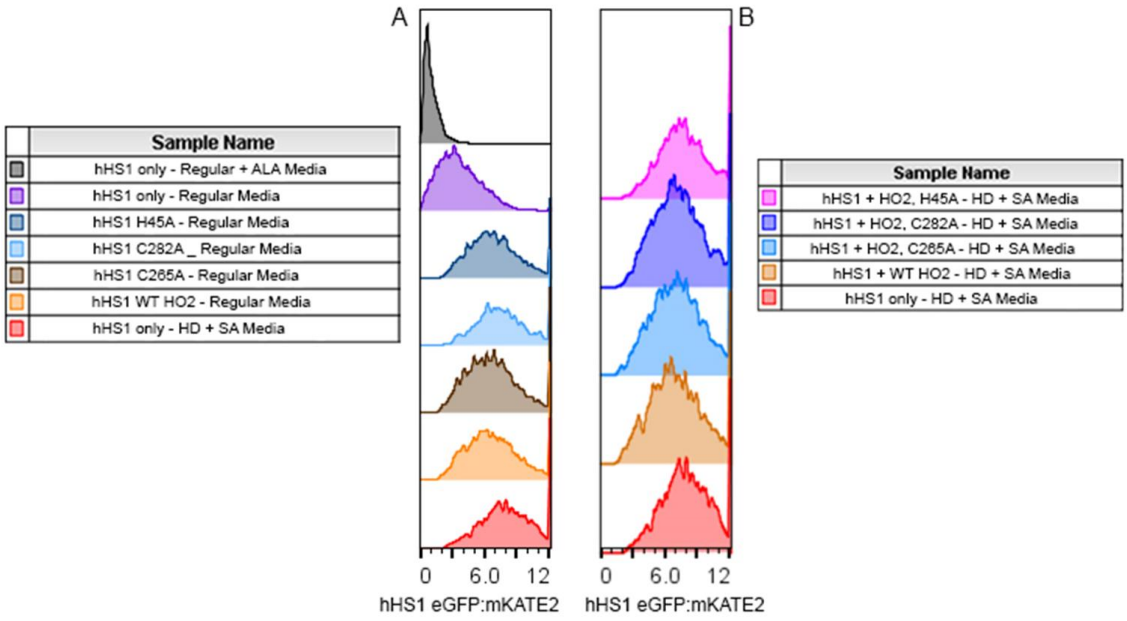

Figure 4.11 – Overexpression of HO2 lowers labile heme availability regardless of catalytic function or either of its HRMs. (**A**) Overexpression of WT HO2 compared to H45A catalytic mutant, and two HRM mutants, C265A and C282A are identical in regular media. Cells expressing hHS1 in regular media, regular media + 300 µM ALA (saturated), and heme depleted HD + SA were analyzed as controls. See legend on the left for the identity of each histogram. (**B**) Overexpression of WT HO2, catalytic mutant, 45A, and the two HRM mutants C265A and C282A do not affect sensor fluorescence when compared in HD + SA media. See legend on the right for the identity of each histogram.

Given that exogenous heme treatment resulted in the same depletion of LH regardless of most HO2 mutations, we next sought to test if the inducible heme oxygenase 1 isoform (HO-1) was compensating for any loss of function within these mutants, masking any contribution they play in effecting LH availability (Figure 4.12E). Indeed, exogenous heme treatment induces expression of HO-1, but the results indicate that HO-1 is not expressed higher in any of the mutants than in hHS1 only or WT HO2

expressing cells (Figure 4.12E). In fact, there appears to be lower HO-1 expression in cells expressing HO2 mutants (Figure 4.12E).

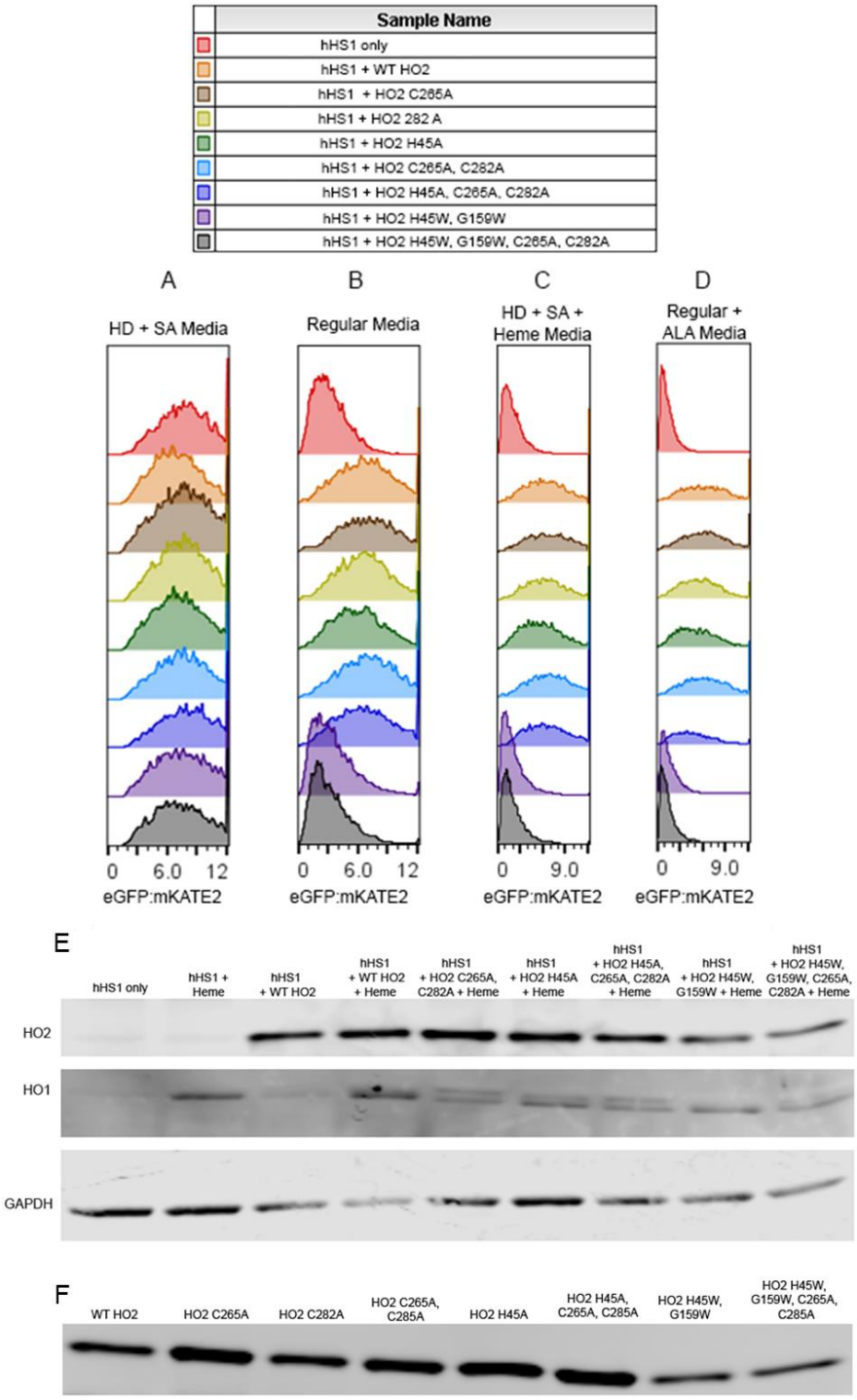

Figure 4.12 – Overexpression of a panel of HO2 mutants for their ability to effect LH availability in (**A**) HD + SA, (**B**) regular, (**C**) HD + SA + 5 µM heme, and (**D**) Regular + 300 µM ALA media, with corresponding western blots for HO2 and HO-1 in HD + SA ± heme with a GAPDH loading control (**E**) and a western blot confirming HO2 overexpression in regular media (**F**).

To further solidify that HO2 is truly acting on LH by sequestering it, we checked that HO2 was not lowering LH via decreasing total heme stores. The results confirm that WT HO2, catalytical deficient H45A, and heme binding HO2 mutant have no impact on total heme availability when overexpressed (Figure 4.13).

.

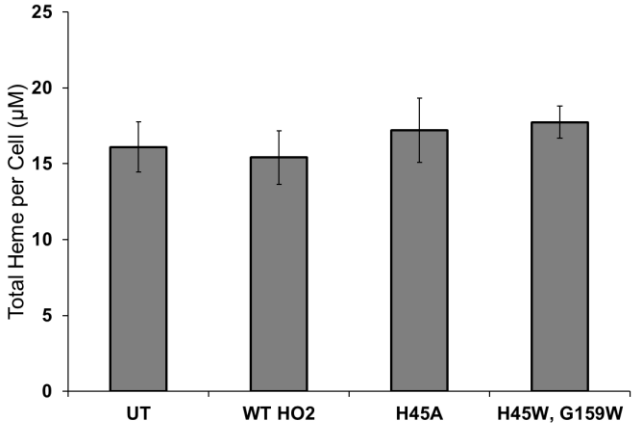

Figure 4.13 – Total heme availability in response to HO2 overexpression in HEK293 cells. Total heme per cell was measured using the porphyrin fluorescence assay to quantify total cellular heme (n = 6)[167].

Lastly, we sought to test if the sequestering of LH by HO2 was unique to the cytosol or if it also affected mitochondrial and nuclear stores of LH. Additionally, we wished to interrogate if any HO2 sequestration of LH depended on origin of the heme, either from heme biosynthesis or from an extracellular source. To these ends, we interrogated HO2 specific changes in LH in each compartment under regular media conditions containing excess endogenous or exogenously supplied heme and under HD + SA media growth with and without excess exogenous heme (Figure 4.14A-C). The results indicate that the overexpression of HO2 affects the nuclear and cytosolic LH heme

pools equally (Figure 4.14A,C); however, the mitochondrial pool of heme is mostly unaffected (Figure 4.14B). Mitochondrial LH under regular media conditions with and without ALA supplementation are completely unaltered by HO2, but heme starved HD + SA cells overexpressing HO2 fed exogenous hemin are completely depleted relative the non-overexpressing HO2 cells in this condition (Figure 4.14B, black histograms).

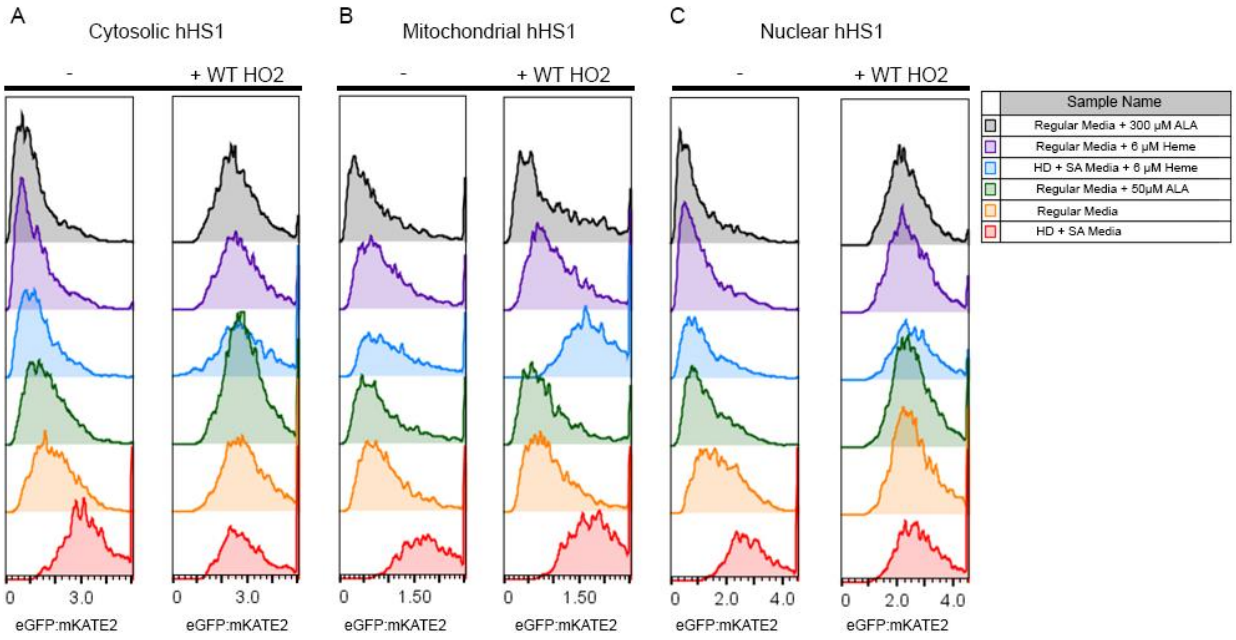

Figure 4.14 – Subcellular LH monitoring in cells with and without the overexpression of HO2. (**A**) Cytosolic, (**B**) mitochondrial, and (**C**) nuclear hHS1 expressing cells were grown in the regular vs HD + SA media with ALA or heme supplementation to determine the effects of HO2 in sequestering exogenous vs endogenously produced heme in each compartment.

4.5 Discussion

Until recently, there was no precise way to quantify or interrogate the nature of LH. The development of novel heme sensors like HS1 have provided concentrations of LH that may be dependent on the probes' ability to access particular heme pools. Additionally, the amount of LH available between cell types is quite variable[2, 28, 111, 222,

[224, 228-230]. Therefore, in order to understand the factors that control LH, it is instrumental to develop several different heme sensing technologies that can together more comprehensively assess the nature of LH of which so little is known. Indeed, the factors that affect LH dynamics, oxidation state, speciation, heme availability, and the differences in these factors amongst different organisms warrants investigation. The knowledge of these factors is imperative to understanding the basis for how new heme dependent processes and signaling are activated as well as understanding how cells must properly manage LH to avoid the deleterious effects of misregulated heme. To these points, in this study, we characterized the use of genetically encoded hHS1 in HEK293 cells to interrogate how they manage LH and to reveal a novel role for the constitutive heme degradation enzyme HO2 in sequestering LH independent of its catalytic function.

Our first results indicate that HEK293 cells tightly regulate their heme pools and will not hyperaccumulate LH as sensed by hHS1 and hHS1-M7A (Figure 4.1). Given the binding affinities of our sensors, we cannot distinguish between ferrous or ferric heme pools in these cells: hHS1 has a dynamic range for ferrous heme spanning between ~1 and ~100 pM and a dynamic range for ferric heme spanning between ~0.3 and 30 nM, while hHS1-M7A sensor has a dynamic range for ferrous heme spanning between ~2.5 and ~250 nM and a dynamic range for ferric heme spanning 0.1 to 100 nM at pH 7[28]. Given the binding affinity of hHS1, the data in Figure 4.1 entails that the hHS1 heme dependent fluorescence changes in cells treated excess 10-50 μM exogenous heme for 24 hours results in pM ferrous or very low nM ferric changes in the buffered concentration of LH. On the other hand, hHS1-M7A cells are unaffected by 10 μM exogenous heme treatment, but this sensor does respond to 25 and 50 μM exogenous heme treatment. The

responses from hHS1-M7A at these high doses suggests that there is either more than 2.5 nM ferrous heme or more than 100 nM ferric heme at these pathophysiological doses of heme treatment, either of which would saturate hHS1. However, the fact that 10 μM exogenous heme saturates hHS1 but leaves hHS1-M7A at 0% bound, may suggest that some amount of the LH pool exists in a ferric state. The details regarding the oxidation state of heme remain unclear. Even so, one might predict that LH is largely ferrous if it were to equilibrate with the cellular redox buffer, glutathione, which poises the $E_m^{Cytosol} \sim$ -320 mV vs. NHE[118]. If free heme, which has redox potentials that can span E_m = -50 mV to -220mV vs NHE, reacts with the glutathione redox buffer (E_m = -250 mV vs NHE), ferric heme should only constitute 0.003 % (using -50 mV vs NHE) to 2.05 % (using -220 mV vs NHE) of LH at equilibrium. Even so, the speciation and redox potentials of buffered LH as well as the degree to which LH assessible to hHS1 equilibrates with the glutathione redox buffer are unknown.

Even so, a considerable fraction of buffered LH may be ferric as previous reporters with activity-based heme reporters report ferric heme on the order of 100s of nM in HEK293 cells. Perhaps these previous values with subcellular localized reporters may be largely ferric due heme oxidation that may result from cell lysis implored with this heme detection method. Even so, the regulatory heme pool is typically thought to comprise of 10% of the total heme quota, which equates to 1-2 μM heme in these cells (Figure 4.4). If cells truly buffer LH to pM levels, which equates to almost no free heme, what can buffer heme to these low levels and be used to regulate heme dependent processes? To better address the specific concentrations and oxidation states of LH and its buffer depth more sensors with different dynamic ranges for ferric and ferrous

affinities need to be utilized, and the degree to which heme equilibrates with the glutathione redox buffer warrants investigation.

Interestingly, the conditions under which hHS1-M7A detects LH were also found to induce the increased formation of heme granules in HEK293 cells as detected by the label-free transient absorption microscopy technique by Chen et al[224]. Perhaps, hHS1-M7A interacts with heme that may accumulate in these enlarged extra-mitochondrial heme granules that abundantly increase under heme stress conditions[224]. This explanation is consistent with the fact that hHS1-M7A cells do not respond to a dose of ALA that saturates hHS1 but do respond to excess exogenous heme treatment (Figure 4.1). The nature of these heme granules and their involvement in controlling LH availability merits further investigation.

All considered, the data in Figure 4.1 clearly demonstrated that hHS1 was much better suited for sensing due to its heme responsiveness, so all further studies were addressed using this sensor. To further assess the sensitivity of hHS1, we subjected heme-starved HD + SA vs regular media cells to low μM doses of exogenous heme. These results indicate that prolonged treatment with 0.2 μM heme are sufficient to considerably alter LH availability in both heme starved and regular media grown cells (Figure 4.2). Additionally, excess of 1 μM exogenous heme treatment is required to make up for the gap between LH availability between HD + SA and regular media cells. This observation between heme starved and regular media cells fed exogenous heme primed us to later investigate what component of LH exists in regular media cells from the import of extracellular heme versus endogenously synthesized heme.

Having optimized the use of cytosolic hHS1, we next investigated the repletion kinetics of cytosolic LH versus total heme. Surprisingly, total heme pools were refilled within two hours, while cytosolic LH was replenished slowly over 24 hours post heme starvation (Figure 4.4). Other studies in yeast looking at LH versus total heme repletion kinetics have indicated that LH is restored concurrently with TH, but this is not the case here in HEK293 cells[231]. The nature of how this total heme and hemoproteins are replenished in HEK293 cells while bypassing the side-by-side refilling of cytosolic LH seen in yeast is of interest. When cells are replenishing LH through synthesis, is there not a pool of LH that is responsible for refilling hemoproteins, or is this heme pool buffered to undetectable levels until other heme proteins are filled? These results might indicate that heme transport to client hemoproteins from the site of synthesis in the mitochondria may rely on some uncharacterized method that may utilize direct protein-protein heme transfer mechanisms circumventing the use of a regulatory LH pool until these proteins acquire heme. The evidence for a heme metabolon with structural components that may facilitate its coordination with different organelles that may integrate scaffolds with signaling proteins[71], in addition to mitochondrial dynamics affecting heme delivery rates to subcellular locals[231], and our data in HEK293 cells, are all consistent with the potential for a novel mechanism of heme delivery that can bypass the LH pool. Complimentary to this theory is the potential for the newly synthesized heme to first be portioned to the ER by translocation through mitochondrial associated membranes (MAMs). Indeed, several factors key in the regulation of heme homeostasis, including coproporphyrinogen III oxidase, ferrochelatase, HBP-1, and HO2, have been found to associate with MAMs[232]. Even so, these results still warrant the question, what is the role of cytosolic LH in

HEK293 cells? And, is there a pool of LH being used under these heme repletion conditions but is either inaccessible or below the detection limit of hHS1?

Regarding the importance of developing several different heme sensors, previous reports of labile heme in cancer cell lines report subcellular labile heme levels of between 20-40 nM in cytosolic, nuclear, mitochondrial, and ER subcellular compartments, indicating roughly equal distribution of LH throughout these cells. Contrary to this, our previous results in *Saccharomyces cerevisiae* indicate that these cells have much lower LH availability in their nuclear and mitochondrial fractions (<2.5 nM), but between 20-40 nM labile heme in the cytosol. The differences in these LH measurements could reflect organism to organism differences but may also arise from the potential of each heme sensor to have differential capacities to equilibrate with proteins that buffer LH. Towards this point, in the current work in HEK293 cells we report pM ferrous or nM ferric cytosolic, nuclear, and mitochondrial LH under basal conditions (Figure 4.7), while previous work with activity-based reporters indicate that LH in HEK293 is buffered to 100s of nM ferric heme. Taken together, there may be several different factors that buffer LH inside these cells, which may serve as regulatory reservoirs for different heme dependent processes. Ultimately these results highlight the importance of the continued development of heme sensors with a variety of binding affinities and heme binding scaffolds to better understand the nature of LH.

Utilizing our calibration methods to assess hHS1 fractional saturation in cells, we were able to give estimates for the maximum amount of ferrous and ferric heme in each compartment, assuming only one oxidation state of heme existed in each compartment (Figure 4.7). When reporting molecules of heme per each compartment, the number of

molecules changed of less than 5 molecules of ferrous heme in each compartment to ~250 -1,100 molecules of ferric heme depending on the particular organelle and the oxidation state of heme being sensed, demonstrating the importance of developing more oxidation state specific sensors for heme.

Interestingly, our results interrogating the compartment specific response to endogenous versus exogenous heme sources indicate that nuclear and mitochondrial LH is affected differently than cytosolic LH under heme starvation (Figure 4.8). Indeed, heme starvation by inhibiting synthesis in heme replete media almost completely depletes cytosolic LH (<5 % hHS1 loading) while mitochondrial and nuclear hHS1 sensors are around 20% bound with heme (Figure 4.9). These results indicate that cells undergoing heme starvation by inhibition of synthesis either hold on to LH in these compartments, or the cell recognizes a need for heme, and uptake it from the extracellular media (Figure 4.9). This same study clearly indicates that mitochondrial LH pools are more sensitive to endogenous heme supply than the cytosolic and nuclear compartments. As seen in Figure 4.9B, mitochondrial LH is almost completely replenished by synthesis alone, where there is very marginal impact on mitochondrial LH in cells being grown in HD versus regular media. Cytosolic and nuclear heme on the other hand, seem to equilibrate more with extracellular heme than the mitochondrial LH pool does, indicated by the increase in their LH availability in response to growth in HD versus regular media. Further, under high heme conditions, the fraction of hHS1 bound to heme in mitochondria indicate that the mitochondria equilibrate with extracellular heme less than cytosol and nucleus in HEK293 cells. Given that total heme is roughly the same between the compared conditions (i.e. regular media vs HD vs regular + SA media, and regular media + heme vs

+ ALA), the changes in fraction bound in each compartment are from compartment specific preferences for heme source more so than from changes in total heme availability (Figure 4.9A,B).

Our observations that HO2 lowers LH independent of its catalytic function, but solely by its potential to bind heme in its catalytic core were quite surprising (Figure 4.11). Further evincing this heme sequestering role of HO2 is the fact that HO2 does not impact total heme stores when overexpressed (Figure 4.13) and acts independently of HO-1 induction (Figure 4.12E). Given that mitochondrial LH is unaffected by HO2 in regular media ± ALA, mitochondria seem to maintain a LH pool that is not impacted by overexpressed HO2, unlike the cytosolic and nuclear LH pools (Figure 4.14A-C). Additionally, as mitochondria are only affected when cells have been heme starved and then fed exogenous heme, overexpressed HO2 likely prevents the translocation of exogenous heme to the mitochondria (Figure 4.14B). HO2 is canonically thought of as a heme degrading enzyme, and not necessarily a heme buffering or trafficking factor as these results mandate. How HO2 functions and its physiological roles for binding LH without degrading it are still unknown, but this newly identified heme buffering role may explain why the catalytic mutant of HO2 benefits cryoprotection to cells confronted with oxidative stress in previous reports[227]. Although we were not able to ascribe a role to the HRMs, which have been thought to tune the affinity of HO2 for heme depending on their redox state[113, 233], we hypothesize that these HRMs modulate the activity of HO2 to switch from heme buffering to heme catabolic roles. The identification of conditions that may satisfy this switch may explain more of the HO2's other implicated roles in cryoprotection in inflammatory and neurogenerative disorders. Indeed, as HO2 seems

have some preference for exogenously supplied heme (Figure 4.14B) it may act to sequester this heme under conditions like hemolytic stress to prevent the deleterious effects of excess free or mishandled heme.

Altogether we have demonstrated the utility of hHS1 in heme sensing in mammalian cells and have employed this sensor in HEK293 cells to both interrogate compartment specific preferences for heme and to identify a new LH sequestering role for HO2. The continued development of sensors with differently tuned affinities for heme are required to establish the specific quantities of LH in these cells, but for now, hHS1 is a sensitive tool that can be utilized in detecting compartment specific fluxes in LH availability and should be used to interrogate the nature of LH in other more relevant mammalian cell lines.

4.6 Materials and Methods

4.6.1 Human Embryonic Kidney (HEK293) cells, Media, and Growth Conditions

HEK293 cells were plated and transfected in 60 mm X 15 mm polystyrenecoated sterile dishes (Corning) for flow cytometry. The cells were plated on day 0 in basal growth medium (Dulbecco's modified eagle medium (DMEM) containing 10% fetal bovine serum. On day 1 or 2, cells were transfected with heme sensor plasmids pcDNA3.1-HS1, pcDNA3.1-HS1-M7A, pcDNA3.1-HS1-M7A, H102A or pEF52α-hHS1 or hHS1-M7A expression constructs for cytosolic, nuclear, or mitochondrial targeting of heme sensor. For HO2 overexpression studies, HO2 expressed by the CMV promoter of pcDNA3.1 were cotransfected into cells with hHS1 using Lipofectamine LTX. If cells were transfected for longer than 60 hours, media was changed 24 hours before

harvesting. See Appendix for details concerning each plasmid and each of the several transfection protocols utilized in this study.

4.6.2 Characterization of Heme Sensors in Human Embryonic Kidney (HEK293) cells

Flow cytometric measurements were performed using a BD FACS Aria Ill Cell Sorter, BD LSR II Flow Cytometer, or BD Fortessa Flow Cytometers, both equipped with an argon laser (ex 488 nm) and yellow-green laser (ex 561 nm). EGFP was excited using the argon laser and was measured using a 530/30 nm bandpass filter. mKATE2 was excited using the yellow- green laser and was measured using a 610/20 nm bandpass filter. Data evaluation was conducted using FlowJo v10.4.2 software. The number of cells measured per experiment was set on an experiment by experiment basis, but a set number of medium fluorescence mKATE2 positive cells, gated on dot plots while analyzing cells, were selected and counted for analysis. The typical range was between 2000-25,000 of these mKATE2 positive cells.

4.6.3 Total heme Quantification

Measurements of total heme were accomplished using a fluorometric assay designed to measure the fluorescence of protoporphyrin IX upon the release of iron from heme as previously described[221]. For most total heme measurements, following harvest, HEK293 cell counts were assessed using automated TC20 cell counter (BioRad). Cells pellets were resuspended in 20 mM oxalic acid overnight at 4°C protected from light. Following the overnight, cell suspensions were treated an equal volume of warm oxalic acid to give a final [oxalic acid] of ~ 1M. This suspensions of samples were split, with half the cell suspension transferred to a heat block set at 100 °C and heated for 30

minutes and the other half of the cell suspension kept at room temperature (~25 °C) for 30 minutes. All suspensions were centrifuged for 2 minutes on a table-top microfuge at 21000 x g and the porphyrin fluorescence (ex: 400 nm, em: 620 nm) of 200 µL of each sample was recorded on a Synergy Mx multi-modal plate reader using black Greiner Bio-one flat bottom fluorescence plates. Heme concentrations were calculated from a standard curve prepared by diluting 500-1500 µM hemin chloride stock solutions in 0.1 M NaOH into blank oxalic acid stocks prepared the same way as for the cell samples. In order to calculate heme concentrations, the fluorescence of the unboiled sample (taken to be the background level of protoporphyrin IX) is subtracted from the fluorescence of the boiled sample (taken to be the free base porphyrin generated upon the release of heme iron). The cellular concentration of heme is determined by dividing the moles of heme determined in this fluorescence assay and dividing by the number of cells analyzed, giving moles of heme per cell, and then converting to a cellular concentration by dividing by the volume of a HEK293 cells approximated to be 1.23 pL[226].

4.6.4 Immunoblotting

Cells were harvested in the same way as described for flow cytometry as outlined in the Appendix. Briefly, cells grown in 6-well plates were aspirated of their media, rinsed with 1 mL DPBS, then harvested by pipetting in 1 mL DPBS. Cells were harvested into microcentrifuge tubes for freeze thaw lysis or in hefty tubes for lysis by bullet blending. To pellet, cells were centrifuged at 400 x g for 4 minutes at 4 °C, aspirated, then resuspended in lysis buffer for 3x freeze thaws or had lysis buffer added for bullet blending. For freeze thawing, cells were frozen twice at 80 °C for at least 1 hour, then thawed in a 37 °C water bath, then frozen a third time then thawed at room temperature.

For bullet blending, lysis was achieved at 4 °C using one pellet volume of zirconium oxide beads and a bead beater (Bullet Blender, Next Advance) on a setting of 8 for 3 minutes[139, 140]. Post lysis with either method, lysates were centrifuged at max speed for 30 minutes to separate cellular debris from the supernatants. Lysate protein concentrations were determined by the Bradford method (Bio-rad) and 14% tris-glycine gels (Invitrogen) were employed for SDS-PAGE[139, 141]. Anti-GAPDH polyclonal antibody (ProScience) and a goat anti-rabbit secondary antibody conjugated to a 790 nm emitting fluorophore (Invitrogen) were used to probe GAPDH. Anti-HO2 (Abcam) and anti-HO-1 (Enzo Life Sciences) polyclonal antibodies were used in sequence to probe HO2 and HO-1 and were both used in conjunction with a goat anti-rabbit secondary antibody conjugated to a 680 nm emitting fluorophore (Biotium). GAPDH was probed with primary anti-GAPDH at room temperature for 1 hour. Primary antibodies for anti-HO2 and anti-HO-1 were each individually applied to membranes overnight treatments at 4 °C. All gels were imaged on a LiCOR Odyssey Infrared imager[139, 141].

CHAPTER 5. CONCLUSION

The means to elucidate the mechanisms underlying heme trafficking and transport as well as the tools to quantitate the amount of labile heme inside cells has been a long sought-after goal as more roles for this multifaceted cofactor and signaling molecule are unveiled. Uncovering these molecular details regarding how cells manage heme, is not only important to understand its potential uses in the cell, but are moreover highlighted by the deleterious effects of mishandled heme and the association of aberrant heme trafficking in many disease states, including hemolytic diseases, cardiovascular disease, neurodegenerative diseases, infectious diseases, and porphyria.

To increase the capacity to address the multitude of unknowns pertaining to the nature and dynamics of labile heme, including its concentration, oxidation state, speciation, distribution and dynamics, we generated genetically encoded sensors for heme. Using these sensors in both microbial and mammalian cells, we have divulged methods to quantitate changes in subcellular LH availability, ascribed a functional role for LH in regulating metabolism, and uncovered novel roles for proteins involved in regulating LH availability, including previous suggested factors like the proteasome and the signaling molecule nitric oxide. Further, we distinguished a condition under which LH is uncoupled due to stress imparted by Pb^{2+} poisoning, where ironically, total cellular heme is depleted while labile heme has been preserved for signaling.

Having identified several conditions that effected labile heme availability, we sought to develop a method for the quantitation of proteins that bind or release heme in response to stress. The application of this approach to Pb^{2+} poisoned cells should reveal

novel heme signaling networks employed by cells to manage stress and may have implications in understanding the pathogenesis of heavy metal toxicity, which has become a real concern in certain communities. Validating the application of our approach to identifying heme signaling networks may poise its use to investigate what proteins are involved in signaling and in several other identified conditions that alter protein heme speciation in response to either chemical or genetic stresses imparted to cells.

With the continued use of the developed heme sensors in ongoing genetic screens and investigations for heme's role in Alzheimer's disease and infectious diseases that require heme for virulence, others are uncovering more factors that are involved in regulating heme availability and are ascribing functional roles for LH in the pathogenesis of these diseases. With the continued development and use of more heme sensors along with cleverly devised biochemical and genetic strategies, who knows, someone may even uncover the mechanism underlying how hemoglobin acquires its heme.

APPENDIX A. SUPPLEMENTARY LIST OF METHODS, OPTIMIZATIONS, ANNECODTAL RESULTS SUPPLEMENTARY TO THE DISSERTATION, AND CATALOGUE OF HEME SENSOR REAGENTS AND STRAIN GENERATION

A.1 Introduction

This appendix is to serve as a supplementary section that includes more detailed methods and explanations of the technical details behind each procedure and the optimization of protocols utilized in the main body of work. Additionally, this appendix is a source for any unpublished data that did not fit with Chapters 2-4. Finally, herein is a catalogue of how I generated all of the yeast strains and plasmids that were relevant to this work.

A.2 Chapter 2 Supplementary Methods

A.2.1 Cellular Heme Imaging Methods: Cytosol – Optimization of the In Situ Calibration of HS1-M7A by Flow Cytometry

Optimization of these calibration procedures with *hem1Δ* cells expressing HS1-M7A by flow cytometry demonstrates that in situ calibration reagents added in parts or without heme have negligible effects on the heme sensor fluorescence ratio (**Error! Reference s ource not found.**). Additionally, the EGFP:mKATE ratio of cells treated with heme are only lowered significantly when cotreated with digitonin (Figure A. 1). When testing the effects of two different reductants, ascorbate and DTT, ascorbate was found better suited

in equipping ferrous binding HS1-M7A with enough reduced heme to saturate its EGFP:mKATE ratio (**Error! Reference source not found.**). Finally, when testing the u se of both DTT and ascorbate consequently, there appear to be heme independent effects on the HS1-M7A sensor ratio (Figure A. 1).

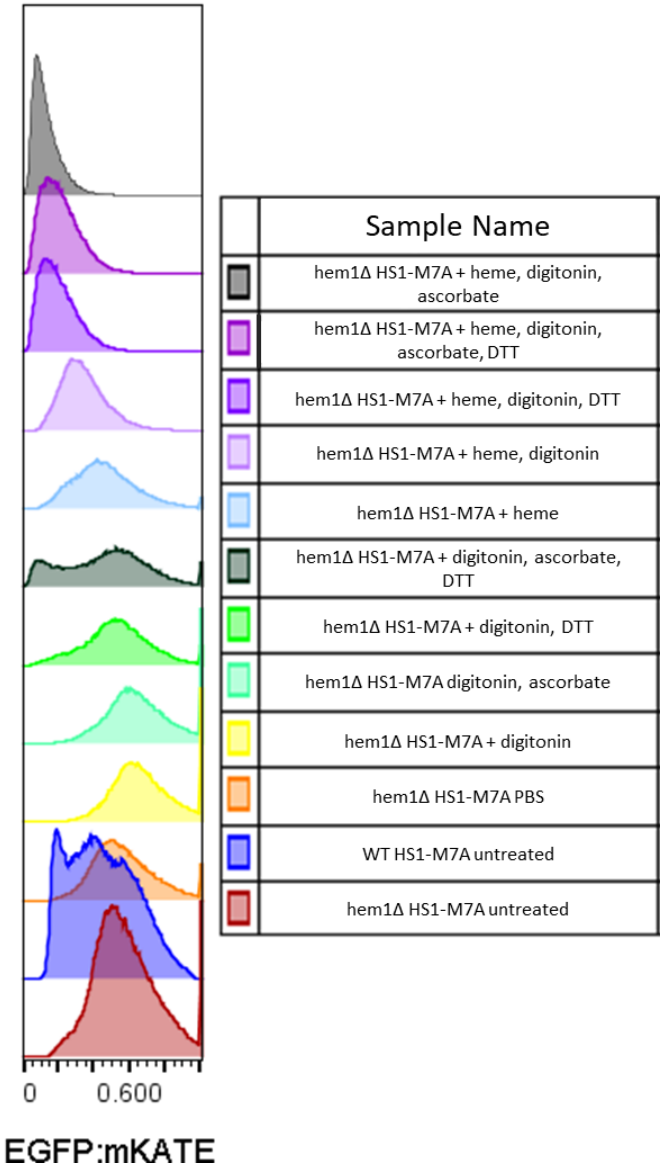

Figure A. 1 - Flow cytometric analysis of the optimization of heme sensor in situ calibration protocol. The effects of the in situ calibration reagents with and without heme and with two different reducing agents were tested. Following the same protocol as in

Figure 2.7, cells were treated with and without 50 µM heme, 200 µg/mL digitonin, 1mM ascorbate, and/or 1mM DTT. The untreated cells, "WT HS1-M7A untreated" and "*hem1Δ* HS1-M7A untreated" were analyzed while all the cells used for the in situ calibration optimization were in PBS undergoing different treatment conditions for 30 minutes at 30 °C (Figure 2.7).

A.2.1.2 Cellular Heme Imaging Methods: Cytosol —Flow Cytometry Gating Yeast Dot Plots to Generate Ratio Histograms

Single cell analysis of EGFP:mKATE2 expressing gives the power to see heterogeneity in cell populations, evincing the tri-modal distribution in labile heme availability in yeast (Figure 2.8) and to see secondary cell populations that arise by treated with excess reductants but are only a subpopulation of cells. (Figure A. 1). To properly analyze these samples, steps must be taken to remove populations that are too much like untransfected or EV fluorescence levels and ro remove events that have heme independent changes in fluorescence ratio. Herein, are the steps to properly gate yeast cell populations expressing HS1-M7A sensor (See Figure A. 2):

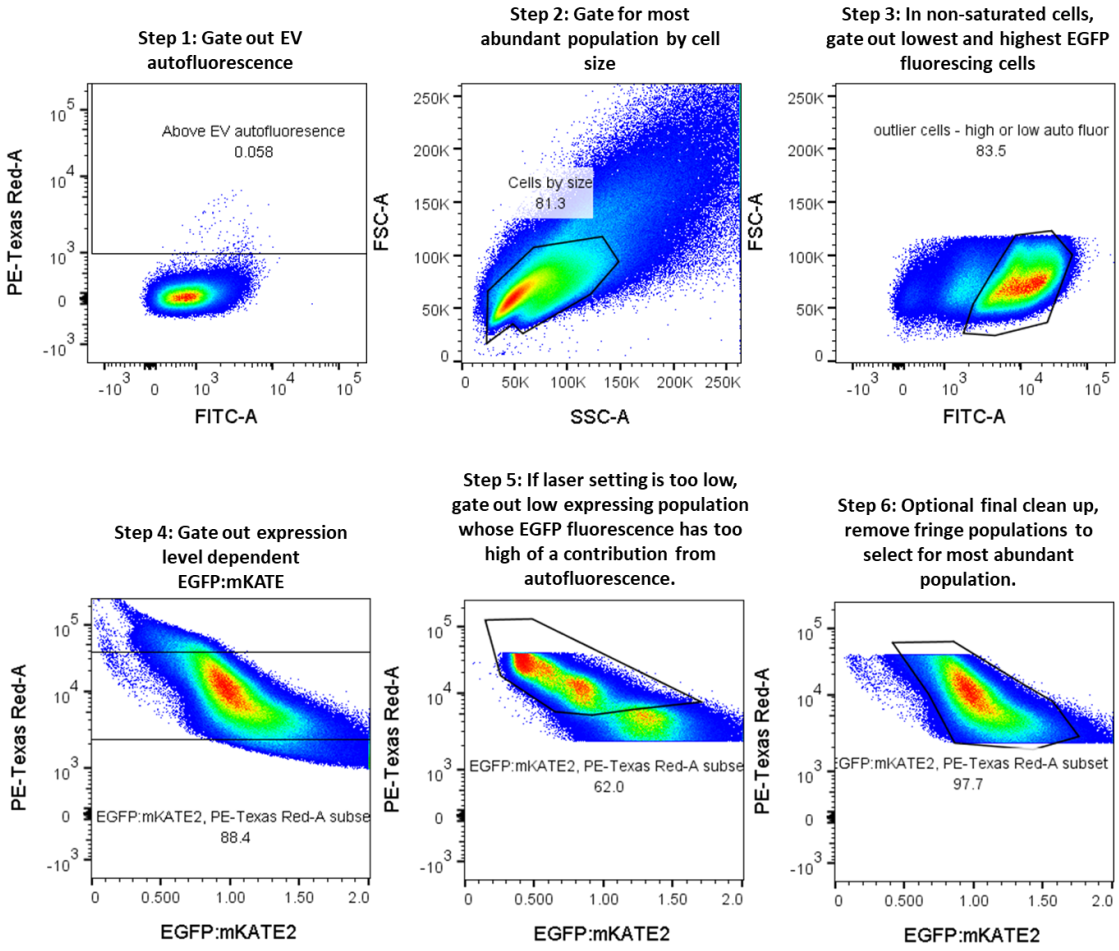

Figure A. 2 - Steps to follow to gate yeast cells expressing HS1-M7A for flow cytometric analyses of heme dependent changes in sensor fluorescence ratio. The steps will ensure that the removal of cells that have heme independent changes in sensor fluorescence ratio and the removal of low fluorescing cells that are influenced too much by EV autofluorescence (Step 5).

1. Use EV cells to create a gate to apply to all cells populations to only accept cells with fluorescence levels above EV autofluorescence (Figure A. 2Figure A. 2 - Steps to follow to gate yeast cells expressing HS1-M7A for flow cytometric analyses of heme dependent changes in sensor fluorescence ratio. The steps will ensure that the removal of cells that have heme independent changes in sensor

fluorescence ratio and the removal of low fluorescing cells that are influenced too much by EV autofluorescence (Step 5)., Step 1 dot plot).

2. To the subpopulations of cells formed using Step 1, apply a gate that keeps the most abundant cell population. Do this by creating a gate that selects for the most abundant cell population in a dot plot of Forward vs. Side Scatter. See Figure A. 2, Step 2 dot plot.
3. The next gate to apply is to subpopulation 2 and removes any remaining cells with low or exceedingly high EGFP autofluorescence using a forward scatter vs EGFP dot plot. Often, but not always, some cells with very low (those that survived Step 1) or very high EGFP fluorescence exist (sometimes from cellular clumping that can arise with some treatments, i.e. excess heme) that need to be removed. Form the gate using a cell sample with high EGFP fluorescing cells like hem1Δ cells expressing heme sensor. This gate should not be applied to remove low fluorescing EGFP cells from heme saturated samples, as the EGFP fluorescence in these heme saturated cells resembles near autofluorescence levels of EGFP. See **Error! Reference source not found.**, Step 3 dot plot.
4. Make a mKATE2 vs EGFP:mKATE2 dot plot on cells that are in subpopulation 3, which shows the heme sensor ratio's dependence on expression. The highest expressing cells have a lower ratio and the lowest fluorescing cells have a very wide distribution, likely because of autofluorescence variability in cells that will affect how much "GFP" fluorescence there is independently of [heme]. These high and low expression populations should be gated out. See Figure A. 2, Step 4 dot plot.

5. In WT cells expressing HS1-M7A, check to see if how the bottom fluorescing cell population looks like relative to *hem1Δ* cells by overlaying their EGFP:mKATE2 histograms. If this dot plot contains a populations population has a very high ratio, which can be higher than the mode hem1Δ ratio, (dark red histogram in Figure A.3**Error! Reference source not found.**), then it should be removed. To gate out this population, make a mKATE2 vs EGFP:mKATE2 ratio dot plot on cells that are in subpopulation 4, and create a gate to remove the lowest expression population See Figure A. 2, Step 5 dot plot. This population of low fluorescing EGFP:mKATE2 cells may have EGFP values too close to EV EGFP autofluorescence if your laser settings for FITC-A are set too low. The fluorescence contributed by a cells autofluorescence in low fluorescing cells may give an artificially high "EGFP" fluorescence value relative to mKATE2 expression, giving an uncharacteristically high EGFP:mKATE ratio. This is one disadvantage of flow cytometry over fluorimetry unless you take the time to export all of the data out of FlowJO and into a software like Excel and determine a good way to subtract out EGFP EV autofluorescence from every cell in your analysis. However, as the EV autofluorescence between cell varies, it is difficult to decide on the best value to subtract from each cell.
6. Finally, to your subpopulation made in the last mKATE2 vs EGFP:mKATE2 Ratio dot plot or an EGFP vs mKATE2 dot blot, remove any outlier or low abundance populations on the fringe of your most highest cell populations on the dot plot countor map (red dots represent the highest abundant cell type on the dot plot, while the blue dots on the fringe are the lowest represented cell type). This is

not a necessary step but cleans your data up a little bit. See Figure A. 2, Step 6 dot plot.

The cells used in creating this methods primer, Steps 1-6, are the cells plotted in the EGFP:mKATE2 histograms in Figure A.3**Error! Reference source not found.**. F ollowing Steps 1-6 exactly will gate cells to optimally demonstrate the *in vivo* heme dependent changes in HS1-M7A sensor fluorescence.

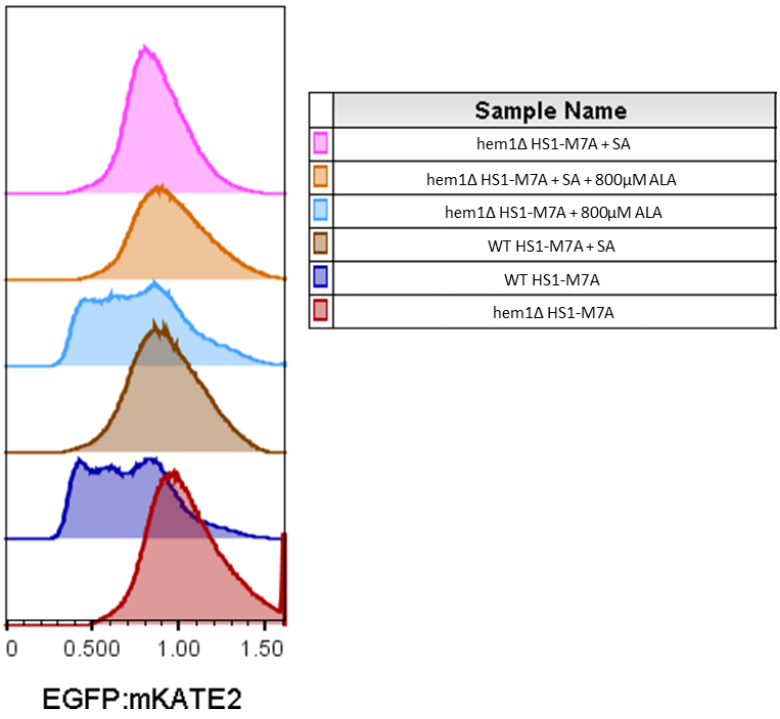

Figure A.3 – Resulting histograms from gating WT and hem1Δ cells expressing HS1-M7A that were treated with a heme depleting dose of SA and heme replenishing dose of ALA for *hem1Δ* cells. Following the gating steps outlined in **Error! Reference source n ot found.** yields a trimodal distribution in cells that are heme replete and express HS1-M7A and yields monomodal distributions of any SA treated cell population (WT or hem1Δ) that is marginally lower in ratio than untreated *hem1Δ* cells expressing HS1-M7A.

Lastly, Figure A.4 and Figure A.5 show all gates applied from Steps 1-6 to *hem1Δ* and WT cells expressing HS1-M7A in FlowJO and are displayed using the “backgating”

function option for each EGFP:mKATE ratio histogram. Each gate that was used to generate the final figures (red histogram for *hem1Δ* and blue histogram for WT) are shown in grey dot plots shown to the right of each coloured histogram. The red dots in each dot blot represent the cells that met the criteria of every gate and are cells that fill the population of the final histograms shown in Figure A.4 and Figure A.5.

hem1Δ cells in Figure A.4 follow Steps 1-4, and 6 for their gating, which ensures that most cells that display heme independent changes in EGFP:mKATE ratio are removed from the analysis. Further gating or a tighter threshold could be applied to Step 4 to remove more of the lower fluorescing cells; however, doing so would only affect the tails of each side of the histogram, without affecting the mode or mean of the distribution significantly. Keeping some of the lower fluorescing cell population in the Step 4 gate, ensures that the tails do not drop off too suddenly, keeping the data from looking too artificial (Figure A.4).

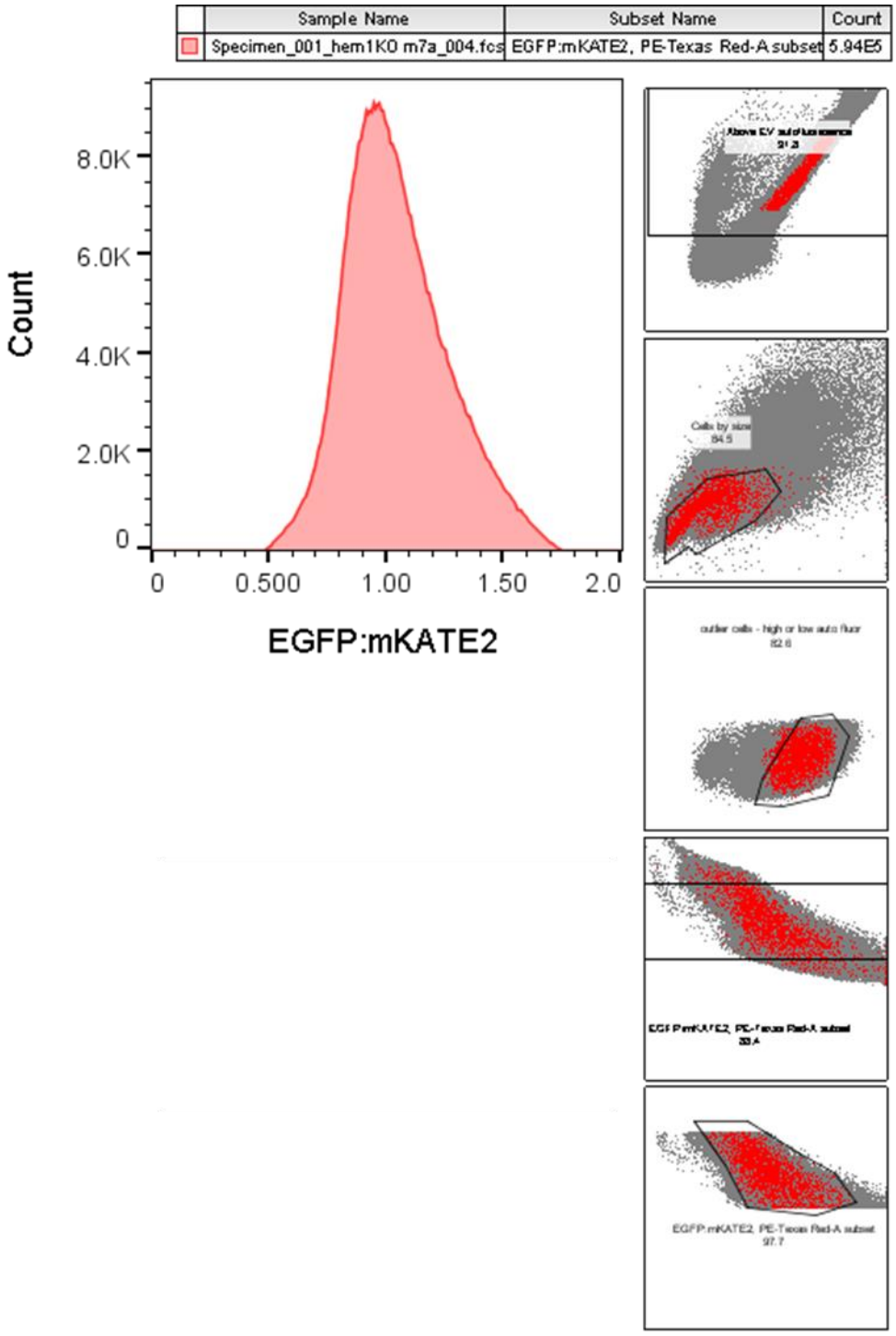

Figure A.4 - Backgating of *hem1Δ* HS1-M7A expressing cells that underwent all of the gates prescribed by Steps 1-4 and 6 as outlined in Figure A. 1. Step 5 does not apply to *hem1Δ* HS1-M7A and is skipped for these cells.

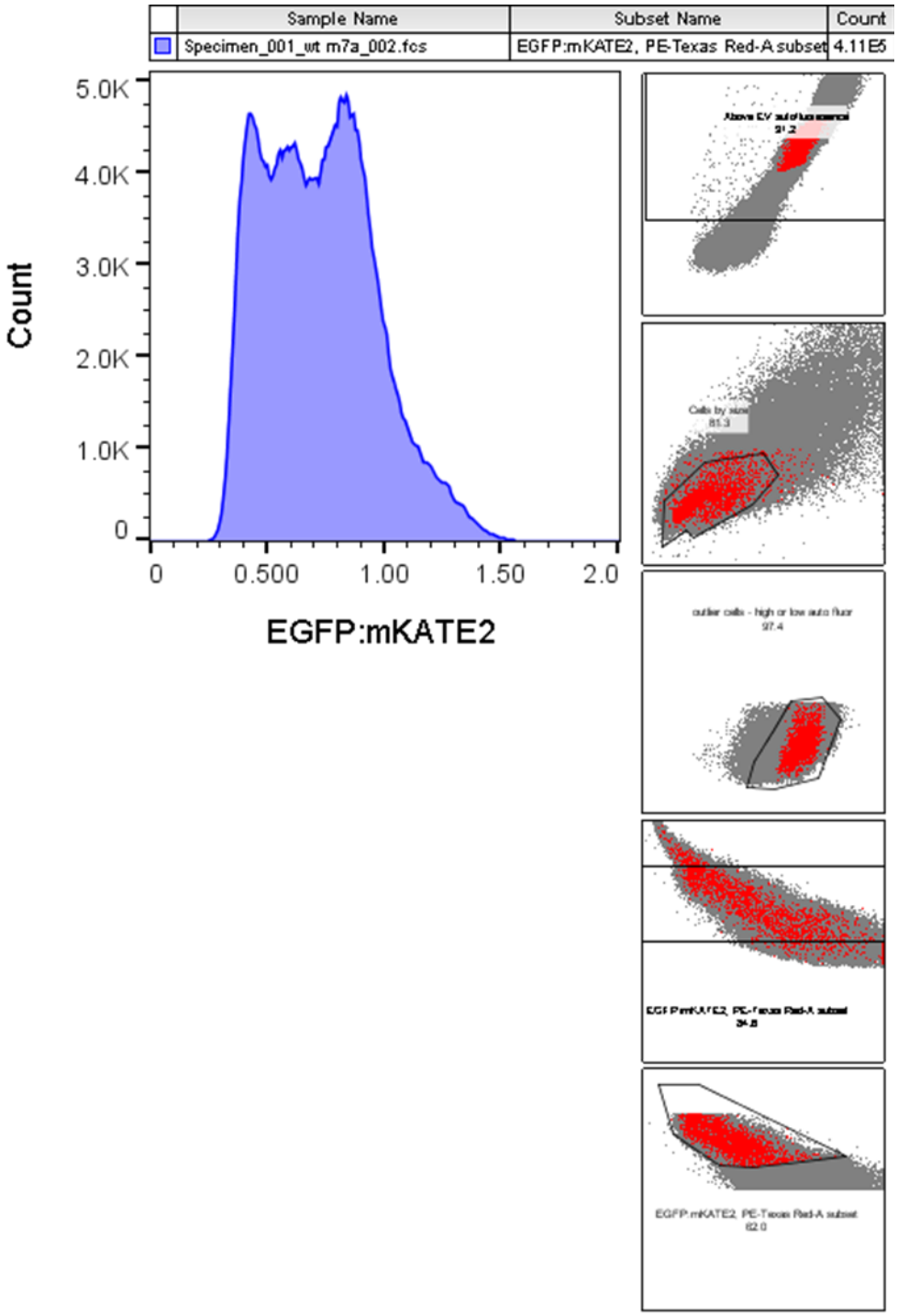

Figure A.5 - Backgating of WT HS1-M7A expressing cells that underwent all of the gates prescribed by Steps 1-6 outlined in Figure A. 2.

Unlike with the hem1Δ HS1-M7A cells, the analysis for WT HS1-M7A expressing cells undergoes all steps outlined in Figure A. 2. to include Step 5. Step 5 is necessary in this case as there is a low expressing sensor population that has an artificially high EGFP:mKATE ratio due to EGFP autofluorescence contributions that affects lower fluorescing cells. Acquiring the data with a lower FITC-A laser setting often mandates that the lowest expression population of HS1-M7A cells be removed. See Figure A.6, which shows this importance of gating out these low fluorescing cells. A higher FITC-A channel laser setting used to analyze the EGFP fluorescence of these cells might put the EGFP fluorescence high enough above background to not be give these cells an artificially higher ratio from the EGFP contributing autofluorescence that comes from a lack of EV autofluorescence subtraction for cells in our analyses. However, the FITC-A channel laser cannot be increased too much as the EGFP fluorescence is already nearing the dynamic range capacity of the flow cytometer's detector in this example (Figure A. 2, Step 3 dot plot, x-axis).

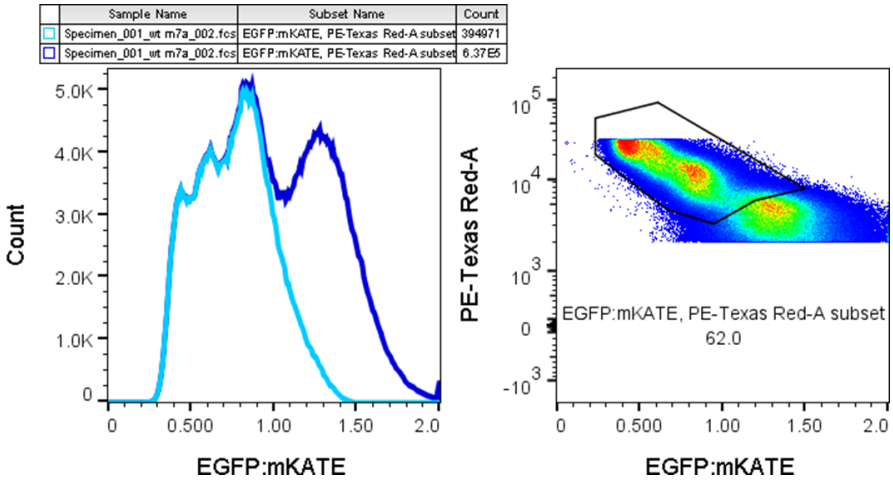

Figure A.6 – Importance of gating lowest fluorescing cell population from WT HS1-M7A expressing cells as outlined in Figure A. 2. Light blue EGFP:mKATE ratio histogram represent the population of cells that went through Steps 1-5 of gating, while

the dark blue histogram are those cells that only went through Steps 1-4 of gating. The dot plot on the right represents cells that passed the criteria of Gates 1-4, and contains gate 5, which removes most of the lowest expressing cell population.

A.2.1.3 Cellular Heme Imaging Methods:Flow Cytometry Gating HEK293 Cell Dot Plots to Generate Ratio Histograms

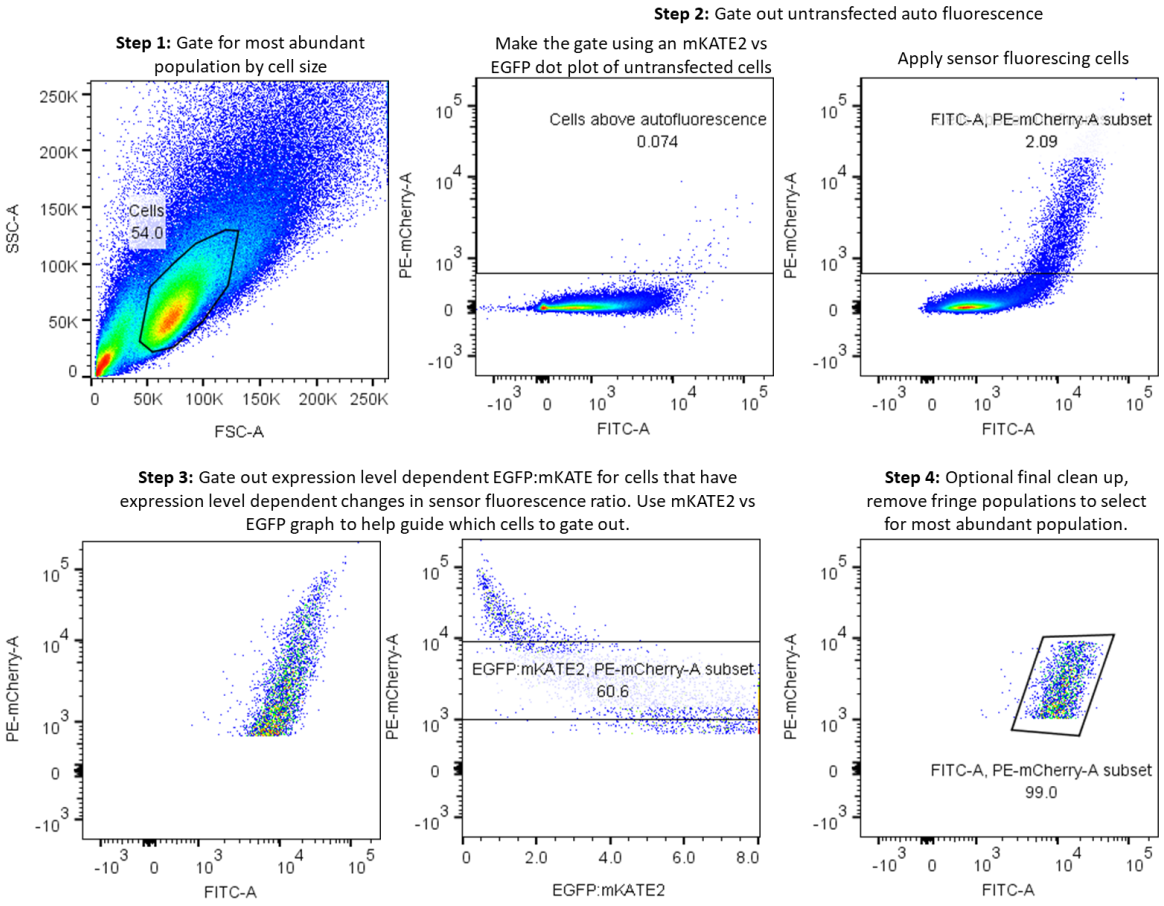

Figure A.7 - Steps to follow to gate transiently transfected HEK293 cells expressing hHS1 sensors. Following each step will select for the events that are cells expressing sensor that have heme dependent changes in their sensor fluorescence ratio by removing debris, untransfected cells, and cells that have heme independent changes in sensor fluorescence ratio. At high expression, hHS1 has heme independent changes in sensor fluorescence ratio, and the lowest expressing cells are influenced too much by EV autofluorescence and should be removed (Step 3).

1. Apply a gate that keeps the most abundant cell population that is not the smallest population using a side scatter (SSC-A) versus forward scatter (FSC-A) dot plot. The medium sized population represents your cells and are referred to as subpopulation 1 of your specimen. See Figure A.7, Step 1.
2. Use analyzed untransfected cells create a gate to apply to all subpopulation 1 cells that will only accept cells with fluorescence levels above the untransfected cells' autofluorescence (Figure A.7, Step 2 dot plot.). The left panel of Step 2 represent the created gate using untransfected cells. The right panel of Step 2 is this gate applied to transfected cells, which removes any remaining untransfected cells and debris. Step 2 generates subpopulation 2.
3. Next, make two dot plots, an mKATE2 vs eGFP:mKATE2 dot plot and an mKATE2 vs eGFP dot plot on cells that are in subpopulation 2. Analyze these dot plots to see where the expression level of sensor begins to cause heme independent changes in ratio, which occurs at both high expression and very low expression of sensor. (See Step 3 dot plots, Figure A.7). Draw a gate around medium mKATE2 expression population on the mKATE2 vs eGFP:mKATE2 dot plot to select for these cells and remove any cells with expression dependent changes in sensor fluorescence ratio. Apply this gate to subpopulation 2 to make subpopulation 3.
4. Finally, to each subpopulation 3 for all your samples, using an eGFP:mKATE2 dot plot , apply a gate that removes any outlier or low abundance populations on the fringe of your highest cell populations. This is not a necessary step but cleans your data up a little bit. See Figure A.7, Step 4.

The cells used in creating this methods primer, Steps 1-4, are the cells plotted in the eGFP:mKATE2 histograms in Figure A.8. Following Steps 1-4 exactly will gate cells to optimally demonstrate the *in vivo* heme dependent changes in hHS1 sensor fluorescence. To see these gates applied to one population of cells, see Figure A.9.

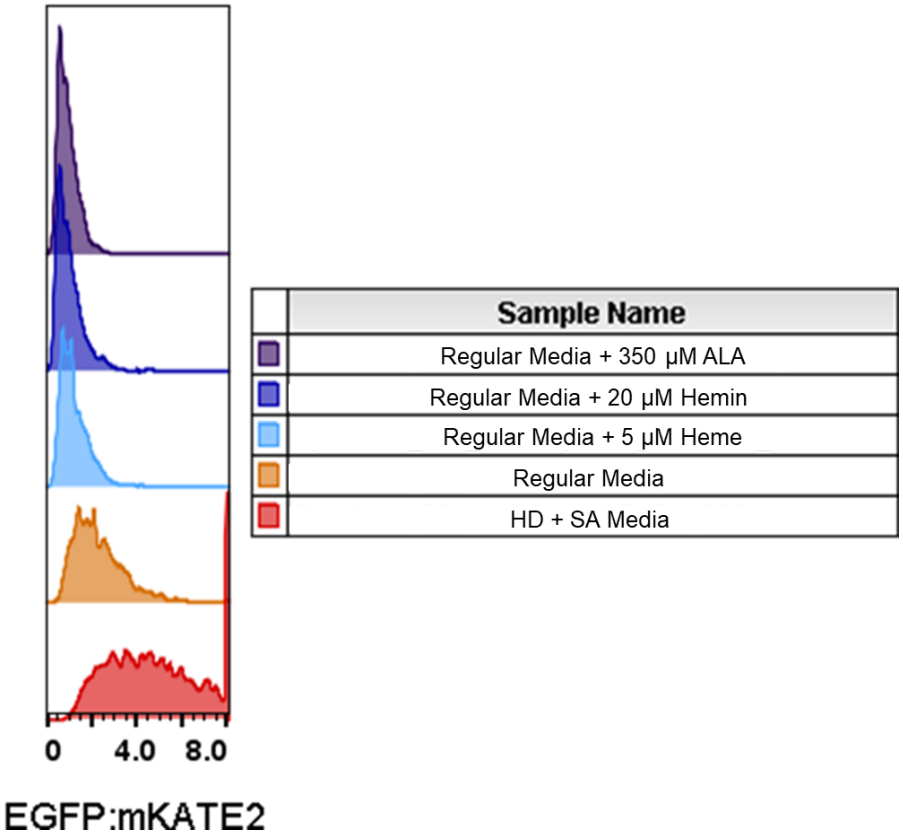

Figure A.8 - Resulting histograms from gating heme depleted (HD +SA media) cells versus cells grown in media with sensor saturating amount of heme or ALA for 24 hours. These histograms contain cells gated exactly as prescribed in Steps 1-4.

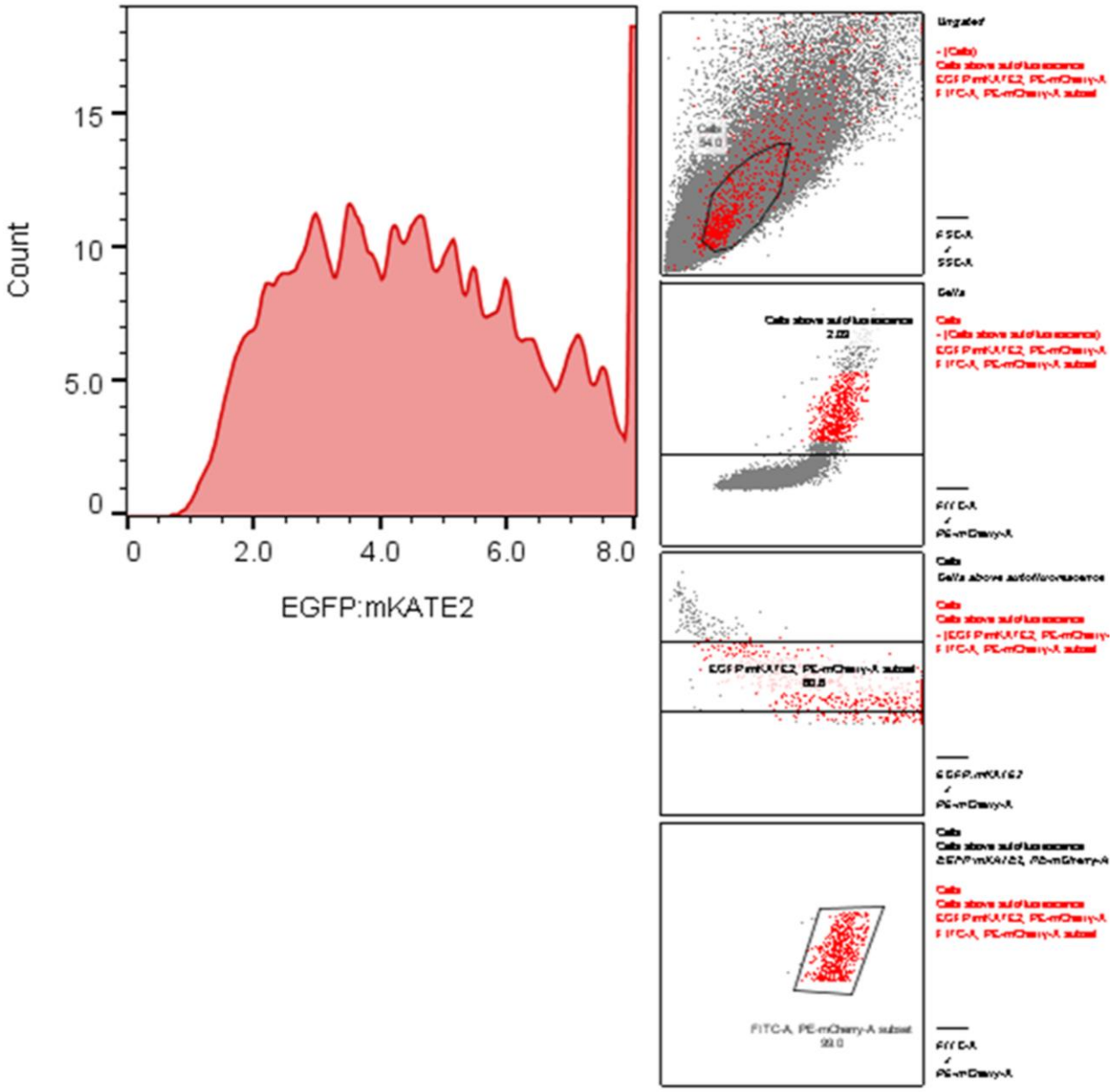

Figure A.9 - FlowJO's backgating function applied to heme deficient HD + SA grown cells to visualize the effects of each gate on cells that make it to the final population analyzed. Each gate applied to the cells that are in the red histogram are shown on the right in gates made following Steps 1 through 4. The top right box represents Step 1 and progresses through the steps ending with Step 4 at the bottom. The gray dots that are shown in each dot plot did not make it to the final histogram. The red dots of each dot plot represent the cells that survived each gate outlined in Steps 1-4 and are the cells plotted in red EGFP:mKATE2 ratio plot.

A.3 Chapter 3 Supplementary Methods and Optimization Procedures

A.3.1 Total Heme Quantification

Measurements of total heme were accomplished using a fluorimetric assay designed to measure the fluorescence of protoporphyrin IX upon the release of iron from heme as previously described[221]. For most total heme measurements, following cell growth, 2 x 10^8 cells were harvested, washed in sterile water, and resuspended in 500 μL of 20 mM oxalic acid and stored in a closed box at 4 °C overnight (16-18 hours). The total heme assay can work with less than 2 x 10^8, with the lowest number attempted being 1 x 10^7 cells. When using cell numbers this low, instead of resuspended cells in 500 μL 20mM oxalic acid, cells should be resuspended in 250 μL to concentrate the cells slightly. After the 4 °C overnight, a 500mL premade stock of 2 M oxalic acid in a 1 L glass media bottle was warmed on a hot plate, with the lid open, in a fume hood. Once the oxalic acid is mostly dissolved, overnight treated cells are moved to room temperature. Next, 50mL of the warmed 2 M oxalic acid was poured into a 100mL glass beaker and from here an equal volume (500 μL in most cases) of 2 M oxalic acid was added to the cell suspensions that were moved to room temperature to give a final [oxalic acid] of ~1M. The samples were moved to room temperature from 4 °C to warm up since concentrate oxalic acid is not soluble at low temperatures. The samples were split, with half the cell suspension transferred to a heat block set at 100 °C and heated for 30-35 minutes and the other half of the cell suspension kept at room temperature (~25 °C) for 28-33 minutes. The room temperature suspensions are centrifuged first followed by the boiled suspensions for 2 minutes on a table-top microfuge at 21000 x g and the porphyrin fluorescence (ex: 400 nm, em: 604 nm) of 200 μL of each sample was recorded on a

Synergy Mx multi-modal plate reader using black Greiner Bio-one flat bottom fluorescence plates. Taking a porphyrin fluorescence spectrum for each sample of each independent experiment showed that 604 em was consistently a good wavelength to use for collection. Heme concentrations were calculated from a standard curve prepared by diluting a 500-1500 μM hemin chloride stock solutions in 0.1 M NaOH into Milli-Q water to make a 10 μM hemin chloride working solution, (the first dilution of the heme stock is always to 100 μM followed by a dilution 10 μM hemin chloride). The 10 μM hemin chloride stock is then added back to extra untreated cell pellets harvested in tandem with the treated cells from the experiment to create a heme standard curve to be analyzed with the cells whose heme are being quantified. In order to calculate heme concentrations, the fluorescence of the unboiled sample (taken to be the background level of protoporphyrin IX) is subtracted from the fluorescence of the boiled sample (taken to be the free base porphyrin generated upon the release of heme iron). The cellular concentration of heme is determined by dividing the moles of heme determined in this fluorescence assay using the heme standard curve to relate the porphyrin fluorescence to moles of heme, and then dividing by the number of cells analyzed, giving moles of heme per cell. After calculating heme per cell to a molarity of hemin by diving the heme per cell by the volume per yeast cell, which is ~50 fL[29]. This fluorescence assay gives similar qualitative trends between samples as an HPLC assay for heme we previously employed[29], but the absolute concentrations tend to be consistently 3-5 fold higher (data not shown).

A.3.2 Preparation and Use of Hemin Agarose and Sepharose Beads to Affinity Purify Proteins from Cellular Lysates and Apo-myoglobin

Pipet desired volume of bead slurry, typically 100uL slurry per compact reaction column (CRC), in a CRC. Pellet at 700 x g in a microcentrifuge for 5 minutes. Discard the collected solvent and conduct 3x1mL 5 minute washes in sodium phosphate lysis buffer (0.1% Triton X-100, 10 mM NaP_i, 50 mM NaCl, 5mM EDTA, pH 7.4, 1 mM PMSF, 1X ProteaseArrest™), double check notebook rotating at 20 rpm. Distribute the washed beads in lysis buffer to aliquot 100 uL of washed slurry per CRC, of which there should be 1 CRC per reaction condition. Per 100 uL of pelleted slurry (~50 uL volume of beads) add 250 uL of cellular lysate at a concentration of a least 1ug/uL achieved by lysing several 25-50 OD cellular pellets using one pellet volume of zirconium oxide beads and a bead beater (Bullet Blender, Next Advance) on a setting of 8 for 3 minutes[29]. The amount of cells depends on the amount of protein required for the analysis, where at least 200 uL of 2 ug/ uL is required for ample detection of eluted proteins from hemin agarose beads treated with cellular lysates (Figure A.12). When affinity purifying purified proteins with hemin agarose or sepharose, prepare 50 uL of bead bed volume per CRC and add at least 2-5ug myoglobin in 200 uL of lysis buffer in lysis buffer.

Following preparation of beads and addition of cellular lysate or myoglobin to the beads, allow the lysate/protein to incubate with the beads for 60-70 minutes at room temperature rotating at 20rpm in the compact reaction columns. After treating cells with lysate/protein, collect flow through by pelleting CRCs at 700 x g for 5 minutes. If the columns still contain much of the flow through spin for multiple 1 minute spins, making sure not to completely dry out the beads but centrifuging until most of the flow through was collected. If collecting most of the flow through is not required for the experiment, instead, remove most of the rest of the volume by aspirating the rest from the bottom of

the CRC with a 1mL pipet tip connected to a hose and vacuum line. After collecting the flow through, conduct 3x10 minutes washes in lysis buffer, rotating at 20 rpm at room temperature. Collect and/or discard the washes in the same manner as the flow throughs. Finally, elute the proteins from the beads with a 15 minute wash in 50-100 uL 1M imidazole in lysis buffer followed by a 2 minute pellet at max speed.

A.3.2.1 Preparation of Apo-myoglobin

Adapted protocol from Ascoli et al with slight modifications[234]. Weighed out 100 mg of horse heart myoglobin (Sigma-Aldrich). In 1 L beaker on thin layer of ice on a magnetic stir plate, precipitated out protein from heme in acid-acetone (2 M HCl, made by addition of concentrated HCl into acetone), by slowly adding 200 mL of acid-acetone to the myoglobin spinning by magnetic stir bar. The precipitate is white, and the acid-acetone should contain all of the heme. Pelleted the 200 mL volume in several 50 mL conical tubes at -19 °C. Decanted acid acetone supernatant from the pelleted protein and washed each pellet in each conical tube with and addition 50 mL of acid-acetone twice, repelleting at 4 °C at 4000 rpm. Allow the resulting mass of pelleted proteins to solubilize in 4 mL MilliQ water at 4 °C for 1-2 days. Next, conduct two rounds of dialysis overnight of the soluble fraction of the pellets against lysis 150 mL of lysis buffer at 4 °C rotating slowly by magnetic stir bar.

Dialyzed half of the soluble fraction of the pellets against each lysis buffer (0.1% Triton X-100, 20 mM Tris, 100 mM NaCl, pH 7.4) using 2 rounds of dialysis with 100-150mL of each buffer against half the soluble protein.

Next, quantify the dialyzed protein by Bradford Reagent assay using known concentrations of BSA to make a standard curve and by UV-VIS spectroscopy[235]. Finally, make dilutions apo-myoglobin with and without a half of a molar equivalent of heme added and measure the UV spectra relative the spectra of just heme to ensure proper binding of heme to myoglobin from the purified, reconstituted protein.

A.3.2.2 Optimization of Elution Conditions for Hemin Agarose using Apo-myoglobin

An elution condition that would remove heme-binding proteins but would not be too harsh to elute non-specific interactors of hemin agarose was required. To optimize such an elution condition, 1 M imidazole, which has a strong affinity for heme and can compete for heme binding versus the heme matrix of the hemin agarose beads was tested for its efficacy versus heat and SDS, which in combination should elute any protein that sticks to hemin agarose via heme-binding or non-heme specific interactions. Finally, testing imidazole with both SDS and heat should determine any difference in the ability of imidazole to elute proteins versus just SDS and heat. Conveniently, there was no difference in elution efficacy between 1 M imidazole alone compared to the plus heat and SDS conditions, indicating that imidazole alone is enough to elute the myoglobin from the beads (Figure A.10).

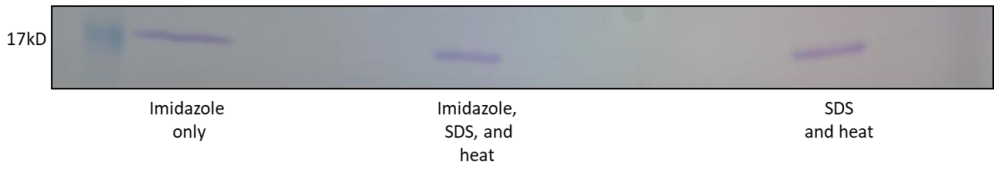

Figure A.10 - Testing apo-myoglobin elution conidtions with 1 M imidazole, 1x SDS loading dye, and heat. Hemin agarose beads were treated with 8 µg of apo-myoglobin at

4°C for 50 minutes. After 3x10 minute 1 mL washes in lysis buffer, the beads were split into 3 equal volumes then eluted with either 1 M imidazole, 1 M imidazole with 1x SDS loading dye, and boiled for 5 minutes, or with 1x SDS loading dye and boiled for 5 minutes. There is no significant difference between the elution conditons indicating the 1 M imidazole alone is sufficent to elute heme-binding proteins off of hemin agarose. This gel is representative of 2 independent trials.

To further validate our elution conditions off of the hemin agarose beads, several other candidate elution conditions were tested against 1 M imidazole, including 8 M urea, lysis buffer alone, 1 % SDS, 100 µM hemin, and heat alone (5 minute boiling of the beads in lysis buffer). To do so, a 200 µL bead bed volume of hemin agarose was prepped and resuspended in 1.2 mL of lysis buffer containing 20 µg of apo-myoglobin. This bead-myoglobin suspension was split into 6 equal parts into 6 compact reaction columns (CRCs) and allowed to incubate at room temperature for an hour. Post treatment and after 3x10 minute washes in lysis buffer, the beads were eluted and analyzed by 1-D PAGE (Figure A.11). 1 M imidazole, 1% SDS, and 100 µM hemin treatment were both the top 3 and the only elution conditions that eluted myoglobin off the beads (Figure A.11). From here, all elutions were conducted using 1 M imidazole in lysis buffer, since 1% SDS is not heme specific, and 100 µM heme may be harder to remove from the eluents if the eluents were to be prepared for MS-MS analysis.

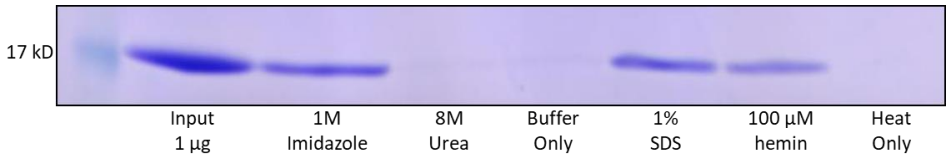

Figure A.11 - Apo-myoglobin eluted off hemin agarose beads by 1 M imidazole versus other candidate elution conditions, including 8 M urea, lysis buffer, 1 % SDS, 100 µM hemin, and heat alone analyzed by 1-D PAGE. 1µg input was completely untreated. Hemin agarose protein treatment was conducted at room temperature, 20 rpm. Each lane was loaded with 70% of its 50 µL elution, giving a theoretical yield of ~2.3 µg per sample. Hence, either not all the myoglobin was eluted off the beads, some myoglobin

never stuck to the beads, or some myoglobin came off during the extensive wash steps (not tested).

After optimizing the elution to remove a canonical heme binding protein from hemin agarose beads, and after having validated that a protein's heme saturation will affect how well the heme-binding protein will bind hemin agarose with the myoglobin studies, we pursued treating hemin agarose with cellular lysates. Previous models and uses of hemin agarose have had success identifying and/or confirming novel heme-binding roles for proteins using hemin agarose [57, 236-239]; however, to date, there has not been a published, comprehensive comparison of a hemin agarose binding proteome analysis between two conditions that are known impact heme signalling or alter cellular protein heme speciation. Specifically, no one for example, no one has devised nor pursued the proper methods to investigate what proteins bind or release heme in response to stress (i.e. heme starvation or Pb^{2+} poisoning) but instead only investigated one or two candidate proteins.

So, to move forward, our next step in establishing such a method with hemin agarose in our yeast models began by optimizing the amount of hemin agarose beads to use in tandem with how much protein lysate to load the beads with for an hour treatment (Figure A.12). The lowest bead bed volume was too low to affinity purify enough protein to be visible by coomassie blue staining (Figure A.12, 12.5 µL column). As there is little difference between 2.5 µg/µL and 5 µg/µL protein lysate loaded, it is possible that the beads have become saturated with proteins at this concentration of protein. Higher amounts of eluted protein resulted from using the highest bead bed volume, but there was not a large difference between this 100 µL and the 50 µL bead bed volume sample

(Figure A.12). Moving forward, all cellular lysates were treated with at least 50 µL bead bed volumes of hemin agarose, with cellular lysate volumes between 200-300 µL with target protein lysate concentrations of ~2 µg/µL.

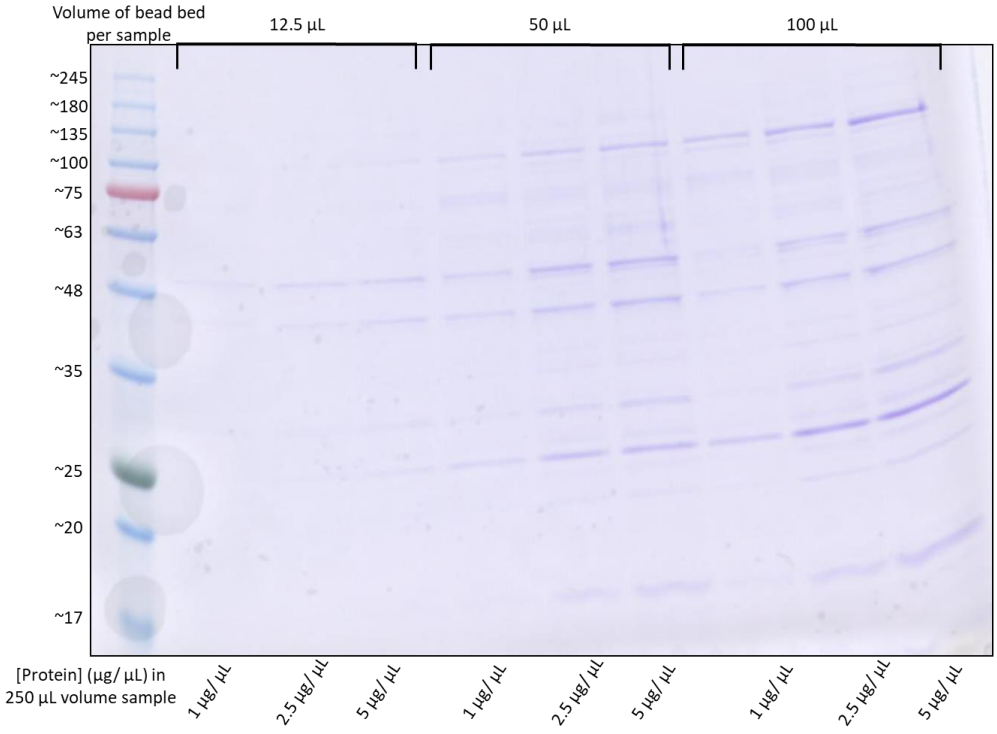

Figure A.12 – Optimization of bead bed volume of hemin agarose versus concentration of protein to load in 250 µL protein lysate for 1-hour room temperature hemin agarose treatments. The results indicate that to optimize the amount of proteins pulled out with hemin agarose, at least a 50 µL bead bed volume (~100 µL of slurry) and ~2 µg/µL but less than 5 µg/µL protein should be used.

A.3.2.3 Attempting by 1-D PAGE with Coomassie Staining and SyproRuby Staining

At this point, our model and hypothesis that proteins will stick to hemin agarose preferentially based on whether they are heme bound or not seems accurate with both pure hemoproteins, like myoglobin, and proteins extracted from differentially heme

starved cellular lysates. Furthermore, the protein interactions are quite heme specific when comparing their relative abundances to the proteins resulting from sepharose bead treatment as analyzed by 1-D PAGE (Figure 3.15). Herein, having established this, we next examined what proteins bind or release heme in response to Pb^{2+} poisoning in yeast by comparing analyzing the relative protein abundances of proteins that stick to hemin agarose versus sepharose in Pb^{2+} poisoned versus non-stressed cells. Any large differences in proteins detected between these two conditions are likely, based off our well supported hypothesis, to be binding and releasing heme in response to Pb^{2+} treatment.

Since the total protein in Pb^{2+} treated cells is much lower than non-stressed cells, analyzing the resulting proteins that stick to hemin agarose from Pb^{2+} and untreated cells was difficult to detect by 1D-PAGE analysis with Coomassie staining, which has a detection limit for protein stained bands of ~10 ng. Even though the cells treated Pb^{2+} were protein limiting, coomassie staining of a 1D-Page gel of the eluted proteins from hemin agarose and sepharose displays that there are many different proteins that stick to hemin agarose versus sepharose in Pb^{2+} stressed versus non-Pb^{2+} treated cells (Figure A. 13). Many faint proteins bands are detected from the hemin agarose elutions of untreated, "-Pb lysates," that do not show up from the treated, "+Pb lysates." Additionally, there are 3 distinct bands that are enhanced in the +Pb hemin agarose treated lysates. (See the -Pb and +Pb "Brightness/Contrast Enhanced Hemin Agarose Lanes" in Figure A. 13).

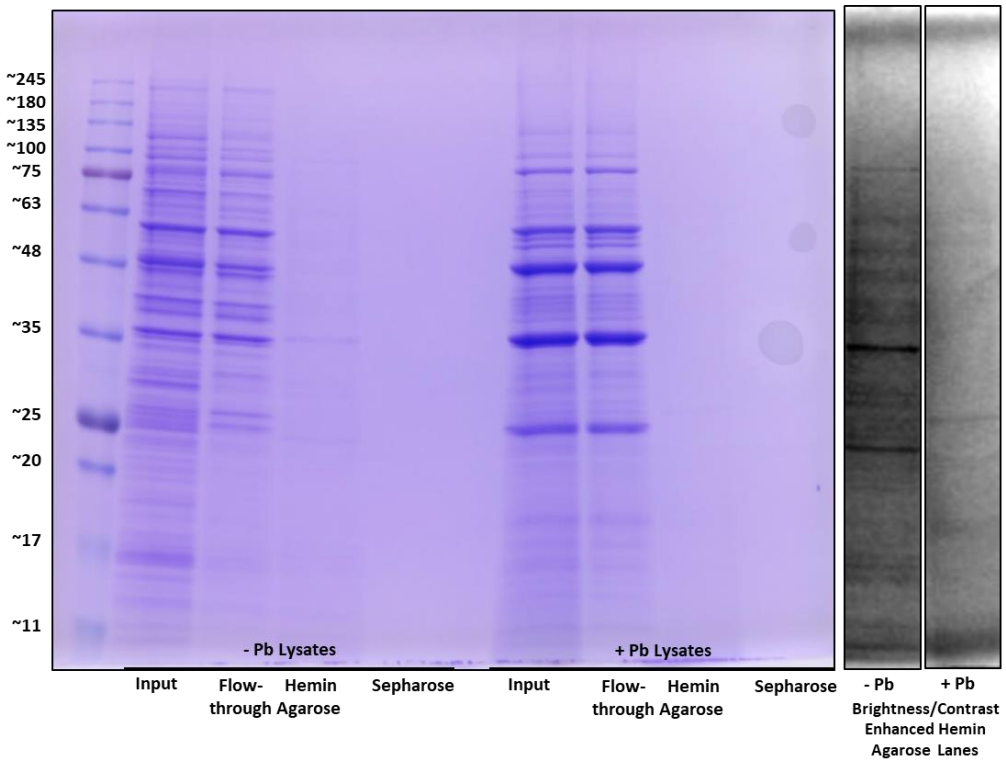

Figure A. 13 –Probing for differential binding to hemin agarose in lysates from nontreated "-Pb" Pb^{2+} treated "+ Pb" cells. 1-D PAGE displaying the input, flow-through, and the resulting hemin agarose and sepharose elutions. The brightness and contrast enhanced lanes for the -Pb and +Pb hemin agarose elutions reveals several differential binders of heme between these two treatment conditions. Protein expression is highly varied between -Pb and +Pb treated cells as seen by the input lanes. This data is representative of two independent trials with at least 2.8 mg of protein lysate loaded per sample of hemin agarose and sepharose beads.

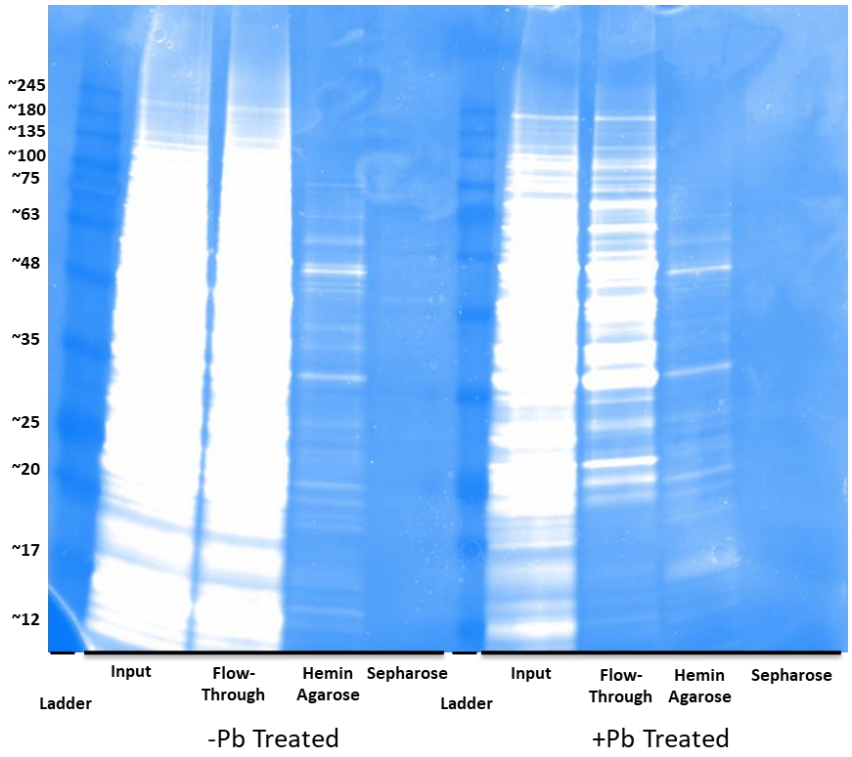

Figure A. 14 - 1-D PAGE and SyproRuby staining of eluents from SILAC labeled eluents that were sent for LC MS-MS analysis (Figure 3.16). Unlike with coomassie staining, many proteins are detected from both -Pb and + Pb hemin agarose elutions with many distinctive bands between the two samples.

From the SILAC labeleing experiment, approximately 10% of the elutent volume from each condition from outlined in Figure 3.16 was saved to conduct an 1-D PAGE analysis with SyproRuby staining while the remaining eluent was sent for LC MS-MS analysis. The SyproRuby stained 1-D PAGE shows numerous protein bands that run with differing intensities between the -Pb and +Pb treatments with some bands that only appear in one of the two treatment conditions (Figure A. 14). The results of the hemin agarose versus sepharose proteomics study are depicted in Figure 3.17B. To help interpret the results of the proteomics data, some SILAC labeled cells from the experiment outlined in Figure 3.16 were set aside to analyze whole proteome abundance changes resulting from Pb^{2+} poisoning (Figure 3.17A).

A.3.2 SILAC Media Preparation and MES Treatment with and without Pb^{2+} to Acquire Light and Heavy Labelled Cells for Sepharose versus Hemin Agarose Enrichment Studies

Step 1: Streaked Ly1D cells from a freezer stock onto YPD plates for 2 days.

Step 2: Prepped 4 L of SD-Lys media. Media was from stock of SD-Lys Powder prepped for 15 L that was made by adding each component of the media and then mixing by magnetic stir bar. Media was made prepped in 4 L beakers with Sterile MilliQ and stirred for 90 minutes with a magnetic stir bar. Afterwards, media was sterilized using the autoclave in 2 x 2 L media bottles. Filter sterilized 20% glucose was added to the media after it cooled. Light or heavy lysine (50 mg/mL) was added to the media after inoculating with cells.

Step 3: Scraped cells to make a 10 OD/mL (A600) cell stock in Sterile MilliQ.

Step 4: Inoculated 1.6 L of SD-Lys media at a density of 0.00075, swirled to mix, then split into 2 x 800 mL cultures in 2 L flasks. To one flask containing 2 L SD-Lys, added 50 mg/mL light lysine. To the other flask, added 50 mg/mL heavy lysine. Split the 800 mL cultures into 2 x 400 mL cultures in 2 L flasks. End result equals, 2 x 400 mL heavy lysine and 2 x 400 mL light lysine cultures with Lys1D cells at 0.00075 OD/mL in 2 L flasks. Conditions are as follows: "– Pb light lysine for sepharose beads, -Pb heavy lysine for hemin agarose beads, + Pb light lysine for sepharose beads, and + Pb heavy lysine for hemin agarose beads.

Step 5: Cells were grown overnight at 30°C at 250 rpm.

Step 6: After 14 hours of growth, checked the density.

Cells will need to grow between 15 and 16 hours and it is vital to read the density at 14 hours to be able to catch the cells before the go over a density of 1.0- read the densities and 14 hours, 15 hours, then every 15 minutes after that by taking out 0.5 to 1 mL media into a microcentrifuge tube to use to read the OD.

Step 7: Cells were grown to final densities between 0.8 and 1.0 (between 10 and 11 doublings), then were vacuum filtered to harvest the cells.

Step 8: Cells were then washed twice with 45 mL Sterile MilliQ.

Step 9: Each pellet was resuspended in 20-30 mL of 10mM pH 6.0 MES then added to new 4-liter flask with total volume of 1 L MES post addition of cells.

Step 10: Add 1 mL sterile MilliQ or 1 mL Pb(NO3)2 to add IC50 dose (85 µM) of Pb2+ to cells.

Step 11: Keep cells in MES buffer for 3 hours, rotating cultures by hand every 15 minutes to ensure cells do not settle to the bottom of the flask.

Step 12: After 3 hours of Pb Shock, take out 1mL aliquots of each culture and pellet in prelabelled 1.5mL microcentrifuge tubes. Pellet and re-suspend in 1mL Sterile MilliQ. Inoculate 100 µL of each washed culture in 10mL of SD-Lys + Light Lys for 20-hour growth to assess toxicity of Pb Shock.

Step 13: Filter the remaining culture to harvest cells. Two flasks were filtered at once.

Step 14: 1 x 90 mL wash to collect all cells off each filter. Cells harvested in 2 x 50 mL conical tubes.

Step 15: Resuspend cells in 25mL of appropriate media (light or heavy lysine added to SD-Lys), and transfer each resuspended cell pellet into appropriately labeled flasks.

Step 16: Add back appropriate media to flask so that total volume is 400 mL SD-Lys + heavy or light lysine

Step 17: Let recover for 4 hours at 30□C, 250 rpm

Step 18: Harvest cells just like in Step 14, but make 3 sets of pellets for each type of pellet in prelabeled tubes:

3 sets:

i. 5 OD pellets for double-checking coomassie banding toxicity phenotype

ii. 50-60 OD pellets for whole proteome analysis

iii. Remainder of cells in 4 x ~50 OD pellets for each condition for sepharose versus hemin agarose bead enrichment

4 types of pellets

i. - Pb light lysine

ii. - Pb heavy lysine

iii. + Pb light lysine

iv. + Pb heavy lysine

A.4 Chapter 4 Supplementary Methods

A.4.1 Transfection of hHS1 Sensor Plasmids into HEK293 Cells for Flow Cytometric Analysis

The protocols described below are for HEK293 cells cultured in 6-well plates. However, the same protocols work for cells transfected in similarly sized wells for microscopy.

A.4.1.1 Transfecting Cells with jetPRIME or PolyJet for Flow Cytometric Analysis

Protocol reproduced from Xiaojing Yuan, Hamza Lab

Day 1: HEK293 cells are seeded at ~40% confluence (0.4 x 10^6 cells / well for 6-well plate). For imaging, you may seed at lower confluence.

Day 2: 30 minutes to 1 hour before transfection, change the medium to fresh medium (basal, HD, SA or HD+SA, or HD + SA + heme). In one Eppendorf tube, add 1ug DNA to 50 µL DPBS. In another Eppendorf tube, add 4 µL PolyJet to 50 µL DPBS. Then add the Polyjet/DPBS solution to DNA/DPBS solution, pipet to mix, wait for 10-15 minutes at RT, and then add to cells.

Day 3: 24 hours post transfection, change to fresh medium (basal, basal + ALA, HD, SA or HD + SA, or HD + SA + heme now).

Day 4: Harvest cells for analysis.

Alternatively, for PolyJet Transfections, you could follow this approach to avoid cell counting:

Day 1 – Split ¼ of T75's cells in a 6 well plate and grow cells for ~40 hours before transfecting, or 1/6 of T75's cells in a 6 well plate and wait 48-60 hours before transfecting

30min to 1h before transfection, change the medium to fresh medium (basal, HD, SA or HD + SA, if plan to do HD + SA + heme, change to HD + SA today). In one Eppendorf tube, add 1-2µg DNA/well that you are transfected to 50µL DPBS/well you are transfecting. In another Eppendorf tube, add (4-8µL PolyJet x n) to (50µL DPBS x n) where "n" = the amount of wells you are transfecting. Then add the PolyJet/DPBS solution to DNA/DPBS solution, pipet to mix, wait for 10-15min at RT, and then add to cells.

The amount of PolyJet:DNA should always be at a ratio of at least 4:1

Example: transfecting a 6 well plate with 5 of 6 wells transfected with 1.5 µg hHS1

Add 250 µL DPBS to two Eppendorf tubes, 1 for to receive DNA, the other to receive a PolyJet.

Add 7.5 µg DNA to the 1st tube, and add 30 uL PolyJet to the 2nd tube

Add the tubes together and mix by pipetting to get 500+ uL DPBS-DNA-PolyJet

Incubate at RT 10-15 minutes

Add to 100 µL to each well

UT would be 50 µL DPBS w/o DNA added and 50 µL DPBS + 6 µL of PolyJet

24hrs post transfection, change to fresh medium (basal, HD, SA or HD+SA, if plan to do HD + SA + heme, change to HD + SA + heme now).

After an overnight, up to 48 hours later, harvest cells for analysis.

A.4.1.2 Transfecting Cells with Lipofectamine LTX

Step 1: HEK293 cells are typically seeded into a 6-well plate with ¼ the cells resulting from splitting a confluent T75 flask. For larger experiments with cells to be from the same parent flask, cells can be split at a lower density to expand the experiment into multiple plates.

Step 2: Once cells are around 50% confluent, 1-2 days after seeding, change the media 30 minutes to 1 hours before transfection. In one Eppendorf tube, add 100 µL room temperature OptiMEM per well that you are transfecting, up to 600 µL OptiMEM per tube. Add 1-2 µg of hHS1 DNA per well to be transfected. Next, add a volume of Lipofectamine Plus Reagent equal in µL to the µg amount of hHS1 DNA added. Then, add the Lipofectamine LTX transfection reagent at a volume that is double the volume of Plus Reagent. Flick tubes or pipet up and down to mix. Incubate at RT for 5 minutes, then add 100 µL of the resulting OptiMEM-DNA-Plus-LTX cocktail to each well. If cotransfecting hHS1 with pCMV-HO2 plasmid, then follow same procedure, adding pCMV-HO2 DNA with the hHS1 plasmid, and add the appropriate amount of additional Plus and LTX reagents in the follow steps.

Step 3: Cells can be harvested within 40 hours post transfection to analyze by flow cytometry. However, if you need to treat cells with a toxicant or growth supplement to investigate the resulting changes on labile heme, wait on harvesting. Instead, around 40 hours post transfection, change media and include the relevant toxicant (i.e. H_2O_2 or Pb^{2+}) or growth supplement (i.e. heme or ALA). Harvest cells post treatment, typically around 20-24 hours for heme or ALA treatment.

A.4.1.3 Transfecting Cells with Lipofectamine 2000

Step 1: HEK293 cells are typically seeded into a 6-well plate with ¼ the cells resulting from splitting a confluent T75 flask. For larger experiments with cells to be from the same parent flask, cells can be split at a lower density to expand the experiment into multiple plates.

Step 2: Transfect cells when they are about 50% confluent. If there are less than 50% confluent, transfect for slightly shorter time, or use less Lipofectamine 2000 per well. Slightly higher than 50% confluency works well, too. Change media to HD + SA or regular media at least 30 minutes before transfection. Aliquot 480 μL OptiMEM to a microcentrifuge tube and around 500 μL OptiMEM to a second microcentrifuge tube. To the first tube, add 20 μL of Lipofectamine 2000, and to the second tube, add an amount of HS1 DNA that gives you ~1 μg of DNA per well. If you added 5 μL of hHS1 DNA to this second tube, then you would have added 5 μL DNA to 495 μL OptiMEM. Incubate these tubes at room temperature for 5 minutes after flicking the tubes to mix. Then, add the contents of each tube together to incubate at room temperature for an additional 25-30 minutes. Next, add 150 μL of the resulting mixture to each well to be transfected with the

heme sensor. If cells were lower than 40% confluent at the time of transfection, add ~140 μL of this cocktail per well. If cells are higher than 50% confluency, add ~155-165 μL per well.

Step 3: Change media around 20 hours post transfection.

Step 4: Harvest cells and analyze 16-40 hours post changing media.

A.4.2 In situ saturation protocols

These methods were optimized to in situ saturate hHS1 in HEK293 cells analyzed by flow cytometry. The digitonin permeabilization was tried by microscopy and analyzed by point scanning confocal microscopy. The cells would not stay attached (data not shown). For others attempting this in the future, it should be possible using the Cyation 3 imaging plate reader, which is less phototoxic. On the other hand, the ALA treatment methods to in situ saturate cells should be easily measured by microscopy.

A.4.2.1 In situ saturation of hHS1 by digitonin permeabilization

Transfect cells with hHS1 for 48 hours using any of the above protocols. If cells are not over 50% confluent, change media and harvest the next day. Before harvesting, pre-warm water baths to 30 °C and 37 °C. Heat regular media to 37 °C. Make 15mM hemin chloride stock (10mg/mL in DMSO), 100mM ascorbate stock (17.6mg/mL in PBS), and 814μM digitonin stock (1mg/mL in PBS). Acquire cells from CO2 incubator and bring to 3D. Aspirate old media. Replace media with 1mL prewarmed 37 °C media. Add 49.2 μL digitonin stock = 40 μM digitonin, add 6.5 μL hemin chloride stock = 100 μM heme, swish cells around to disperse digitonin and heme, then add 10 μL of ascorbate

stock = 1 mM ascorbate. Swish around again. Next, pipet cells up and down to detach them from dish using 1 mL blue pipet set to 700-800 μL and stick cells in prelabelled Eppendorf tubes. Once all cells to be in situ calibrated are harvested, put them in 30 °C water bath for 30 minutes. Then pellet at 400 x g (0.4 x 1000g) for 4 minutes at 4 °C. Aspirate heme saturating media. 1mL PBS wash, then pellet again but at RT. Aspirate. Resuspend in 500μL PBS 1mM ascorbate. Then pass through BD Falcon tube and analyze by flow cytometry after running all other harvested samples.

This protocol only saturates the cytosolic and nuclear hHS1 but not mitochondrial hHS1.

A.4.2.2 In situ saturation of hHS1 by digitonin permeabilization

Transfect cells with hHS1 for 40-48 hours using any of the above protocols. Next, change media to include a well that has 300 to 350 μM ALA in each well that you want to in situ saturate with heme. Treat with this media for anytime between 20-24 hours. Harvest and analyze by flow cytometry.

A.5 Catalase Activity Assay – Unpublished

Any alternative method for investigating cellular heme availability is by interrogating heme dependent activity in the cell. If the design and characterization of the heme sensors did not work, we were going to conduct genetic screens to look at proteins that affect heme accessible to catalase, whose activity can be easily monitored in either in-gel or in-solution assays. I developed the in-solution assay to be used on a 96 well

plate scale to screen the yeast gene knockout collection for genes that alter catalase heme acquisition, which should lead to some proteins that affect heme trafficking.

A.5.1 Cytosolic catalase acquires heme posttranslationally

Applying the in-gel activity assay to *ctt1Δ*, *hem1Δ* expressing either EV or a constitutively expressed Ctt1 reveals that catalase acquires its heme post translationally. Cells treated with cycloheximide, which arrests new protein synthesis, has about 45 % less catalase activity than the untreated sample, indicating that there may be a fraction of catalase that acquires its heme cotranslationally (Figure A. 15).

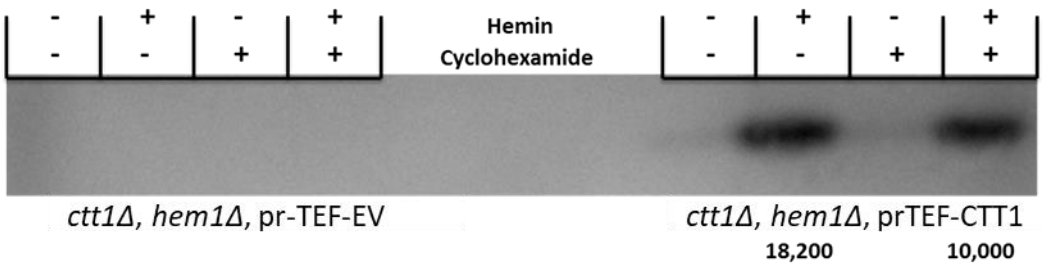

Figure A. 15 – Posttranslational and cotranslational heme acquisition by cytosolic catalase. Heme deficient *ctt1Δ*, *hem1Δ* cells with and without constitutive expression of cytosolic catalase protein, ctt1p, by the TEF promoter (prTEF) reveals that heme can be acquired by catalase post translationally. Cells were grown in 10mL cultures of SCE-LEU media to an OD of 1.0, washed in Sterile MilliQ, resuspended in fresh media to an OD of 0.65, and then treated with and without 10 μg/mL cycloheximide for 60 minutes to arrest new protein synthesis. The cycloheximide treatment was followed by a 60 minute ± 38 μM hemin treatment from a 10 mg/mL hemin chloride DMSO stock of hemin to facilitate heme acquisition in these heme deficient cells. Cells were harvested and washed 3 times in MilliQ water, lysed, and ran on a native gel and stained for catalase activity. The results indicate strong catalase activity in heme treated cells that express the constitutively expressed ctt1p, and there is 1.8-fold more catalase activity in cells untreated with cycloheximide, suggesting that some component of catalase heme acquisition may happen cotranslationally, assuming there is no change in catalase expression between the two samples.

A.5.2 Catalase activity assay developed for en masse screen of the yeast knockout collection

To conduct the stain to cells in solution, cells resuspended in 100 µL MilliQ have 35 µL of a catalase staining solution added to them. The catalase staining solution contains 1 part Dopamine (20mg/mL) in pH 8 0.2 M KPi buffer, 1 part para-phenylenediamine (3.5mg/mL) in pH 8 0.2M KPi, 1 part 15% H_2O_2, and 2 parts DMSO were mixed in the order listed. The cells' response is measured in a kinetics run measuring absorbance at 530 nm. At the point that the activity levels off, deemed the endpoint, the A_{530} of each well was taken to be its catalase activity.

To be quantitative in a 96 well format, the procedure was optimized to ensure differences in cell growth could be accounted for between each well.

First, grow cells in 96-well plate(s), pellet the plate(s) at 4000 rpm, decant, and resuspend in MilliQ. From here, the A_{600} is taken to assess growth, and the A_{530}, the wavelength that catalase activity is measured, is taken to get a background measurement to be subtracted from each well's final A_{530}. The A_{600} can be used to normalize each well to account for growth as there is a strong linear relationship of A_{600} and catalase activity measured for cells with an A_{600} between 0.1 and 1.5 measured in the 96-well plate in the BioTEK Synergy Mx multi-modal plate reader (Figure A. 16). The A_{530} is subtracted from each well's catalase activity measured post adding reagent.

These methods were successful used to quantitate differences in catalase activity between mutants in the yeast gene knockout collection but was only applied manually to a few plates. The whole knockout collection should be screened thoroughly for genes that

contribute to differences in catalase activity in tandem with screens that affect HS1 or HS1-M7A sensor loading.

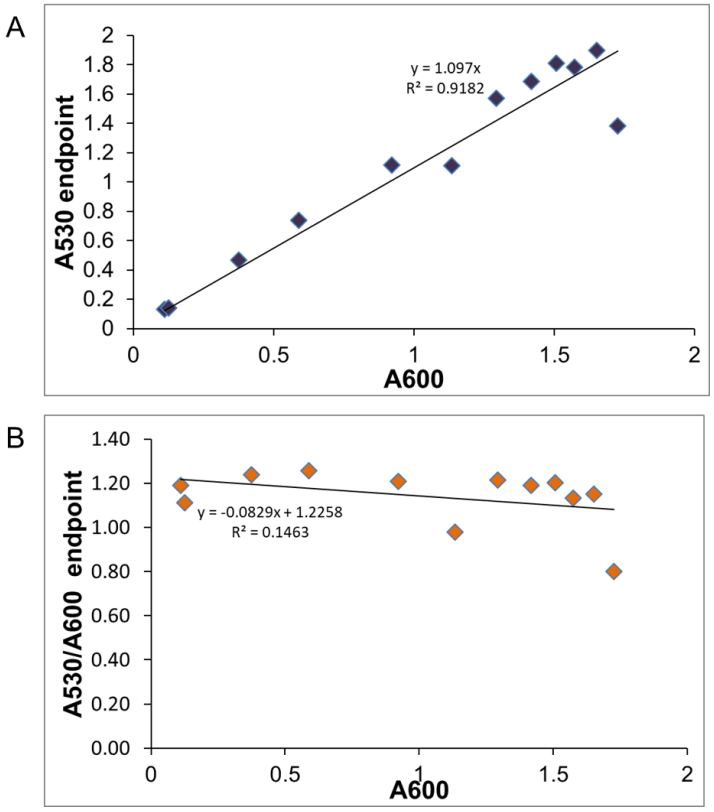

Figure A. 16 – Linear relationship between catalase activity versus activity. (**A**) Plot showing linear relation between catalase activity measured at 530nm at the endpoint of a kinetic run monitoring the change in catalase activity versus the amount of cells measured by at 600 nm. (**B**) Normalizing the activity at 530 nm by dividing by growth measured at 600 nm results in a flat line.

A.6 Plasmid Constructions and Heme Sensor Gene Sequences

A.6.1 Plasmids

Heme Sensor (HS1) Expression Plasmids. The synthetic gene for Heme sensor 1, **HS1**, was obtained from GENSCRIPT as codon optimized constructs for expression in

yeast/*E. coli* or human cell lines. **HS1** was generated by fusing **mKATE2**[240, 241] and **CG6**[107].

The amino acid sequence of **HS1** is as follows:
HMVSELIKENMHMKLYMEGTVNNHHFKCTSEGEGKPYEGTQTMRIKAVEGGPL
PFAFDILATSFMYGSKTFINHTQGIPDFFKQSFPEGFTWERVTTYEDGGVLTATQD
TSLQDGCLIYNVKIRGVNFPSNGPVMQKKTLGWEASTETLYPADGGLEGRADM
ALKLVGGGHLICNLKTTYRSKKPAKNLKMPGVYYVDRRLERIKEADKETYVEQ
HEVAVARYCDLPSKLGHRGGSMVSKGEELFTGVVPILVELDGDVNGHKFSVSGE
GEGDATFGGSADLEDN**M**ETLNDNLKVIEKADNAAQVKDALTKMRAAALDAQK
ATPPKLEDKSPDSPEMKDFRHGFDILVGQIDDALKLANEGKVKEAQAAAEQLKT
TRNAY**H**QKYRGGKLTLKFICTTGKLPVPWPTLVTTLGYGVQCFSRYPDHMKQH
DFFKSAMPEGYVQERTIFFKDDGNYKTRAEVKFEGDTLVNRIELKGIDFKEDGNI
LGHKLEYNYNSHNVYIMADKQKNGIKVNFKIRHNIEDGSVQLADHYQQNTPIGD
GPVLLPDNHYLSTQSALSKDPNEKRDHMVLLEFVTAAGITLGMDELYK

Red = mKATE2 Black = Linkers Green = EGFP Blue = Cyt b_{562}

Bold = Heme Iron Coordinating Residues

For yeast and *E. coli* expression, **CG6** and **mKATE2** were ordered as two separate gene constructs from GENSCRIPT. The **CG6** gene was flanked by 5'/3' BamHI/HindIII sites and subcloned into plasmid pUC57.

The DNA sequence for *E. coli*/yeast codon optimized **CG6** is as follows:

ATGGTGTCCAAAGGTGAAGAACTGTTTACTGGTGTAGTGCCGATTTTAGTTGA
ATTAGACGGTGATGTGAATGGTCATAAGTTTAGCGTGTCGGGTGAAGGCGAA
GGTGATGCTACCTTTGGTGGCTCTGCAGATCTGGAAGACAACATGGAAACTC
TGAACGATAACTTGAAGGTTATCGAAAAGGCCGATAATGCTGCACAAGTGAA
AGACGCGTTAACAAAGATGCGCGCCGCGGCTTTGGATGCTCAGAAAGCAACG
CCACCGAAACTGGAGGATAAGTCTCCTGACTCACCAGAAATGAAAGATTTTC
GTCATGGCTTCGACATTTTAGTGGGTCAAATCGATGACGCCTTGAAACTGGCG
AACGAGGGTAAAGTCAAGGAAGCTCAAGCAGCCGCGGAACAGCTGAAGACC
ACTCGTAATGCATATCATCAGAAATACAGAGGTGGCAAACTGACCTTGAAGT
TTATCTGTACAACGGGTAAACTGCCTGTTCCATGGCCGACTTTGGTGACCACT
CTGGGCTATGGTGTACAATGCTTCTCACGTTACCCAGATCATATGAAACAGCA
CGACTTTTTCAAGAGCGCCATGCCGGAAGGCTACGTTCAAGAACGCACTATT

TTCTTTAAGGATGACGGTAACTACAAGACACGTGCGGAAGTCAAATTTGAAG
GCGATACGCTGGTAAACAGAATCGAATTGAAGGGTATCGATTTCAAGGAAGA
CGGCAACATCTTGGGTCATAAATTGGAATACAACTACAACTCCCACAACGTC
TACATCATGGCTGATAAGCAAAAGAATGGCATCAAGGTAAACTTCAAGATCA
GACATAACATCGAAGATGGTTCTGTTCAGCTGGCTGACCACTATCAACAGAA
TACACCTATTGGCGATGGTCCGGTGCTGTTACCTGATAACCATTACTTGAGCA
CGCAGAGTGCACTGTCCAAAGATCCAAATGAAAAGCGCGACCACATGGTCTT
GTTGGAATTTGTCACCGCTGCTGGTATCACTTTGGGTATGGATGAACTGTATA
AATGA

The DNA sequence for *E. coli*/yeast codon optimized **mKATE2** is as follows:

CATATGCACATGGTATCGGAACTGATCAAGGAAAACATGCACATGAAGCTGT
ATATGGAAGGCACGGTCAACAACCACCACTTTAAATGCACCTCAGAAGGCGA
AGGTAAACCTTATGAAGGTACCCAAACTATGAGAATTAAGGCTGTCGAAGGT
GGCCCACTGCCGTTTGCCTTCGATATCTTAGCGACTTCTTTTATGTACGGCTCA
AAGACATTCATCAACCATACGCAAGGTATCCCAGATTTCTTTAAACAGTCCTT
TCCGGAAGGCTTCACCTGGGAACGCGTTACCACTTATGAAGACGGTGGCGTG
CTGACAGCTACGCAAGATACTTCGTTACAGGACGGTTGTTTGATTTACAACGT
CAAAATCCGTGGCGTAAATTTTCCTAGCAACGGTCCAGTCATGCAGAAAAAG
ACATTAGGCTGGGAAGCTAGTACCGAAACTTTGTATCCGGCAGATGGTGGCC
TGGAAGGTCGCGCTGACATGGCACTGAAATTAGTAGGTGGCGGTCACTTGAT
TTGCAATCTGAAGACAACGTACCGTAGTAAAAAGCCGGCCAAAAACTTAAAG
ATGCCTGGTGTTTATTACGTGGATCGTAGATTGGAAAGAATCAAAGAAGCGG
ACAAGGAAACGTATGTGGAACAGCACGAAGTCGCCGTCGCACGCTACTGTGA
TTTACCGTCCAAGTTAGGTCATAGAGGT

For expression in human cell lines, **HS1** was ordered as a codon-optimized single fusion gene construct from GENSCRIPT.

ATGCACATGGTCAGCGAGCTGATCAAGGAAAACATGCACATGAAACTGTACA
TGGAGGGGACTGTGAACAATCACCATTTCAAATGCACCTCCGAGGGCGAAGG
GAAGCCCTACGAGGGCACACAGACTATGAGGATCAAGGCAGTGGAGGGAGG
ACCACTGCCATTCGCCTTTGACATTCTGGCTACCTCATTCATGTACGGCAGCA
AAACCTTCATCAATCACACTCAGGGGATTCCCGACTTCTTTAAGCAGTCTTTC
CCTGAAGGCTTTACTTGGGAGCGAGTGACCACATACGAGGATGGAGGCGTCC
TGACCGCCACACAGGACACAAGTCTGCAGGATGGCTGTCTGATCTATAACGT
GAAGATTCGCGGGGTCAACTTTCCCAGTAATGGACCTGTGATGCAGAAGAAA
ACCCTGGGATGGGAGGCTTCAACTGAAACCCTGTACCCAGCAGACGGAGGAC
TGGAGGGACGAGCAGATATGGCTCTGAAACTGGTGGGCGGGGGACACCTGA
TCTGCAACCTGAAGACTACCTATCGGTCCAAGAAACCTGCTAAGAATCTGAA
AATGCCAGGCGTGTACTATGTGGACCGGAGACTGGAGAGAATTAAGGAAGC
AGATAAAGAGACCTACGTGGAGCAGCACGAAGTGGCTGTCGCACGATATTGT

GACCTGCCTTCTAAACTGGGCCATCGGGGCGGGTCTATGGTGAGTAAGGGCG
AGGAACTGTTCACAGGGGTGGTCCCAATCCTGGTGGAACTGGACGGCGATGT
CAATGGGCACAAGTTCAGCGTGTCCGGAGAGGGAGAAGGGGACGCAACCTT
TGGAGGCAGCGCCGACCTGGAAGATAATATGGAGACACTGAACGATAATCTG
AAAGTGATCGAGAAAGCCGACAACGCCGCTCAGGTCAAGGATGCTCTGACTA
AAATGAGGGCAGCCGCTCTGGATGCACAGAAAGCCACCCCCCCTAAGCTGGA
AGACAAATCACCTGATAGCCCAGAGATGAAGGACTTCCGCCACGGATTTGAT
ATCCTGGTCGGCCAGATTGACGATGCTCTGAAGCTGGCAAATGAAGGCAAGG
TGAAAGAGGCACAGGCAGCCGCTGAGCAGCTGAAAACAACTAGGAACGCCT
ACCATCAGAAGTATCGCGGGGGAAAGCTGACACTGAAATTCATCTGCACCAC
AGGCAAGCTGCCCGTGCCCTGGCCAACTCTGGTCACTACCCTGGGATACGGC
GTGCAGTGTTTTTCCCGCTATCCAGACCACATGAAGCAGCATGATTTCTTTAA
ATCTGCCATGCCCGAAGGCTACGTGCAGGAGAGAACCATCTTCTTTAAGGAC
GATGGAAACTATAAAACAAGGGCTGAAGTGAAGTTCGAGGGAGACACTCTG
GTCAACCGCATCGAACTGAAGGGCATTGACTTTAAAGAGGATGGAAATATTC
TGGGCCACAAGCTGGAATACAACTATAATAGCCATAACGTGTACATCATGGC
CGATAAGCAGAAAAACGGCATTAAGGTCAATTTCAAAATCCGGCACAATATT
GAGGACGGGAGCGTGCAGCTGGCCGATCATTACCAGCAGAACACCCCAATC
GGGGACGGACCAGTGCTGCTGCCCGATAATCACTATCTGTCCACACAGTCTG
CCCTGAGTAAGGACCCTAACGAAAAAAGAGATCACATGGTGCTGCTGGAGTT
TGTCACCGCAGCCGGGATTACACTGGGAATGGACGAGCTGTACAAGTGA

For yeast expression, **HS1** was generated by sub-cloning the 5' XbaI/3' BamHI **mKATE2** fragment and the 5' BamHI/3' HindIII **CG6** fragment into p415-ADH1, p415-TEF, and p415-GPD yeast centromeric plasmids[137]. The BamHI site between the mKATE2 and CG6 gene sequences create a GlySer linker between the mKATE2 and CG6 domains.

For *E. coli* expression, **HS1** was sub-cloned into a variant of pET30a(+) (EMD Millipore), pAR1008. pAR1008 is derived from pET30(+), but has a Tobacco Etch Virus (TEV) protease site (ENLFYQS) flanked by a 3' BamHI site in place of the original thrombin protease site. Sub-cloning of a 5'/3' BamHI/BamHI fragment of **mKATE2** and a 5'/3' BamHI/HindIII **CG6** fragment, both generated by PCR, results in an expression plasmid that has a His_6 tag, followed by a TEV protease site linked to HS1 via a GlySer linker.

For expression in human cell lines, the human codon optimized **HS1** gene was sub- cloned into the 5' BamHI and 3' XhoI site of pcDNA3-EGFP (Addgene). This plasmid drives protein expression using a CMV promoter.

Heme Sensor Variants. PCR based mutagenesis was used to generate variants of HS1 with an additional Gly Ser linker between mKATE2 and CG6, or with mKATE2 at the C-terminus of CG6. For the latter, one or two (Gly Ser) linkers between CG6 and mKATE2 were introduced. In addition, a stop codon was introduced into mKATE2 using Quick Change mutagenesis (Agilent Technologies). These constructs are highlighted in Figure 2.6 and are driven by the GPD promoter in p415-GPD. Using similar PCR based approaches, an mKATE2-EGFP fusion construct lacking Cytochrome b_{562} was generated and sub-cloned into appropriate expression yeast, *E. coli*, or mammalian cell expression plasmids.

For mitochondrial matrix or nuclear targeting in yeast, heme sensors were fused to N-terminal COX4[118] or C-terminal SV40[121] localization sequences, respectively. For mitochondrial matrix targeting, a COX4 matrix-targeting pre-sequence was amplified from yeast genomic DNA with a 5' SpeI site and a 3' HindIII site. HS1 was PCR amplified to include a 5' HindIII site and a 3' SalI site. The COX4 and HS1 amplicons were then sub-cloned into the SpeI and SalI sites of p415-TEF.

For nuclear targeting, HS1 was PCR amplified using mutagenic primers that incorporate the SV40 NLS sequence (5'-CCTAAGAAGAAGAGGAAGGTT-3') prior to the stop codon. The HS1-SV40 amplicon included 5' SpeI and 3' HindIII sites for sub-cloning into p415-GPD.

For all expression plasmids, heme binding site mutations of HS1 in which Met_7 or His_{102} are mutated to Ala were generated by Quick Change mutagenesis (Agilent Technologies). The numbering refers to its position in Cytochrome b_{562} and is highlighted in bold in the sequence for HS1.

For subcellular targeting:

Yeast cyto HS1 is p4XX-XXX-[usually SpeI]-HS1-[usually HindIII], depending on the construct there are a few different ones made for different subcloning purposes but most are

p4X5-XXX-[SpeI]-HS1-[HindIII]

Underlined, bold text is Restriction Enzyme Site

Start and stop codons are in lower case to distinguish them in the sequences.

In cyto HS1 gene sequence, I show mKATE in CAPITALIZED letter and CG6 in *lower* case letters:

ACTAGTatgTCTAGACATATGCACATGGTATCGGAACTGATCAAGGAAAACAT
GCACATGAAGCTGTATATGGAAGGCACGGTCAACAACCACCACTTTAAATGC
ACCTCAGAAGGCGAAGGTAAACCTTATGAAGGTACCCAAACTATGAGAATTA
AGGCTGTCGAAGGTGGCCCACTGCCGTTTGCCTTCGATATCTTAGCGACTTCT
TTTATGTACGGCTCAAAGACATTCATCAACCATACGCAAGGTATCCCAGATTT
CTTTAAACAGTCCTTTCCGGAAGGCTTCACCTGGGAACGCGTTACCACTTATG
AAGACGGTGGCGTGCTGACAGCTACGCAAGATACTTCGTTACAGGACGGTTG
TTTGATTTACAACGTCAAAATCCGTGGCGTAAATTTTCCTAGCAACGGTCCAG
TCATGCAGAAAAAGACATTAGGCTGGGAAGCTAGTACCGAAACTTTGTATCC
GGCAGATGGTGGCCTGGAAGGTCGCGCTGACATGGCACTGAAATTAGTAGGT
GGCGGTCACTTGATTTGCAATCTGAAGACAACGTACCGTAGTAAAAAGCCGG
CCAAAAACTTAAAGATGCCTGGTGTTTATTACGTGGATCGTAGATTGGAAAG

AATCAAAGAAGCGGACAAGGAAACGTATGTGGAACAGCACGAAGTCGCCGT
CGCACGCTACTGTGATTTACCGTCCAAGTTAGGTCATAGAGGT**GGATCC***atggt*
gtccaaaggtgaagaactgtttactggtgtagtgccgattttagttgaattagacggtgatgtgaatggtcataagtttagcgtg
tcgggtgaaggcgaaggtgatgctacctttggtggctctgcagatctggaagacaacatggaaactctgaacgataacttga
aggttatcgaaaaggccgataatgctgcacaagtgaaagacgcgttaacaaagatgcgcgccgcggctttggatgctcag
aaagcaacgccaccgaaactggaggataagtctcctgactcaccagaaatgaaagattttcgtcatggcttcgacattttagt
gggtcaaatcgatgacgccttgaaactggcgaacgagggtaaagtcaaggaagctcaagcagccgcggaacagctgaa
gaccactcgtaatgcatatcatcagaaatacagaggtggcaaactgaccttgaagtttatctgtacaacgggtaaactgcct
gttccatggccgactttggtgaccactctgggctatggtgtacaatgcttctcacgttacccagatcatatgaaacagcacgac
tttttcaagagcgccatgccggaaggctacgttcaagaacgcactattttctttaaggatgacggtaactacaagacacgtgc
ggaagtcaaatttgaaggcgatacgctggtaaacagaatcgaattgaagggtatcgatttcaaggaagacggcaacatctt
gggtcataaattggaatacaactacaactcccacaacgtctacatcatggctgataagcaaaagaatggcatcaaggtaaa
cttcaagatcagacataacatcgaagatggttctgttcagctggctgaccactatcaacagaatacacctattggcgatggtc
cggtgctgttacctgataaccattacttgagcacgcagagtgcactgtccaaagatccaaatgaaaagcgcgaccacatgg
*tcttgttggaatttgtcaccgctgctggtatcactttgggtatggatgaactgtataaatga***AAGCTT**

The p4X5-XXX-[SpeI]-HS1-[HindIII] plasmids can be amplified using:

prDH011; GCGAATGCAACTAGTCATATGCACATGG; 5’ to 3’; contains SpeI restriction site; Forward Primer

prRC007; GGATATAAGCTTTCATTTATACAGTTCATCCATACCC; 3’ to 5’; Contains HindIII restriction site; Reverse Primer

Mitochondrial targeted plasmid, originally made as, pDH049-3; p415-TEF-[SpeI]-Cox4-[HindIII]-HS1-[SalI]

Lower case is 5’ or 3’ UTR on plasmid in addition to start and stop codons.

gccatacaaatagataaca**ACTAGT**atgCTTTCACTACGTCAATCTATAAGATTTTTCAAG
CCAGCCACAAGAACTTTGTGTAGCTCTAGATATCTGCTT**AAGCTT**TCTAGACA
TATGCACATGGTATCGGAACTGATCAAGGAAAACATGCACATGAAGCTGTAT
ATGGAAGGCACGGTCAACAACCACCACTTTAAATGCACCTCAGAAGGCGAA
GGTAAACCTTATGAAGGTACCCAAACTATGAGAATTAAGGCTGTCGAAGGTG

GCCCACTGCCGTTTGCCTTCGATATCTTAGCGACTTCTTTTATGTACGGCTCAA
AGACATTCATCAACCATACGCAAGGTATCCCAGATTTCTTTAAACAGTCCTTT
CCGGAAGGCTTCACCTGGGAACGCGTTACCACTTATGAAGACGGTGGCGTGC
TGACAGCTACGCAAGATACTTCGTTACAGGACGGTTGTTTGATTTACAACGTC
AAAATCCGTGGCGTAAATTTTCCTAGCAACGGTCCAGTCATGCAGAAAAAGA
CATTAGGCTGGGAAGCTAGTACCGAAACTTTGTATCCGGCAGATGGTGGCCT
GGAAGGTCGCGCTGACATGGCACTGAAATTAGTAGGTGGCGGTCACTTGATT
TGCAATCTGAAGACAACGTACCGTAGTAAAAAGCCGGCCAAAAACTTAAAG
ATGCCTGGTGTTTATTACGTGGATCGTAGATTGGAAAGAATCAAAGAAGCGG
ACAAGGAAACGTATGTGGAACAGCACGAAGTCGCCGTCGCACGCTACTGTGA
TTTACCGTCCAAGTTAGGTCATAGAGGT**GGATCC**ATGGTGTCCAAAGGTGAA
GAACTGTTTACTGGTGTAGTGCCGATTTTAGTTGAATTAGACGGTGATGTGAA
TGGTCATAAGTTTAGCGTGTCGGGTGAAGGCGAAGGTGATGCTACCTTTGGT
GGCTCTGCAGATCTGGAAGACAACATGGAAACTCTGAACGATAACTTGAAGG
TTATCGAAAAGGCCGATAATGCTGCACAAGTGAAAGACGCGTTAACAAAGAT
GCGCGCCGCGGCTTTGGATGCTCAGAAAGCAACGCCACCGAAACTGGAGGAT
AAGTCTCCTGACTCACCAGAAATGAAAGATTTTCGTCATGGCTTCGACATTTT
AGTGGGTCAAATCGATGACGCCTTGAAACTGGCGAACGAGGGTAAAGTCAA
GGAAGCTCAAGCAGCCGCGGAACAGCTGAAGACCACTCGTAATGCATATCAT
CAGAAATACAGAGGTGGCAAACTGACCTTGAAGTTTATCTGTACAACGGGTA
AACTGCCTGTTCCATGGCCGACTTTGGTGACCACTCTGGGCTATGGTGTACAA
TGCTTCTCACGTTACCCAGATCATATGAAACAGCACGACTTTTTCAAGAGCGC
CATGCCGGAAGGCTACGTTCAAGAACGCACTATTTTCTTTAAGGATGACGGT
AACTACAAGACACGTGCGGAAGTCAAATTTGAAGGCGATACGCTGGTAAACA
GAATCGAATTGAAGGGTATCGATTTCAAGGAAGACGGCAACATCTTGGGTCA
TAAATTGGAATACAACTACAACTCCCACAACGTCTACATCATGGCTGATAAG
CAAAAGAATGGCATCAAGGTAAACTTCAAGATCAGACATAACATCGAAGAT
GGTTCTGTTCAGCTGGCTGACCACTATCAACAGAATACACCTATTGGCGATGG
TCCGGTGCTGTTACCTGATAACCATTACTTGAGCACGCAGAGTGCACTGTCCA
AAGATCCAAATGAAAAGCGCGACCACATGGTCTTGTTGGAATTTGTCACCGC
TGCTGGTATCACTTTGGGTATGGATGAACTGTATAAATGA**GTCGAC**atatcc

The ; p415-TEF-[SpeI]-Cox4-[HindIII]-HS1-[SalI] plasmids can be amplified using:

prDH015; GCCATACAAATAGATAACAACTAGTATGCTTTCACTACG; 5' to 3'; contains overlap with Cox4 targeting presequence and SpeI Restriction site; Forward Primer

prDH034; GGATATGTCGACTCATTTATACAGTTCATCCATACCC; 3' to 5'; contains SalI Restriction site; Reverse primer

Mitochondrial targeted plasmid, originally made as pDH046-1; p415-GPD-[SpeI]-HS1-NLS-[HindIII]

ACTAGTatgTCTAGACATATGCACATGGTATCGGAACTGATCAAGGAAAACAT
GCACATGAAGCTGTATATGGAAGGCACGGTCAACAACCACCACTTTAAATGC
ACCTCAGAAGGCGAAGGTAAACCTTATGAAGGTACCCAAACTATGAGAATTA
AGGCTGTCGAAGGTGGCCCACTGCCGTTTGCCTTCGATATCTTAGCGACTTCT
TTTATGTACGGCTCAAAGACATTCATCAACCATACGCAAGGTATCCCAGATTT
CTTTAAACAGTCCTTTCCGGAAGGCTTCACCTGGGAACGCGTTACCACTTATG
AAGACGGTGGCGTGCTGACAGCTACGCAAGATACTTCGTTACAGGACGGTTG
TTTGATTTACAACGTCAAAATCCGTGGCGTAAATTTTCCTAGCAACGGTCCAG
TCATGCAGAAAAAGACATTAGGCTGGGAAGCTAGTACCGAAACTTTGTATCC
GGCAGATGGTGGCCTGGAAGGTCGCGCTGACATGGCACTGAAATTAGTAGGT
GGCGGTCACTTGATTTGCAATCTGAAGACAACGTACCGTAGTAAAAAGCCGG
CCAAAAACTTAAAGATGCCTGGTGTTTATTACGTGGATCGTAGATTGGAAAG
AATCAAAGAAGCGGACAAGGAAACGTATGTGGAACAGCACGAAGTCGCCGT
CGCACGCTACTGTGATTTACCGTCCAAGTTAGGTCATAGAGGTGGATCCATG
GTGTCCAAAGGTGAAGAACTGTTTACTGGTGTAGTGCCGATTTTAGTTGAATT
AGACGGTGATGTGAATGGTCATAAGTTTAGCGTGTCGGGTGAAGGCGAAGGT
GATGCTACCTTTGGTGGCTCTGCAGATCTGGAAGACAACATGGAAACTCTGA
ACGATAACTTGAAGGTTATCGAAAAGGCCGATAATGCTGCACAAGTGAAAGA
CGCGTTAACAAAGATGCGCGCCGCGGCTTTGGATGCTCAGAAAGCAACGCCA

CCGAAACTGGAGGATAAGTCTCCTGACTCACCAGAAATGAAAGATTTTCGTC

ATGGCTTCGACATTTTAGTGGGTCAAATCGATGACGCCTTGAAACTGGCGAA

CGAGGGTAAAGTCAAGGAAGCTCAAGCAGCCGCGGAACAGCTGAAGACCAC

TCGTAATGCATATCATCAGAAATACAGAGGTGGCAAACTGACCTTGAAGTTT

ATCTGTACAACGGGTAAACTGCCTGTTCCATGGCCGACTTTGGTGACCACTCT

GGGCTATGGTGTACAATGCTTCTCACGTTACCCAGATCATATGAAACAGCAC

GACTTTTTCAAGAGCGCCATGCCGGAAGGCTACGTTCAAGAACGCACTATTTT

CTTTAAGGATGACGGTAACTACAAGACACGTGCGGAAGTCAAATTTGAAGGC

GATACGCTGGTAAACAGAATCGAATTGAAGGGTATCGATTTCAAGGAAGACG

GCAACATCTTGGGTCATAAATTGGAATACAACTACAACTCCCACAACGTCTA

CATCATGGCTGATAAGCAAAAGAATGGCATCAAGGTAAACTTCAAGATCAGA

CATAACATCGAAGATGGTTCTGTTCAGCTGGCTGACCACTATCAACAGAATA

CACCTATTGGCGATGGTCCGGTGCTGTTACCTGATAACCATTACTTGAGCACG

CAGAGTGCACTGTCCAAAGATCCAAATGAAAAGCGCGACCACATGGTCTTGT

TGGAATTTGTCACCGCTGCTGGTATCACTTTGGGTATGGATGAACTGTATAAA

GTATGGATGAACTGTATAAACCTAAGAAGAAGAGGAAGGTTtga**AAGCTT**

(NLS tag from prDH024)

The ; p415-GPD-[SpeI]-HS1-NLS-[HindIII] plasmids can be amplified using:

prDH015; GCGAATGCAACTAGTCATATGCACATGG; 5’ to 3’; contains SpeI restriction site; Forward primer

prDH034;

GTTCGATATCAAGCTTTCAAACCTTCCTCTTCTTCTTAGGTTTATACAGTTCAT CCATAC; 3’ to 5’; contains NLS sequence and HindIII restriction site; Reverse primer

A.6.2 Gene Knockout Construction and Validation

*hem1::HIS3 Knockout Plasmid and hem1*Δ *Strain Generation*. In order to generate a *hem1*::HIS3 knockout plasmid, the 5’ and 3’ untranslated regions (UTR’s) of *HEM1* were amplified from yeast genomic DNA. The 5’ UTR (-300 to +79) was amplified to include 5’ BamHI and 3’ SalI sites. The 3’ UTR (+1695 to +2195) was amplified to include 5’ EagI and 3’ BamHI sites. The 5’ and 3’ UTRs were digested with the enzymes indicated and ligated in a trimolecular reaction into the *HIS3* integrating plasmid pRS403 [242] digested with EagI and SalI, resulting in pDH001. Transformation of BY4741 with pDH001 linearized with BamHI resulted in deletion of *HEM1* sequences from +80 to +1694. *hem1*Δ cells were initially selected for on SC-HIS media supplemented with 50 μg/mL 5-ALA. After isolation of single colonies, *bona fide hem1*Δ cells were selected for their heme auxotrophy. That is to say, strains that exhibited limited growth in YPD or SC media, and robust growth in media supplemented with 50 μg/mL of 5-ALA or hemin, were deemed genuine *hem1*Δ cells.

Primers used for the construction the 5’ UTR of *HEM1* include:

Forward primer: prDH001; contains BamHI site; covers --300 to -273; GCCTTGCCCATTGTTCGGATCCATGCG

Reverse primer: prDH002; contains SalI site; covers 49 to 79; GCTGTCGTCGACAGCCTATTCAGTGTGG

Primers used for the construction the 5’ UTR of *HEM15* include:

Forward primer: prDH003; contains EagI site; covers 1170 to 1200; CCAATATATGCATCGGCCGAGATAGAGGTACAAGG

Reverse primer: prDH004; contains BamHI site; covers 2163 to 2195; CGCTGATGTTCCATTGGATCCAGAGTCTAAGGC

*hem15::HIS3 Knockout Plasmid and hem1*Δ *Strain Generation*. In order to generate a *hem15*::HIS3 knockout plasmid, the 5’ and 3’ untranslated regions (UTR’s) of *HEM15* were amplified from yeast genomic DNA. The 5’ UTR (-836 to +218) was amplified to include 5’ BamHI and 3’ SalI sites. The 3’ UTR (+1170 to +1648) was amplified to include 5’ EagI and 3’ BamHI sites. The 5’ and 3’ UTRs were digested with the enzymes indicated and ligated in a trimolecular reaction into the HIS3 integrating plasmid pRS403 [242] digested with EagI and BamHI, resulting in pDH019. Transformation of BY4741 with pDH019 linearized with BamHI resulted in deletion of *HEM15* sequences from +219 to +1. *hem15*Δ cells were initially selected for on SC-HIS media supplemented with 25 μM hemin chloride, 0.16% DMSO. After isolation of single colonies, *bona fide hem15*Δ cells were selected for their heme auxotrophy. That is to say, strains that exhibited limited growth in YPD or SC media, and robust growth in media supplemented with hemin were deemed genuine *hem15*Δ cells.

Primers used for the construction the 5’ UTR of *HEM15* include:

Forward primer: hem15-1; contains BamHI site; covers -836 to -801; GCATTCAGTGGGAAGGATCCCAATAAGCAGATAGC

Reverse primer: hem15-2; contains SalI site; covers -245 to -218; GGCAGCAACTCCGTCGACATATAAGGC

Primers used for the construction the 3' UTR of *HEM15* include:

Forward primer: hem15-3; contains EagI site; covers 1170 to 1200; CGAATCTACTTGATAACGGCCGTTCATCCC

Reverse primer: hem15-4; contains BamHI site; covers 1614 to 1648; GGCCTTTGTGCACAATGGGATCCCAACAATTATCC

REFERENCES

1. Chiabrando, D.; Vinchi, F.; Fiorito, V.; Mercurio, S.; Tolosano, E., Heme in pathophysiology: a matter of scavenging, metabolism and trafficking across cell membranes. *Front Pharmacol* **2014,** *5*, 61.

2. Hanna, D. A.; Martinez-Guzman, O.; Reddi, A. R., Heme Gazing: Illuminating Eukaryotic Heme Trafficking, Dynamics, and Signaling with Fluorescent Heme Sensors. *Biochemistry* **2017,** *56* (13), 1815-1823.

3. Severance, S.; Hamza, I., Trafficking of heme and porphyrins in metazoa. *Chem Rev* **2009,** *109* (10), 4596-616.

4. Fleming, M. D.; Hamza, I., Mitochondrial heme: an exit strategy at last. *J Clin Invest* **2012,** *122* (12), 4328-30.

5. Atamna, H.; Frey, W. H., 2nd, A role for heme in Alzheimer's disease: heme binds amyloid beta and has altered metabolism. *Proc Natl Acad Sci U S A* **2004,** *101* (30), 11153-8.

6. Atamna, H., Heme, iron, and the mitochondrial decay of ageing. *Ageing Res Rev* **2004,** *3* (3), 303-18.

7. Fang, X.; An, P.; Wang, H.; Wang, X.; Shen, X.; Li, X.; Min, J.; Liu, S.; Wang, F., Dietary intake of heme iron and risk of cardiovascular disease: a dose-response meta-analysis of prospective cohort studies. *Nutr Metab Cardiovasc Dis* **2015,** *25* (1), 24-35.

8. Gudjoncik, A.; Guenancia, C.; Zeller, M.; Cottin, Y.; Vergely, C.; Rochette, L., Iron, oxidative stress, and redox signaling in the cardiovascular system. *Mol Nutr Food Res* **2014,** *58* (8), 1721-38.

9. Daglas, M.; Adlard, P. A., The Involvement of Iron in Traumatic Brain Injury and Neurodegenerative Disease. *Front Neurosci* **2018,** *12*, 981.

10. Cheesman, M. R.; Oganesyan, V. S.; Watmough, N. J.; Butler, C. S.; Thomson, A. J., The nature of the exchange coupling between high-spin Fe(III) heme o3 and CuBII in Escherichia coli quinol oxidase, cytochrome bo3: MCD and EPR studies. *J Am Chem Soc* **2004,** *126* (13), 4157-66.

11. Layer, G.; Reichelt, J.; Jahn, D.; Heinz, D. W., Structure and function of enzymes in heme biosynthesis. *Protein Sci* **2010,** *19* (6), 1137-61.

12. Schultz, I. J.; Chen, C.; Paw, B. H.; Hamza, I., Iron and porphyrin trafficking in heme biogenesis. *J Biol Chem* **2010,** *285* (35), 26753-9.

13. Hamza, I.; Dailey, H. A., One ring to rule them all: trafficking of heme and heme synthesis intermediates in the metazoans. *Biochim Biophys Acta* **2012,** *1823* (9), 1617-32.

14. Korolnek, T.; Hamza, I., Like iron in the blood of the people: the requirement for heme trafficking in iron metabolism. *Front Pharmacol* **2014,** *5*, 126.

15. Girvan, H. M.; Munro, A. W., Heme sensor proteins. *J Biol Chem* **2013,** *288* (19), 13194-203.

16. Williams, D. E.; Nisbett, L. M.; Bacon, B.; Boon, E., Bacterial Heme-Based Sensors of Nitric Oxide. *Antioxid Redox Signal* **2018,** *29* (18), 1872-1887.

17. Shimizu, T.; Huang, D.; Yan, F.; Stranava, M.; Bartosova, M.; Fojtikova, V.; Martinkova, M., Gaseous O2, NO, and CO in signal transduction: structure and function relationships of heme-based gas sensors and heme-redox sensors. *Chem Rev* **2015,** *115* (13), 6491-533.

18. Ragsdale, S. W., Life with carbon monoxide. *Crit Rev Biochem Mol Biol* **2004,** *39* (3), 165-95.

19. Kabil, O.; Yadav, V.; Banerjee, R., Heme-dependent Metabolite Switching Regulates H2S Synthesis in Response to Endoplasmic Reticulum (ER) Stress. *J Biol Chem* **2016,** *291* (32), 16418-16423.

20. Xu, X.; Cho, M.; Spencer, N. Y.; Patel, N.; Huang, Z.; Shields, H.; King, S. B.; Gladwin, M. T.; Hogg, N.; Kim-Shapiro, D. B., Measurements of nitric oxide on the heme iron and beta-93 thiol of human hemoglobin during cycles of oxygenation and deoxygenation. *Proc Natl Acad Sci U S A* **2003,** *100* (20), 11303-8.

21. Helms, C.; Kim-Shapiro, D. B., Hemoglobin-mediated nitric oxide signaling. *Free Radic Biol Med* **2013,** *61*, 464-72.

22. Coppola, D.; Giordano, D.; Milazzo, L.; Howes, B. D.; Ascenzi, P.; di Prisco, G.; Smulevich, G.; Poole, R. K.; Verde, C., Coexistence of multiple globin genes conferring protection against nitrosative stress to the Antarctic bacterium Pseudoalteromonas haloplanktis TAC125. *Nitric Oxide* **2018,** *73*, 39-51.

23. Stevanin, T. M.; Poole, R. K.; Demoncheaux, E. A.; Read, R. C., Flavohemoglobin Hmp protects Salmonella enterica serovar typhimurium from nitric oxide-related killing by human macrophages. *Infect Immun* **2002,** *70* (8), 4399-405.

24. Kathiresan, M.; English, A. M., Targeted proteomics identify metabolism-dependent interactors of yeast cytochrome c peroxidase: implications in stress response and heme trafficking. *Metallomics* **2016,** *8* (4), 434-43.

25. Cao, C.; Leng, Y.; Kufe, D., Catalase activity is regulated by c-Abl and Arg in the oxidative stress response. *J Biol Chem* **2003,** *278* (32), 29667-75.

26. Baureder, M.; Hederstedt, L., Genes important for catalase activity in Enterococcus faecalis. *PLoS One* **2012,** *7* (5), e36725.

27. Mense, S. M.; Zhang, L., Heme: a versatile signaling molecule controlling the activities of diverse regulators ranging from transcription factors to MAP kinases. *Cell Res* **2006,** *16* (8), 681-92.

28. David A. Hanna, R. M. H., Osiris Martinez-Guzman, Xiaojing Yuan, Bindu Chandrasekharan, Gheevarghese Raju, F. Wayne Outten, Iqbal Hamza, and Amit R. Reddi, Heme Dynamics and Trafficking Factors Revealed by Genetically Encoded Fluorescent Heme Sensors. *PNAS* **2016**.

29. Hanna, D. A.; Harvey, R. M.; Martinez-Guzman, O.; Yuan, X.; Chandrasekharan, B.; Raju, G.; Outten, F. W.; Hamza, I.; Reddi, A. R., Heme dynamics and trafficking factors revealed by genetically encoded fluorescent heme sensors. *Proc Natl Acad Sci U S A* **2016,** *113* (27), 7539-44.

30. Pfeifer, K.; Kim, K. S.; Kogan, S.; Guarente, L., Functional dissection and sequence of yeast HAP1 activator. *Cell* **1989,** *56* (2), 291-301.

31. Zhang, L.; Guarente, L., Heme binds to a short sequence that serves a regulatory function in diverse proteins. *EMBO J* **1995,** *14* (2), 313-20.

32. Igarashi, K.; Sun, J., The heme-Bach1 pathway in the regulation of oxidative stress response and erythroid differentiation. *Antioxid Redox Signal* **2006,** *8* (1-2), 107-18.

33. Ogawa, K.; Sun, J.; Taketani, S.; Nakajima, O.; Nishitani, C.; Sassa, S.; Hayashi, N.; Yamamoto, M.; Shibahara, S.; Fujita, H.; Igarashi, K., Heme mediates derepression of Maf recognition element through direct binding to transcription repressor Bach1. *EMBO J* **2001,** *20* (11), 2835-43.

34. Shen, J.; Sheng, X.; Chang, Z.; Wu, Q.; Wang, S.; Xuan, Z.; Li, D.; Wu, Y.; Shang, Y.; Kong, X.; Yu, L.; Li, L.; Ruan, K.; Hu, H.; Huang, Y.; Hui, L.; Xie, D.; Wang, F.; Hu, R., Iron metabolism regulates p53 signaling through direct heme-p53 interaction and modulation of p53 localization, stability, and function. *Cell Rep* **2014,** *7* (1), 180-93.

35. Raghuram, S.; Stayrook, K. R.; Huang, P.; Rogers, P. M.; Nosie, A. K.; McClure, D. B.; Burris, L. L.; Khorasanizadeh, S.; Burris, T. P.; Rastinejad, F., Identification of heme as the ligand for the orphan nuclear receptors REV-ERBalpha and REV-ERBbeta. *Nat Struct Mol Biol* **2007,** *14* (12), 1207-13.

36. Barr, I.; Smith, A. T.; Chen, Y.; Senturia, R.; Burstyn, J. N.; Guo, F., Ferric, not ferrous, heme activates RNA-binding protein DGCR8 for primary microRNA processing. *Proc Natl Acad Sci U S A* **2012,** *109* (6), 1919-24.

37. Kathiresan, M.; Martins, D.; English, A. M., Respiration triggers heme transfer from cytochrome c peroxidase to catalase in yeast mitochondria. *Proc Natl Acad Sci U S A* **2014,** *111* (49), 17468-73.

38. Burton, M. J.; Kapetanaki, S. M.; Chernova, T.; Jamieson, A. G.; Dorlet, P.; Santolini, J.; Moody, P. C.; Mitcheson, J. S.; Davies, N. W.; Schmid, R.; Raven, E. L.; Storey, N. M., A heme-binding domain controls regulation of ATP-dependent potassium channels. *Proc Natl Acad Sci U S A* **2016,** *113* (14), 3785-90.

39. Kapetanaki, S. M.; Burton, M. J.; Basran, J.; Uragami, C.; Moody, P. C. E.; Mitcheson, J. S.; Schmid, R.; Davies, N. W.; Dorlet, P.; Vos, M. H.; Storey, N. M.; Raven, E., A mechanism for CO regulation of ion channels. *Nat Commun* **2018,** *9* (1), 907.

40. Sweeny, E. A.; Singh, A. B.; Chakravarti, R.; Martinez-Guzman, O.; Saini, A.; Haque, M. M.; Garee, G.; Dans, P. D.; Hannibal, L.; Reddi, A. R.; Stuehr, D. J., Glyceraldehyde-3-phosphate dehydrogenase is a chaperone that allocates labile heme in cells. *J Biol Chem* **2018,** *293* (37), 14557-14568.

41. Chakravarti, R.; Aulak, K. S.; Fox, P. L.; Stuehr, D. J., GAPDH regulates cellular heme insertion into inducible nitric oxide synthase. *Proc Natl Acad Sci U S A* **2010,** *107* (42), 18004-9.

42. Waheed, S. M.; Ghosh, A.; Chakravarti, R.; Biswas, A.; Haque, M. M.; Panda, K.; Stuehr, D. J., Nitric oxide blocks cellular heme insertion into a broad range of heme proteins. *Free Radic Biol Med* **2010,** *48* (11), 1548-58.

43. Chakravarti, R.; Gupta, K.; Majors, A.; Ruple, L.; Aronica, M.; Stuehr, D., NO and denitrosylases regulate maturation of active catalase by influencing its heme incorporation and tetrameric structure. *Nitric Oxide-Biol Ch* **2014,** *42*, 117-117.

44. Sassa, S., Why heme needs to be degraded to iron, biliverdin IXalpha, and carbon monoxide? *Antioxid Redox Signal* **2004,** *6* (5), 819-24.

45. Donegan, R. K.; Moore, C. M.; Hanna, D. A.; Reddi, A. R., Handling heme: The mechanisms underlying the movement of heme within and between cells. *Free Radic Biol Med* **2019,** *133*, 88-100.

46. Kumar, S.; Bandyopadhyay, U., Free heme toxicity and its detoxification systems in human. *Toxicol Lett* **2005,** *157* (3), 175-88.

47. Belcher, J. D.; Mahaseth, H.; Welch, T. E.; Otterbein, L. E.; Hebbel, R. P.; Vercellotti, G. M., Heme oxygenase-1 is a modulator of inflammation and vaso-occlusion in transgenic sickle mice. *J Clin Invest* **2006,** *116* (3), 808-16.

48. Kozlowski, H.; Janicka-Klos, A.; Brasun, J.; Gaggelli, E.; Valensin, D.; Valensin, G., Copper, iron, and zinc ions homeostasis and their role in neurodegenerative disorders (metal uptake, transport, distribution and regulation). *Coordin Chem Rev* **2009,** *253* (21-22), 2665-2685.

49. Reddi, A. R.; Hamza, I., Heme Mobilization in Animals: A Metallolipid's Journey. *Acc Chem Res* **2016,** *49* (6), 1104-10.

50. Severance, S.; Rajagopal, A.; Rao, A. U.; Cerqueira, G. C.; Mitreva, M.; El-Sayed, N. M.; Krause, M.; Hamza, I., Genome-wide analysis reveals novel genes essential for heme homeostasis in Caenorhabditis elegans. *PLoS Genet* **2010,** *6* (7), e1001044.

51. Sinclair, J.; Pinter, K.; Samuel, T.; Beardsley, S.; Yuan, X.; Zhang, J.; Meng, K.; Yun, S.; Krause, M.; Hamza, I., Inter-organ signalling by HRG-7 promotes systemic haem homeostasis. *Nat Cell Biol* **2017,** *19* (7), 799-807.

52. Marciano, O.; Moskovitz, Y.; Hamza, I.; Ruthstein, S., Histidine residues are important for preserving the structure and heme binding to the C. elegans HRG-3 heme-trafficking protein. *J Biol Inorg Chem* **2015,** *20* (8), 1253-61.

53. Yuan, X.; Protchenko, O.; Philpott, C. C.; Hamza, I., Topologically conserved residues direct heme transport in HRG-1-related proteins. *J Biol Chem* **2012,** *287* (7), 4914-24.

54. Rajagopal, A.; Rao, A. U.; Amigo, J.; Tian, M.; Upadhyay, S. K.; Hall, C.; Uhm, S.; Mathew, M. K.; Fleming, M. D.; Paw, B. H.; Krause, M.; Hamza, I., Haem homeostasis is regulated by the conserved and concerted functions of HRG-1 proteins. *Nature* **2008,** *453* (7198), 1127-31.

55. Cabello-Donayre, M.; Malagarie-Cazenave, S.; Campos-Salinas, J.; Galvez, F. J.; Rodriguez-Martinez, A.; Pineda-Molina, E.; Orrego, L. M.; Martinez-Garcia, M.; Sanchez-Canete, M. P.; Estevez, A. M.; Perez-Victoria, J. M., Trypanosomatid parasites rescue heme from endocytosed hemoglobin through lysosomal HRG transporters. *Mol Microbiol* **2016,** *101* (6), 895-908.

56. O'Callaghan, K. M.; Ayllon, V.; O'Keeffe, J.; Wang, Y.; Cox, O. T.; Loughran, G.; Forgac, M.; O'Connor, R., Heme-binding protein HRG-1 is induced by insulin-like growth factor I and associates with the vacuolar H+-ATPase to control endosomal pH and receptor trafficking. *J Biol Chem* **2010,** *285* (1), 381-91.

57. Chakravarti, R.; Aulak, K. S.; Fox, P. L.; Stuehr, D. J., GAPDH regulates cellular heme insertion into inducible nitric oxide synthase. *P Natl Acad Sci USA* **2010,** *107* (42), 18004-18009.

58. Chakravarti, R.; Gupta, K.; Majors, A.; Ruple, L.; Aronica, M.; Stuehr, D. J., Novel insights in mammalian catalase heme maturation: Effect of NO and thioredoxin-1. *Free Radical Bio Med* **2015,** *82*, 105-113.

59. Ghosh, A.; Stasch, J. P.; Papapetropoulos, A.; Stuehr, D. J., Nitric Oxide and Heat Shock Protein 90 Activate Soluble Guanylate Cyclase by Driving Rapid Change in Its Subunit Interactions and Heme Content. *J Biol Chem* **2014,** *289* (22), 15259-15271.

60. Yee, E. L.; Pitt, B. R.; Billiar, T. R.; Kim, Y. M., Effect of nitric oxide on heme metabolism in pulmonary artery endothelial cells. *Am J Physiol* **1996,** *271* (4 Pt 1), L512-8.

61. Motterlini, R.; Foresti, R.; Intaglietta, M.; Winslow, R. M., NO-mediated activation of heme oxygenase: endogenous cytoprotection against oxidative stress to endothelium. *Am J Physiol* **1996,** *270* (1 Pt 2), H107-14.

62. Cooper, C. E., Nitric oxide and iron proteins. *Biochim Biophys Acta* **1999,** *1411* (2-3), 290-309.

63. Herzik, M. A.; Jonnalagadda, R.; Kuriyan, J.; Marletta, M. A., Structural insights into the role of iron-histidine bond cleavage in nitric oxide-induced activation of H-NOX gas sensor proteins. *P Natl Acad Sci USA* **2014,** *111* (40), E4156-E4164.

64. Straub, A. C.; Lohman, A. W.; Billaud, M.; Johnstone, S. R.; Dwyer, S. T.; Lee, M. Y.; Bortz, P. S.; Best, A. K.; Columbus, L.; Gaston, B.; Isakson, B. E., Endothelial cell expression of haemoglobin alpha regulates nitric oxide signalling. *Nature* **2012,** *491* (7424), 473-7.

65. Hematian, S.; Siegler, M. A.; Karlin, K. D., Heme/Copper Assembly Mediated Nitrite and Nitric Oxide Interconversion. *Journal of the American Chemical Society* **2012,** *134* (46), 18912-18915.

66. Schreiter, E. R.; Rodriguez, M. M.; Weichsel, A.; Montfort, W. R.; Bonaventura, J., S-nitrosylation-induced conformational change in blackfin tuna myoglobin. *J Biol Chem* **2007,** *282* (27), 19773-80.

67. Weichsel, A.; Maes, E. M.; Andersen, J. F.; Valenzuela, J. G.; Shokhireva, T.; Walker, F. A.; Montfort, W. R., Heme-assisted S-nitrosation of a proximal thiolate in a nitric oxide transport protein. *Proc Natl Acad Sci U S A* **2005,** *102* (3), 594-9.

68. Sharma, J. N.; Al-Omran, A.; Parvathy, S. S., Role of nitric oxide in inflammatory diseases. *Inflammopharmacology* **2007,** *15* (6), 252-9.

69. Kleschyov, A. L., The NO-heme signaling hypothesis. *Free Radic Biol Med* **2017,** *112*, 544-552.

70. Fiorito, V.; Chiabrando, D.; Tolosano, E., Mitochondrial Targeting in Neurodegeneration: A Heme Perspective. *Pharmaceuticals (Basel)* **2018,** *11* (3).

71. Piel, R. B., 3rd; Dailey, H. A., Jr.; Medlock, A. E., The mitochondrial heme metabolon: Insights into the complex(ity) of heme synthesis and distribution. *Mol Genet Metab* **2019**.

72. Bonkovsky, H. L.; Guo, J. T.; Hou, W.; Li, T.; Narang, T.; Thapar, M., Porphyrin and heme metabolism and the porphyrias. *Compr Physiol* **2013,** *3* (1), 365-401.

73. Peoc'h, K.; Martin-Schmitt, C.; Talbi, N.; Deybach, J. C.; Gouya, L.; Puy, H., [Porphyrias and haem related disorders]. *Rev Med Interne* **2016,** *37* (3), 173-85.

74. Medlock, A. E.; Shiferaw, M. T.; Marcero, J. R.; Vashisht, A. A.; Wohlschlegel, J. A.; Phillips, J. D.; Dailey, H. A., Identification of the Mitochondrial Heme Metabolism Complex. *PLoS One* **2015,** *10* (8), e0135896.

75. Sass, G.; Seyfried, S.; Parreira Soares, M.; Yamashita, K.; Kaczmarek, E.; Neuhuber, W. L.; Tiegs, G., Cooperative effect of biliverdin and carbon monoxide on survival of mice in immune-mediated liver injury. *Hepatology* **2004,** *40* (5), 1128-35.

76. Ding, Y.; Hou, X.; Chen, L.; Zhou, H.; Gong, Y.; Dai, L.; Zheng, Y., Heme oxygenase-1 dependant pathway contributes to protection by tetramethylpyrazine against chronic hypoxic injury on medulla oblongata in rats. *J Neurol Sci* **2016,** *361*, 101-11.

77. Chen, H.; Wang, X.; Zhao, Q.; Zhang, Z.; Ye, X.; Hua, F.; Cui, G., Dual effects of heme oxygenase-1 on astrocyte injury induced by hemin in vitro. *Brain Inj* **2016,** *30* (1), 36-42.

78. Schallner, N.; Pandit, R.; LeBlanc, R., 3rd; Thomas, A. J.; Ogilvy, C. S.; Zuckerbraun, B. S.; Gallo, D.; Otterbein, L. E.; Hanafy, K. A., Microglia regulate blood clearance in subarachnoid hemorrhage by heme oxygenase-1. *J Clin Invest* **2015,** *125* (7), 2609-25.

79. Baranano, D. E.; Snyder, S. H., Neural roles for heme oxygenase: contrasts to nitric oxide synthase. *Proc Natl Acad Sci U S A* **2001,** *98* (20), 10996-1002.

80. Wang, J.; Dore, S., Heme oxygenase 2 deficiency increases brain swelling and inflammation after intracerebral hemorrhage. *Neuroscience* **2008,** *155* (4), 1133-41.

81. Wang, J.; Zhuang, H.; Dore, S., Heme oxygenase 2 is neuroprotective against intracerebral hemorrhage. *Neurobiol Dis* **2006,** *22* (3), 473-6.

82. Ambegaokar, S. S.; Kolson, D. L., Heme oxygenase-1 dysregulation in the brain: implications for HIV-associated neurocognitive disorders. *Curr HIV Res* **2014,** *12* (3), 174-88.

83. Kovacsics, C. E.; Gill, A. J.; Ambegaokar, S. S.; Gelman, B. B.; Kolson, D. L., Degradation of heme oxygenase-1 by the immunoproteasome in astrocytes: A potential interferon-gamma-dependent mechanism contributing to HIV neuropathogenesis. *Glia* **2017,** *65* (8), 1264-1277.

84. Soares, M. P.; Bozza, M. T., Red alert: labile heme is an alarmin. *Curr Opin Immunol* **2016,** *38*, 94-100.

85. Dutra, F. F.; Alves, L. S.; Rodrigues, D.; Fernandez, P. L.; de Oliveira, R. B.; Golenbock, D. T.; Zamboni, D. S.; Bozza, M. T., Hemolysis-induced lethality involves inflammasome activation by heme. *Proc Natl Acad Sci U S A* **2014,** *111* (39), E4110-8.

86. Petrillo, S.; Chiabrando, D.; Genova, T.; Fiorito, V.; Ingoglia, G.; Vinchi, F.; Mussano, F.; Carossa, S.; Silengo, L.; Altruda, F.; Merlo, G. R.; Munaron, L.; Tolosano, E., Heme accumulation in endothelial cells impairs angiogenesis by triggering paraptosis. *Cell Death Differ* **2018,** *25* (3), 573-588.

87. Belcher, J. D.; Chen, C.; Nguyen, J.; Milbauer, L.; Abdulla, F.; Alayash, A. I.; Smith, A.; Nath, K. A.; Hebbel, R. P.; Vercellotti, G. M., Heme triggers TLR4 signaling leading to endothelial cell activation and vaso-occlusion in murine sickle cell disease. *Blood* **2014,** *123* (3), 377-90.

88. Liu, Y.; Zhong, H.; Vinchi, F.; Mendelson, A.; Yazdanbakhsh, K., Patrolling monocytes in sickle cell hemolytic conditions. *Transfus Clin Biol* **2019**.

89. Okombo, J.; Chibale, K., Insights into Integrated Lead Generation and Target Identification in Malaria and Tuberculosis Drug Discovery. *Acc Chem Res* **2017,** *50* (7), 1606-1616.

90. McLean, K. J.; Munro, A. W., Drug targeting of heme proteins in Mycobacterium tuberculosis. *Drug Discov Today* **2017,** *22* (3), 566-575.

91. Higgins, L. S., Tuberculosis and porphyria. *Clin Infect Dis* **1999,** *29* (3), 693-4.

92. Chiziane, E.; Telemann, H.; Krueger, M.; Adler, J.; Arnhold, J.; Alia, A.; Flemmig, J., Free Heme and Amyloid-beta: A Fatal Liaison in Alzheimer's Disease. *J Alzheimers Dis* **2018,** *61* (3), 963-984.

93. Flemmig, J.; Zamocky, M.; Alia, A., Amyloid beta and free heme: bloody new insights into the pathogenesis of Alzheimer's disease. *Neural Regen Res* **2018,** *13* (7), 1170-1174.

94. Vidal, C.; Daescu, K.; Fitzgerald, K. E.; Starokadomska, A.; Bezprozvanny, I.; Zhang, L., Amyloid beta perturbs elevated heme flux induced with neuronal development. *Alzheimers Dement (N Y)* **2019,** *5*, 27-37.

95. Sankar, S. B.; Donegan, R. K.; Shah, K. J.; Reddi, A. R.; Wood, L. B., Heme and hemoglobin suppress amyloid beta-mediated inflammatory activation of mouse astrocytes. *J Biol Chem* **2018,** *293* (29), 11358-11373.

96. Ghosh, C.; Pramanik, D.; Mukherjee, S.; Dey, A.; Dey, S. G., Interaction of NO with Cu and heme-bound Abeta peptides associated with Alzheimer's disease. *Inorg Chem* **2013,** *52* (1), 362-8.

97. Keel, S. B.; Doty, R. T.; Yang, Z.; Quigley, J. G.; Chen, J.; Knoblaugh, S.; Kingsley, P. D.; De Domenico, I.; Vaughn, M. B.; Kaplan, J.; Palis, J.; Abkowitz, J. L.,

A heme export protein is required for red blood cell differentiation and iron homeostasis. *Science* **2008,** *319* (5864), 825-8.

98. Haldar, M.; Kohyama, M.; So, A. Y.; Kc, W.; Wu, X.; Briseno, C. G.; Satpathy, A. T.; Kretzer, N. M.; Arase, H.; Rajasekaran, N. S.; Wang, L.; Egawa, T.; Igarashi, K.; Baltimore, D.; Murphy, T. L.; Murphy, K. M., Heme-mediated SPI-C induction promotes monocyte differentiation into iron-recycling macrophages. *Cell* **2014,** *156* (6), 1223-34.

99. Dutra, F. F.; Bozza, M. T., Heme on innate immunity and inflammation. *Front Pharmacol* **2014,** *5*, 115.

100. Hou, S.; Reynolds, M. F.; Horrigan, F. T.; Heinemann, S. H.; Hoshi, T., Reversible binding of heme to proteins in cellular signal transduction. *Acc Chem Res* **2006,** *39* (12), 918-24.

101. Quigley, J. G.; Yang, Z.; Worthington, M. T.; Phillips, J. D.; Sabo, K. M.; Sabath, D. E.; Berg, C. L.; Sassa, S.; Wood, B. L.; Abkowitz, J. L., Identification of a human heme exporter that is essential for erythropoiesis. *Cell* **2004,** *118* (6), 757-66.

102. Robinson, C. R.; Liu, Y.; Thomson, J. A.; Sturtevant, J. M.; Sligar, S. G., Energetics of heme binding to native and denatured states of cytochrome b562. *Biochemistry* **1997,** *36* (51), 16141-6.

103. Takeda, S.; Kamiya, N.; Nagamune, T., A novel protein-based heme sensor consisting of green fluorescent protein and apocytochrome b(562). *Anal Biochem* **2003,** *317* (1), 116-9.

104. Takeda, S.; Kamiya, N.; Arai, R.; Nagamune, T., Design of an artificial light-harvesting unit by protein engineering: cytochrome b(562)-green fluorescent Protein chimera. *Biochem Biophys Res Commun* **2001,** *289* (1), 299-304.

105. Shcherbo, D.; Murphy, C. S.; Ermakova, G. V.; Solovieva, E. A.; Chepurnykh, T. V.; Shcheglov, A. S.; Verkhusha, V. V.; Pletnev, V. Z.; Hazelwood, K. L.; Roche, P. M.; Lukyanov, S.; Zaraisky, A. G.; Davidson, M. W.; Chudakov, D. M., Far-red fluorescent tags for protein imaging in living tissues. *Biochem J* **2009,** *418* (3), 567-74.

106. Bregestovski, P., Arosio, D., Green fluorescent protein-based chloride ion sensors for in vivo imaging. In *Fluorescent Proteins II: Application of Fluorescent Protein Technology*, Jung, G., Ed. Springer-Verlag: Berlin Heidelberg, 2012; Vol. 12, pp 99-125.

107. Arpino, J. A.; Czapinska, H.; Piasecka, A.; Edwards, W. R.; Barker, P.; Gajda, M. J.; Bochtler, M.; Jones, D. D., Structural basis for efficient chromophore communication and energy transfer in a constructed didomain protein scaffold. *J Am Chem Soc* **2012,** *134* (33), 13632-40.

108. Conant, J. B.; Tongberg, C. O., The oxidation-reduction potentials of hemin and related substances: I. The potentials of various hemins and hematins in the abscence and presence of pyridine. *J Biol Chem* **1930,** *86*, 733-741.

109. Reddi, A. R.; Reedy, C. J.; Mui, S.; Gibney, B. R., Thermodynamic investigation into the mechanisms of proton-coupled electron transfer events in heme protein maquettes. *Biochemistry* **2007,** *46* (1), 291-305.

110. Reedy, C. J.; Elvekrog, M. M.; Gibney, B. R., Development of a heme protein structure-electrochemical function database. *Nucleic Acids Res* **2008,** *36* (Database issue), D307-13.

111. Song, Y.; Yang, M.; Wegner, S. V.; Zhao, J.; Zhu, R.; Wu, Y.; He, C.; Chen, P. R., A Genetically Encoded FRET Sensor for Intracellular Heme. *ACS Chem Biol* **2015,** *10* (7), 1610-5.

112. Gupta, N.; Ragsdale, S. W., Thiol-disulfide redox dependence of heme binding and heme ligand switching in nuclear hormone receptor rev-erb{beta}. *J Biol Chem* **2011,** *286* (6), 4392-403.

113. Fleischhacker, A. S.; Sharma, A.; Choi, M.; Spencer, A. M.; Bagai, I.; Hoffman, B. M.; Ragsdale, S. W., The C-terminal heme regulatory motifs of heme oxygenase-2 are redox-regulated heme binding sites. *Biochemistry* **2015,** *54* (17), 2709-18.

114. Ness, F.; Achstetter, T.; Duport, C.; Karst, F.; Spagnoli, R.; Degryse, E., Sterol uptake in Saccharomyces cerevisiae heme auxotrophic mutants is affected by ergosterol and oleate but not by palmitoleate or by sterol esterification. *J Bacteriol* **1998,** *180* (7), 1913-9.

115. Labbe-Bois, R., The ferrochelatase from Saccharomyces cerevisiae. Sequence, disruption, and expression of its structural gene HEM15. *J Biol Chem* **1990,** *265* (13), 7278-83.

116. Grynkiewicz, G.; Poenie, M.; Tsien, R. Y., A new generation of Ca2+ indicators with greatly improved fluorescence properties. *J Biol Chem* **1985,** *260* (6), 3440-50.

117. Orij, R.; Postmus, J.; Ter Beek, A.; Brul, S.; Smits, G. J., In vivo measurement of cytosolic and mitochondrial pH using a pH-sensitive GFP derivative in Saccharomyces cerevisiae reveals a relation between intracellular pH and growth. *Microbiology* **2009,** *155* (Pt 1), 268-78.

118. Hu, J.; Dong, L.; Outten, C. E., The redox environment in the mitochondrial intermembrane space is maintained separately from the cytosol and matrix. *J Biol Chem* **2008,** *283* (43), 29126-34.

119. Garber Morales, J.; Holmes-Hampton, G. P.; Miao, R.; Guo, Y.; Munck, E.; Lindahl, P. A., Biophysical characterization of iron in mitochondria isolated from respiring and fermenting yeast. *Biochemistry* **2010,** *49* (26), 5436-44.

120. Protchenko, O.; Shakoury-Elizeh, M.; Keane, P.; Storey, J.; Androphy, R.; Philpott, C. C., Role of PUG1 in inducible porphyrin and heme transport in Saccharomyces cerevisiae. *Eukaryot Cell* **2008,** *7* (5), 859-71.

121. Tsang C. K., L., Y., Thomas, J., Zhang. Y., Zheng X. F., Superoxide dismutase 1 acts as a nuclear transcription factor to regulate oxidative stress resistance. *Nat Commun* **2014,** *5*, 3446.

122. Jorgensen, P.; Edgington, N. P.; Schneider, B. L.; Rupes, I.; Tyers, M.; Futcher, B., The size of the nucleus increases as yeast cells grow. *Mol Biol Cell* **2007,** *18* (9), 3523-32.

123. Rafelski, S. M.; Viana, M. P.; Zhang, Y.; Chan, Y. H.; Thorn, K. S.; Yam, P.; Fung, J. C.; Li, H.; Costa Lda, F.; Marshall, W. F., Mitochondrial network size scaling in budding yeast. *Science* **2012,** *338* (6108), 822-4.

124. Maragos, C. M.; Wang, J. M.; Hrabie, J. A.; Oppenheim, J. J.; Keefer, L. K., Nitric oxide/nucleophile complexes inhibit the in vitro proliferation of A375 melanoma cells via nitric oxide release. *Cancer Res* **1993,** *53* (3), 564-8.

125. Butler, A. R.; White, J. H.; Folawiyo, Y.; Edlin, A.; Gardiner, D.; Stark, M. J., Two Saccharomyces cerevisiae genes which control sensitivity to G1 arrest induced by Kluyveromyces lactis toxin. *Mol Cell Biol* **1994,** *14* (9), 6306-16.

126. Cardon, C. M.; Beck, T.; Hall, M. N.; Rutter, J., PAS kinase promotes cell survival and growth through activation of Rho1. *Sci Signal* **2012,** *5* (209), ra9.

127. Chloupkova, M.; LeBard, L. S.; Koeller, D. M., MDL1 is a high copy suppressor of ATM1: evidence for a role in resistance to oxidative stress. *J Mol Biol* **2003,** *331* (1), 155-65.

128. Sanders, E. R., Aseptic laboratory techniques: plating methods. *J Vis Exp* **2012,** (63), e3064.

129. Shayeghi, M.; Latunde-Dada, G. O.; Oakhill, J. S.; Laftah, A. H.; Takeuchi, K.; Halliday, N.; Khan, Y.; Warley, A.; McCann, F. E.; Hider, R. C.; Frazer, D. M.; Anderson, G. J.; Vulpe, C. D.; Simpson, R. J.; McKie, A. T., Identification of an intestinal heme transporter. *Cell* **2005,** *122* (5), 789-801.

130. Brickman, T. J.; Cummings, C. A.; Liew, S. Y.; Relman, D. A.; Armstrong, S. K., Transcriptional profiling of the iron starvation response in Bordetella pertussis provides new insights into siderophore utilization and virulence gene expression. *J Bacteriol* **2011,** *193* (18), 4798-812.

131. Carlson, P. E., Jr.; Carr, K. A.; Janes, B. K.; Anderson, E. C.; Hanna, P. C., Transcriptional profiling of Bacillus anthracis Sterne (34F2) during iron starvation. *PLoS One* **2009,** *4* (9), e6988.

132. Bucci, M.; Roviezzo, F.; Posadas, I.; Yu, J.; Parente, L.; Sessa, W. C.; Ignarro, L. J.; Cirino, G., Endothelial nitric oxide synthase activation is critical for vascular leakage during acute inflammation in vivo. *Proc Natl Acad Sci U S A* **2005,** *102* (3), 904-8.

133. Predonzani, A.; Cali, B.; Agnellini, A. H.; Molon, B., Spotlights on immunological effects of reactive nitrogen species: When inflammation says nitric oxide. *World J Exp Med* **2015,** *5* (2), 64-76.

134. Gietz, R. D.; Schiestl, R. H., Applications of high efficiency lithium acetate trasformation of intact yeast cells using single-stranded nucleic acids as carrier. *Yeast* **1991,** *7*, 253-263.

135. Bertani, G., Lysogeny at mid-twentieth century: P1, P2, and other experimental systems. *J Bacteriol* **2004,** *186* (3), 595-600.

136. Schneider, C. A.; Rasband, W. S.; Eliceiri, K. W., NIH Image to ImageJ: 25 years of image analysis. *Nat Methods* **2012,** *9* (7), 671-5.

137. Mumberg, D.; Muller, R.; Funk, M., Yeast vectors for the controlled expression of heterologous proteins in different genetic backgrounds. *Gene* **1995,** *156* (1), 119-22.

138. Ebert, P. S.; Hess, R. A.; Frykholm, B. C.; Tschudy, D. P., Succinylacetone, a potent inhibitor of heme biosynthesis: effect on cell growth, heme content and delta-aminolevulinic acid dehydratase activity of malignant murine erythroleukemia cells. *Biochem Biophys Res Commun* **1979,** *88* (4), 1382-90.

139. Reddi, A. R.; Culotta, V. C., SOD1 integrates signals from oxygen and glucose to repress respiration. *Cell* **2013,** *152* (1-2), 224-35.

140. Reddi, A. R.; Culotta, V. C., Regulation of Manganese Antioxidants by Nutrient Sensing Pathways in Saccharomyces cerevisiae. *Genetics* **2011,** *189*, 1261-70.

141. Reddi, A. R.; Culotta, V. C., Regulation of manganese antioxidants by nutrient sensing pathways in Saccharomyces cerevisiae. *Genetics* **2011,** *189* (4), 1261-70.

142. Zhang, L.; Bermingham-McDonogh, O.; Turcotte, B.; Guarente, L., Antibody-promoted dimerization bypasses the regulation of DNA binding by the heme domain of the yeast transcriptional activator HAP1. *Proc Natl Acad Sci U S A* **1993,** *90* (7), 2851-5.

143. Zhang, L.; Hach, A., Molecular mechanism of heme signaling in yeast: the transcriptional activator Hap1 serves as the key mediator. *Cell Mol Life Sci* **1999,** *56* (5-6), 415-26.

144. Feng, Y.; Sligar, S. G.; Wand, A. J., Solution structure of apocytochrome b562. *Nat Struct Biol* **1994,** *1* (1), 30-5.

145. Feng, Y. Q.; Sligar, S. G., Effect of heme binding on the structure and stability of Escherichia coli apocytochrome b562. *Biochemistry* **1991,** *30* (42), 10150-5.

146. Itagaki, E.; Palmer, G.; Hager, L. P., Studies on cytochrome b562 of Escherichia coli. II. Reconstitution of cytochrome b562 from apoprotein and hemin. *J Biol Chem* **1967,** *242* (9), 2272-7.

147. Nikkila, H.; Gennis, R. B.; Sligar, S. G., Cloning and expression of the gene encoding the soluble cytochrome b562 of Escherichia coli. *Eur J Biochem* **1991,** *202* (2), 309-13.

148. Kiktev, D. A.; Patterson, J. C.; Muller, S.; Bariar, B.; Pan, T.; Chernoff, Y. O., Regulation of chaperone effects on a yeast prion by cochaperone Sgt2. *Mol Cell Biol* **2012,** *32* (24), 4960-70.

149. Barker, P. D.; Freund, S. M., Bis-methionine ligation to heme iron in mutants of cytochrome b562. 2. Characterization by NMR of heme-ligand interactions. *Biochemistry* **1996,** *35* (42), 13627-35.

150. Sassa, S.; Kappas, A., Succinylacetone inhibits delta-aminolevulinate dehydratase and potentiates the drug and steroid induction of delta-aminolevulinate synthase in liver. *Trans Assoc Am Physicians* **1982,** *95*, 42-52.

151. Zhang, L.; Hach, A.; Wang, C., Molecular mechanism governing heme signaling in yeast: a higher-order complex mediates heme regulation of the transcriptional activator HAP1. *Mol Cell Biol* **1998,** *18* (7), 3819-28.

152. Correia, M. A.; Sinclair, P. R.; De Matteis, F., Cytochrome P450 regulation: the interplay between its heme and apoprotein moieties in synthesis, assembly, repair, and disposal. *Drug Metab Rev* **2011,** *43* (1), 1-26.

153. De Matteis, F.; Gibbs, A. H.; Smith, A. G., Inhibition of protohaem ferro-lyase by N-substituted porphyrins. Structural requirements for the inhibitory effect. *Biochem J* **1980,** *189* (3), 645-8.

154. De Matteis, F.; Marks, G. S., The effect of N-methylprotoporphyrin and succinyl-acetone on the regulation of heme biosynthesis in chicken hepatocytes in culture. *FEBS Lett* **1983,** *159* (1-2), 127-31.

155. Ortiz de Montellano, P. R.; Mico, B. A.; Yost, G. S., Suicidal inactivation of cytochrome P-450. Formation of a heme-substrate covalent adduct. *Biochem Biophys Res Commun* **1978,** *83* (1), 132-7.

156. Smith, A. G.; Clothier, B.; Carthew, P.; Childs, N. L.; Sinclair, P. R.; Nebert, D. W.; Dalton, T. P., Protection of the Cyp1a2(-/-) null mouse against uroporphyria and

hepatic injury following exposure to 2,3,7,8-tetrachlorodibenzo-p-dioxin. *Toxicol Appl Pharmacol* **2001,** *173* (2), 89-98.

157. Urquhart, A. J.; Elder, G. H.; Roberts, A. G.; Lambrecht, R. W.; Sinclair, P. R.; Bement, W. J.; Gorman, N.; Sinclair, J. A., Uroporphyria produced in mice by 20-methylcholanthrene and 5-aminolaevulinic acid. *Biochem J* **1988,** *253* (2), 357-62.

158. Schauder, A.; Avital, A.; Malik, Z., Regulation and gene expression of heme synthesis under heavy metal exposure--review. *J Environ Pathol Toxicol Oncol* **2010,** *29* (2), 137-58.

159. Sharma, B.; Singh, S.; Siddiqi, N. J., Biomedical implications of heavy metals induced imbalances in redox systems. *Biomed Res Int* **2014,** *2014*, 640754.

160. Lubran, M. M., Lead toxicity and heme biosynthesis. *Ann Clin Lab Sci* **1980,** *10* (5), 402-13.

161. Cohen, A. R.; Trotzky, M. S.; Pincus, D., Reassessment of the microcytic anemia of lead poisoning. *Pediatrics* **1981,** *67* (6), 904-6.

162. Wani, A. L.; Ara, A.; Usmani, J. A., Lead toxicity: a review. *Interdiscip Toxicol* **2015,** *8* (2), 55-64.

163. Flora, G.; Gupta, D.; Tiwari, A., Toxicity of lead: A review with recent updates. *Interdiscip Toxicol* **2012,** *5* (2), 47-58.

164. Alam, J.; Cai, J.; Smith, A., Isolation and characterization of the mouse heme oxygenase-1 gene. Distal 5' sequences are required for induction by heme or heavy metals. *J Biol Chem* **1994,** *269* (2), 1001-9.

165. Gozzelino, R.; Jeney, V.; Soares, M. P., Mechanisms of cell protection by heme oxygenase-1. *Annu Rev Pharmacol Toxicol* **2010,** *50*, 323-54.

166. Van der Heggen, M.; Martins, S.; Flores, G.; Soares, E. V., Lead toxicity in Saccharomyces cerevisiae. *Appl Microbiol Biotechnol* **2010,** *88* (6), 1355-61.

167. Hanna, D. A.; Hu, R.; Kim, H.; Martinez-Guzman, O.; Torres, M. P.; Reddi, A. R., Heme bioavailability and signaling in response to stress in yeast cells. *J Biol Chem* **2018,** *293* (32), 12378-12393.

168. Qian, Z. M.; Morgan, E. H., Effect of lead on the transport of transferrin-free and transferrin-bound iron into rabbit reticulocytes. *Biochem Pharmacol* **1990,** *40* (5), 1049-54.

169. Fu, X.; Zeng, A.; Zheng, W.; Du, Y., Upregulation of zinc transporter 2 in the blood-CSF barrier following lead exposure. *Exp Biol Med (Maywood)* **2014,** *239* (2), 202-12.

170. Pounds, J. G., Effect of lead intoxication on calcium homeostasis and calcium-mediated cell function: a review. *Neurotoxicology* **1984,** *5* (3), 295-331.

171. Quintanar-Escorza, M. A.; Gonzalez-Martinez, M. T.; del Pilar, I. O.; Calderon-Salinas, J. V., Oxidative damage increases intracellular free calcium [Ca2+]i concentration in human erythrocytes incubated with lead. *Toxicol In Vitro* **2010,** *24* (5), 1338-46.

172. Zheng, G.; Zhang, J.; Xu, Y.; Shen, X.; Song, H.; Jing, J.; Luo, W.; Zheng, W.; Chen, J., Involvement of CTR1 and ATP7A in lead (Pb)-induced copper (Cu) accumulation in choroidal epithelial cells. *Toxicol Lett* **2014,** *225* (1), 110-8.

173. Dongre, N. N.; Suryakar, A. N.; Patil, A. J.; Hundekari, I. A.; Devarnavadagi, B. B., Biochemical effects of lead exposure on battery manufacture workers with reference to blood pressure, calcium metabolism and bone mineral density. *Indian J Clin Biochem* **2013,** *28* (1), 65-70.

174. Schulze, H.; Brand, J. J., Lead toxicity and phosphate deficiency in chlamydomonas. *Plant Physiol* **1978,** *62* (5), 727-30.

175. Jaishankar, M.; Tseten, T.; Anbalagan, N.; Mathew, B. B.; Beeregowda, K. N., Toxicity, mechanism and health effects of some heavy metals. *Interdiscip Toxicol* **2014,** *7* (2), 60-72.

176. Mendoza-Cozatl, D.; Loza-Tavera, H.; Hernandez-Navarro, A.; Moreno-Sanchez, R., Sulfur assimilation and glutathione metabolism under cadmium stress in yeast, protists and plants. *FEMS Microbiol Rev* **2005,** *29* (4), 653-71.

177. Ernst, W. H.; Krauss, G. J.; Verkleij, J. A.; Wesenberg, D., Interaction of heavy metals with the sulphur metabolism in angiosperms from an ecological point of view. *Plant Cell Environ* **2008,** *31* (1), 123-43.

178. Protchenko, O.; Philpott, C. C., Regulation of intracellular heme levels by HMX1, a homologue of heme oxygenase, in Saccharomyces cerevisiae. *J Biol Chem* **2003,** *278* (38), 36582-7.

179. Collinson, E. J.; Wimmer-Kleikamp, S.; Gerega, S. K.; Yang, Y. H.; Parish, C. R.; Dawes, I. W.; Stocker, R., The yeast homolog of heme oxygenase-1 affords cellular antioxidant protection via the transcriptional regulation of known antioxidant genes. *J Biol Chem* **2011,** *286* (3), 2205-14.

180. Elsasser, S.; Chandler-Militello, D.; Muller, B.; Hanna, J.; Finley, D., Rad23 and Rpn10 serve as alternative ubiquitin receptors for the proteasome. *J Biol Chem* **2004,** *279* (26), 26817-22.

181. Marques, M.; Mojzita, D.; Amorim, M. A.; Almeida, T.; Hohmann, S.; Moradas-Ferreira, P.; Costa, V., The Pep4p vacuolar proteinase contributes to the turnover of oxidized proteins but PEP4 overexpression is not sufficient to increase

chronological lifespan in Saccharomyces cerevisiae. *Microbiology* **2006,** *152* (Pt 12), 3595-605.

182. Papinski, D.; Kraft, C., Regulation of Autophagy By Signaling Through the Atg1/ULK1 Complex. *J Mol Biol* **2016,** *428* (9 Pt A), 1725-41.

183. Liu, S. C.; Zhai, S.; Palek, J., Detection of hemin release during hemoglobin S denaturation. *Blood* **1988,** *71* (6), 1755-8.

184. Aich, A.; Freundlich, M.; Vekilov, P. G., The free heme concentration in healthy human erythrocytes. *Blood Cells Mol Dis* **2015,** *55* (4), 402-9.

185. Bonkovsky, H. L.; Healey, J. F.; Lourie, A. N.; Gerron, G. G., Intravenous heme-albumin in acute intermittent porphyria: evidence for repletion of hepatic hemoproteins and regulatory heme pools. *Am J Gastroenterol* **1991,** *86* (8), 1050-6.

186. Zhang, T.; Bu, P.; Zeng, J.; Vancura, A., Increased heme synthesis in yeast induces a metabolic switch from fermentation to respiration even under conditions of glucose repression. *J Biol Chem* **2017,** *292* (41), 16942-16954.

187. Tu, B. P.; Mohler, R. E.; Liu, J. C.; Dombek, K. M.; Young, E. T.; Synovec, R. E.; McKnight, S. L., Cyclic changes in metabolic state during the life of a yeast cell. *Proc Natl Acad Sci U S A* **2007,** *104* (43), 16886-91.

188. Tu, B. P.; McKnight, S. L., Evidence of carbon monoxide-mediated phase advancement of the yeast metabolic cycle. *Proc Natl Acad Sci U S A* **2009,** *106* (34), 14293-6.

189. Sousa, C. A.; Soares, E. V., Mitochondria are the main source and one of the targets of Pb (lead)-induced oxidative stress in the yeast Saccharomyces cerevisiae. *Appl Microbiol Biotechnol* **2014,** *98* (11), 5153-60.

190. Perez, R. R.; Sousa, C. A.; Vankeersbilck, T.; Machado, M. D.; Soares, E. V., Evaluation of the role of glutathione in the lead-induced toxicity in Saccharomyces cerevisiae. *Curr Microbiol* **2013,** *67* (3), 300-5.

191. Lanphear, B. P.; Burgoon, D. A.; Rust, S. W.; Eberly, S.; Galke, W., Environmental exposures to lead and urban children's blood lead levels. *Environ Res* **1998,** *76* (2), 120-30.

192. Piomelli, S.; Seaman, C.; Zullow, D.; Curran, A.; Davidow, B., Threshold for lead damage to heme synthesis in urban children. *Proc Natl Acad Sci U S A* **1982,** *79* (10), 3335-9.

193. Gillis, B. S.; Arbieva, Z.; Gavin, I. M., Analysis of lead toxicity in human cells. *BMC Genomics* **2012,** *13*, 344.

194. Lidsky, T. I.; Schneider, J. S., Lead neurotoxicity in children: basic mechanisms and clinical correlates. *Brain* **2003,** *126* (Pt 1), 5-19.

195. Yedjou, C. G.; Milner, J. N.; Howard, C. B.; Tchounwou, P. B., Basic apoptotic mechanisms of lead toxicity in human leukemia (HL-60) cells. *Int J Environ Res Public Health* **2010,** *7* (5), 2008-17.

196. Chen, C.; Wang, J., Response of Saccharomyces cerevisiae to lead ion stress. *Appl Microbiol Biotechnol* **2007,** *74* (3), 683-7.

197. Bussche, J. V.; Soares, E. V., Lead induces oxidative stress and phenotypic markers of apoptosis in Saccharomyces cerevisiae. *Appl Microbiol Biotechnol* **2011,** *90* (2), 679-87.

198. Wysocki, R.; Tamas, M. J., How Saccharomyces cerevisiae copes with toxic metals and metalloids. *FEMS Microbiol Rev* **2010,** *34* (6), 925-51.

199. Magyar, J. S.; Weng, T. C.; Stern, C. M.; Dye, D. F.; Rous, B. W.; Payne, J. C.; Bridgewater, B. M.; Mijovilovich, A.; Parkin, G.; Zaleski, J. M.; Penner-Hahn, J. E.; Godwin, H. A., Reexamination of lead(II) coordination preferences in sulfur-rich sites: implications for a critical mechanism of lead poisoning. *J Am Chem Soc* **2005,** *127* (26), 9495-505.

200. Grunberg-Etkovitz, N.; Lev, N.; Ickowicz, D.; Avital, A.; Offen, D.; Malik, Z., Accelerated proteasomal activity induced by Pb2+, Ga3+, or Cu2+ exposure does not induce degradation of alpha-synuclein. *J Environ Pathol Toxicol Oncol* **2009,** *28* (1), 5-24.

201. Guo, G. G.; Gu, M.; Etlinger, J. D., 240-kDa proteasome inhibitor (CF-2) is identical to delta-aminolevulinic acid dehydratase. *J Biol Chem* **1994,** *269* (17), 12399-402.

202. Vallelian, F.; Deuel, J. W.; Opitz, L.; Schaer, C. A.; Puglia, M.; Lonn, M.; Engelsberger, W.; Schauer, S.; Karnaukhova, E.; Spahn, D. R.; Stocker, R.; Buehler, P. W.; Schaer, D. J., Proteasome inhibition and oxidative reactions disrupt cellular homeostasis during heme stress. *Cell Death Differ* **2015,** *22* (4), 597-611.

203. Lopes, A. C.; Peixe, T. S.; Mesas, A. E.; Paoliello, M. M., Lead Exposure and Oxidative Stress: A Systematic Review. *Rev Environ Contam Toxicol* **2016,** *236*, 193-238.

204. Lee, K. H.; Lee, S. K.; Kim, H. S.; Cho, E. J.; Joo, H. K.; Lee, E. J.; Lee, J. Y.; Park, M. S.; Chang, S. J.; Cho, C. H.; Park, J. B.; Jeon, B. H., Overexpression of Ref-1 Inhibits Lead-induced Endothelial Cell Death via the Upregulation of Catalase. *Korean J Physiol Pharmacol* **2009,** *13* (6), 431-6.

205. May, B. K.; Bhasker, C. R.; Bawden, M. J.; Cox, T. C., Molecular regulation of 5-aminolevulinate synthase. Diseases related to heme biosynthesis. *Mol Biol Med* **1990,** *7* (5), 405-21.

206. Fleischhacker, A. S.; Ragsdale, S. W., An unlikely heme chaperone confirmed at last. *J Biol Chem* **2018,** *293* (37), 14569-14570.

207. Ghosh, A.; Stasch, J. P.; Papapetropoulos, A.; Stuehr, D. J., Nitric oxide and heat shock protein 90 activate soluble guanylate cyclase by driving rapid change in its subunit interactions and heme content. *J Biol Chem* **2014,** *289* (22), 15259-71.

208. Ghosh, A.; Garee, G.; Sweeny, E. A.; Nakamura, Y.; Stuehr, D. J., Hsp90 chaperones hemoglobin maturation in erythroid and nonerythroid cells. *Proc Natl Acad Sci U S A* **2018,** *115* (6), E1117-E1126.

209. Ghosh, A.; Stuehr, D. J., Regulation of sGC via hsp90, Cellular Heme, sGC Agonists, and NO: New Pathways and Clinical Perspectives. *Antioxid Redox Signal* **2017,** *26* (4), 182-190.

210. Billecke, S. S.; Draganov, D. I.; Morishima, Y.; Murphy, P. J.; Dunbar, A. Y.; Pratt, W. B.; Osawa, Y., The role of hsp90 in heme-dependent activation of apo-neuronal nitric-oxide synthase. *J Biol Chem* **2004,** *279* (29), 30252-8.

211. Xu, Z.; Pal, J. K.; Thulasiraman, V.; Hahn, H. P.; Chen, J. J.; Matts, R. L., The role of the 90-kDa heat-shock protein and its associated cohorts in stabilizing the heme-regulated eIF-2alpha kinase in reticulocyte lysates during heat stress. *Eur J Biochem* **1997,** *246* (2), 461-70.

212. Szyszka, R.; Kramer, G.; Hardesty, B., The phosphorylation state of the reticulocyte 90-kDa heat shock protein affects its ability to increase phosphorylation of peptide initiation factor 2 alpha subunit by the heme-sensitive kinase. *Biochemistry* **1989,** *28* (4), 1435-8.

213. Padmanabhan, N.; Fichtner, L.; Dickmanns, A.; Ficner, R.; Schulz, J. B.; Braus, G. H., The yeast HtrA orthologue Ynm3 is a protease with chaperone activity that aids survival under heat stress. *Mol Biol Cell* **2009,** *20* (1), 68-77.

214. Jo, H.; Patterson, V.; Stoessel, S.; Kuan, C. Y.; Hoh, J., Protoporphyrins enhance oligomerization and enzymatic activity of HtrA1 serine protease. *PLoS One* **2014,** *9* (12), e115362.

215. Otto, B. R.; Sijbrandi, R.; Luirink, J.; Oudega, B.; Heddle, J. G.; Mizutani, K.; Park, S. Y.; Tame, J. R., Crystal structure of hemoglobin protease, a heme binding autotransporter protein from pathogenic Escherichia coli. *J Biol Chem* **2005,** *280* (17), 17339-45.

216. Tachibana, S.; Kuba, N.; Kawai, F.; Duine, J. A.; Yasuda, M., Involvement of a quinoprotein (PQQ-containing) alcohol dehydrogenase in the degradation of

polypropylene glycols by the bacterium Stenotrophomonas maltophilia. *FEMS Microbiol Lett* **2003,** *218* (2), 345-9.

217. Chavez-Pacheco, J. L.; Contreras-Zentella, M.; Membrillo-Hernandez, J.; Arreguin-Espinoza, R.; Mendoza-Hernandez, G.; Gomez-Manzo, S.; Escamilla, J. E., The quinohaemoprotein alcohol dehydrogenase from Gluconacetobacter xylinus: molecular and catalytic properties. *Arch Microbiol* **2010,** *192* (9), 703-13.

218. Gomez-Manzo, S.; Gonzalez-Valdez, A. A.; Oria-Hernandez, J.; Reyes-Vivas, H.; Arreguin-Espinosa, R.; Kroneck, P. M.; Sosa-Torres, M. E.; Escamilla, J. E., The active (ADHa) and inactive (ADHi) forms of the PQQ-alcohol dehydrogenase from Gluconacetobacter diazotrophicus differ in their respective oligomeric structures and redox state of their corresponding prosthetic groups. *FEMS Microbiol Lett* **2012,** *328* (2), 106-13.

219. Oubrie, A.; Rozeboom, H. J.; Kalk, K. H.; Huizinga, E. G.; Dijkstra, B. W., Crystal structure of quinohemoprotein alcohol dehydrogenase from Comamonas testosteroni: structural basis for substrate oxidation and electron transfer. *J Biol Chem* **2002,** *277* (5), 3727-32.

220. Tamas, M. J.; Sharma, S. K.; Ibstedt, S.; Jacobson, T.; Christen, P., Heavy metals and metalloids as a cause for protein misfolding and aggregation. *Biomolecules* **2014,** *4* (1), 252-67.

221. Michener, J. K.; Nielsen, J.; Smolke, C. D., Identification and treatment of heme depletion attributed to overexpression of a lineage of evolved P450 monooxygenases. *Proc Natl Acad Sci U S A* **2012,** *109* (47), 19504-9.

222. Yuan, X.; Rietzschel, N.; Kwon, H.; Walter Nuno, A. B.; Hanna, D. A.; Phillips, J. D.; Raven, E. L.; Reddi, A. R.; Hamza, I., Regulation of intracellular heme trafficking revealed by subcellular reporters. *Proceedings of the National Academy of Sciences* **2016,** *113* (35), E5144-E5152.

223. Abshire, J. R.; Rowlands, C. J.; Ganesan, S. M.; So, P. T. C.; Niles, J. C., Quantification of labile heme in live malaria parasites using a genetically encoded biosensor. *P Natl Acad Sci USA* **2017,** *114* (11), E2068-E2076.

224. Chen, A. J.; Yuan, X.; Li, J.; Dong, P.; Hamza, I.; Cheng, J. X., Label-Free Imaging of Heme Dynamics in Living Organisms by Transient Absorption Microscopy. *Anal Chem* **2018,** *90* (5), 3395-3401.

225. Kempe, H.; Schwabe, A.; Cremazy, F.; Verschure, P. J.; Bruggeman, F. J., The volumes and transcript counts of single cells reveal concentration homeostasis and capture biological noise. *Mol Biol Cell* **2015,** *26* (4), 797-804.

226. Chien, H. C.; Zur, A. A.; Maurer, T. S.; Yee, S. W.; Tolsma, J.; Jasper, P.; Scott, D. O.; Giacomini, K. M., Rapid Method To Determine Intracellular Drug Concentrations in Cellular Uptake Assays: Application to Metformin in Organic Cation

Transporter 1-Transfected Human Embryonic Kidney 293 Cells. *Drug Metab Dispos* **2016,** *44* (3), 356-64.

227. Kim, Y. S.; Dore, S., Catalytically inactive heme oxygenase-2 mutant is cytoprotective. *Free Radic Biol Med* **2005,** *39* (4), 558-64.

228. Abshire, J. R.; Rowlands, C. J.; Ganesan, S. M.; So, P. T.; Niles, J. C., Quantification of labile heme in live malaria parasites using a genetically encoded biosensor. *Proc Natl Acad Sci U S A* **2017,** *114* (11), E2068-E2076.

229. Gouveia, Z.; Carlos, A. R.; Yuan, X.; Aires-da-Silva, F.; Stocker, R.; Maghzal, G. J.; Leal, S. S.; Gomes, C. M.; Todorovic, S.; Iranzo, O.; Ramos, S.; Santos, A. C.; Hamza, I.; Goncalves, J.; Soares, M. P., Characterization of plasma labile heme in hemolytic conditions. *Febs J* **2017,** *284* (19), 3278-3301.

230. Wissbrock, A.; Imhof, D., A Tough Nut to Crack: Intracellular Detection and Quantification of Heme in Malaria Parasites by a Genetically Encoded Protein Sensor. *Chembiochem* **2017,** *18* (16), 1561-1564.

231. Martinez-Guzman, O.; Dietz, J. V.; Bohovych, I.; Medlock, A. W.; Khalimonchuk, O.; Reddi, A. R., Mitochondrial-nuclear heme trafficking is regulated by GTPases that control mitochondrial dynamics. *bioRxiv* **2019**, 539254.

232. Poston, C. N.; Duong, E.; Cao, Y.; Bazemore-Walker, C. R., Proteomic analysis of lipid raft-enriched membranes isolated from internal organelles. *Biochem Biophys Res Commun* **2011,** *415* (2), 355-60.

233. Bagai, I.; Sarangi, R.; Fleischhacker, A. S.; Sharma, A.; Hoffman, B. M.; Zuiderweg, E. R.; Ragsdale, S. W., Spectroscopic studies reveal that the heme regulatory motifs of heme oxygenase-2 are dynamically disordered and exhibit redox-dependent interaction with heme. *Biochemistry* **2015,** *54* (17), 2693-708.

234. Ascoli, F.; Fanelli, M. R.; Antonini, E., Preparation and properties of apohemoglobin and reconstituted hemoglobins. *Methods Enzymol* **1981,** *76*, 72-87.

235. Bowen, W. J., The absorption spectra and extinction coefficients of myoglobin. *J Biol Chem* **1949,** *179* (1), 235-45.

236. Mourer, T.; Jacques, J. F.; Brault, A.; Bisaillon, M.; Labbe, S., Shu1 Is a Cell-surface Protein Involved in Iron Acquisition from Heme in Schizosaccharomyces pombe. *J Biol Chem* **2015,** *290* (16), 10176-10190.

237. Saito, N.; Iio, T.; Yoshikawa, Y.; Ohtsuka, H.; Orino, K., Heme-binding of bovine lactoferrin: the potential presence of a heme-binding capacity in an ancestral transferrin gene. *Biometals* **2018,** *31* (1), 131-138.

238. Sengupta, S.; Tripathi, J.; Tandon, R.; Raje, M.; Roy, R. P.; Basu, S. K.; Mukhopadhyay, A., Hemoglobin endocytosis in Leishmania is mediated through a 46-kDa protein located in the flagellar pocket. *J Biol Chem* **1999,** *274* (5), 2758-2765.

239. Sultana, S.; Nirodi, C. S.; Ram, N.; Prabhu, L.; Padmanaban, G., A 65-kDa protein mediates the positive role of heme in regulating the transcription of CYP2B1/B2 gene in rat liver. *J Biol Chem* **1997,** *272* (14), 8895-8900.

240. Vuletic, I.; Liu, J.; Wu, H.; Ding, Y.; Lei, Y.; Li, C.; Zhu, D.; Ren, Q.; Sun, H.; Li, J., Establishment of an mKate2-Expressing Cell Line for Non-Invasive Real-Time Breast Cancer In Vivo Imaging. *Mol Imaging Biol* **2015**.

241. Li, D.; Shen, M.; Zhang, B.; Li, Z. R.; Pang, P. F.; Zhu, K. S.; Wang, J.; Huang, M. S.; Meng, X. C.; Shan, H., [Labeling of liver cancer cell for fluorescence imaging study by far-red fluorescence protein reporter gene mKate2]. *Zhonghua Yi Xue Za Zhi* **2011,** *91* (19), 1344-7.

242. Sikorski, R. S.; Hieter, P., A system of shuttle vectors and yeast host strains designed for efficient manipulation of DNA in *Saccharomyces ceresiviae*. *Genetics* **1989,** *122*, 19-27.